Methods to Improve nZVI Adsorbance on Silicates Surface for Nitrate Reduction

By

Handayani Putri Fraser

A Thesis

Submitted to the Victoria University of Wellington

In fulfilment of the requirements for the degree of

Doctor of Philosophy

TE WHARE WĀNANGA O TE ŪPOKO O TE IKA A MĀUI

VICTORIA
UNIVERSITY OF WELLINGTON

Victoria University of Wellington

February 2018

For my boys: James and George.

My sunshine, my rays of joy,

I am helping to make this world a better place for you to grow up in!

May the Force be with you—Always!

Declaration

This dissertation is the result of my own work and includes nothing which is the outcome of work done in collaboration except where specifically indicated in the text. It has not been previously submitted, in part or whole, to any university of institution for any degree, diploma, or other qualification.

In accordance with the Faculty of Science guidelines, this thesis is does not exceed 100,000 words.

Signed:_____

Date:_____

Handayani Putri Fraser

Victoria University of Wellington

Abstract

Efforts to remove excess nitrate in the groundwater typically involves expensive ion-exchange membranes or slow reacting bio-reactors.   Nano-sized zero valent iron (nZVI) has been used successfully to reduce nitrate into ammonia in various sites in USA and Europe. However, nZVI has a number of major setbacks associated with it, namely the tendency to agglomerate due to magnetic properties, and the possible toxicity due to the nano-sized material.

To circumvent these two setbacks, nZVI could be adsorbed onto solid support. In this research, geothermal sediment microsilicate 600 (Misi) was utilised as a support.   Initial results suggested that Misi has potential as a support for nZVI, however modifications were required to improve the adsorbance of nZVI onto Misi surface.   Calcination, activation, acid wash and iron oxyhydroxide coating were used as surface modifications for Misi. It was found that the two most important modifications for nZVI adsorption was calcination at either 400 or 600 $^\circ$C and acid washing in 5.6 M HCl.

Equipped with this knowledge, other silica and silicates were also used to adsorb nZVI. For pure silica surfaces, 3-APTES and 3-TPTMS ligands and pore enlarging methods of calcination of porogen and salt wash were also used. nZVI was not able to be fully adsorbed on pure silica surfaces. Four other silicates were examined: Rice husk ash, Western Australia silica fume, Mt Piper fly ash, and precipitated aluminium silicate. Of these, only Western Australia silica fume and precipitated aluminium silicate showed potential as nZVI support. Based on the SEM-EDS XRD data of all the silica and silicates, it could be tentatively concluded that nZVI requires an aluminium silicate surface for successful adsorption. Aluminium silicate surfaces typically has an exchangeable cation present, and this cation might play a part in nZVI adsorption.

The nZVI/Misi surface was then utilised to reduce nitrate. It was discovered that even though activation and FeOOH did not play a part in nZVI adsorption onto Misi surface, these two steps were important in reduction of nitrate, as the presence of activation and FeOOH increase the reduction of nitrate significantly within 60 minutes. The Misi-supported nZVI were also shown to be more stable in dispersion, and less agglomerated as shown in a sand column experiment.

Acknowledgements

over many conversation about music, food, and family and banter about my impatience and his sloth-like movements, we have bonded. Thank you very much for all your help with the technical bits, but most of all, thanks for being there for me and being my friend.

And there are my other friends: My Friday Night drinking buddies, consoling me over many things, bantering over too many bad jokes, putting up with loud and drunken me: Erin, Amira, Ash, Amy, Chriselle, Tomas, Mat, Sarah, Dan, Shaymal, Geoffry, Kathryn, Nicoló, Justinas, Nick, and Claire. Thanks mates!

The 7.30 am #17 Bus with Casey and the Brain Trust kept me going for a long time, and introduced me to one of my best friend Alex da Silva, whom I was glad to have to confide in and bitch with.

My best friend outside Uni, Nicky, kept me going and fueled me by getting me to go out and have lunches and shopping trips with her. You're my VVS A colour 2 ct diamond girl!

Erin and Geoffry have also proofread my thesis, so all the grammatical mistake are theirs (I wish). Thanks guys! Much appreciated!

I have also two other sources of sustenance: comedy and music. I have been known to email Matinee Idle during the summer break while I was writing my Thesis. Thanks Si and Phil for the humour and the bad music. On similar note, Chris (aka 'The Boy') introduced me to Elis James and John Robins show podcast, and I am proud to say that I am a retro-1-er, a 98-er and a PCD. The two broadly fine comedians picks me up when I am heading towards the darkness. Chris also introduced me to some fine indie UK bands, which become the soundtracks of my thesis: Courteneers, C-fish and the B-man, The Cribs, TLSP, Mystery Jets, Jamie T, Alt-J, aside from my three other mainstays: The Killers, DMB and Bastille.

When you are a working studying mother of two, there is no way you can do it without the help of friends and family. Pat and Hugh, my in-laws have been super helpful with picking up the boys and minding them over the breaks. Other families have also picked up our boys and entertain them every now and then: the Hunt, Heerdergen, and Ernst. My nannies/demi pair: Jodie, Leon, Lizzie, Rebecca, Oz, Nicole, Livia, and Maria. My ante-natal girls: Elle, Sarah, Jules, Em, Sharyn, Tara, Amy and Becs, for the wine nights and catch ups. Thank you to you all, I cannot do it without your help.

And to keep the best for last: my family. I am honoured to be the first person in my wide family to gain a PhD qualification. My Mum didn't finish junior high and Dad only finished high school. However, they instilled the love of education in me and even though they sometimes wonder when I will stop going to school, they are very proud and supportive of what I am doing. Thanks Mami and Papi. Yiwen started out as a homestay student, but now she is an integral part of the family. Thank you for helping out and making dinner and just being there with us.

My husband, Peter, always believed that I have the brain to do my PhD. He supported me throughout my 8 years of study with full confidence that I will finish it with flourish. Thank you love. To my boys James and George, thanks you for putting up with your busy mum, now you can have your mummy back!

Contents

List of Tables

List of Figures

List of Abbreviations and Acronyms

AAS   : Atomic absorption spectroscopy

AS   : Amino-functionalised silica sphere

BET   : Brunaeur-Emmett-Teller measurement

COMPO   : Composite image, contrast SEM image based on difference in atomic weight.

EDS   : Energy dispersion spectroscopy, based on characteristic X-Ray

gFe^0 : Granular zero-valent iron, typically sized in micrometers

IR   : Infrared spectroscopy

Misi   : Microsilica 600, a geothermal silica provided by Golden Bay Cement

nZVI   : Nano Zero-Valent Iron

PFA   : Mt Piper Fly Ash

ppm   : Parts per million (mg/kg)

RHA   : Rice Husk Ash

SEI   : Secondary Electron Image, SEM image showing morphology of sample.

SEM   : Scanning electron microscope

SS   : Synthetic silica sphere

TGA   : Thermogravimetric analysis

UV-Vis   : Ultraviolet-visible spectroscopy

WA   : Western Australia silica fume

XRD   : X-Ray powder Diffraction

List of Appendices

1 Introduction

1.1 Overview

Nano zero valent iron (nZVI) has been postulated as a useful material for environmental remediation over the past two decades. Its use for eliminating contaminants such as heavy metals, inorganic anions and organic pollutants has been well established. As with any new technology, concerns about nZVI safety in general use has been raised, especially with respect to eco-toxicity. Nano-sized materials are more reactive than their bulk material. Loose nano-sized material may cause unforeseen environmental issues such as bio-accumulation of nano-material in gills of aquatic animals. In this work, nZVI supported by various silicates and silica were synthesised to increase the bulk size of nZVI while maintaining its nano-size reactivity. These materials were then used to reduce nitrate, one of the major pollutants in New Zealand waterways. Based on previous work by the candidate, Microsilica 600 (**Misi**), a by-product of geothermal energy generation, was chosen for further study. Misi adsorbed nZVI more evenly compared to other sources of silicates. However, the distribution of nZVI on Misi was not optimal, and hence the main aim of this research was to modify the surface of silicates, especially Misi, to make them a better support for nZVI. Once these modifications were established, investigations were made to see whether these steps can be applied to both pure silica and other types of silicates to improve their ability to adsorb nZVI. The capabilities of the Misi-nZVI system to reduce nitrate under various conditions were also investigated. Finally, the ability of the support system to improve mobility in a soil-like environment was also investigated.

1.2 State of New Zealand environment

Dairy products are one of the major export commodities for New Zealand. As a percentage of gross domestic product (GDP), the dairy sector contributed 2-3% of GDP, equivalent to $5.3 billion in 2012, and accounted for up to 25% of cargo value exported from New Zealand ports ($11 billion in 2012) (Figure 1). The pay out from Fonterra, NZ's major dairy processor, increased from $4.46/kg of milk solid in 2006/2007 season to $7.76 in 2007/2008. This led to a rise in conversion of farm lands, mostly beef and sheep farms, to dairy farms. In 2007, dairy farms covered 1.9 million ha, approximately 13% of all farm land in New Zealand; in 2012 they

covered up to 2.4 million ha, or 17% of all farm land. The high value of the dairy industry is important for the New Zealand economy; however dairy farm conversion and intensification (increase of stocking rate) of the farms have major environmental impacts in the form of excess nutrient pollution in the waterways and increased water demand. Thus there is a need to reduce the negative impact of dairy farms while still supporting the growth of the dairy industry.
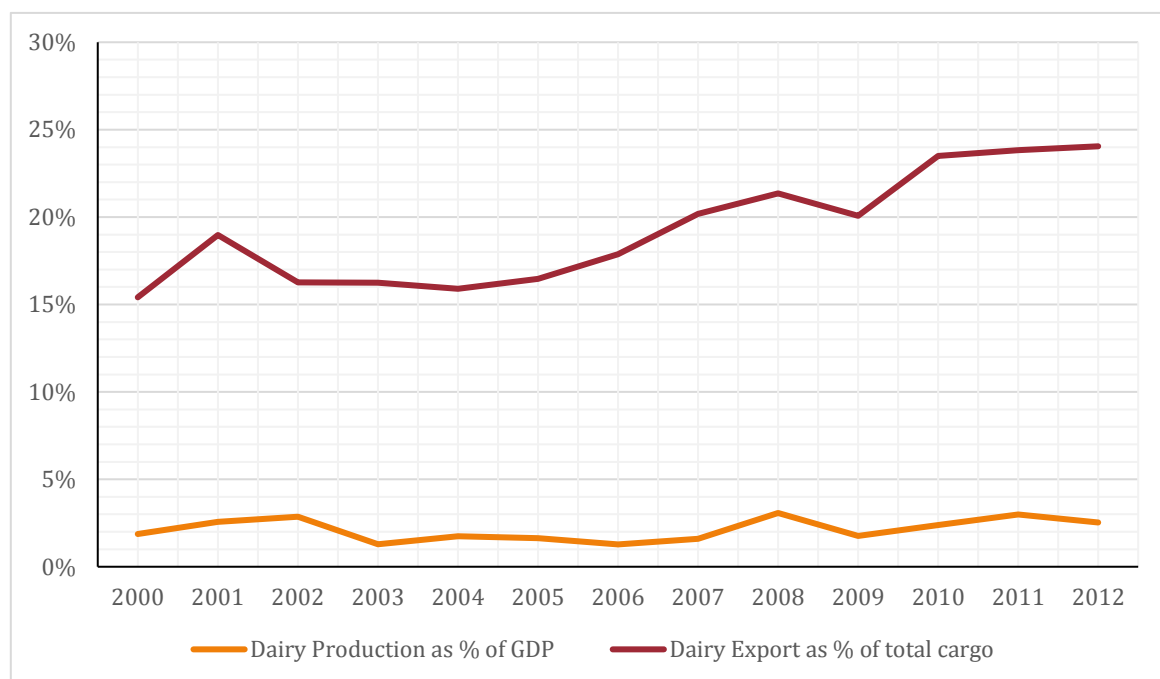
Figure 1.1. Value of NZ dairy industry as percentage of GDP and Cargo Export Value from year 2000-2012. Source: Statistics NZ

Dairy farms are one of the major users of nitrogen-based fertilisers. Even though dairy farms comprise of only 17% of all farming area in New Zealand, they consume more than half of all nitrogen-based fertilisers used in New Zealand. The main reason for this is that dairy farms have intensive grazing due to their high stocking rate (2.85 cattle per hectare, 104 kg of N-fertiliser per cattle), and thus these farms require more fertiliser to improve pasture growth and quality. As a comparison, beef and sheep farms, which occupy more than 60% of all farming areas, use less than 30% of the total nitrogen-based fertiliser used in New Zealand, or 23 kg of N-fertiliser per cattle-equivalent (Figure 1.2).

3
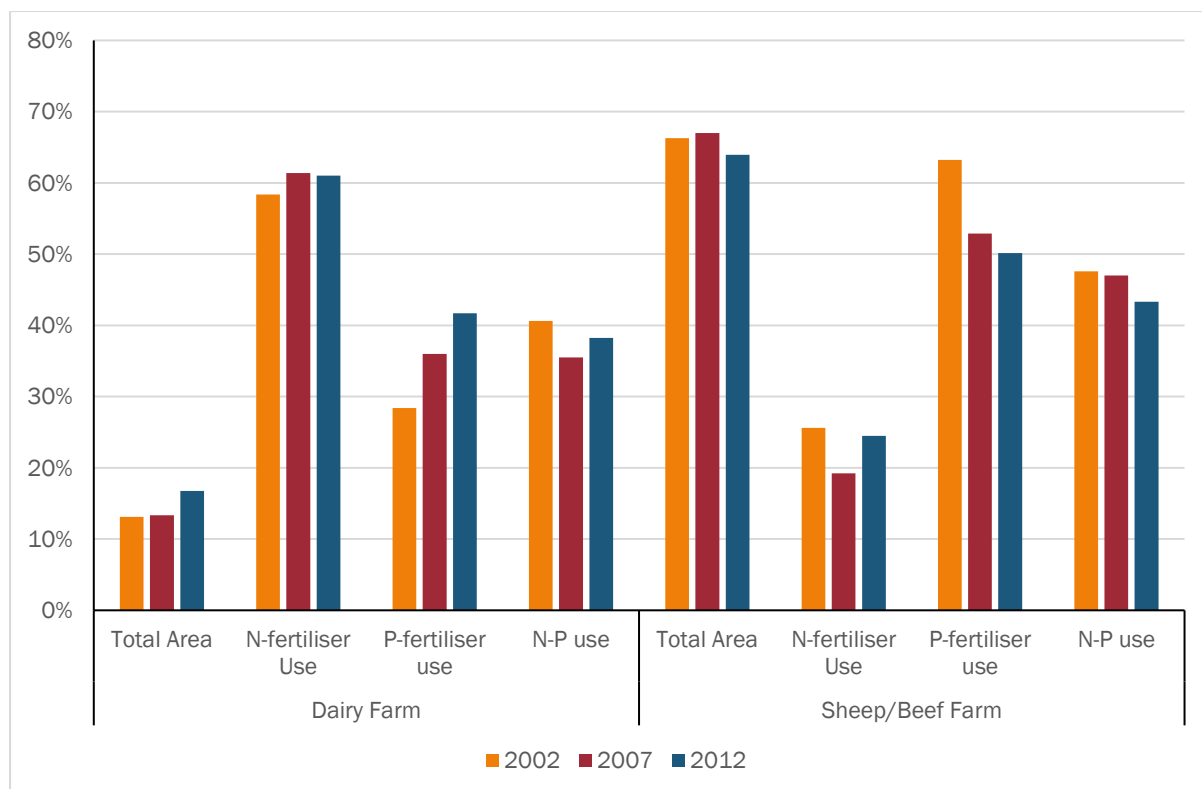
Figure 1.2. Comparison between dairy and beef/sheep farm in fertiliser usage. N-fertiliser: nitrogen based fertiliser, P-fertiliser, Phosphorous based, N-P, fertiliser that has both N and P. Source: Statistic NZ

Ideally, all of the fertiliser applied on farms would be utilised by plants and therefore leaching of the applied nutrients to the surrounding environment would not occur. Statistic New Zealand reported that on average, 108 kg/Ha of N-based fertiliser was applied in the Waikato region in the 2002 Agricultural census. In 2002-2003, Environment Waikato found that on average, 50 kg/Ha of N was leached from soil per year, and 80% of this was from dairy farms.[1] Over the same period it was found that 40% of farms had excessive levels of phosphorous. Furthermore, as cows' urine contains a high level of urea, it has been estimated that nitrogen loading in a dairy cow urine patch is in the region of 1000 kg N/Ha in areas of high stocking rate.[2,3] When grassland pastures are ploughed in winter, a large amount of bound nitrogen was lost due to mineralisation after ploughing, and hence more fertiliser was needed to be added for the next planting season.[4] At the current dairy farming practice of high stocking rate, it is inevitable that nitrogen as nitrate and phosphorous as phosphate will end up in the waterways.

4

Excess phosphate and nitrate in the waterways cause *eutrophication*, which is defined as "the process of increased organic enrichment of an ecosystem, generally through increased nutrient input".[5]   The excess nutrients fuel the growth of algae, cyanobacteria and nuisance weeds. The uncontrolled growth of cyanobacteria, commonly known as a toxic algae bloom, is dangerous due to both the biomass and the toxins they produce.[5] These toxins may cause injuries and mortalities in wild and farmed fish.   In humans and other mammals, damage is caused through contact, exposure and ingestion of contaminated water and consumption of shellfish that have ingested toxic algae.   The overgrowth of weeds also impairs native fish spawning through habitat alteration. When the algae and weeds die, the rotting masses reduce the amount of dissolved oxygen available in the waterways, which, in turn, reduces the number of fish and other aquatic animals.[7]

Excess nutrients in streams also accelerate terrestrial carbon (C) loss from the stream.[8] Terrestrial carbon is important in riverine food webs as it acts as food source for aquatic life. Excess nutrients not only encourage accumulation of carbon in weeds, but it also encourages mineralisation of organic carbon, which in turn releases carbon as CO_2 to the atmosphere.

1.2.1 Phosphorus

Phosphorus (P) is abundant in soil, but has limited bioavailability for uptake by plant roots.[9] A large portion of phosphorus (20 – 80%) is contained in soil microbial mass as DNA and phospholipids and other P-containing components. [10] Another dominant form of phosphorus in soils is insoluble/immobilised inorganic P, commonly formed when phosphates (PO_4^{3-}) are adsorbed on soil surface or precipitated ('fixed') by free Fe^{3+}, Al^{3+} or Ca^{2+} in the soil. Only a small amount (~0.1%) of total P is in a soluble form and bioavailable for plant uptake.[11] Due to this limited bioavailability, fertilisers containing phosphate are required by farms even though only 30% of these are bioavailable to plants as P is readily fixed in soil.[9]

Farms are not the only source of phosphorus in the environment. Untreated animal and sewage effluent, household detergents, wastewater from dairy factories, meatworks (abattoir/ slaughterhouses), pulp and paper plants are also considered significant point sources of phosphorus.[12]

5

Phosphorus enters waterways through erosion and/or flooding events. The effect of excess phosphorus in the waterways might not immediately be seen, due to a delay, which is dependent on the vulnerability of the system.[13] Ideally, total phosphorous in waterways should be less than 0.04 ppm.[14] Due to its propensity for precipitation and biological assimilation, phosphate is usually the limiting nutrient in the growth of algae and weeds in waterways. [15,16] If a lake or waterways is balanced nutritionally, phosphate remains in the sediment layer, bound by Fe^{3+}.[17] However, when the waterways become eutrophic, the bottom water often becomes anoxic, and the pH increases. This will reduce Fe^{3+} to Fe^{2+} resulting in the release of phosphorus back into the water column as soluble phosphate. This in turns fuels further eutrophication (Figure 1.3).
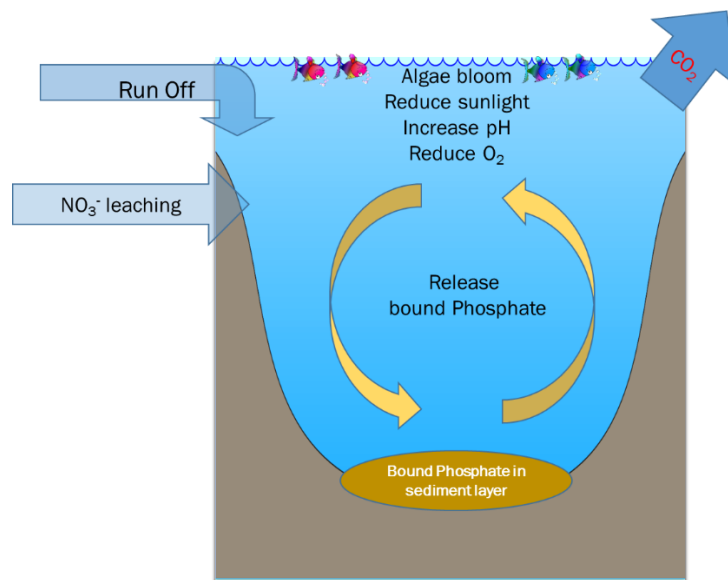
Figure 1.3. Eutrophication cycle.

In the developed world, eutrophication is mainly caused by fertiliser runoff from agriculture and urban landscaping, and therefore land and soil management are important.[13,19] Understanding the phosphorus cycle is the first step, ensuring the amount added as fertiliser to soil is what will be utilised.[20] Effort has also been made to utilise soil microbes that transform immobilised phosphorus into bioavailable soluble phosphorus and hence reduce the amount of phosphorus fertiliser required.[9]

Another method of managing phosphate pollution is by stopping the erosion of P-laden soils into waterways. Riparian strips are a 5 - 30 m band of trees and bushes planted along a river

that act as barrier for erosion and prevents cattle from getting into waterways. As riparian strips reduce erosion incidents, they are pivotal in reducing the amount of soil-adsorbed and insoluble phosphate entering the waterways. Furthermore, riparian strips are helpful in reducing the amount of pathogens, such as *E.coli*, entering waterways, and provides shade for aquatic life.[21]

Chemically, phosphates are very stable as they are not readily reduced. They can be removed from wastewater by adsorption onto a variety of different materials, including alumina (Al_2O_3),[22] zeolite,[23–25] fly ash,[26,27] and specialist products including NCaSil (nano-structured calcium silicate), which was developed at Victoria University of Wellington.[28–30] Phosphate can also be sequestered by precipitating and concentrating soluble phosphate in wastewater/effluent by utilising the redox chemistry of iron to bind and recover phosphate.[31]

1.2.2 Nitrate

Nitrogen is vital to all life. Plants and microorganisms uptake nitrogen as nitrate (NO_3^-) and ammonium (NH_4^+) ions. As mentioned previously, excess nitrate in waterways accelerates eutrophication. Nitrate is also toxic to fish at concentrations as low as 0.8 ppm nitrogen as nitrate (NO_3^--N).[14] Excess nitrate in drinking water is also one of the co-factors in methemoglobinemia, or blue-baby syndrome, in infants under four months old. This occurs when water containing high nitrate concentration (>10 ppm) is used to make their formula. The ingested nitrate is reduced into nitrite (NO_2^-), which can irreversibly oxidise Hemoglobin to form MetHb (methemoglobulin) (Figure 1.4). As MetHb contains Fe^{3+}, it is unable to bind to dioxygen (O_2). Thus methemoglobinemia is characterised by cyanosis (blue-tinged skin), stupor and cerebral anoxia. Healthy humans have less than 2% of total hemoglobin circulating as MetHb, but in patients with methemoglobinemia, >10% of total hemoglobin is MetHb. Newborn infants are more susceptible to MetHb formation as fetal hemoglobin is more readily oxidised than adult hemoglobin.[32]
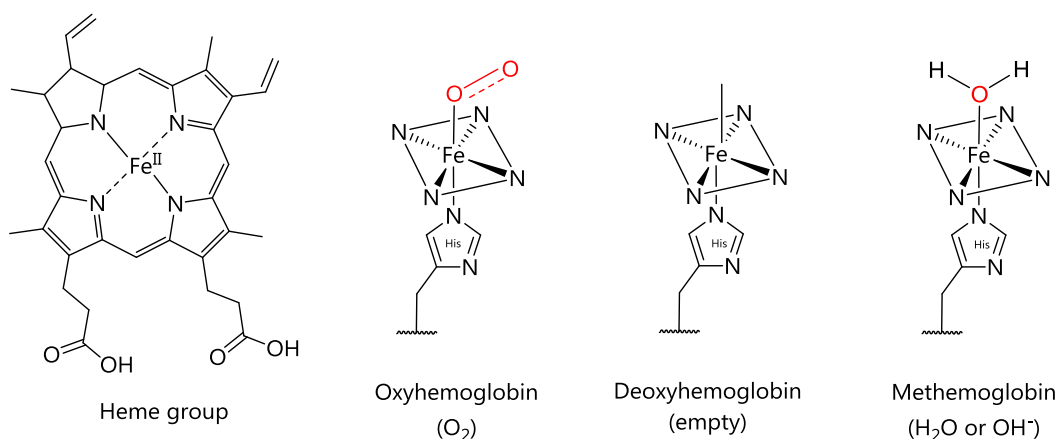
Figure 1.4. Heme group and various state of hemoglobin

The maximum accepted value of nitrate in NZ drinking water is 50 mg/L as nitrate (11 ppm NO_3^--N),[33] but higher levels have been found in contaminated ground water. Ammonia/ammonium (NH_3/NH_4^+) are also considered as pollutants, in addition to nitrite. Nitrite is carcinogenic in large dosages and, as previously discussed, is implicated in methemoglobinemia. The acceptable value of nitrite in NZ drinking water is 3 mg/L (or 0.9 ppm NO_2^- -N).[34] Ammonia is also toxic to aquatic life with the maximum acceptable value in waterways of 0.88 ppm NH_3-N.[14] Despite its toxicity, the presence of ammonia in soil is preferred compared to nitrate. Ammonia can be retained in soil due to its positive charge allowing for the formation of hydrogen bonds to the soil structure.[35] In contrast, nitrates have a highly delocalised negative charge that will not interact with the negatively charged surface of soils thus they readily leach.

Attempts to mitigate nitrate pollution can be classified into four major themes: on-farm usage reduction, nitrate sequestration, and biological and non-biological reduction of nitrate.

1.2.2.1 On-Farm usage/leaching reduction

Leaching reduction

In July 2013, the Sustainable Dairying Water Accord was launched, which set out good farming management practices to help keep New Zealand's freshwater system clean.[36] The accord targeted five key areas: riparian management, nutrient management, effluent management,

water use management and conversions. The first three areas related to reducing excess nutrients leaching to waterways.

Riparian management includes excluding cattle from waterways by fencing and planting riparian strips where they would provide water quality benefit. Nutrient management begins with collecting nutrient management data and inputting this data through computer programs such as OVERSEER®, which is a nutrient management computer model developed by AgResearch in conjunction with Ministry of Primary Industry and FANZ.[37] With OVERSEER®, nutrients can be budgeted and the right amount can be applied to maintain the soil's current fertility level. Another approach has been developed by Grazing System Limited where the aim is not just nutrient management but also optimising stocking rate based on the farm condition so that extra feeding and nutrients are minimised and, by corollary, nutrient leaching is also minimised.[38] AgResearch is also conducting experimental research to see whether different types of pasture species (e.g. chicory, plantain, ryegrass) can reduce nitrate leaching.[39]

For effluent management, the installation of effluent ponds is essential in reducing the amount of effluent going to waterways. Furthermore, the ponds allow effluent to be stored until the situation is right for spraying effluent onto the pastures. Careful effluent spraying both reduces the amount of fertiliser needed and the amount of nutrients leaching into waterways.

Nitrification Inhibitor

Another on-farm method that has been was tested was the use of nitrification inhibitor chemicals such as DCD (dicyandiamide). Nitrification inhibitors reduce the amount of ammonium oxidised by microbes into nitrite and nitrate. By spraying urine patches with DCD, nitrogen becomes trapped as ammonium and thus retained by the soil.[40] Unfortunately, when cattle ingest grass that has been sprayed with DCD, enough DCD is ingested such as that it can be found in trace amounts in milk. As there has not been any research on the effect of DCD on human health, its use was discontinued in 2013.[41]

1.2.2.2 Nitrate sequestration

Nitrate is a very stable ion, and has a very limited chemical reactivity. Nitrate pollution can be mitigated by sequestering nitrate, and creating a more concentrated brine. This method is

9

typically employed in waste water treatment plants, low level nuclear waste sites, and drinking water plants. Nitrate ions can be sequestered using a physical adsorber, such as nano-alumina,[42] bamboo charcoal,[43] nanocomposite of chitosan, zeolite and ZrO_2,[44] HCl-activated sepiolites and activated carbon,[45] and ion exchange resin.[46,47] The surface properties of the adsorbent material attract nitrate anions and collect the anions on the surface. Nitrate ions can be desorbed and the adsorber regenerated.

Aside from absorption, nitrate ions can also be selectively removed using reverse osmosis[48], and electrodialysis.[49,50] In reverse osmosis, the nitrate-rich water is pushed through a semi-permeable membrane, which keeps ions and other solutes on the pressurised side and allows purer water to continue to the unpressurised side. The size of the pores and pressure determines which molecules or ions are separated out. Electrodialysis removes ionic components through an ion exchange membrane under an electric field, where the voltage applied determines which ions are attracted to the ion exchange membrane.[50] Electrodialysis thus removes both contaminant ions and reduces water hardness and salinity. The major problems with reverse osmosis and electrodialysis are that they are expensive and produce concentrated waste brines that need to be treated separately.

1.2.2.3 Biological reduction of nitrate

The goal of nitrate reduction is to chemically reduce nitrate to less harmful substances, ideally dinitrogen (N_2) gas. In a natural nitrogen cycle, several types of microbes act as nature's denitrification system in soil, groundwater or freshwater systems.[51] Microbial denitrification occurs when bacteria use nitrate instead of oxygen as their terminal electron acceptor during the respiratory process, with N_2 as the final product. A typical reduction occurs in several steps (eq. 1).

$$NO_3^- \longrightarrow NO_2^- \longrightarrow NO_{(g)} \longrightarrow N_2O_{(g)} \longrightarrow N_{2(g)} \qquad (1)$$
$$+5 \qquad\quad +3 \qquad\quad +2 \qquad\quad +1 \qquad\quad 0$$
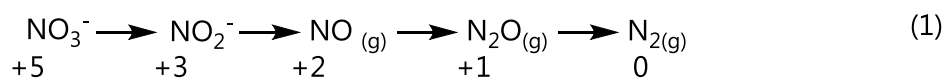
Bioreactors utilise microbial denitrification in reducing nitrate. The main requirement for microbial denitrification are suitable carbon and energy sources. As these are sometimes

lacking in soil or groundwater, a bioreactor's function is to provide carbon and energy for the microbes.

Bioreactors can be placed in the aquifer as injection wells. These are trenches where contaminated water can flow through or on top of an aquifer where water is pumped from and injected back to after the treatment. A heterotrophic system uses organic compounds such as methanol,[52] newspaper,[53] cotton,[54] or woodchips[55–57] as the source of carbon. An autotrophic system uses inorganic carbon, such as carbonates, as the source of carbon and inorganic substrates such as hydrogen gas and various reduced-sulfur compounds as the energy source.[51]

If the efficiency of the bioreactor is not optimal, then N_2O, a potent greenhouse gas, is released instead of N_2. This becomes more common as bioreactors age.[55,57] Denitrification processes also produce biomass that has to be filtered and flushed out periodically to maintain the bioreactor. Denitrified water often still contains microbes and residual organic carbon and thus, intensive post-treatment is sometimes required.[58]

1.2.2.4 Non-biological reduction of nitrate

Nitrate can also be directly reduced either using chemicals or by an external source of energy.[59] There are a number of chemical reductants that can be used. These can be broadly categorised as inorganic and organic reductants, active metals, and a mixture of metal/organic or inorganic/organic reductants. Aside from using a chemical reductant, a number of external energy sources can also be used to reduce nitrate including photochemical, electrochemical and thermal energy.

Chemical Reduction

Based on standard reduction potentials (Table 1.1),[59,60] any reductant that has reduction potential of at least 0.86 V should be able to reduce nitrate to ammonium under acidic conditions (entry 1). Nitrate can be reduced to N_2 readily in either acidic or basic conditions (entry 2 and 4), though the reduction potential is more favourable in acidic condition. Nitrate can only be reduced by ammonia in basic conditions under high pressure and temperature despite the favourable reduction potential (entry 4 and 7).[61]

Table 1.1. *Redox couple and E°of selected N compounds in acidic and basic conditions.*

Entry	Redox couple	Condition	E° (V)
1	NO_3^-/NH_4^+	acidic	0.87
2	NO_3^-/N_2	acidic	1.25
3	NO_3^-/NO_2-	basic	0.49
4	NO_3^-/N_2	basic	0.43
5	NO_3^-/NH_3	basic	-0.01
6	NO_2^-/N_2	basic	1.45
7	N_2/NH_3	basic	0.27

Other inorganic reductants such as sodium borohydride ($NaBH_4$), or organic reductants such as formic acid had also been used to reduce nitrate with some success. For instance, H_2 gas had been used as a reductant, although the presence of a catalyst was required. [62,63]

Sodium borohydride could only reduce nitrate in the presence of Cu/Zn or Cu^{2+} under basic condition at 65 °C, with nitrite as the initial product before turning into ammonia. [59] Formic acid could be used to reduce nitrate in concentrated sulfuric acid (eq. 2). As the reaction was highly exothermic, it was potentially hazardous.[64,65] Formic acid had also been used in conjunction with either platinum group metals[66] or nitrite[67] to reduce nitric acid in nuclear waste. Without a catalyst, these reactions required an input of energy by boiling the nitric acid, and hence this was not very practical for environmental remediation. However, when formic acid was used with either Pd^0/Sn^0 or Pd^0/Si as catalyst, the nitrate reduction could proceed at room temperature and pressure, with the final product a mixture of ammonia and N_2.[68]

$$HCOOH + NO_3^- + H^+ \longrightarrow HNO_2 + CO_2 + H_2O \qquad (2)$$

Aside from iron, which will be discussed at length in the next section, other metallic elements and amalgams had also been used to reduce nitrate. Amalgamated Cd/$HgCl_2$, [69] and spongy precipitated Cd[70] had been used to reduce nitrate to nitrite. These reductants were not useful for water treatment due to the toxicity of cadmium and mercury.

Catalysts such as bimetallic Pd/Cu could be used to reduce nitrate in the presence of H_2 gas as the reductant. (eq. 3-5).[62,63]   Although these catalysts were able to reduce nitrate to dinitrogen, the conversion was only 80%, with the product mixture consisting of 20% unreduced NO_3^- -N, 40% NH_4^+-N and 40% N_2. When Pd/Cu was mounted on γ-Al_2O_3 and coupled with ion-exchange resin, the conversion to ammonia was 100% within 2 hours.

$$2NO_3^- + 5H_{2(g)} \xrightarrow{\text{Cat.}} N_{2(g)} + 4H_2O + 2OH^- \qquad (3)$$

$$NO_3^- + H_{2(g)} \xrightarrow{\text{Cat.}} NO_2^- + H_2O \qquad (4)$$

$$NO_3^- + 4H_{2(g)} \xrightarrow{\text{Cat.}} NH_4^+ + H_2O + 2OH^- \qquad (5)$$
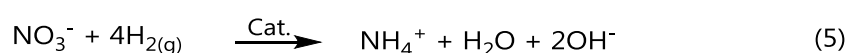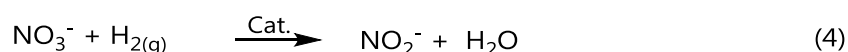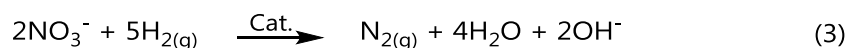
Photocatalytic reduction

Photocatalytic reduction of nitrate is promising as it is able reduce a large percentage of nitrate to N_2 rather than ammonia. TiO_2 based materials had been used to reduce nitrate photocatalytically. For example, catalytic Pd and Cu had been impregnated on TiO_2 to reduce nitrate.[71] In these experiments, formic acid, ethanol, methanol or humic acid were used as hole scavengers, H_2 as the reductant and CO_2 as the buffer.   Hole scavengers are molecules sacrificed as electron donors to react with the generated holes (h^+) to stop recombination of h^+ with the generated electron. In this system 95% of nitrate were reduced to ammonia and N_2 in a 1:1 ratio.

A combination of TiO_2/Pt and non-photocatalyst SnPd/Al_2O_3 with glucose as the hole scavenger had also been used with mixed results.[72] The conversion of nitrate to either N_2 or ammonia was very low (23%), but selectivity for N_2 was much higher at 75%. Furthermore, no extra H_2 was required, as H_2 was produced by the cleavage of water by Pd/TiO_2 under light irradiation. The hydrogen gas produced was then utilised by the SnPd/Al_2O_3 catalyst to reduce nitrate. This low conversion was due to poisoning of the photocatalyst by sulfate and silicate ions that were present in groundwater sample used.

TiO_2 had also been coupled with Fe^0 and UV radiation with the purpose of increasing conversion of nitrate to N_2.[73]   The coupled system could remove 98% of nitrate compared to 100% by Fe^0 alone within 30 minutes, but it increased selectivity of N_2 from 10% in Fe^0 system to 45% in TiO_2/Fe^0 system with a 1:10 ratio of TiO_2:Fe^0.

Aside from TiO_2, $LiNbO_3$ had also been used as a photocatalyst to reduce nitrate with formic acid, KI and humic acid as the hole scavengers and H_2 as the reductant. The conversion achieved was 98.4%, with 95.8% of nitrate converted to N_2.[74]

Electrochemical reduction

While electrodialysis only separated nitrate ions from other compounds in water, electrochemical reduction reduced nitrate into nitrite, ammonium, or dinitrogen. In a typical nitrate-reduction electrochemical cell, water was electrolysed, evolving hydrogen and oxygen (eq. 6 - 7).[75] The electrons released from the cathode reduces nitrate into ammonia and nitrite (eq. 8 - 10). Sodium bicarbonate was added to counter the alkalinity of the electrolyte as the reaction progresses (eq. 11). Dinitrogen was produced while chloride from NaCl electrolyte was oxidised to chlorine (eq. 12). The reaction between chlorine and water formed hypochlorite (eq. 13) that lead to the oxidation of nitrite and ammonium back to nitrate and dinitrogen, respectively (eq. 14 - 15).[76]

$$2H_2O + 2e^- \longrightarrow H_2 + 2OH^- \tag{6}$$

$$4OH^- \longrightarrow O_2 + 2H_2O + 4e^- \tag{7}$$

$$NO_3^- + H_2O + 2e^- \longrightarrow NO_2^- + 2OH^- \tag{8}$$

$$NO_2^- + 5H_2O + 6e^- \longrightarrow NH_3 + 7OH^- \tag{9}$$

$$NO_3^- + 2H_2O \longrightarrow NH_3 + 2O_2 + OH^- \tag{10}$$

$$NO_3^- + HCO_3^- + H_2O \longrightarrow NH_3 + 2O_2 + CO_3^{2-} \tag{11}$$

$$2Cl^- \longrightarrow Cl_2 + 2e^- \tag{12}$$

$$Cl_2 + H_2O \longrightarrow HOCl + H^+ + Cl^- \tag{13}$$

$$NO_2^- + HOCl \longrightarrow NO_3^- + Cl^- + H_2O \tag{14}$$

$$2NH_4^+ + 2HOCl \longrightarrow N_2 + 5H^+ + 3Cl^- + 3H_2O \tag{15}$$
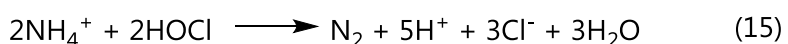
There are six parameters that influence the effectiveness of the electrochemical cell: electrode material, current input, pH, conductivity, concentration of NaCl, and initial concentration of nitrate and nitrite. From these six parameters, the electrode material has been the most widely researched. Various anodes have been used, for example Pt/Ti,[77] diamond and Ti. For

cathodes, Cu/Zn,[76] TiO$_2$, and Fe had been used. The best combination to date was the Ti/IrO$_2$-Pt anode coupled with a Cu/Zn cathode that can remove up to 90.3% nitrate within 5 hours.[78]

The mechanism of nitrate reduction by a single electrode were still unclear. In a study using Pt/Rh electrode, it was discovered that applying different potential yielded different product.[79] Potential between 0.3 – 0.4 V cleaved oxygen atoms off nitrate forming NO, and then coupled with another N to form N$_2$O. At potential between 0 – 0.2 V however only NH$_4^+$ was formed. When the potential applied was below 0, H$^+$ started to evolve from water, and various product were formed: N$_2$H$_2$, NH$_2$OH, N$_2$, NH$_4^+$, N$_2$O, NO, suggesting various different pathways.

Thermal reduction

In the absence of any catalyst, when nitrate was heated to temperature between 650°-750°C, N$_2$ and O$_2$ gas were produced, while at higher temperatures, a mixture of N$_2$ and NO$_x$ gasses were formed.[80] Thermal reduction could be used in conjunction with other reductants to lower the activation temperature. For example, the addition of formic acid reduced the required temperature to 350 °C, converting almost all nitrate to N$_2$.[61]

1.3 Iron and nano-particles for environmental remediation

1.3.1 Iron in environmental remediation

Contaminated groundwater was traditionally treated using a pump-and-treat method. In this method, contaminated water was pumped to the surface (*ex situ*) to be treated, before being injected back to the aquifer or discharged into a stream or waterways (Figure 1.5).[81] Pump-and-treat methods were expensive in cost and time. In 2001, US EPA calculated that a pump-and-treat site, on average, cost US\$ 767,000 per site annually, and USD\$ 9.4 million to fully clean a site. The treatment of the contaminated water also created a lot of toxic waste, and in most cases, the remediation success rate was very low.[82]

A newer and more successful technique is the use of a permeable reactive barrier (PRB, Figure 1.5).[83] PRB is an engineered zone of reactive material that extends below the water table.[84] PRB is designed to intercept and treat contaminated groundwater as it flows naturally through the aquifer (*in situ*). The contaminants were either degraded or adsorbed by the reactive

barrier. As of 2004, around 60% of all PRB worldwide used some form of iron as the reactive barrier, as elemental iron is effective in degrading various contaminants. Typical PRBs cost around $60-$245 per ton of material treated.
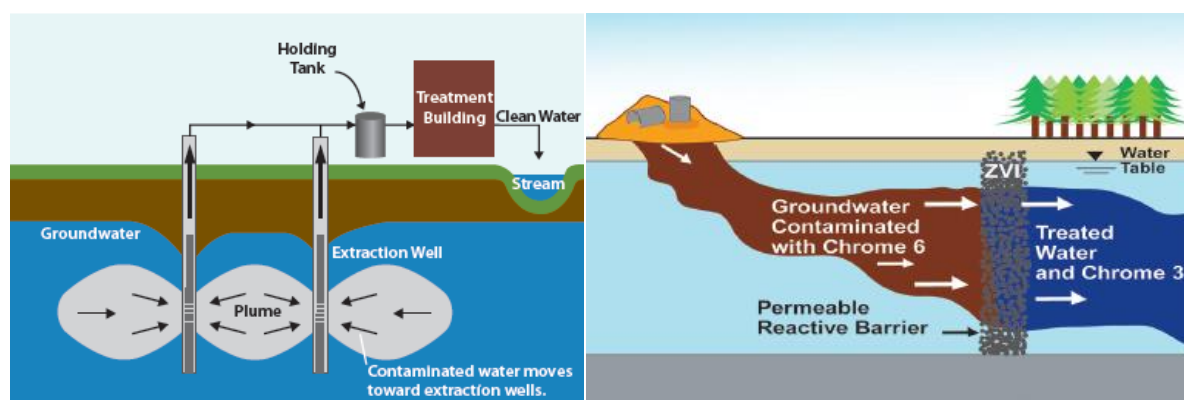
Figure 1.5. Illustration of ex-situ *pump-and-treat method (left) and* in-situ *permeable reactive barrier (right). Images courtesy of CLU-IN, US-EPA.*[85,86]

Table 1.2. Major iron oxides and oxyhydroxides.[87,88]

Type	Formula	Mineral	Colour	Magnetism	Structure
Oxy-hyrdroxides	α-FeOOH	Goethite	blackish brown, yellow in thin section	A	Orthorhombic
	β-FeOOH	Akaganeite	Yellowish brown	A	Monoclinic
	γ-FeOOH	Lepidocrocite	Ruby red to reddish brown	A	Orthorhombic
	δ-FeOOH	Feroxyhyte	Brown, yellow brown	F	Hexagonal
Oxides	$Fe_5HO_8 \cdot H_2O$	Ferrihydrite	Yellow brown	A	Hexagonal
	α-Fe_2O_3	Hematite	Steel grey	F (w)	Hexagonal
	β-Fe_2O_3	Maghemite	Brown, bluish black	F	Cubic
	Fe_3O_4	Magnetite	Black	F	cubic
A: Antiferromagnetism. F: Ferrimagnetism (w): weakly					

The iron by-product in these PRBs is typically an iron oxide. The iron used is typically Fe^0; however as Fe^0 reacts readily with O_2 and H_2O, an oxide coating is formed on top of the zero valent iron. Table 1.2 listed the 8 major oxides and oxide hydroxides of iron. These minerals

can change from one form to another depending on temperature, pressure, pH and oxidative or reductive environment. The oxide coating for ZVI is typically hematite and magnetite.

One of the most persistent contaminants in the environment is halogenated hydrocarbons, such as 1,2-dibromo-3-chloropropane (DBCP). Granular zero valent iron (gFe^0) of various sizes were used to reduce DBCP with and without the presence of nitrate ions.[89] It was found that the smaller sized iron grains (3.5 μm) were faster in reducing DBCP compared to the larger ones (11.7 μm), at 0.39 and 0.22 min^{-1} respectively (pseudo first order rate). When nitrate was present in the system, the nitrate was reduced prior to DBCP reduction. Nitrate (10 ppm) can be removed by medium sized iron grains (3.5 - 11.7 μm) in 14 minutes. gFe^0 performed comparably to reductants such as H_2 with Pt catalyst which reduced DBCP at 0.36 μM/min. However it was more sensitive to the influence of interfering ions in groundwater compared to H_2/Pt. As granular iron did not require an external H_2 source, it was more suitable for *in-situ* remediation.

In acidic mine wastewater, granular zero valent iron (gFe^0; 0.3 - 2.36 mm and <0.150 mm) had also been used to treat metals such as Al, Hg, Cd, Cu, Mn, Ni, and Zn, and semimetals such as As.[90] In low pH (2.5), gFe^0 was transformed into ferrihydrite and green rusts. These iron oxides neutralised the acidity of the solution while providing adsorption surfaces for most of the metals listed above except for Mn as the final pH (6.5) was not enough to precipitate Mn as its hydroxide.

When gFe^0 was placed in a flow-through column and coupled with iron reducing bacteria, the amount of tetrachloroethene (TCE) removed increased from 50 – 70% (only gFe^0) to 80% (gFe^0/bacteria).[83] Additionally, the coupled system also enhanced nitrate removal from 15 to 80%. At the same time, the coupled system reduced Cr^{6+} to Cr^{3+}, which was not achieved by gFe^0. The bacteria, *Shewanella algae* BRY, solvated the passive iron oxide layer formed as the reaction progresses, thus making the surface active for longer period of time.

Granular iron (with α-Fe_2O_3, γ-Fe_2O_3 and Fe_3O_4 layer) was also used to reduce TCE in the presence of nitrate. It was found that nitrate hinders the reduction of TCE by preventing the removal of protective high valent species such as Fe_2O_3 and FeOOH.[91] The efficiency of granular iron in reducing nitrate (22 ppm) in the presence of TCE was very low (23%) after 13

17

hours, and the reduction product was ammonia. Only 40% of TCE was reduced, with the end product acetylene instead of the desired ethene and ethane.

Reduction of nitrate by gFe^0 requires acidic solution, with pH 2-3 being the optimal range, and ammonium as the reduction product.[92–94] The ratio of $Fe^0:NO_3^-$- N required was related to the grain size of Fe^0 (Table 1.3). Larger Fe^0 grain size necessitated more Fe for the reaction. For example with grain size of 0.5 mm, 0.8 - 2 g of Fe^0 was required for each ppm of nitrate. [92,93] With grain size of around 6 - 10 μm, 0.5 g of Fe^0 was enough to treat 10 ppm of nitrate.[94] Nitrate could be reduced by granular iron, but it required a very low pH and the amount of iron required was relatively high.

Table 1.3. Nitrate reduction by granular iron.

Iron size	Fe^0: NO_3^--N ratio	[NO_3^- -N]	Variables investigated	Results
>0.5mm[92]	2g/1 ppm	20 ppm	Organic/inorganic Acid	t½ ranges from 7.59 ± 0.23 h (HCl) to 250 ± 2.8 h (H_3PO_4)
~0.5 mm[93]	0.8 g/1 ppm	30 ppm	Low pH	100% reduction at 20 mins (pH 2), 25 mins (pH 3), pH> 3 not completed within 45 mins
6-10 μm[94]	0.5g/10 ppm	11.3-113 ppm	Effect of pH control	pH control required or no reaction after 1 minutes. At pH2, 95% removal at 30 mins

While Fe^0 was used mostly as a reductant and adsorbent, ferrous ions had been used as an oxidant in Fenton-like reactions with hydrogen peroxide to provide hydroxyl radicals. The first step of the reaction was chain initiation (eq. 16), followed by chain termination (eq. 17).[95] The reaction did not stop there however, as the newly formed ferric ions can catalyse the breakdown of hydrogen peroxide into water and oxygen through several steps (eq. 18 - 22).

$$Fe^{2+} + H_2O_2 \longrightarrow Fe^{3+} + OH^{\bullet} + OH^- \qquad (16)$$

$$OH^{\bullet} + Fe^{2+} \longrightarrow OH^- + Fe^{3+} \qquad (17)$$

$$Fe^{3+} + H_2O_2 \longrightarrow Fe^{2+}\text{-}OOH + H^+ \qquad (18)$$

$$Fe\text{-}OOH^{2+} \longrightarrow HO_2^{\bullet} + Fe^{2+} \qquad (19)$$

$$Fe^{2+} + HO_2^{\bullet} \longrightarrow Fe^{3+} + HO_2^- \qquad (20)$$

$$Fe^{3+} + HO_2^{\bullet} \longrightarrow Fe^{2+} + O_2 + H^+ \qquad (21)$$

$$OH^{\bullet} + H_2O_2 \longrightarrow H_2O + HO_2^{\bullet} \qquad (22)$$
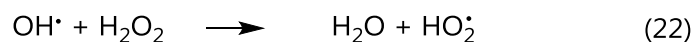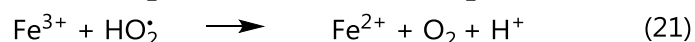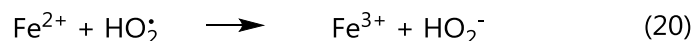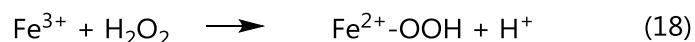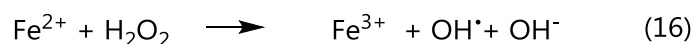
As an oxidant, ferrous iron were mostly used to decompose organic compounds such as phenols,[96] tetracycline hydrochloride,[97] various dyes such as methylene blue,[98] and non-organic compounds such as ammonia.[99] The low pH requirement (<4), and the volatility of a high concentration of peroxide (>40%) when H_2O_2 was not generated *in situ* limit the use of Fenton chemistry for *in-situ* environmental remediation.

1.3.2 Nano-sized particles

Nanotechnology is the science and engineering of materials on the nano scale (10^{-9} m).[52] Nanoparticles are defined as particles being below 100 nm in at least one dimension although they can be of any shape.[100,101] Nanoparticles can be synthetically made, but they are also naturally occurring. Soot, a product of burning carbon, is an example of naturally occurring nanoparticles.

Nanoparticles have unique properties due to their surface area to volume ratio. For example, a cube with a volume of 1 cm^3 (1 cm x 1 cm x 1 cm), has a surface area of 6 cm^2 (6 of 1 cm x 1 cm) area. When each side is divided by two, 8 (2^3) new cubes form (Figure 1.6). The volume remains the same, but the surface area is now 12 cm^2 (8 x 6 of 0.5 cm x 0.5 cm). When the original cube is divided by 100 on each sides, 1 million new cubes of 1 μm^3 form with a total surface area of 600 cm^2 (1,000,000 x 6 of 0.01 cm x 0.01 cm). Nano cubes of 50 nm divided from the same 1 cm^3 cube have a total surface area of 1,200,000 cm^3.
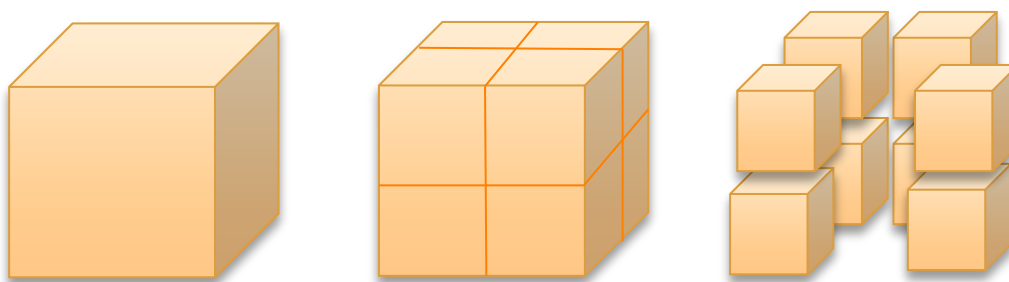
Figure 1.6. How surface area is related to volume.

The implications of the increased surface area associated with nanoparticles are two-fold. Firstly, the particles are now relatively more reactive as more reaction or impact sites are available. Additionally, the particles do not behave as atoms or bulk materials as their total surface area is similar to their total interior volume. This increased ratio between surface area and total interior volume changes the properties of the materials. For example, in its bulk form, gold has a metallic lustre with golden colour, gold ions solution (such as $AuCl_3$) are yellow in colour, whilst the colour of gold nanoparticle can be tuned to from pink to grey.[102,103]

Nanoparticles had been used in a wide variety of applications, including creating superhydrophobic materials,[104] as electrodes for the electroanalysis of ascorbic acid,[105] hydrogen peroxide,[106] and hydrazine[107], as biosensors for detecting bacterial infections,[108] acetaminophen,[109] pesticides,[110] and enzymatic activities.[111] In the renewable energy sector, nanoparticles had been utilised for capturing solar energy,[112–116] storing energy,[117,118] and splitting water.[119,120] Magnetic nanoparticles had also been developed to identify lymph nodes,[121] diagnose tumours,[122,123] and as anti-cancer agents.[124,125] In environmental remediation, nanoparticles had been used either as adsorbent, reductant, or oxidant of various pollutants. Nanoalumina (Al_2O_3) adsorbed arsenic,[126] heavy metal ions[127] and nitrate.[42] Nanosilver (Ag) has very strong antimicrobial activity and therefore can be used to disinfect water and as an antifouling agent.[128–130] A combination of TiO_2/Au nanoparticles had been successfully used to degrade SO_2.[131]

20

1.3.3 Scope of nZVI

When nano zero valent iron was synthesised, the scope of usage for environmental remediation widened. Nano-sized zero valent iron (nZVI) was able to increase pollutant removal rates at lower dosages and control the release of toxic intermediates due to the extra reactivity of nZVI. [132] nZVI can be synthesised through either physical or chemical methods.[133] Physical methods involve ball-milling, condensation or evaporation techniques. In ball-milling, larger particles are ground down to nano-sized particles.[134,135] Condensation techniques involve laser vaporization,[136] and gas-phase synthesis.[137] Chemical methods revolve around reducing iron precursors, usually ferrous or ferric salts, into elemental iron. The most common reductant used is sodium or potassium borohydride (eq. 23 - 24),[138,139] although polyphenols from various leaves, such as those present on green tea, were also able to reduce ferric or ferrous ions to nZVI.[140–144]

$$Fe^{2+}_{(aq)} + 2BH_4^-{}_{(aq)} + 6H_2O \longrightarrow Fe_{(s)} + 2B(OH)_{3aq)} + 7H_{2(g)} \qquad (23)$$

$$2Fe^{3+}_{(aq)} + 6BH_4^-{}_{(aq)} + 18H_2O \longrightarrow 2Fe_{(s)} + 6B(OH)_{3aq)} + 21H_{2\,(g)} \qquad (24)$$

nZVI is a mild reductant ($E^0 = -0.44$ V). In water, it undergoes a redox reaction with dissolved oxygen to form ferrous (Fe^{2+}) and ferric (Fe^{3+}) ions in both acidic (eq. 25 - 26) and neutral (eq. 27 - 28) conditions.[145]

$$2Fe^0_{\,(s)} + 4H^+_{\,(aq)} + O_{2\,(aq)} \longrightarrow 2Fe^{2+} + 2H_2O \qquad (25)$$

$$2Fe^{2+} + 2H^+_{(aq)} + {}^1\!/_2O_{2\,(aq)} \longrightarrow 2Fe^{3+} + H_2O \qquad (26)$$

$$Fe^0_{(s)} + 2H_2O_{\,(l)} \longrightarrow Fe^{2+} + H_{2\,(g)} + 2OH^-_{(aq)} \qquad (27)$$

$$2Fe^{2+} + 2H_2O_{\,(l)} \longrightarrow 2Fe^{3+} + H_{2\,(g)} + 2OH^-_{\,(aq)} \qquad (28)$$
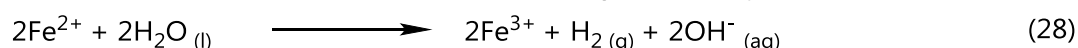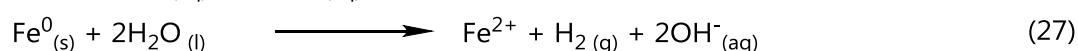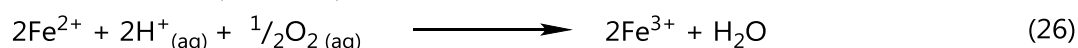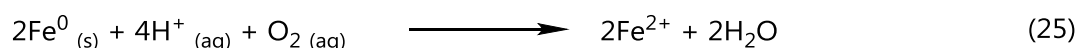
Metal pollutants were removed by nZVI through a number of mechanisms, depending on the standard reduction potential of the metal (Figure 1.7). Metal ions with reduction potentials more positive than nZVI underwent surface-mediated reductive precipitation. Example of metals in this category were Cr^{6+} ($E^o = +1.33$ V),[146–148] Hg^{2+} ($E^o = +1.33$ V)[149] and Cu^{2+} ($E^o = +0.34$ V)[150]. Metal ions with reduction potential only slightly more positive than nZVI were adsorbed and then partially reduced, for example Pb^{2+} ($E^o = -0.36$ V).[151,152] Metals with reduction potential very close to or more negative than nZVI, for example Zn^{2+} ($E^o = -0.76$ V),[148,149] Cd^{2+} ($E^o = -0.40$

V)[153,154], Ni^{2+} (E^o= -0.25 V)[148] were usually removed through surface-mediated complexation. Arsenic is a special case, in which As^{5+} (E^o= 0.56 V) is reduced to the more soluble As^{3+}. It then co-precipitates with iron oxyhydroxide (FeOOH), the product of Fe^0 oxidation.[155–157] Thus, this is effectively a combination of reduction and complexation processes.

Surface-Mediated Reductive Precipitation
Hg^{2+}, Cu^{2+}, Cr^{6+}, UO_2^{2+}

$E^o >>$

Reduction/Co-precipitation
As^{5+}

Fe^0
E^o= -0.44V

$E^o >$ Adsorbtion/Reduction
Pb^{2+}

$E^o <$

Surface-Mediated Complexation
Zn^{2+}, Cd^{2+}, Ni^{2+}
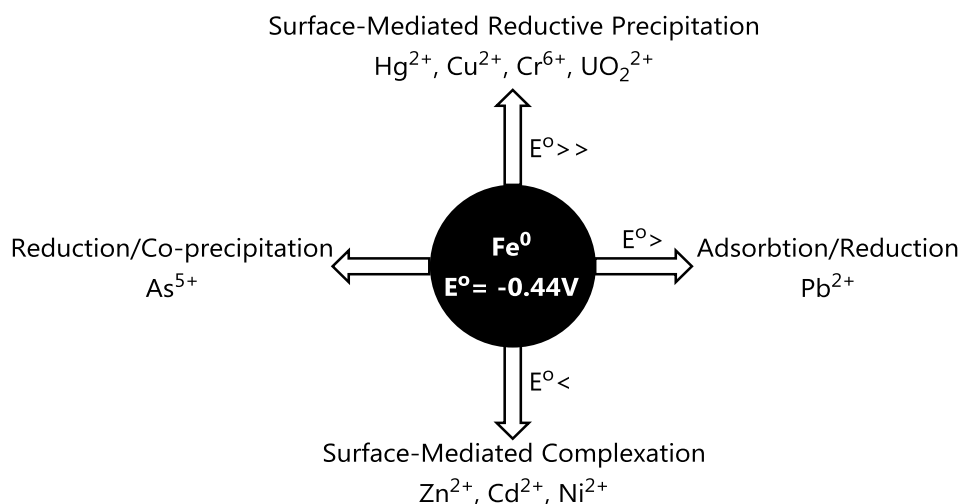
Figure 1.7. Mechanism of metal ion removal by nzVI.

Organic pollutants were removed via a variety of different pathways. TCE is degraded to ethane, butane and chloride ions.[158] Polychlorinated dibenzo-*p*-dioxins and furans were dechlorinated, leaving dibenzo-*p*-dioxins as the final product.[159] Dinitro-toluene is reduced to diaminotoluene.[160] Inorganic anion pollutants were generally reduced or adsorbed. Nitrates and nitrites were reduced,[161–163] phosphates were adsorbed,[164] and sulfates can either be adsorbed onto nZVI surface,[165] or reduced to hydrogen sulfide.[166]

nZVI can also be utilised as a Fenton-like catalyst. In the presence of H_2O_2, nZVI were able to degrade various organic material such as dyes,[98] phenols,[167] and sulfamethazine[168] in near neutral pH instead of low pH. In these reactions nZVI were oxidised by peroxide to Fe^{2+} and the rest of the reaction progresses as a normal Fenton reaction (eq. 16 – 22).

nZVI hae been trialled *in-situ* in contaminated sites to remediate chlorinated hydrocarbon and Cr^{6+}.[81] Similar to gFe^0, nZVI could be used in PRB. However, the small size of nZVI made it easier to inject into the treatment wells. nZVI is more commonly utilised in direct push injection, recirculation using injection/extraction wall, or by pneumatic fracturing. These

methods allow nZVI to reach areas not easily accessed by other method. However, bare nZVI was not expected to migrate more than a few centimetres due to collision and contact with surfaces such as groundwater aquifers. After injection of nZVI to groundwater plume, if there was enough nZVI and the nZVI had not been passivated, the pH of the plume increased to around 8. The oxidation reduction potential (ORP) of the plume was then reduced to below -400 mV, consistent with a highly reducing environment.[169]

In Europe, nZVI had been used in three full-scale remediation and around 15 pilot tests since 2005.[170] Bornheim, Germany was the site of first full-scale remediation in which nZVI was used, with polychlorinatedethenes (PCE) as the main contaminant. The site was previously treated using pump-and-treat method and soil vapour extraction method with a cost of €200/kg of PCE, taking 14 years to remove 5 tons of PCE. The remaining 2 tons of PCE was removed by a mixture of nZVI and gFe^0 at the cost of €290/kg of PCE within 2 years of injection. Furthermore, the treatment also removes the TCE and DCE by-product, leaving only hydrocarbons. Another site that was treated by 100% nZVI used 300 kg of nZVI to treat 70 ppm PCE, TCE and DCE, with 60-75% of original contaminant removed within one year. As of 2011, nZVI has only been used to treat groundwater, and only monometallic nZVI has been used in European *in-situ* trials.

In the US, nZVI had been used for both soil and groundwater remediation, and as of 2017, the US EPA reported at least 70 sites have been described as using nZVI for remediation.[171] Both mono-metallic nZVI and bimetallic nZVI had been used. A special emulsion-based ZVI/nZVI has also been widely used to treat dense non aqueous phase liquid (DNAPL) contaminants, such as TCE.[172]

1.3.4 nZVI and nitrate

The standard electrode potential of nitrate reduction shows positive values across the different types of redox couples (Table 1). This suggested that nZVI should be able to reduce nitrate given that the E^o of nZVI was more negative than the second least positive value of 0.43 V (NO_3^-/N_2, basic conditions). The reduction of nitrate usually requires acidic media (eq. 29 -

30). Several studies suggested pH of about 5 for effective reduction,[93,173] although other studies had found that reduction still occurred at higher pH values. [174,175]

$$Fe^0_{(s)} + NO_3^- + 2H^+ \longrightarrow Fe^{2+} + NO_2^- + H_2O \qquad (29)$$

$$3Fe^0_{(s)} + NO_2^- + 8H^+ \longrightarrow 3Fe^{2+} + NH_4^+ + 2H_2O \qquad (30)$$
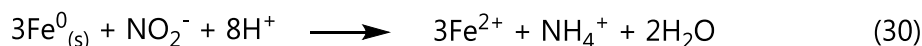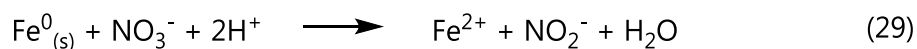
At pH above 10.8 - 11.5, the equilibrium between ammonium and ammonia (eq. 31) favoured the production of ammonia gas, and as the gas left the solution, the equilibrium moved towards the production of ammonia in a process called 'stripping'.[176]

$$NH_4^+ + OH^- \rightleftharpoons NH_{3\,(g)} + H_2O \qquad (31)$$
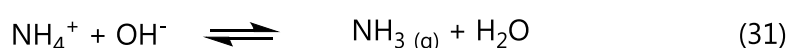
Several studies had investigated the kinetics and activation energy of the reduction of nitrate by ZVI/nZVI (Table 1.4). It was worth noting that the rate constant (k) and activation energy (Ea) varied across different condition which was not expected. However, the systems investigated were heterogenous, and hence calculation of k and Ea were problematic as the exact concentration of Fe^0 available was unknown. The general trend suggested that k was larger for smaller particle size or buffered systems. Activation energy was also lowered by buffering the solution and reducing particle size suggesting that buffer and size of particles somehow acted as catalyst for the reaction.

Table 1.4. Rate Constant and Activation Energy of ZVI/nitrate Reduction

Type of ZVI	Condition	Order of reaction	k	Ea
Cast iron grind (1 mm Ø average)[177]	buffered	Pseudo first order	$0.214 \pm 0.015\ h^{-1}$	$28.2 \pm 0.3\ kJ \cdot mol^{-1}$
	Not buffered	Pseudo first order	$0.072 \pm 0.006\ h^{-1}$	$39.5 \pm 0.1\ kJ \cdot mol^{-1}$
Microscale (~149 μm)[178]	Not buffered (2.21 mol Fe:N)	Pseudo first order	$0.04 \times 10^{-2}\ min^{-1}$	$42.5\ kJ \cdot mol^{-1}$
nZVI (80-90 nm)[178]	Not buffered (2.21 mol Fe:N)	Pseudo first order	$1.37 \times 10^{-2}\ min^{-1}$	$25.8\ kJ \cdot mol^{-1}$
nZVI (1-100 nm)[179]	pH adjusted, 14.72 mol Fe:N	Nth order : 0.42	$0.83\ min^{-1}$	
	7.36 mol Fe:N	Nth order: 0.90	$0.03\ min^{-1}$	

1.3.5 Drawbacks of nZVI

In 2012, Crane and Scott stipulated that for *in-situ* remediation of polluted groundwater, engineered nanoparticles must have the following key properties: high reactivity for contaminant removal, sufficient reactive longevity when in use, sufficient mobility within porous media, low toxicity and cost-effectiveness.[145] nZVI is highly reactive towards contaminants and is cost effective with regards to reagents and starting materials; however, nZVI has potential longevity, mobility, and toxicity issues. For instance, due to its high reactivity, it decomposes to a variety of iron oxides when exposed for prolonged periods to water and oxygen. For storage purposes, nZVI must be kept in dry environments, preferably under N_2 or vacuum, although it can also be stored in degassed ethanol.[180]

One of the main problems in applying nZVI for *in-situ* soil treatment is that nZVI has the tendency to agglomerate due to its magnetic properties. [181] Agglomeration reduced mobility of nZVI in soil systems.[147] In the treatment of nitrate pollution, pH increased due to the production of ammonium. This can cause problems as the zeta (ζ) potential of nZVI is almost zero at pH 8.1. A zero zeta potential indicated no repulsion between particles suggesting that as nitrate is being reduced, the agglomeration problem will increase.[182]

Even though iron is essential in several bioactivities and has biological function, excess iron poses threats such as DNA damage and hemochromatosis.[183] The toxicity of iron is due to its ability to catalyse the formation of radicals via Fenton reactions, manifesting in reactive oxygen intermediate species (ROIs). These ROIs influence antioxidant enzymes, modify nucleic acids and may cause cell injury and death. [184] In a study using *Oryzias latipes* (medaka fish) embryos and full grown adult, it was found that 5 ppm nZVI (30 nm) was enough to cause serious oxidative damage to the embryos, however there was no damage at 0.5 ppm nZVI. [183] Oxidative damage was measured by the level of antioxidant enzymatic activities via superoxide dismutase (SOD) and lipid peroxidation via the malondialdehyde level (MDA). Oxidative damage was also observed on the liver and brain of the adult medaka fish, however at longer exposure level, the damage was reversed, possibly due to endogenous antioxidant enzymes at gene level. The damage to the adult fish could be seen in their gills. At both 5 and 50 ppm, the surface of the gills was full of breakages, and a large number of nZVI particles were found.

The structure of the laminae was almost destroyed. Similar damage could also be seen in the intestine, where accumulation of black particles can be seen. The intestinal villi were sparse and short and the intestinal wall thinner in some parts compared to healthy intestine of unexposed fish.

The toxicity of coated nZVI, aged coated nZVI, uncoated nZVI, nano magnetite (nFe_3O_4) along with Fe^{2+} were explored in a study with medaka fish.[185,186] Carboxymethycellulose (CMC), a biodegradable surfactant, was used as coating on nZVI as it has no or little toxic effect in medaka larvae. The highest mortality was observed when medaka fish were exposed to Fe^{2+} (Table 1.5). Both nFe_3O_4 and uncoated nZVI bio accumulated in the fish intestinal track to a larger degree than coated nZVI; however, the CMC-coated nZVI resulted in higher mortality than uncoated nZVI. nFe_2O_3 did not result in any fish mortality, and aged CMC-coated nZVI also resulted in smaller mortality, presumably due to the relatively higher amount of iron oxides within this system.

Table 1.5. Mortality Rate of Medaka Fish from Different Type of Iron Particle and Dose

Particle type and size	% Mortality at day 1			% Mortality at day 3		
	5 ppm	50 ppm	100 ppm	5ppm	50 ppm	100 ppm
CMC-nZVI (75 nm)	0%	11.7%	47%	0%	11.7%	56.7%
CMC-nZVI aged (75 nm)	0%	0%	0%	0%	5%	5%
Uncoated nZVI (25 - 75 nm)	0%	0%	40%	0%	5%	40%
nFe_3O_4 (27 nm)	0%	0%	0%	0%	0%	0%
Fe^{2+}	0%	25%	85%	0%	67.5%	100%

The toxicity of nZVI on lower order aquatic animals were also investigated using marine phytoplanktons *(Isochrysis galbana, Dunaliella tertiolecta* and *Thalssiosira pseudonana)*, freshwater phytoplanktons (*Pseudokirchneriella subcapitata*) and freshwater zooplankton herbivore (*Daphnia magna*).[184] In this study, two commercially available nZVI (Nanofer 25S and NanoStar) were used. Nanofer 25S is 80-120 nm in size, and has a coating of polyethylene glycol sorbitan monostrearate. NanoStar is 100-200 nm in size and only has an FeO coating. The statistically significant toxic effect could be found from concentrations as low as 0.42 ppm

for Nanofer 25S and from 0.5 ppm for NanoStar (Table 1.6). Fe^{2+} was mildly toxic in an aquatic environment, and for freshwater phytoplankton *P. subcapitata*, Fe^{2+} was more toxic than nZVI, which was consistent with the result with medaka fish. This indicated that care must be applied not only with the nZVI particles but also the Fe^{2+} by-product.

Table 1.6. Effect of different iron on phytoplanktons and zooplankton.

Iron species used	Statistically Significant Toxic Effect (ppm)				
	I. galbana	D. tertiolecta	T. pseudonana	P.subcapitata	D. magna
Nanofer 25S	3.1	1.3	0.42	8.24	0.5
Nanostar	>100	ND	ND	12.4	0.5
Fe^{2+}	50	ND	ND	5	1
Fe^{3+}	75	ND	ND	25	15
*ND: Not determined					

The toxic effect of nZVI on *D. magna* was not limited to only sub-200 nm particles. A recent study using larger nZVI (805 nm) found that at 48 hours, the concentration of nZVI that was responsible for immobilisation half the population of *D. magna* (EC_{50}) was 0.931 ppm.[187] The EC_{50} was lower for *Chironomus sp.* larvae (a non-biting midge fly) at 0.445 ppm.

Figure 1.8. Chironomus sp. *(a) larvae (b) adult (c)* D. magna *(animal is 4 mm long) (d)* D. tertiolecta
Attribution: (a) and (b) Biopix.dk (c) by Dieter Ebert, CC BY-SA 4.0 (d) by CSIRO, CC BY-3.0.

1.3.6 Solutions for nZVI

To summarise the previous sections, the major drawback of nZVI are: (1) nZVI can be too reactive to easily store, (2) nZVI has a tendency to aggregate and hence has limited mobility, and (3), nZVI is potentially toxic due to its small size. The approach in solving all these problems can be categorised into three groups: coating with surfactants or polyelectrolytes, core-shell support and adsorbing onto a solid surface.

1.3.6.1 Coating

Surfactants such as cetyl trimethylammonium bromide (CTAB) and sodium *n*-dodecylsulfate (SDS) had been used to provide bulk hindrance to counteract the electrical and dipolar attraction between nano particles while providing colloidal stability. [188] For the treatment of TCE in soil, anionic surfactants such as SDS and CTAB could be useful as they promoted the solvation of TCE to the aqueous phase as TCE was desorbed from soil.[189]   As soil contains

charged groups such as NH_4^+ and OH_2^+, these anionic surfactants could be desorbed from nZVI and attached to soil instead, especially at pH <8, leaving nZVI bare and unstable. [189]

Polyelectrolyte coating differs from surfactants in that they were irreversibly bound to the particles. The coatings used were generally high molecular weight polymers that promoted colloidal stability and steric hindrance. Several polymers had been tested as nZVI coating with varying degrees of success including carboxymethylcellulose (CMC),[190] guar gum,[47,191] oleate,[192] chitosan,[144,193] and potato starch.[158] CMC and guar gum coated nZVI was stable in suspension, had high dispersability, and hence easier to inject *in-situ*. As CMC and guar gum-coated nZVI reduced aggregation, the resulting particles had high mobility in porous medium. As CMC is more commonly used as coating, a lot of research has gone into its safety; as previously mentioned, unfortunately CMC-nZVI was more toxic towards medaka fish compared to uncoated nZVI.[185,186]

1.3.6.2 Core-Shell support

In order to reduce aggregation, a protective shell can also be placed around nZVI particles. Some of the materials that had been tested as protective shells were: silica,[194] polyvinyl alcohol/polyacrylic acid (pVA/pAA) composite,[133] and carbon.[195] Silica coated nZVI had been synthesised for the reduction of Cr^{6+}.[196] The particles overall size was around 25 nm, with 8 nm coating of SiO_2. pAA could be toxic to *D. magna* larvae with LC_{50} of 1323 ppm, and hence must be used with caution.[185] Carbon had also been used to coat nZVI for the reduction of Cr^{6+}, with an average particle size of 15 nm.[195]

1.3.6.3 Adsorbance on solid support

nZVI can be adsorbed on solid support, which increases the overall particle size with little or no reduction in reactivity. Carbon,[197] chitosan, calcium-alginate capsule,[198] bentonite,[146,199,200] montmorillonite,[201] TiO_2 nanotubes,[73] polystyrene resins,[202,203] silica fume,[147] silica gels[204] and mesoporous silica[205–208] had all been investigated as solid supports for nZVI. nZVI adsorbed on chitosan and calcium-alginate capsules did not show improvement in mobility in porous media compared to unsupported nZVI, but the shelf life of these materials was longer than unsupported nZVI. nZVI adsorbed on silica fumes, mesoporous silica, or montmorillonite

showed improved mobility in porous media, and increased the effectiveness of nZVI. The use of silica/silicate as support will be discussed in detail later in the chapter.

1.3.6.4 Finding the right support/coating

Particle mobility is important in *in-situ* soil remediation. When nZVI is injected into soil, a more even dispersion of nZVI in the media means an increase in the area treated. This also means that fewer injection sites were required to treat the same area of soil. Crane and Scott suggested that, depending on the permeability of the soil, particles within the size range of 100 nm - 2 µm have the highest mobility in soil. Particles of this size range are also less toxic than the sub-100 nm particles. The larger sized particles (>500 nm) can also be handled as powder rather than slurry, reducing the material volume and improving material handling.[145] Therefore, the right support or coating for nZVI are those that will increase its bulk size to 500 nm - 2 µm.

In-situ remediation is the preferred method of field treatment due to its lower operating cost, therefore a support or coating system that is not toxic is required. A support system that contributes to the remediation process by adsorbing the by-product is also desirable. Furthermore, nZVI particles should have a good adsorption on the support material or the coating should have a good adhesion to nZVI with little or no reduction in effectiveness of nZVI. Also, the adsorption or coating process should be efficient and cost-effective.

Based on these criteria, this research focussed on the use of silica and silicates as support, as they come in a variety of sizes and can be functionalised. Silicate minerals make up over 90% of the earth's crust,[209] and most silica and silicates are compatible with environmental remediation. The chemistry of silica and silicate is discussed in the next section, followed by a discussion of nZVI supported by silicates systems that have been synthesised by other researchers.

1.4 Chemistry of silica and silicates

Silicon (Si) is the second most abundant element in the earth's crust after oxygen.[210] Silicon does not exist as a pure element in earth's crust, instead it exists as silica (SiO_2) and silicates (SiO_4^{-4}). Silicon forms strong bond with oxygen, with a bond enthalpy of 466 kJ mol^{-1}, much higher than the Si-Si (226 kJ mol^{-1}) or Si-H (326 kJ mol^{-1}) bond. Silica is the oxide of silicon and is typically built from a 3-dimensional tetrahedral '"SiO_4^{4-}"structure. The units are connected to each other by sharing the corner O, forming O-Si-O. Silica is a type of silicate when the composition of the silicate contains only silicon and oxygen. For instance, quartz is a silicate that consists only of pure silica. However, other types of silicates contain additional metal cations (e.g. Na, K, Fe, Mg, Al) as well as silicon and oxygen. Thus, silicates will be used as the generic SiO_2-containing support in this thesis.

Silicates can either be crystalline or amorphous.[211] Commonly used silicates are naturally occurring, a by-product of other processes, or synthesised in high purity. Pure synthetic silica is typically generated using the Stöber process where a silicon source such as tetraethylorthosilicate (TEOS), is hydrolysed using suitable bases (Figure 1.9).[212] The Stöber process can be modified to control size,[213] functional group availability,[214] and pore size.[215]

Tetraethylorthosilicate (TEOS) 3-thiopropyltrimethylsilane (3-TPTMS) 3-aminopropyltriethylsilane (3-APTES)
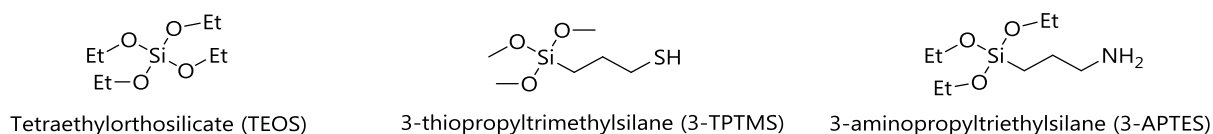
Figure 1.9. Different silicates and silanes used for syntheses of silica and functionalised silica.

The active sites on silica and silicates can be different. As silica does not have other cations or counter ions, reactivity at the surface is based purely on Si-O-H bonds.[216] Silanols are considered as strong adsorption sites and hydrophilic (Figure 1.10). Siloxane sites are hydrophobic as they cannot form hydrogen bonds with water or other adsorbates. Siloxane sites are relatively unreactive with most molecules.[217,218] Silanoxy sites are the result of alkaline treatment of silanol sites, and are also hydrophobic. Due to the negative charge, silanoxy sites

are attracted to electrophilic molecules. Silica surfaces can also be functionalised by grafting organic silane groups onto silica,[219,220] or by adding organic silane as the silica is synthesised.[214,221] Depending on the functional group required, 3-aminopropyltriethoxysilane (3-APTES) or 3-thiopropyltrimethoxysilane (3-TPTMS) were usually used as the organic silane in conjunction with tetraethylorthosilicate (TEOS) as the source of silicon (Figure 1.10).
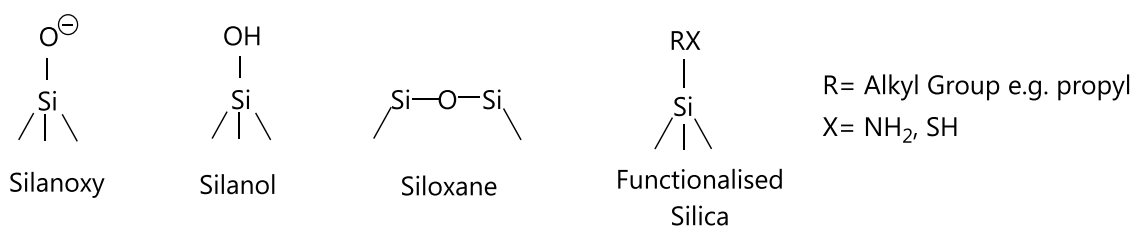
Figure 1.10. Types of Si-O bonds on silica surface.

Based how many tetrahedral SiO_4^{4-} units share their corner oxygen and the arrangements of these connected tetrahedral units, there are a number of different possible silicate groups (Figure 1.11).[210] In **neosilicates,** SiO_4^{4-} groups are independent of each other and instead the oxygen is shared with other cations such as Ti^{4+}, Mg^{2+}, Fe^{2+} as in olivine $(Mg,Fe)_2[SiO_4]$, and both synthetic β- and γ-$Ca_2[SiO_4]$. A **Sorosilicate** group is formed when two tetrahedron of SiO_4^{4-} share an oxygen, making a basic unit of $Si_2O_7^{6-}$. An example of a member of the sorosilicate group is thortveitite $(Sc_2[Si_2O_7])$.

When considering larger silicates, it is easier to represent the SiO_4^- unit as tetrahedral with oxygen (red circle) on the corners and silicon in the middle of the tetrahedral. A **Cyclosilicate** group can be formed from three, four, five or six tetrahedral groups, with the basic group being $Si_3O_9^{6-}$, $Si_4O_{12}^{8-}$, $Si_5O_{15}^{-10}$, and $Si_6O_{18}^{-12}$ respectively. Examples of these groups include α-wollastonite $(Ca_3[Si_3O_9])$ and beryl $(Be_3Al_2[Si_6O_{18}])$. **Inosilicates** can be formed from either a single chain of linked tetrahedra (**pyroxene** group) or two connected chains (**amphibole** group). The pyroxene group has a basic group of $Si_2O_6^{4-}$ or SiO_3^{2-}, and examples of this group are β-wollastonite $(Ca[SiO_3])$ and orthopyroxenes $(Mg,Fe)[SiO_3]$. Asbestos contains tremolite

Neosilicates $(SiO_4)^{4-}$ *Sorosilicates $(Si_2O_7)^{6-}$*
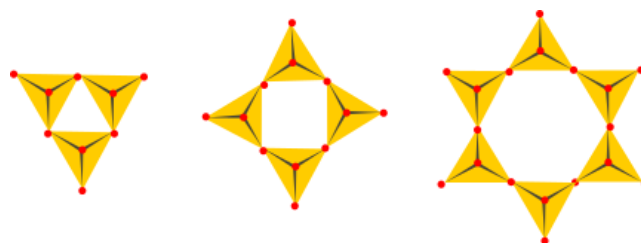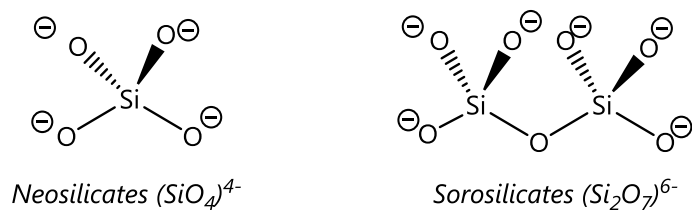
Cyclosilicates: thrree-$(Si_3O_9)^{6-}$, four- $(Si_4O_{12})^{8-}$, and six-$(Si_6O_{18})^{12-}$ membered rings.
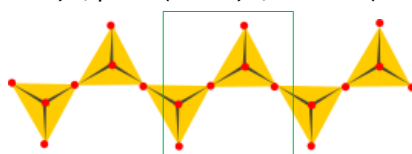
Pyroxene group $(Si_2O_6)^{4-}$
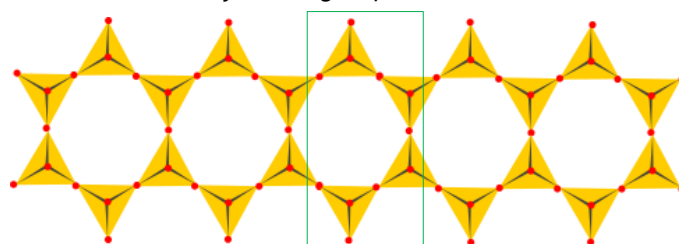
Amphiboles group $(Si_4O_{11})^{6-}$
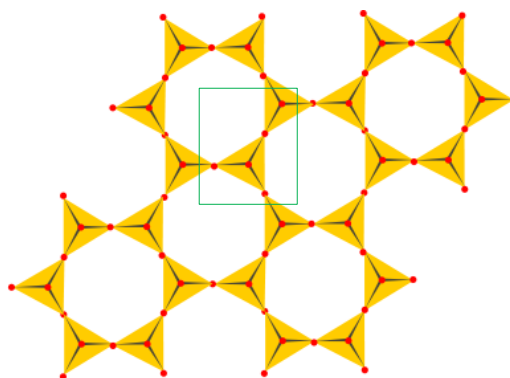
Phyllosilicate/sheet silicates $(Si_2O_5)^{2-}$

Figure 1.11. Different groups of silicate based on the arrangement of base tetrahedral shape. The green box indicate the basic repeating unit.

33

(Ca$_2$Mg$_5$[Si$_4$O$_{11}$]$_2$(OH)$_2$, a member of the amphibole group, which has the basic structural group of Si$_4$O$_{11}$$^{6-}$. The next group is phyllosilicates where three of the oxygen atoms are shared, forming an infinite sheet of connected tetrahedral, with the basic unit of Si$_2$O$_5$$^{2-}$. Mica, clays, such as kaolinite, Al$_4$[Si$_4$O$_{10}$](OH)$_8$ and halloysite, Al$_4$(H$_2$O)$_4$[Si$_4$O$_{10}$](OH)$_8$, along with talc, Mg$_3$(Si$_2$O$_5$)$_2$(OH)$_2$ are members of this group. The last class in the silicates is called **tectosilicates** (framework silicate) where all of the oxygens are shared with another SiO$_4$ tetrahedron, and the basic structural group is then SiO$_2$. In tectosilicates, the framework can be made from just SiO$_4$ tetrahedra, such as in quartz and cristobalite, or with some of the silicon replaced with aluminium. Example of where aluminium replaces silica is the feldspars series (Na[AlSi$_3$O$_8$]-K(AlSi$_3$O$_8$]-Ca[Al$_2$Si$_2$O$_8$]) and in zeolites, an aluminosilicate that has a very high water absorbing capacity.

Aluminosilicate is a special class of silicates where one or more of the SiO$_4$$^{4-}$ tetrahedra is replaced with AlO$_4$$^{5-}$ tetrahedra and another metal cation to balance the overall charge (Figure 1.12). Aluminosilicates are very common as ionic radii of Si^{4+} and Al^{3+} ions are similar, at 26 and 39 pm, respectively. The ratio of displacement of silicon with aluminium varies widely, from orthoclase (K[AlSi$_3$O$_8$]) with one in four silica tetrahedra replaced with aluminium tetrahedra, to sodalite (Na$_4$[AlSiO$_4$]$_3$Cl), where half of the silica is replaced with aluminium. Aluminosilicate typically occurs in tectosilicates, although examples of cylcloaluminosilicates also exist such as in the corderite minerals groups, Mg$_2$Al$_3$[AlSi$_5$O$_{18}$]. Aside from aluminium, other metallic tetrahedra can also replace SiO$_4$$^{4-}$, for example borates (BO$_4$$^{5-}$) form borosilicates, zirconoate (ZrO$_4$$^{4-}$) form zirconosilicates, and titanoate (TiO$_4$$^{4-}$) form titanosilicates.

In older publications, distinctions were made between aluminosilicate and aluminium silicate.[222] In aluminosilicate, aluminium tetrahedra replaces silica tetrahedra, for example in celsian (Ba[Al$_2$Si$_2$O$_8$]) (tectosilicate with SiO$_2$ basic group). In aluminium silicates, aluminium acts as a counter cation, for example in beryl rings, Be$_3$Al$_2$[Si$_6$O$_8$], cyclosilicates with Si$_6$O$_{18}$$^{12-}$ basic group, connected by AlO$_6$ octahedras.

Figure 1.12. Aluminosilicates tetrahedra.

The chemistry of the silicate surface is more complicated as the reactivity also depends on the counter ions and cation replacement, along with the structure of the silicate.

1.5 nZVI adsorbance on silica and silicates

Due to their abundance as well as ease of synthesis, silicates, including silica, have been investigated as potential supports for nZVI. This section discussed both the use of pure silica as well as other silicates, including aluminosilicates for nZVI support.

As previously mentioned, pure silica had been used to coat nZVI. However, synthetic silica spheres had also been examined as a potential support for nZVI. Qiu *et al* examined the effect of silica support on both the adsorption and reactivity of nZVI-supported silica.[223] In these studies, an FeOOH layer on silica was created by soaking silica spheres in a $FeSO_4$ solution in the presence of polyethylene glycol (PEG), and then nZVI was generated on this surface (SiO_2@FeOOH@nZVI). Although the role of PEG was never fully explained, it was found that the reactivity of the FeOOH-coated system in the nZVI-mediated degradation of decabromodiphenyl ether was faster than without the FeOOH system (SiO_2@nZVI).

The FeOOH-coated silica had a larger zeta potential than the unmodified silica (-15.78 mV versus -25.78 mV, respectively), thus it was postulated that this increase in surface charge increased the attraction of the nZVI particles. Although the presence of adsorbed nZVI on silica was supported by TEM images of SiO_2@FeOOH@nZVI, there were no TEM images of SiO_2@nZVI for comparison, and no corresponding SEM images to analyse the overall dispersion of nZVI on the silica particles.

In a similar study, nZVI was adsorbed onto the nano-silica coated with FeOOH ($nSiO_2$@FeOOH@nZVI). [224] As the particle size was small (20 nm), sonication was required to disperse the particles before reduction of nitrate. The best removal of nitrate (29 ppm) was

achieved using 4 mg/L of Fe^0-SiO_2 system, taking 100 minutes to remove 99.84% of nitrate at pH 3. Despite the success of removing nitrate, the evidence for the actual material used was not strong. The SEM images presented did not have the necessary resolution in order to determine if nZVI was adsorbed onto the surface of $nSiO_2$@FeOOH or existed as agglomerated chains of nZVI. The XRD data presented revealed the presence of nZVI; however, the resolution of this technique also did not confirm if nZVI was adsorbed to the silica surface (see 3.4.1).

A good dispersion of nZVI on silica surface can also be achieved by aerosolising the silica and iron salt mixture before drying at 400°C. The particles were able to reduce TCE to ethane within 96 hours. However, when the SiO_2@nZVI particles were made with both Pd and Fe, the reduction rate was faster with almost 95% of TCE removed within 1 hour. The SiO_2@nZVI/Pd particles produced showed good dispersion, however the technique required specialist atomizer and heating equipment.

Functionalized silica had been used to support nZVI. [197] For instance, nZVI had been adsorbed on sulfonate-functionalised silica colloid and silica gel and used to reduce TCE. The nZVI particle size was between 20-30 nm. The dechlorination rate was approximately 50% in 50 hours. In this study the nZVI could be observed to be adsorbing onto the silica gel surface, however the dispersion was not even as aggregates of nZVI were also observed on the silica surface.

Two types of clay, bentonite (montmorillonite) and kaolin had been used as a support for nZVI. Bentonite-supported nZVI were able to remove Cr^{6+}, Pb^{2+}, and Cu^{2+} successfully, and upon washing with ethylenediaminetetraacetic acid (EDTA), bentonite-nZVI could be reused although the efficiency was reduced by 70%.[199] Montmorillonite-supported nZVI were able to sequester U^{6+} and Se^{4+}.[225] The rate of sequestration was enhanced due to the ability of montmorillonite to adsorb U^{6+} and Se^{4+}. Bentonite supported nZVI had been used to remove methyl orange, doubling the performance of nZVI from 40% to 79% removal, for bare iron and bentonite supported nZVI respectively.[200]

A bentonite-nZVI system had also been utilised to reduce nitrobenzene.[226] In a comparison of efficiency, it was found that nZVI supported in bentonite was more successful in reducing nitrobenzene compared to nZVI/raw bentonite or bare nZVI. Bentonite was prepared by cation

36

exchange between Na and cethyltrimethyl ammonium. Kaolinite had also been used to support nZVI to remove Cu^{2+} and Co^{2+} ions successfully[227].

Silica fume (from blast furnace) was also used as support for nZVI (SF@nZVI) in nZVI mediated reduction of Cr^{6+}.[147] The size of SF@nZVI particles was established at 150-450 nm. The researchers found that the suspension of SF@nZVI was well dispersed in an aqueous medium for up to 48 hours. The reactivity with Cr^{6+} was very good as SF@nZVI was capable of removing 97% of 40 ppm Cr^{6+} within 120 minutes with only 0.5 g/L of SF@nZVI (compared to 85.2% removal with unsupported iron). Mobility wise, 51.5% of SF-nZVI was eluted through a vertical sand column and 38.3% eluted through a horizontal sand column. In contrast, unsupported nZVI could not be eluted from sand columns.

For nitrate reduction, nZVI had been used alongside clays, where clay acted as an adsorbent for the reduction process,[228,229] or as a support with nZVI adsorbed to the clay particles.[201] In the clay-supported nZVI, 50 mg of nZVI were used to reduce 100 mL of 50 ppm NO_3^-, (molar ratio of 100:1) and 95% of nitrate was reduced within 1 hour to ammonium. The evidence of nZVI adsorption onto the clay was via a TEM image and XRD.

Mesoporous silica beads had been used as support for nZVI to reduce nitrate with some success, reducing nitrate into ammonia.[207] The size of beads were quite large at 1 mm, and the reduction of 30 ppm NO_3^--N was complete in 36 hours. Similar to other studies mentioned previously, there was no conclusive evidence that nZVI was adsorbed onto the beads' surface as there were no COMPO images or TEM contrast that showed the presence of iron particles.

Choice of support and organisation of thesis

Previous work by the candidate for an VUW Honour's project investigated nitrate reduction by nZVI adsorbed on various waste silicates.[230] There were 10 different silicate tested: 4 types of silica fume, 3 types of fly ash, fumed silica, crystalline quartz and glass flour. Based on the preliminary results, it was decided to do further work with Microsilica 600 (Misi) as this silicate was the most promising in terms of adsorption of nZVI and reactivity toward nitrate reduction. Misi is a powdered silicate from a geothermal source in Rotorua. It was supplied by Golden Bay Cement, and commonly used as partial replacement for cement in concrete products. Misi

has pozzolanic properties as it contains amorphous silicate and aluminium silicates that react with calcium hydroxide in the presence of water to form cementitious product.[231] This pozzolanic nature of Misi means that in alkaline conditions, Misi becomes partially soluble and reactive, a useful characteristic in cement chemistry.

In the research reported within this thesis, nZVI was also adsorbed on pure silica surfaces (commercially available silica gel and Stöber silica), and four other silicates (rice husk ash, Western Australia silica fume, Mt Piper fly ash and precipitated aluminium silicate). The ability of nZVI adsorbed on Misi to reduce nitrate, and other environmental concern are also discussed.

The structure of this thesis is as follows:

Chapter 2 discusses into the methods and techniques used throughout this thesis. Included in this chapter were methods for synthesis of pure silica, surface functionalisation and modifications of silicate surfaces, nZVI adsorbance onto silicates, and nitrate reduction. This chapter also outlines methods developed by the author to quantify agglomeration of nZVI on silicate surfaces (*A*-value). A discussion and methods on all characterisation methods used were also explained: atomic absorption spectroscopy (AAS), Zeta potential, surface area analysis via Brunaeur-Emmett-Teller isotherm (BET), scanning electron microscope and energy dispersive X-Ray spectroscopy (SEM and EDS), X-Ray Powder diffraction (XRD) and thermogravimetric analysis (TGA).

Chapter 3 focusses on nZVI adsorption onto Misi. In this chapter the surface chemistry of Misi and the effect of different modification techniques (calcination, acid wash, boiling and FeOOH layer) were discussed. The role of each of these modifications to nZVI adsorption were explained. Discriminate analysis was conducted to classify the quality of adsorption of nZVI on the Misi surface. Univariate analysis was used to determine the significance of each treatment on the adsorption of nZVI onto the Misi surface.

Chapter 4 explores the adsorption of nZVI on a pure silica surface. In this chapter, silica gel and spherical synthetic silica were used as support for nZVI. The silica surfaces were modified

using the same sets of treatment as in Misi along with other methods such as functionalisation and pore enlargement.

Chapter 5 investigates how nZVI adsorbs on different types of silicates, focussing on silicate with different crystallinity and aluminium content compared to Misi. In addition, nZVI was also adsorbed on amorphous precipitated aluminium silicate that were relatively free of other metals.

Chapter 6 investigates the ability of selected nZVI-Misi material to reduce nitrate. The role of *A*-value as well as other ions in the reduction of nitrate were also explored. Furthermore, the effect of support to nZVI aggregation was examined.

Chapter 7 summarises all the findings in this thesis, and suggested the future direction of work in supported nZVI.

2 Methodology

2.1 Materials

2.1.1 Naturally Occurring Silicates

Microsilica 600 (Misi) was donated by Golden Bay Cement in a 25 kg bag. Misi was then divided into 5 kg airtight plastic bags to maintain its purity and protect against humidity. Mt Piper fly ash, Western Australia silica fume and rice husk ash were gifted by Dr. Neil Milestone from Callaghan Innovation and stored in a plastic ziplock bag.

2.1.2 Stöber silica

Synthetic silica was synthesised using a modified Stöber process where dodecylamine was used as both the base and template to create uniform spherical silica as described by Qiu *et al* (2011).[212,223] In a typical synthesis, 0.222 g (1.20 mmol) of dodecylamine (DDA) was added to ~30 mL of 62.5% $^v/_v$ EtOH/ deionised-H_2O (DI-H_2O, MilliQ, 18.1 MΩ). After all of the DDA was dissolved, 1.16 mL (5.20 mmol) of tetraethylorthosilicate (TEOS) was added. The solution was stirred for a further 30 s with a mixing speed of 300 rpm, then left to react (unstirred) for 3 hours.

After 3 hours, white powder was observed on the bottom of the conical flask. The silica was then separated using a centrifuge at 5000 rpm for 5 minutes. Silica was then washed and dried using the alcohol dehydration method to reduce agglomeration.[232] In this method, silica was progressively sonicated and then separated using a centrifuge at 3000 rpm for 3 minutes with EtOH/H_2O ratio of 1:1, 3:2, 1:0, 1:0, before drying at 60 °C oven to remove the ethanol.

The silica was then calcined at 600 °C for 6 hours to remove the organic template, yielding SS-C600. This material was reactivated by boiling in DI-H_2O for 2 hours, yielding SS-C600-A.

2.2 Surface Modification Treatments

2.2.1 Calcination

Silica and silicates were placed on ceramic crucibles and heated at either 400 °C or 600 °C for 6 hours under air. When nitrogen atmosphere was required, the silica and silicates were

calcined using a programmable tube furnace (MTI High Temperature Furnace GSL-1500X) with 99.999% N_2 (BOC).

2.2.2 Regeneration of Silanol Sites

2.2.2.1 Acid washing

To 50 mL PPE centrifuge tube containing 4.0 g of silica/silicate, ~50 mL of 5.6 M, 2.8 M or 1.1 M HCl in DI-H_2O were added. The tubes were then shaken and placed in a sonicator (Elma S40H Elmasonic) for 30 mins before being centrifuged (5000 rpm, 3 minutes) to separate the solids from the solution. After discarding the acidic liquor, the solids were washed with ~50 mL DI-H_2O twice and then with ~30 mL EtOH. The solids were then dried at 60 °C overnight.

2.2.2.2 Boiling

In a typical procedure, 4.0 g of silica/silicate were placed in a 250 mL Erlenmeyer flask, and ~100 mL of DI-H_2O were added, and the suspension was heated until boiling gently without reflux for 2 hours. The suspension was then centrifuged (5000 rpm, 3 minutes), decanted and placed in a 60 °C oven to dry overnight.

2.2.3 Surface Functionalisation

2.2.3.1 Amino-functionalised silica (co-condensation method)

Aminopropyl functionalised silica was synthesised following the method by Miyake *et al* (2009).[214] In a typical synthesis, 0.222 g (1.20 mmol) of dodecylamine was solvated with ~30 mL of 60% $^v/_v$ EtOH/DI-H_2O. To this solution, 1.30 mL (5.82 mmol) of tetraethylorthosilicate (TEOS), and an appropriate amount of 3-aminopropyltriethoxysilane (3-APTES/ $NH_2(CH_2)_3Si(OEt)_3$) was added (3 mol%, 5 mol% or 10 mol%). This was allowed to mix for 30 s and then left to react overnight at room temperature. The resulting silica, denoted as AS-3%, AS-5% and AS-10% respectively, were washed using water, dehydrated using ethanol, and dried in a 60 °C oven for 2 h.

2.2.3.2 Ligand-functionalised silica (reflux)

Using methods developed by Goswami[219], 3 g of silica gel (Silica Gel 60, Pure Science) was refluxed in 10 mL of dry toluene and 1 mL of either 3-APTES or 3-TPTMS, then washed with ~10 mL toluene, followed by ~10 mL EtOH, then ~10 mL Et_2O and then dried in drying pistol at 100 °C under vacuum.

2.2.4 Pore Enlargement

Calcination of Amino-functionalised silica (AS): Aminopropyl functionalised silica was heated at 600 °C for 6 hours to create microporous silica spheres as described by Vacassy (2000), resulting in a fine white powder, denoted as AS3%-C600, AS5%-C600, and AS10%-C600 respectively.[233]

Pore creation in SS: A 50 mL PE centrifuge tube containing 2.0 g of SS-C600 was charged with 45 mL of 20:5:5 w/w NaCl: LiCl: KNO_3 solution (150 g/L) following a procedure outlined by Wang *et al.*[234] Upon addition of the salt solution, fizzing and cracking sounds were heard, and a cloud of steam was observed. The mixture was then sonicated for 30 minutes, centrifuged (5000 rpm, 3 minutes), and decanted. Calcination at 300 °C for 2 hours was required after decanting, however no detail was given on whether the solid needed to be washed prior to or after calcination. Therefore, three variations were trialled. In the first group, the solids were washed three times with ~50 mL of DI-H_2O, centrifuged (5000 rpm, 3 minutes), and then calcined, yielding SS-C600-WBC (washed before calcination). In the second group, the solids were calcined after decanting, and then washed three times with ~50 mL of DI-H_2O, centrifuged (5000 rpm, 3 minutes), decanted and dried in a 60°C oven for 2 h yielding SS-C600-WAC, (washed after calcination). In the third group, the solid remains unwashed, but calcined, denoted as SS-C600-uW (unwashed).

2.2.5 FeOOH layer

The FeOOH layer was generated by soaking silica/silicate in a ferrous salt solution (2:1 SiO_2: $FeSO_4 \cdot 7H_2O$ $^w/_w$), followed by heating the solids in air. In a typical synthesis, 2.0 g of silica/silicate and 1.0 g of $FeSO_4 \cdot 7H_2O$ were added to a 50 mL PE centrifuge tube and then made up to 50 mL with DI-H_2O. The mixture was then sonicated for 30 min and centrifuged

(5000 rpm, 3 minutes), decanted and dried at 60 °C overnight before being placed in a 120 °C oven for 2 hours to encourage the formation of the FeOOH layer.

2.3 nZVI Adsorbance

2.3.1 Sodium Borohydride Reduction

The synthesis of nZVI-SiO$_2$ and unsupported nZVI was performed under N$_2$ atmosphere using standard Schlenk techniques. In a typical procedure, 1.0 g of silica/silicate was re-suspended using ~30 mL DI-H$_2$O and added to a Schlenk flask containing FeSO$_4$·7H$_2$O (0.5 g, 1.7 mmol). The solution was then deoxygenated by bubbling N$_2$ through the solution for 15 minutes. A glass coated magnetic stir-bar was used for mixing The silica/iron suspension was then left to stir for approximately 10 minutes until all the light green FeSO$_4$·7H$_2$O crystals dissolved. NaBH$_4$ (0.2 g, 5.3 mmol) and deoxygenated DI-H$_2$O (10 mL) was directly added directly to a 20 mL plastic syringe. Using a syringe pump (NE-1000, New Era Pump System), NaBH$_4$ solution was added to the iron/silicate solution at a rate of 0.2 mL/minute. A black precipitate was observed upon addition of the NaBH$_4$ solution. After the addition of all NaBH$_4$ solution, the mixture was left to stir for another 10 minutes. The resulting magnetic particles were separated using a strong magnet, and the liquor removed via cannula. The precipitate was then washed twice with ~50 mL deoxygenated DI-H$_2$O, then with ~50 mL of deoxygenated EtOH. The particles were then dried under vacuum. Unsupported nZVI was made using a similar method except no silica/silicate was added to Schlenk flask.

2.3.2 Physisorption method

Sonication: In a typical procedure, 0.1 g of pre-formed nZVI and 1 g of silicate were added to a Schlenk flask, degassed, and 50 mL of de-oxygenated DI-H$_2$O were added. The Schlenk flask was sonicated for 2 hours under nitrogen atmosphere. The resulting nZVI/silicate was separated using a strong magnet, decanted, washed with EtOH and dried under vacuum.

Grinding: In a typical procedure, 0.1 g of pre-formed nZVI was grinded together with 1 g of silicate using an agate mortar and pestle, until a uniformly black mixture can be observed.

2.3.3 Determination of nZVI dispersity

FIJI applet from ImageJ is commonly used by nano-particle scientists to measure the size of their nano-particles based on contrast between particles and background. Typically in these images, the nano-particles were formed from heavy metals with carbon background, and hence in COMPO images, the contrast is high enough that the nanoparticles can be separated from the background image by FIJI. However, our system requires contrasting between silicon and iron. As COMPO image contrast is based on atomic number difference, the contrast between silicon and iron were sometimes not high enough to be picked up by FIJI (Figure 2.1). Thus, Picasa3[TM] freeware was utilised to increase the contrast between the lighter shaded areas representing iron nano particles and darker grey areas of silica/silicate. Once the high contrast were obtained, the white areas corresponding to iron nanoparticles were isolated using the FIJI applet from ImageJ. [235] FIJI then isolated these white areas, inverted the colour, calculated the size of each area, and counted how many areas were there in total. For step-by-step instruction please see Appendix A.

Figure 2.1. Original and processed COMPO images using Picasa3[TM] and FIJI.

Analysing the data. The raw data yielded several variables that can potentially be used as a yardstick for measuring the dispersity of the particles: mean size of particles (Mean), standard deviation (SD), percentage of particles under 2000 nm^2 (%under) and total number of particles counted (TC). As the productions of nZVI was not controlled for size, the size distribution can be quite wide as seen on the previous example. Based on discriminate analysis using SPSS (v.23 © IBM, section 3.5.1), it was determined that the mean particle size did not contribute in differentiating the amount of aggregate formed, and aggregate value (*A*-value) was related to these measurements only: SD, TC and %under. The formula for *A*-value based on the analysis was determined to be:

$$A\ value = \frac{(0.89\ \times \%under) + (0.978\ \times SD) - (0.393 * TC)}{1000}$$
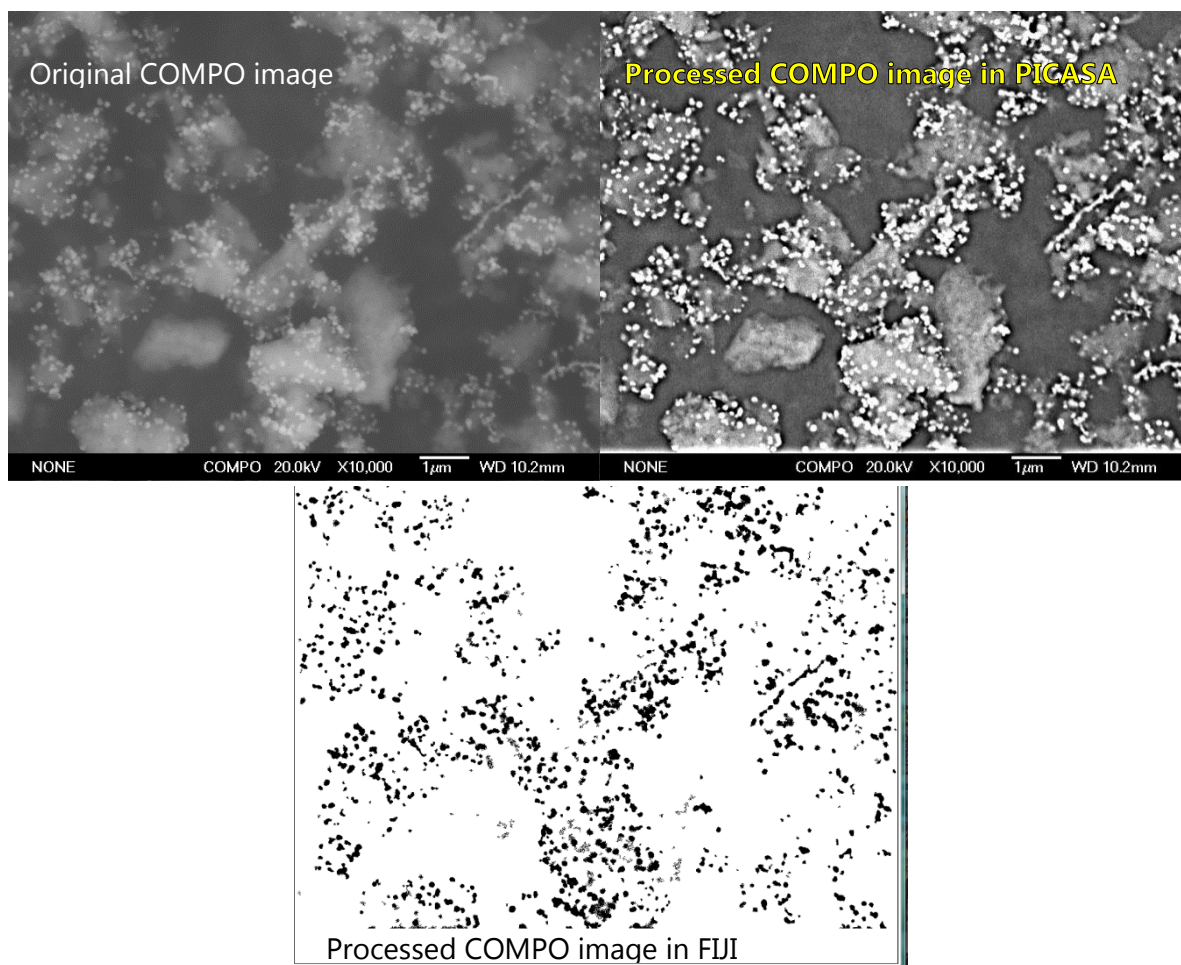
2.4 Nitrate Reduction

To prepare a 100 ppm NO_3^--N solution, oven-dried (105 °C, 24 hour) KNO_3 (0.7218 g, 7.100 mmol) was made up to a 1.000 L solution with DI-H_2O in a volumetric flask. For 10 ppm NO_3^--N solution, 100.00 mL of the 100 ppm solution was transferred quantitatively via a volumetric flask to a 1.000 L volumetric flask and DI-H_2O was added to the mark.

In a typical nitrate reduction experiment, 100 mL of 10 ppm KNO_3 was deoxygenated and 1.0 g of nZVI-silica particles was added under N_2 atmosphere and the suspension was stirred continuously using a glass-coated magnetic stir bar. Aliquots (3-5 mL) were taken at set time points. The aliquots were passed through a 0.25 μm acetate cellulose syringe filter to remove the particulates. Assuming that a typical nZVI/silicate system consists of 10% nZVI, then in a typical reduction experiment, the molar ratio of NO_3^- to Fe was 1:25.

2.4.1 Quantifying Nitrate

In this research, two methods were employed to quantify nitrate: UV-Vis spectroscopy and ion chromatography. The spectrum were obtained using a Cary Bio-50 spectrophotometer at 220 nm (ε (NO_3^-) = 5.161 x 10^{-3} mol/dm^2). Using a quartz cuvette, the concentration of nitrate was quantified against a known standard curve from about 0.1 - 10 ppm range.

2.4.1.1 Ion Chromatography

Principles behind IC

The basis of ion chromatography (IC) is the separation of ions, based on their affinity to the stationary phase. IC can detect several anions in the same measurement.

Method

Approximately 5 mL of sample were passed through 0.25 μm acetate cellulose syringe filters into a PolyVial^{TM} and capped.   The samples were loaded to an auto sampler along with at least 3 known standards that cover both the low and high end of possible nitrate concentration. In this study, Thermofisher IC 1100 was used with Dionex IonPac AS14 column, Dionex IonPac AG 14 column guard, Dionex AERS 500 suppressor and injection volume of 25μL. The eluent used was Dionex AS23 Eluent concentrate, diluted to 3.5 mM Na_2CO_3/1 mM $NaHCO_3$.

2.5 Characterisation Methods

2.5.1 Atomic Absorption Spectrometry

AAS analysis for iron content was conducted using ThermoFisher iCE 3500 with SOLAAR™ software. The range of detection is between 0.1-10 ppm, and all sample were diluted to fit the range of concentration. Standards were prepared from a Sigma-Aldrich Fe standard for AA (1000 ppm), diluted with DI-H_2O to appropriate concentration.

For each measurement, approximately 10 cm^3 of sample was required. The samples were filtered with a 0.22 μm cellulose acetate syringe filter then charged into PE test tubes for sampling and loaded to the auto sampler.   A set of known standards (1, 2, 5, and 10 ppm) were included for each set of measurements.   Each solution was sampled three times and the value reported was the average of the three values.

2.5.2 Zeta potential

Principle behind Zeta potential measurement

A colloid is a dispersion of small particles (<500 nm) of one material in another.[236] Generally they are too small to see with an ordinary optical microscope, and pass through filter paper. The particles however can be detected by light scattering and sedimentation. The surfaces of particles in colloid have electrical charge that is one of the major causes of instability in colloid. Nanoparticles with a net charge will have a layer of ions of opposite charge strongly bound to their surface. This layer of charge is referred to as the Stern layer, and these charges are relatively immobile. A second diffuse outer layer consists of loosely associated ions. These two layers are called the diffuse double layer, which effectively screen or neutralise a portion of the inherent surface charge. The electric potential at the edge of Stern layer relative to its value in the distance bulk medium is called zeta potential or electro kinetic potential, and this is related to the surface charge of the particles. In zeta potential measurements, an electric field is applied to the sample, and the movement of the particles is measured by laser Doppler velocimetry (LDV).[237]

For Zeta potential measurement, approximately 0.005 - 0.0065 g of silica/silicate was added to 10 mL of deionised water, and sonicated to make a stable cloudy white suspension. The solution was then injected to disposable, folded capillary cells. Initial pH measurement of the silica was taken before base (NaOH) was added to the solution to reach pH 10-11, and then auto-titrated to pH 2 with HCl, while measuring zeta potential. Zeta potential was measured using Malvern ZetaSizer nano ZS.

2.5.3 Brunaeur-Emmett-Teller (BET) measurement

Principle behind BET measurement

Surface area and pore size are commonly determined by using a BET isotherm.[238] A BET isotherm assumes the formation of a multilayer of adsorbed molecules rather just one layer as in the Langmuir approach. The BET model assumes that the adsorption of the first monolayer has a characteristic heat of adsorption, but the subsequent layers are controlled by heat of condensation. The adsorbate most commonly employed for BET surface area and pore size determination is nitrogen (0.162 nm^2 effective area per molecule at 77K). If the surface measured is porous, then there will be a pressure difference between adsorption and desorption process due to capillary condensation in pores. If the pressure in the capillaries is lower than normal saturation vapour pressure, condensation can happen at lower partial vapour pressure. The difference between the adsorption and desorption pressure (pore filling pressure) can be used to calculate pore size.

Method

For each BET measurement, approximately 0.1 g of silica/silicates were required for each sample. BET was measured using Micromeritics FlowSorb II 2300. Approximately 0.1 g of silica/silicates were charged into U-shaped tubes and accurately weighed. The tubes were placed in 120 °C oven for 1 hour to ensure all adsorbed water had evaporated. The tube was then placed in the holder and degassed for 20 minutes before being placed in liquid N_2 to measure adsorption. The amount of N_2 adsorbed relates to the voltage reading of the system,

and hence the surface area can be read as volts in the voltmeter, a reading of 10 mV equals to surface area of 1 m^2.

2.5.4 Infrared Spectroscopy

Infrared spectrophotometry is based on the interaction of infrared radiation with matter. In this study, mid infrared, approximately 4000-400 cm^{-1} is used to investigate the vibrations of the molecules. For IR to work, the molecules must have a change in dipole moment, which rules out symmetric diatomic molecules such as N_2, O_2, and H_2. Solid samples can be loaded directly using attenuated total reflectance (ATR) mode or made into transparent discs using KBr as the carrier in Fourier transform infrared (FTIR) mode.

KBr was purified by recrystallizing in boiling distilled water (1 mL/g).[239] The crystals were then separated using Buchner filtration, washed in 95% EtOH, followed by Et_2O. After drying in air, KBr was dried in 115 °C oven for 1 hour, pulverised and dried in a drying pistol at 130 °C under vacuum for 4 hours. The resulting KBr powder was free from bands usually associated with C-O stretch of ethanol at around 1100 cm^{-1} that allows investigation on possible sulfate bands at 1104 cm^{-1}.

All the IR spectra were taken using FTIR mode, with approximately 10 mg of sample to 2 - 3 g of KBr powder made into discs, using PerkinElmer Spectrum One FTIR spectrometer. Measuring IR spectra via ATR mode was also trialled, but discontinued due to inability to pick up some of the smaller peaks.

2.5.5 Scanning Electron Microscopy

Principle behind Scanning Electron Microscopy

In a scanning electron microscope (SEM), an electron beam is used instead of optical light.[240] When the electron beam irradiates the sample, the beam interacts with electrons from various depths/areas in the sample, yielding a variety of information depending on the area from which electrons are detected/analysed (Figure 2.2).
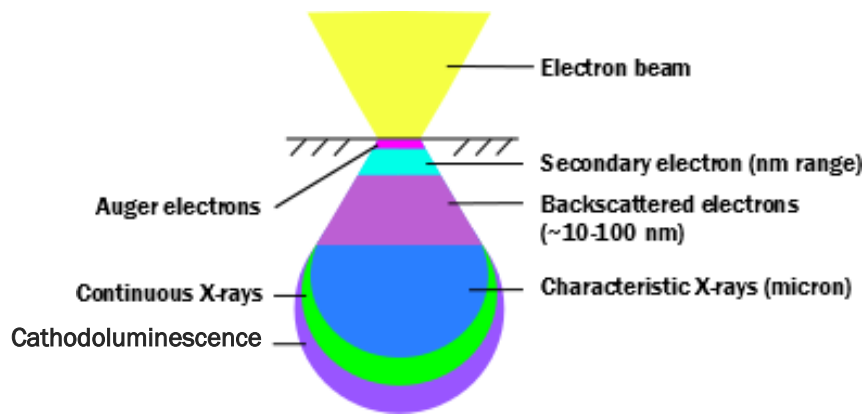
Figure 2.2. Illustration showing the regions from where information from SEM is produced. Adapted from JEOL.

In SEM, secondary electrons, back scattered electrons and characteristic X-ray data are commonly detected and analysed. Secondary electrons are emitted in all directions, and tend to have low energy (< 50 eV). Secondary electrons allow investigation of morphology of the surface. Images collected using secondary electron are commonly known as Secondary Electron Images (SEI).

Backscattered electrons have higher energy than secondary electrons (up to 30 KeV), and hence carry information from deeper layers of the specimen surface. Backscattered electrons depend largely on the specimen composition, they also vary in their amount and direction with surface topography, crystallinity and magnetism of the sample. The generation region on the backscattered electrons is larger than secondary electrons, and hence the spatial resolution is poorer. The combination of backscattered electrons and surface topography gives a composition image (COMPO) when backscatter electron detectors are used. A COMPO image shows a contrast based on the mean atomic number of the elements in the sample, with heavier elements in lighter colour. This feature is useful when the sample consists of elements of very different atomic numbers.

X-Ray spectroscopy can also be collected on SEMs. When the sample is irradiated with an electron beam, electrons from the inner shell are ejected, and vacancies formed. As outer shell electrons transfer to the vacancies, they release energy in the form of an electromagnetic wave in the X-ray region. The X-rays generated by these electron transfers are characteristic of the

51

element, and elemental compositions can be generated from collected these images. EDS (energy dispersion spectroscopy) is a method of analysing these characteristic X-rays where a semiconductor detector is used to detect the energy of the incident X-rays.   The different types of images generated can be seen on Figure 2.3 which showed the same area using SEI, COMPO, and EDS (showing Fe as green and Si as red).
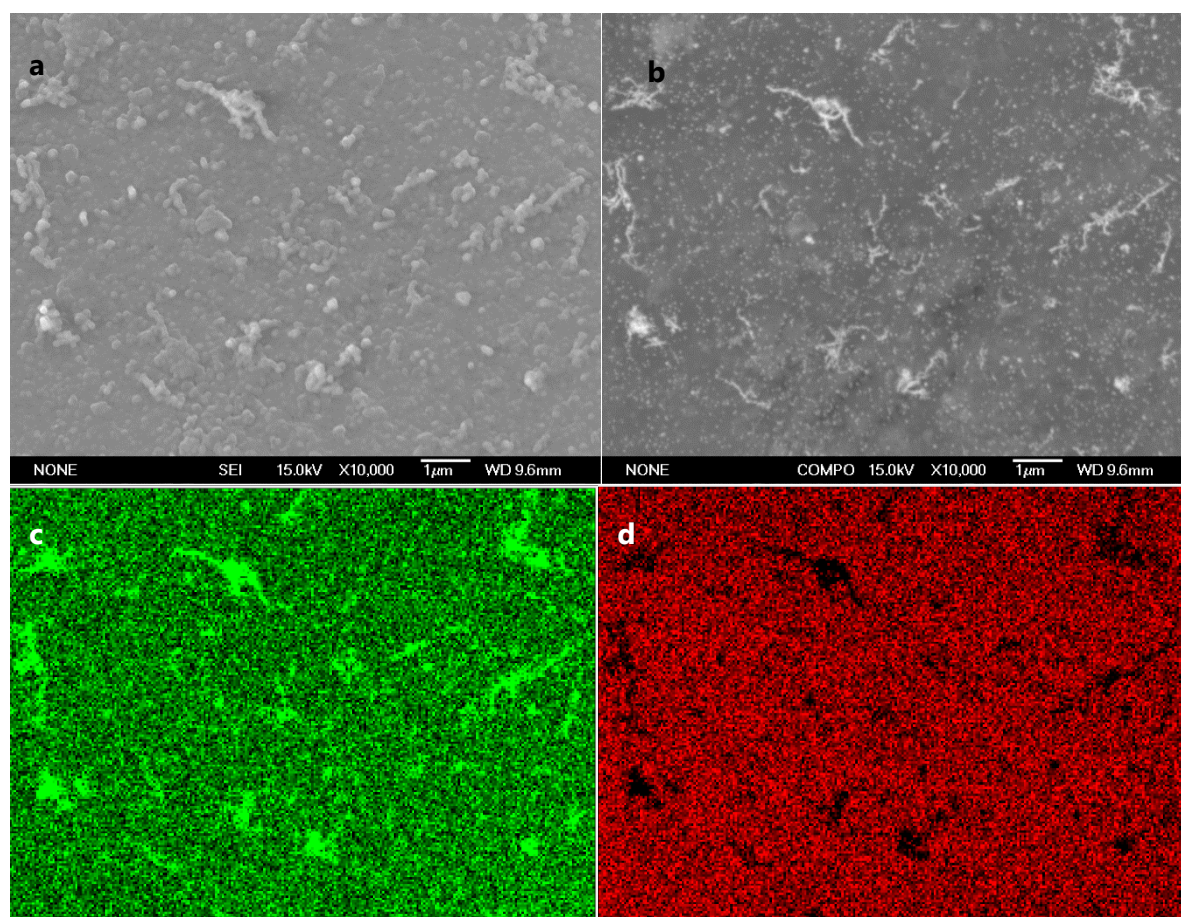
Figure 2.3. Comparison of the three types of imaging from SEM. The sample is iron on silica, magnified x10,000. (a) secondary electron image (SEI), (b) backscattered electron (COMPO), EDS showing presence of iron (c) and silicon (d).

<u>Method</u>

All SEM images were taken under high vacuum with JEOL 6500F SEM. The probe current used was either 15 kV (SEI only) or 20 kV (SEI and EDS). Working distance used was 9-10 mm. Samples were loaded on carbon tape placed on an 1 cm aluminium stub, vacuum dried for at least 6 hours before being coated with 7-9 nm carbon using Quorum Q150T E carbon coater prior to use.

2.5.6 X-Ray powder diffraction

Principle behind X-Ray powder diffraction (XRD)

XRD is mainly used to identify compounds by their diffraction pattern.[241,242] In X-ray diffractometer, a monochromatic beam of radiation is used to yield information about *d* spacing and intensities from a single crystal or crystalline powder.

XRD is based on Bragg's Law. When a beam of monochromatic X-rays falls onto a crystal lattice, a diffracted beam will only result in certain direction due to the periodic arrangement of atoms in a lattice. When all the waves emitted by all atoms lying in a single plane are in phase, and the scattering of the waves by successive planes are also in phase, the x-ray will be diffracted. The spaces between the planes are referred to as *d* spacing. As the x-ray is diffracted on the same angle it arrived on sample, the angle between the incident x-ray and scattering planes (θ) can be measured, and relationship between *d* spacing, θ, and the wavelength of the incident ray used can be expressed as Bragg's law: $n\lambda = 2d\sin\theta$. X-ray diffractometers measure the intensity and the angle of the diffraction. As in EDS, these intensity and angles are characteristic to each element/compound.

Method

XRD were taken of pulverised samples using PANalytical X'Pert PRO diffractometer. Samples were loaded to a specialised stainless steel holder, and the samples compacted down to achieve a smooth surface. The X-Ray source is a CuKα tube operating at 40 mA current and 45 kV voltage with a PIXcel detector. Scans were determined in the region of 5 - 70° with 0.013° step. The peaks were identified using HighScore software provided by PANalytical. This identification was also confirmed through RRUFF.info site that provides a complete set of identification (Raman, IR, and XRD) of minerals. RRUFF.info is a mineralogy database maintained by University of Arkansas.[243] The comparison spectra in XRD images were obtained from RRUFF.info, with the RRUFF ID given for each spectra.

2.5.7 Thermogravimetric analysis

Principle behind thermogravimetric analysis (TGA)

TGA is a technique in which the mass of a substance is monitored as a function of temperature and/or time as the substance is subjected to a controlled change in temperature. The loss/gain of mass can usually be attributed to loss of water or solvent, decomposition, oxidation, pyrolysis, and in organic matter, decarboxylation and loss of plasticiser. A TGA unit usually has temperature range up to 1000 °C.[244]

Method

TGA were conducted using a TGA-50H from Shimadzu. Approximately 10-20 mg of sample was placed in a platinum crucible, and the crucible was then placed in a hang-down pan. The temperature increment was set at 10 °C/minute with a holding temperature at 120, 400, and 600 °C for 15 minutes. The atmosphere was either dry air or N_2, with flow rate of 100 mL/min.

3 Determining the Role of Surface Modification on nZVI adsorption on Misi.

3.1 Introduction

In this chapter, the methodology developed to increase the adsorption of nZVI onto naturally occurring microsilicate Misi is described. The results of the surface treatments on nZVI adsorption were also explored. Preliminary result from the candidate's Honors' year project showed that nZVI was unevenly adsorbed by untreated Misi with a significant proportion of nZVI forming aggregates (Figure 3.1). However, on close inspection of the SEM images, it was observed that some nZVI had adsorbed onto the Misi surface in contrast to other materials where adsorption was not observed. Thus it was postulated that adsorption could be improved by subjecting Misi to a number of different treatments. Before discussing the different modifications performed, the chemistry and characterisation of raw Misi needed to be defined.
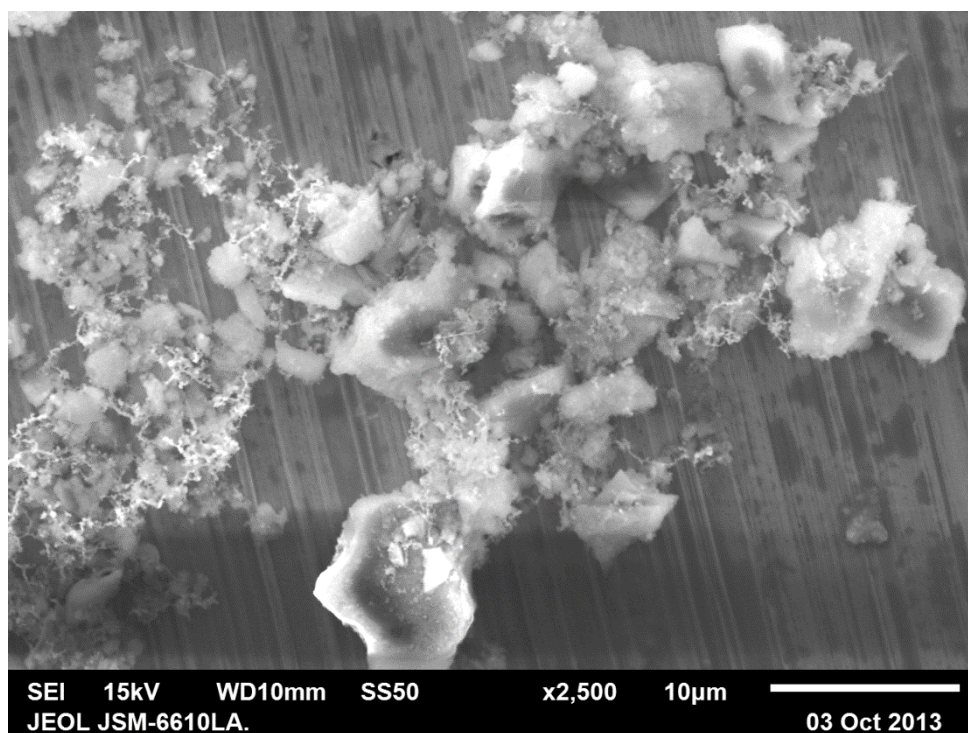
Figure 3.1. SEM image of adsorption of nZVI on raw Misi.

3.2 Characterisation of raw Misi

Misi is a naturally occurring geothermal silicate sold by the Golden Bay Cement Company and is used a cement additive. It has pozzolanic properties in which the reactive silicate or aluminium silicates will form cementitious material upon reaction with calcium hydroxide.[245]

During the production of Misi, there is a strict adherence of specification to NZ Standards NZS 3122:1995-Specification for Portland and Blended Cements, which are primarily concerned with SO_3 content (< 1.0%), mass loss on ignition (< 6.0%), SiO_2 content (min 85%), particle size (max 10% > 45μm) and pozzolanic activity (min 85%).[245] The reported composition of Misi showed that Misi consists primarily of SiO_2 and Al_2O_3, with a trace amount of TiO_2, K_2O , Fe_2O_3, CaO, Na_2O (Table 3.1). The composition of Misi has small permutations between batches and presumably testing facilities. The elemental compositions of silicates were listed as their elemental oxides (i.e. K_2O). However, no information is given as to the speciation of the elements.   Table 3.2 lists the analysis as provided by Golden Bay Cement for the size of Misi particles, which showed that at least 84% of Misi particles were below 5 μm, and all of them were below 100 μm. Though important, these two sets of data were not enough to provide a complete picture on the surface chemistry and properties of Misi, and hence further analysis in the form of XRD, SEM, IR, zeta potential, and surface area measurements were performed.

Table 3.1. Elemental composition of Misi.

Composition		
Oxide	% Mass according to Golden Bay	% Mass according to CRL (independent testing)
SiO_2	87.99	86.22
Al_2O_3	4.31	4.93
TiO_2	1.16	0.69
Fe_2O_3	0.59	0.46
K_2O	0.49	0.66
CaO	0.32	0.30
Na_2O	0.14	0.19
SO_3	0.13	0.03
P_2O_5	0.05	0.04
MnO	0.03	0.02
MgO	<0.02	0.08

Table 3.2. Particle size of Misi 600 according to Golden Bay Cement

Particle Size	
Micron	%Passing
100	100
50	99.6
20	97.9
10	94.5
5	84.6
2	55.6
1	35.0
0.4	12.2

3.2.1 XRD analysis

XRD analysis was used for determining the mineral speciation of silicates.[246,247] The XRD analysis on raw Misi revealed that the main components were two phases of crystalline SiO_2, quartz and cristobalite (Figure 3.2). The broad hump at 2Θ between 20° - 30° suggested that raw Misi also contained an amorphous silicate phase. Aside from quartz and cristobalite, there were a number of unassigned peaks. As Misi was a composite, not all of the mineral species can be identified.
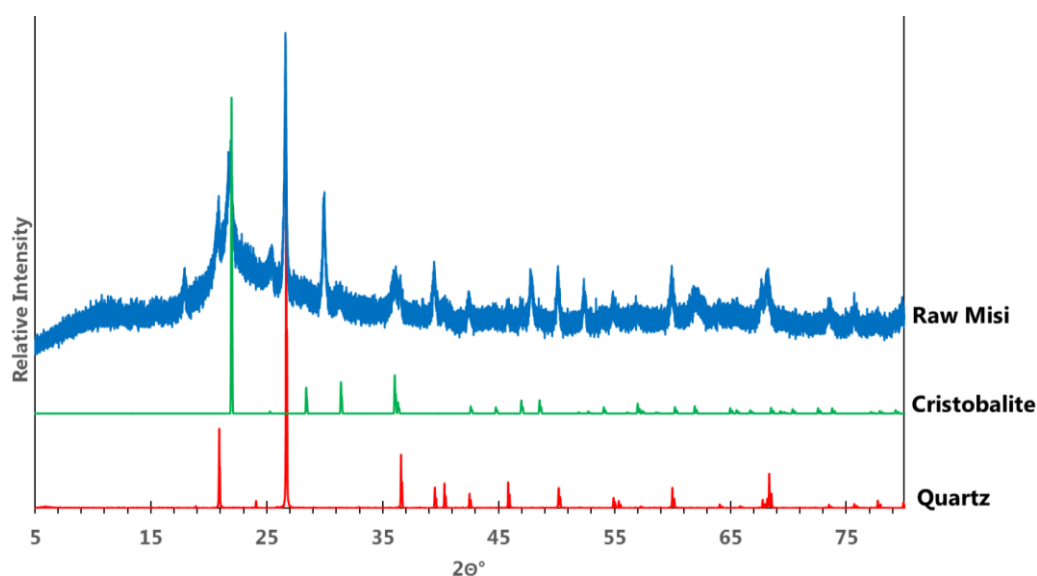
Figure 3.2. Powder X-Ray diffraction of Raw Misi overlaid with quartz (RRUFF ID#R040031) and cristobalite (RRUFF ID#061107)

3.2.2 SEM analysis

Raw Misi was analysed using SEM and EDS to examine the morphology of the Misi and elemental distribution on raw Misi surfaces. The images showed raw Misi as having heterogeneous sizes and shapes. EDS mapping on raw Misi (Figure 3.3) showed an even distribution of aluminium and silicon. Although this suggested the presence of aluminosilicate, this material was not detected by XRD, potentially due to its amorphous nature. Titanium was unevenly dispersed on the silicate. Although detected in much lower amounts, iron and sulfur were both evenly dispersed. Other elements investigated were below detection limits and could not be distinguished from noise.
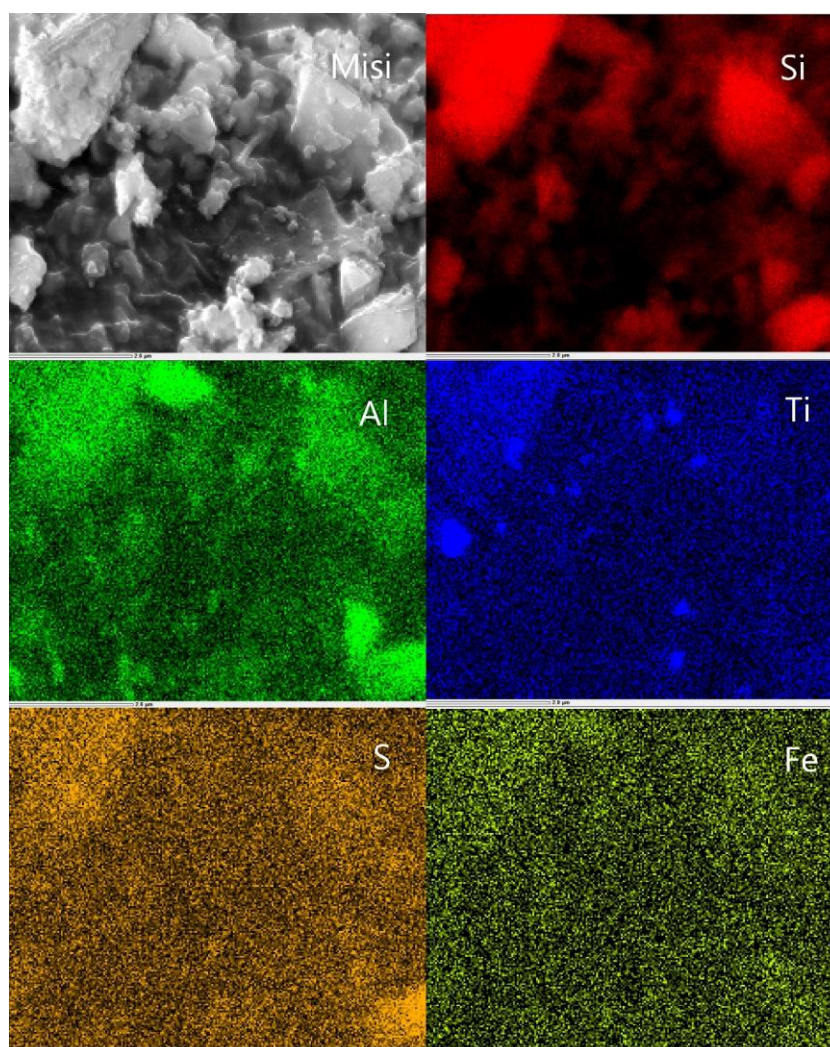
Figure 3.3. EDS mapping of Raw Misi (20,000x magnification) showing density of an element from the same sample.

3.2.3 IR spectroscopy

IR spectroscopy was used to further examine the surface of raw Misi (Figure 3.4). A very strong siloxane Si-O-Si band was found at 1096 cm^{-1}. This overlapped with Si-O-metal stretches at around 900-950 cm^{-1} and therefore the presence of bonds between silica and other metals could not be confirmed using this technique. The bands at 797 and 698 cm^{-1} were consistent with the Si-O bend of cristobalite.[248,249] A band associated with a surface-bound water bend was found at 1628 cm^{-1}. The broad bands between 3000 - 3750 cm^{-1} corresponded to hydroxy functionalities, potentially due to a combination of vicinal, geminal, and isolated silanols, along with adsorbed water stretching. The typical assignments of silicon related peaks were listed in Table 3.3.
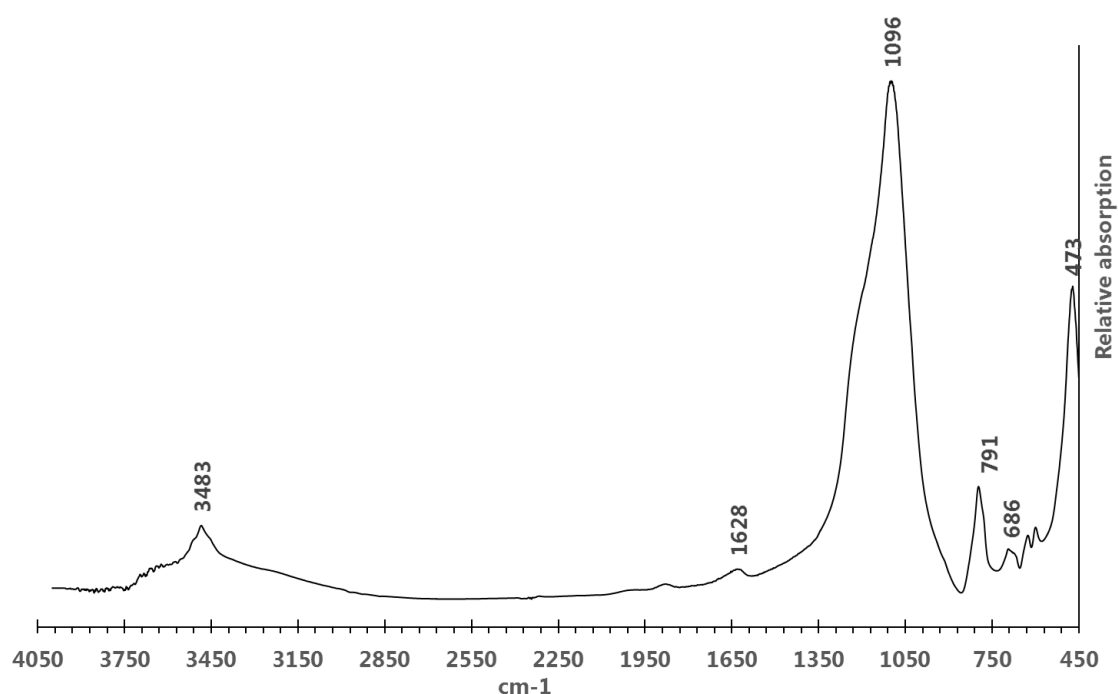
Figure 3.4. IR absorption spectra of raw Misi

Table 3.3. Typical assignment of Si-O related peaks in IR spectroscopy

Wavenumber (cm⁻¹)	Assignment	Mode	Notes (and reference)
3750	Si-OH	ν_a	Isolated silanols [249]
3650-3660	Si-OH	ν	Vicinal silanols [249]
3450, 1630	H-OH	ν,δ	Adsorbed water [249]
1200, 795, 620	Si-O-Si		Si-O-Si for Cristobalite [248]
1170, 800, 780	Si-O-Si		Si-O-Si for α-Quartz [248]
1100-1080	Si-O-Si	ν_a	network Si-O-Si, angle ~144° [248]
1035	Si-O-Si	ν_a	silicon suboxide, angle <144° [250]
1000-900	Si-O-metal		Silanolates, strong band. [248]
990	Si-O	ν_a	HSi-O-SiH [250]
950-810	Si-OH		Si-OH compounds [248]
925	Si-O-Ti		Strong band [248]
850-760	Si-O-Si	δ	In plane bending [217]
430	Si-O-Si	δ	In plane bending [250]

Mode: ν= stretching; δ= bending; a= asymmetric, s= symmetric

3.2.4 Surface area analysis

The surface area and pore sizes of a solid material play important roles when the material is used as an adsorbent.[251] The difference in surface area and pore size after a particular treatment indicated chemical and physical changes to the material. The surface area of raw Misi as determined by BET was 17.53 (± 0.04) m^2/g, with pore size of 161 Å. The surface area was similar to natural platelet clay kaolinites, which range from 10 - 20 m^2/g, and much lower than sepiolites, a type of fibrous silicate, at 300 m^2/g.[252] The pore size fell in the mesopore range (pore size between 10 - 500 Å)[253] typical of silica and alumina.

3.2.5 Zeta potential measurement

Zeta potential measures the surface charge of particles in a colloid. If the surface charges of nZVI and Misi were opposite, then the adsorption of nZVI onto Misi might be favoured. Silica surfaces can be either be negatively charged (silanoxy) or neutral (silanol, siloxane). In contrast, silicates can have a range of zeta potential from negative value as found in sodium

saturated montmorillonite (from pH 2-10) to positive value as observed in aluminium-saturated montmorillonite (at pH <7).[225]

The pH of raw Misi in DI-H$_2$O was 6.27 (650 ppm), and the zeta potential remained negative (-50 to -10 mV) between pH 1.5 to 12. Attempts were made to measure the zeta potential of nZVI, but as our equipment was unable to measure zeta potential under nitrogen atmosphere, nZVI was oxidised and the zeta measurements were not reliable. A positive zeta potential had been reported for nZVI for pH less than 8.1.[254]

3.3 Surface modifications of Misi

A change in the surface of silicate, both chemically and physically, can alter its ability to adsorb various materials.[214,217,251,255] Chemically, a surface can be modified to contain more active sites where adsorption can occur or to eliminate sites that hinder adsorption. Physically, the surface area can be increased by creating rougher surfaces, which might provide more adsorption sites or create more pores to act as anchoring sites. Based on several studies performed by other groups, a number of different treatments were performed to modify the surface of Misi, as well as silica (Chapter 4) and other silicates (Chapter 5)   As there were multiple treatments conducted, the naming convention of the samples was as follows: first was the type of silica/silicates, and then, in order, the treatment conducted on the samples.

The treatments (and different variables of each) applied were:

1. *Calcination*: uncalcined (**uC**), calcined at 400 °C (**C400**), calcined at 600 °C (**C600**)
2. *Acid wash*: 5.6 M HCl (**5**), 2.8 M HCl (**2**), 1.1 M HCl (**1**)
3. *Activation* by boiling: Activated (**A**), non-activated (**nA**)
4. *FeOOH coating*: Layer present (**F**), not present (**nF**)

So, for example, Misi-uC-AF-nZVI referred to Microsilica 600 that was not calcined, but activated by boiling in water for 2 hr, had a layer of FeOOH added to it, and then nZVI was synthesised on this pre-prepared silica via sodium borohydride reduction. SS-C600-5-nAnF was synthetic silica that had been calcined at 600 °C, washed in 5.6 M HCl, not activated and had no FeOOH layer, and nZVI had not been adsorbed onto it (see Chapter 4). The reasoning and the results of each step is discussed in the next section.

3.3.1 Calcination

3.3.1.1 Determination of calcination temperature

Calcination is the easiest way to alter a silicate surface, as the activity and presence of silanols are dependent on temperature, and these silanol groups regulate the reactivity of silicate surfaces.[211] At 120 °C, all physically adsorbed water is removed. At 200 °C, the strongly held monolayer of water is removed, leaving mostly isolated silanols and some bridged (vicinal) silanols (Figure 3.5).[211,251] At 200 °C, the dehydration reaction is still reversible, meaning water can be easily re-adsorbed onto the surface. At 400 – 500 °C, all vicinal silanols are removed leaving only isolated silanols. Silica with only isolated silanols have stronger adsorption sites, as isolated silanols are highly acidic and therefore reactive. The stronger sites are undesirable in chromatography as it will change retention times, but may prove useful in the adsorption of iron nanoparticles. After calcination at 400 °C, silica can still be slowly rehydrated. Above 600 °C, isolated silanols are progressively removed, and rehydration is very difficult and by 1200 °C, dehydroxylation is complete and irreversible, rendering the silica surface hydrophobic as only siloxane remains on the surface.
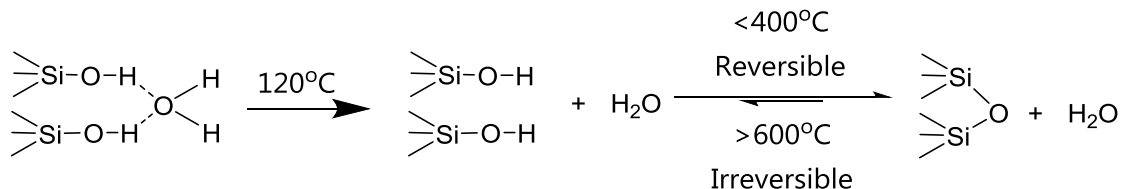
Figure 3.5. Dehydration and dehydroxylation of a silica surface.

Most synthetic silica and silicates require calcination after formation to remove their organic template.[205,212,256] Natural silicates are usually not calcined prior to their usage as adsorbents, although they are calcined prior to use as pozzolans.[257] Calcination can also be used as a method to create more pores. For instance, calcination of amino-propyl functionalised synthetic silica at 600 °C had created pores on an otherwise smooth silica spheres (see section 4.3).[214]

TGA was performed on Misi to determine the optimal temperature for calcination. Two major region of mass loss were observed, the first one beginning at 210 °C and ending at 345 °C, and the second one from 500 °C to 600 °C Figure 3.6).   From this data, two calcination temperatures were chosen, the first one to fall in between the two major loss areas at 400 °C, and the second one at 600 °C, which was at the lower threshold of irreversible dehydroxylation. Calcination at 600 °C was also chosen to ensure that there were no phase change for α-quartz or cristobalite, the two main components in Misi, which can happen at 1000 °C.[258]

The mass loss was slightly greater when TGA analysis was performed under nitrogen atmosphere. During both experiments, the temperature was held constant at 120 °, 400 ° and 600 °C to ensure complete removal of water and hydroxy groups.
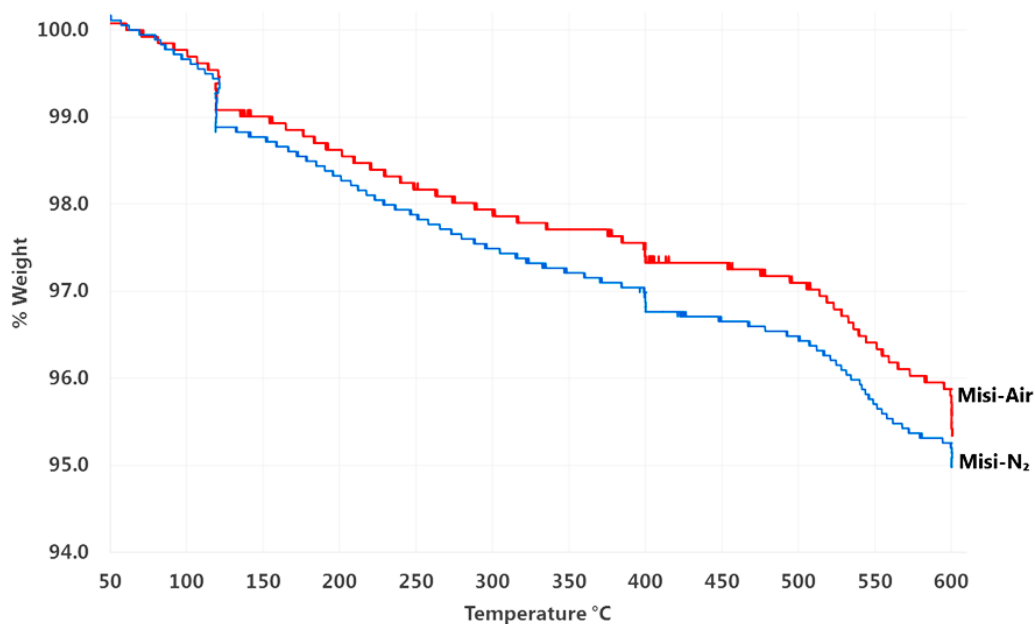
Figure 3.6. TGA results of Misi, conducted under both dry air and nitrogen atmosphere. At 120°, 400° and 600° C the temperature was held constant for 10 minutes to ensure complete removal of water and hydroxy groups.

3.3.1.2 Effect of calcination on Misi

Calcination of Misi at 600 °C resulted in a noticeable colour change (Figure 3.7). The resulting material had a stronger pinkish hue compared to the creamy colour of the uncalcined Misi. The reason for this colour change was not determined

Figure 3.7. Change of Misi colour observed, left before calcination, right after calcination at 600 °C.

The surface area of Misi decreased upon calcination to 600 °C, from 17.53 m^2/g to 11.66 m^2/g. Calcination at 400 °C did not produce a significant change in surface area (17.42 m^2/g). The data suggested a collapse and coalescence of the silicate structure at 600 °C; however this could not be detected in SEM analysis of the material. Figure 3.8 showed the SEMs of raw Misi, Misi C400, and Misi C600. As shown in these images, the structure of the silicate had not visibly changed.
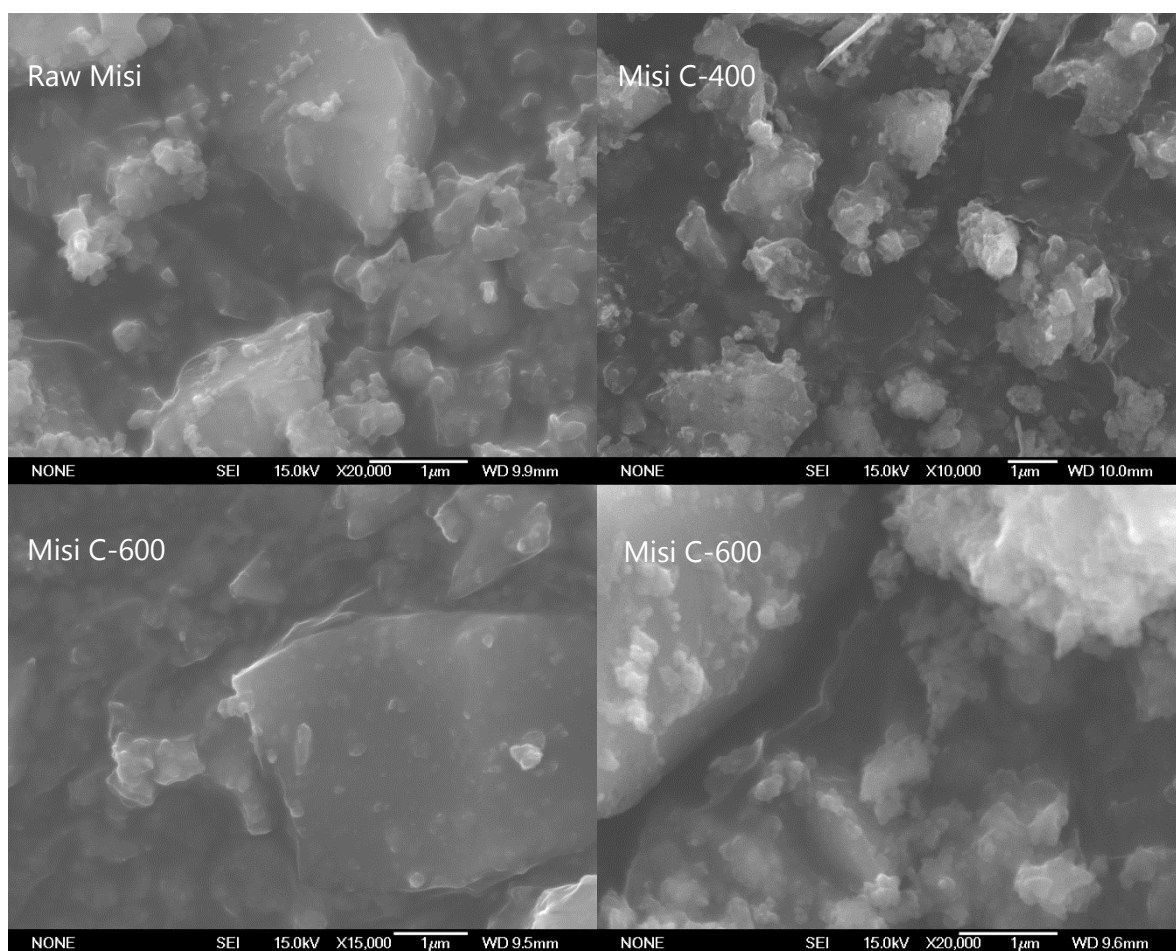
Figure 3.8. SEM images of raw and calcined Misi.

IR spectroscopy was used to determine changes in the surface of Misi after calcination. In these experiments, a 1:50 mass ratio of Misi to KBr was used to ensure consistency between the IR samples. The IR spectra of Misi calcined at 400°C and raw Misi were similar, while the IR spectrum of Misi calcined at 600°C showed a more marked difference (Figure 3.9). The broad band of water and silanol at 3750 - 3000 cm^{-1} remained when Misi is calcined at 400 °C and disappeared when Misi is calcined at 600 °C, indicating that the hydroxy groups were still present at 400 °C. The major Si-O band at 1099 cm^{-1} decreased in intensity upon calcination at 600 °C compared to the uncalcined Misi. The bands at 693, 621 and 599 cm^{-1} were not present when Misi was calcined at 600 °C. The assignment of these bands were still unknown, as they did not correspond to standard silicate bands.
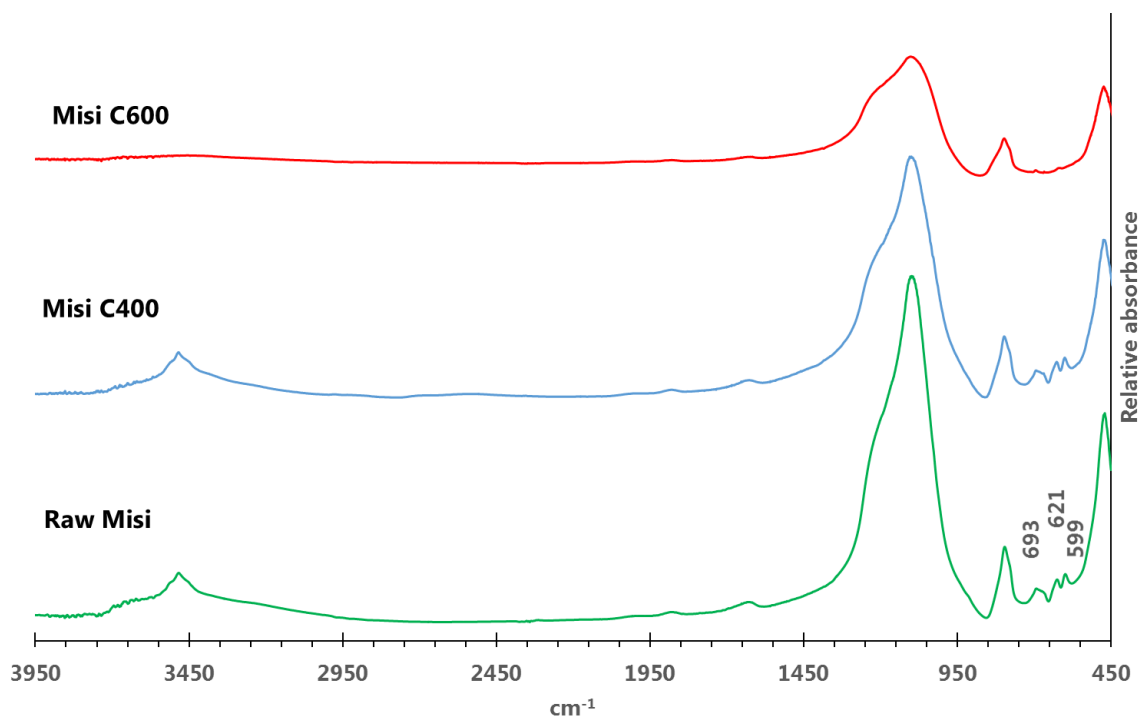
Figure 3.9. IR Spectra of uncalcined and calcined (C400 and C600) Misi. The spectra were obtained using the same KBr: Misi ratio.

XRD was also used to investigate changes to Misi after calcination. Similar to their IR spectra, there were no noticeable change in XRD spectra between raw Misi and Misi C400; however peaks at 2Θ 25.4, 29.9, 47.9 and 52.4° did not appear in the XRD of Misi C600 (Figure 3.10). These peak matched with greigite (Fe_3S_4), a naturally occurring iron sulfide mineral with a spinel structure.[12] Greigite has a cubic crystal system, and typically has very fine-grained crystals. Greigite can be found in hydrothermal veins and are formed by magnetotactic and sulfate-reducing bacteria.[88] It is isostructural with Fe_3O_4 (magnetite) and, like magnetite, is strongly magnetic. Upon heating to 585°C in air, greigite is transformed into hematite (α-Fe_2O_3) (eq. 18).[260]

$$2Fe_3S_4 + 12^1/_2O_2 \xrightarrow{585^oC} 3\alpha Fe_2O_3 + 8SO_2(g) \quad (18)$$
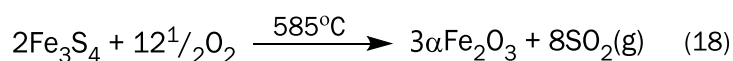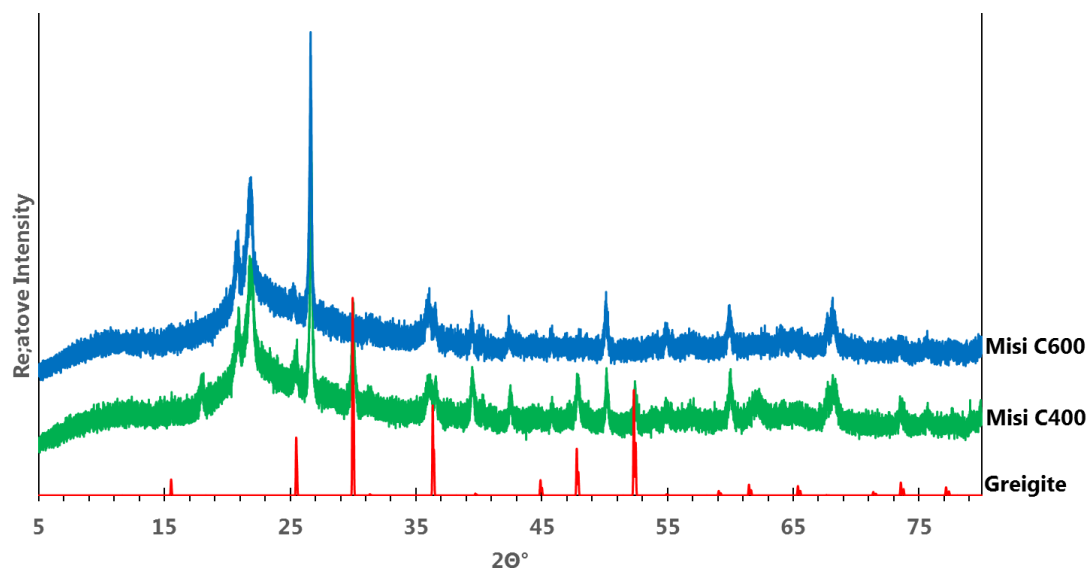
Figure 3.10. Powder X-Ray diffraction spectra of raw Misi and calcined Misi at 400 °C and 600 °C with greigite (RRUFF ID R120103)

Since Misi is a product of geothermal sedimentation, then it is possible that Misi contains greigite. However the expected hematite product (α-Fe_2O_3) was not detected in the final product (2Θ of 24.1, 33.2, 35.6, 49.5, 54.1, 64.0 and 64.2°). This was potentially due to hematite being non-crystalline, thus not observable (Figure 3.11).
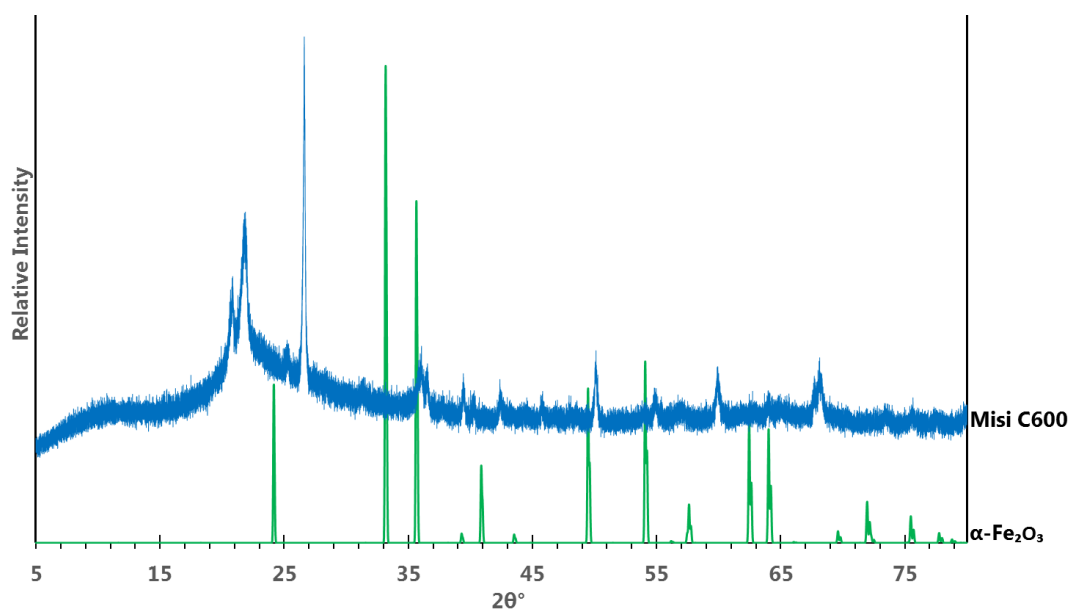
Figure 3.11. Powder X-Ray diffraction spectra of Misi C600 compared to α-Fe_2O_3 (RRUFF ID: R110013)

When greigite is heated in limited supply of oxygen, the product is not hematite but magnetite (Fe_3O_4). In the absence of oxygen the product is magnetite and pyyrhotite ($Fe_{1-x}S$; x=0-0.2).[261] Unfortunately the XRD spectrum of raw Misi calcined at 600°C in N_2 did not show either magnetite or pyyrhotite peaks (Figure 3.12).
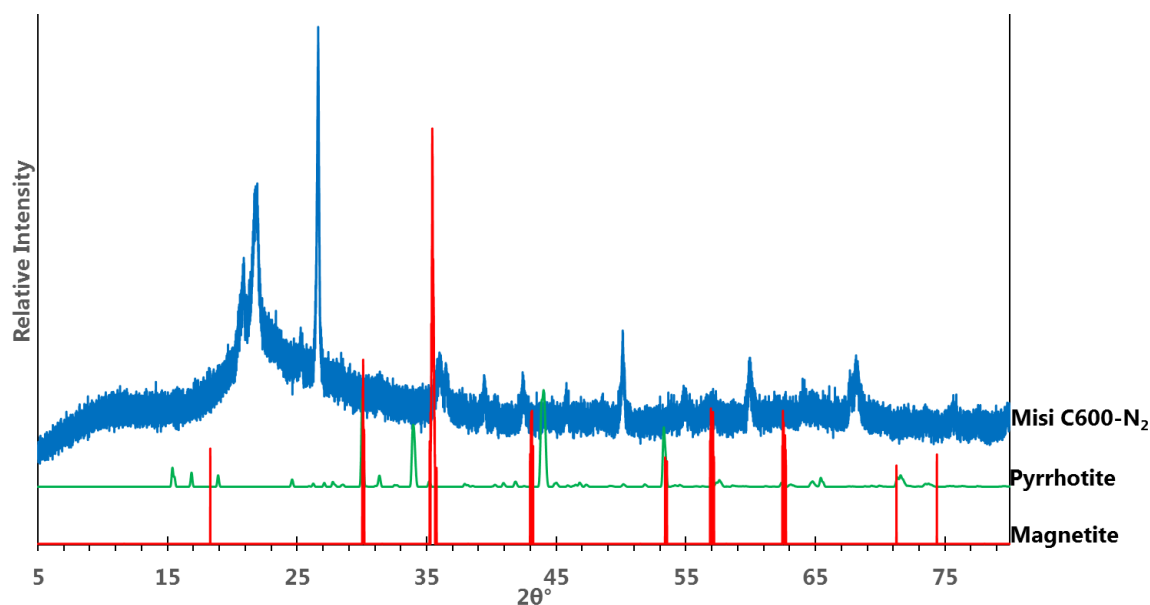
Figure 3.12. Powder X-Ray diffraction of Misi C600-N$_2$ compared to pyrrhotite (RRUFF ID: R061127.9) and magnetite (RRUFF ID: R080025).

Calcination was also associated with weight loss in the samples. To investigate this, raw Misi was calcined using three different instruments: normal programmable oven, tube furnace and TGA. In the normal programmable oven, typically three crucibles of the same material (approximately 5 g each) were calcined at the same time under normal air. Using the tube furnace, only one sample could be calcined at a time, at around 1 g per sample, under 99.999% N_2 atmosphere. In TGA, the sample size was approximately 20 mg, and the atmosphere could be either dry air or O_2-free N_2, both from a gas cylinder.

In the oven, calcination at 400 °C (C400) resulted in a 2.48 % loss in weight, while calcination at 600°C (C600) resulted in 5.45 % loss (Table 3.4). When Misi was calcined at 600 °C in the tube furnace under N_2, the weight loss increased to 6.0 % (Table 3.5). These results were similar to the TGA analysis (Figure 3.6). The weight loss was not significantly larger when it was

calcined under N_2, but the trend for both methods was similar in that raw Misi calcined under N_2 had larger weight loss.

Table 3.4. Weight loss after calcination in oven at different temperature

Atmosphere	Temperature (°C)	% weight loss	Standard deviation
Air	400	2.48	0.03
	600	5.45	0.05
N_2	600	6.0	0.6

Table 3.5. Percentage weight loss for Misi at 400°C and 600°C based on TGA

Atmosphere	% Weight lost at 400°C	% Weight lost at 600°C
Dry air	2.60	4.66
N_2	3.24	5.02

3.3.2 Acid washing

Washing Misi in strong acid could modify its surface both physically and chemically. In chromatography, silica gel is sometimes washed in acid to remove any trace metals as well as metal oxide impurities. [251] Similar to silica gel, acid washing of silicates (or sometimes referred to as acid activation) had been used to remove some metal sulfide (e.g. FeS, PbS), [262] and dissolved any metal that was not bound tightly to the silicate structure. In their use as adsorbent, pillared clay such as montmorillonite and bentonite were often activated in acid to increase their adsorbent capacity.[263] This hydrothermal acid activation increased the surface area of the clay, possibly due to the release of finely dispersed SiO_2 from the mineral system, removal of amorphous aluminium or other silica components, and the creation and filling of cracks, pores and voids.

Chemically, acid activation of clay (an aluminosilicate) also increased the number of weak acidic surface functional groups whilst decreasing the number of strongly acidic ones (pKa ≈ 4).[264] A strongly acidic surface functional group could come from positively charged $Al(OH)_x$, while the weakly acidic surface functional groups were typically the result of formation of amorphous silica as the mineral structure was destroyed. The change of balance between

strongly acidic and weakly acidic surface functional groups could be due to removal of amorphous aluminium and the release of amorphous silica from the structure respectively.

As Misi was sourced from geothermal precipitations, and may contain various types of metal sulfide, for example PbS, ZnS, FeS, [265] acid washing might help to modify Misi surface. In this project, three different concentration of acid (HCl) were used: 5.6 M, 2.8 M and 1.1 M. The washing time was 30 minutes and no heat was applied. Misi was washed prior to calcination for 2.8 M and 1.1M HCl, and either before or after calcination for the 5.6M HCl.
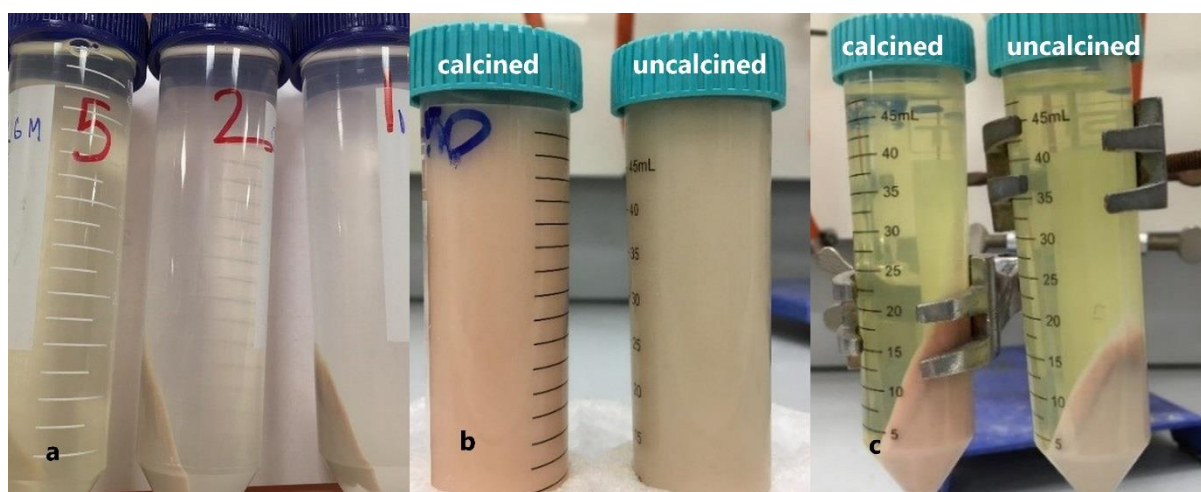
Figure 3.13. Acid washed Misi. On (a) colour of filtrate after washing at 3 different acid concentration. (b) & (c) Misi washed in 5.6 M HCl. (b): after acid was added, (c) after centrifuge. On (b & c), the tube on the left held pre-calcined Misi (C600) while the right held uncalcined Misi (uC).

It had been reported that upon acid treatment of metal sulfide impurities, sulfides were lost as H_2S,[265] the presence of which were difficult to detect unless by olfactory sensation or with a GC-MS unit attached to the heating unit. Thus, H_2S was not measured for our system. However, the liquor from washing with 5.6 M HCl was noticeably yellow whilst liquor from 2.8 M and 1.1 M HCl were almost colourless (Figure 3.13). The only metal analysed for in the AA spectroscopy was iron.[266] The elemental analysis of raw Misi suggested that it contained 3.9 mg of iron per gram of sample. When an aliquot of the filtered solution (5.6 M) was analysed using atomic adsorption spectroscopy (AAS), it was found that the solution contained 640 μg Fe per gram of Misi washed. Whether acid washing was done before or after calcination, the

amount of iron removed was similar (610 µg and 640 µg respectively). Thus, acid washing did not remove all of the iron. The XRD spectra (Figure 3.14) showed acid washing did not eliminate the potential greigite peaks However, greigite has only been reported to dissolve in hot 9M HCl over the course of 20 hours, thus should not be removed after washing in 5.6 M HCl at room temperature for 30 minutes.[259]
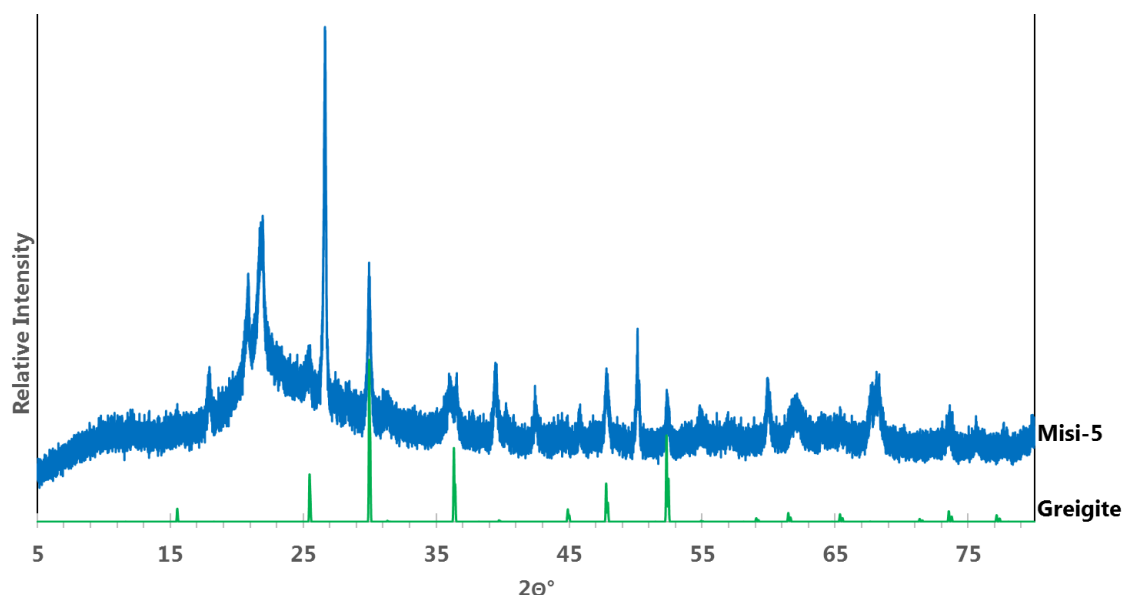
Figure 3.14. Powder X-Ray diffraction of Mis-5 (acid washed) and greigite (RRUFF ID R120103)

Washing with 5.6 M acid reduced the surface area of raw Misi to 14.92 m^2/g from 17.53 m^2/g (Table 3.6).   This was in contrast to acid treatment (10M HCl) of silica gel in which the surface was reported to stay the same.[267]   However, the surface area of various acid treated clays such as bentonite, biotite, kaolin and vermiculite increased by as much as 3.5 times (5M HCl, r.t., 2 weeks).[268] These reported results correspond to the metal content of each system: silica gel has less than 0.04 % metal impurities, while clay contains varying degree of metal, from 0.2 % (kaolin) to 2.8 % in biotite.

Table 3.6. Specific surface area of acid washed Misi

Silicate	Surface Area (m^2/g)
Raw Misi	17.53 (± 0.04)
Misi 5	14.92 (± 0.07)
Misi 5-C400	18.9 (± 0.6)
Misi 5-C600	17.1 (± 0.2)

72
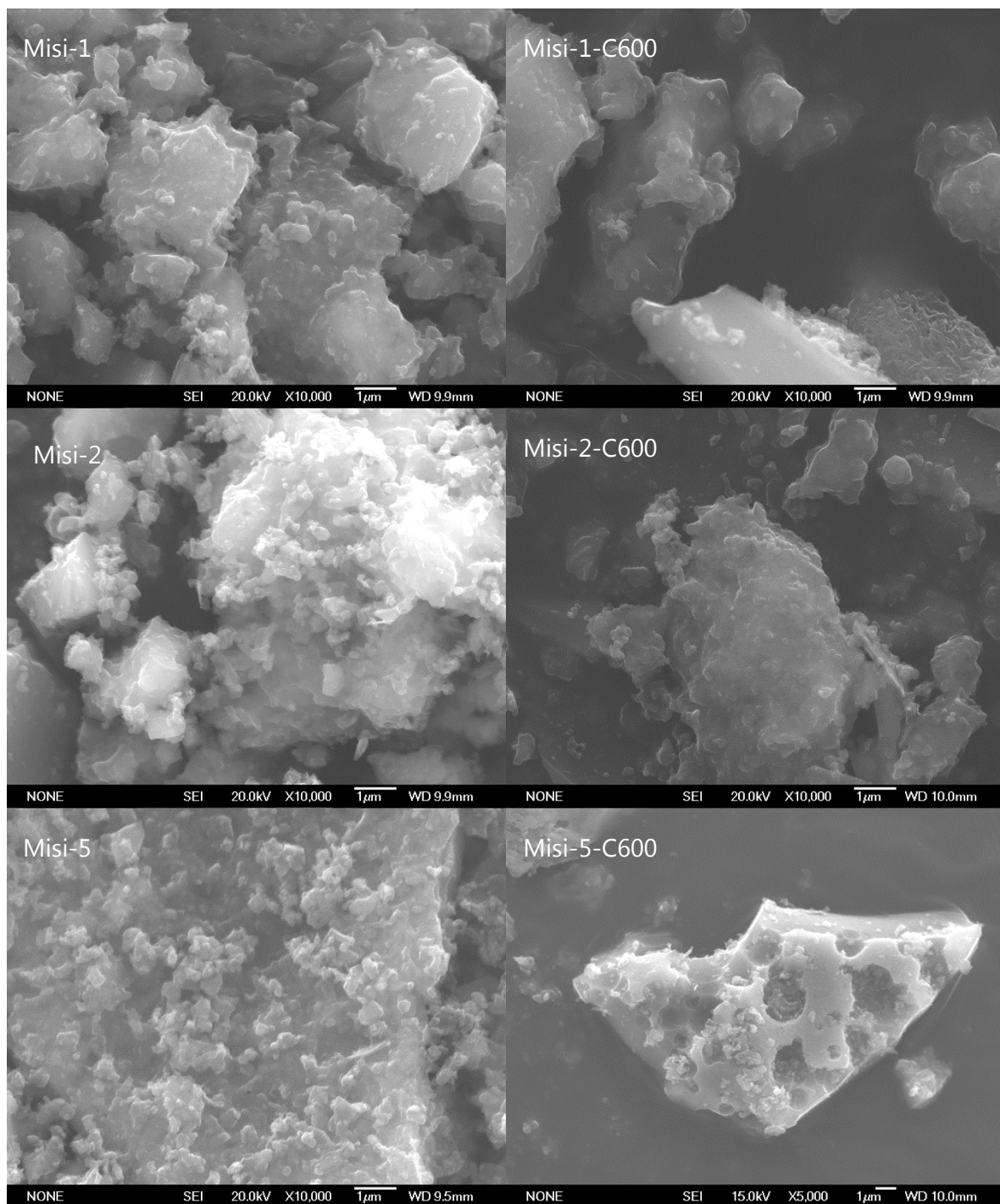
Figure 3.15. Effect of acid wash and calcination on Misi surface

When the calcination was conducted after acid wash, the surface area increased again, especially when calcined at 400 °C. SEM analysis to the acid washed Misi revealed that pits were formed on the surface upon exposure to 5.6 M HCl. No visible changes were observed upon acid washing with either 1.1 or 2.8 M HCl (Figure 3.15).

The weight loss of Misi-5 calcined at either 400 °C or 600 °C was smaller than that of Misi (Table 3.7). As the cause of mass loss upon heating was undetermined, the identity of these species were unknown.

Table 3.7. Weight loss in calcination after acid washing

Silicate	Atmosphere	% Weight lost at 400°C	% Weight lost at 600°C
Misi	Air	2.48 (± 0.03)	5.45 (± 0.05)
Misi-5		1.0 (± 0.2)	4.5 (± 0.3)
Misi	N$_2$	-	6.0 (± 0.6)
Misi-5		-	4.8 (± 0.4)

3.3.3 Activation: regeneration of silanol functional group by boiling.

After calcination, silica and silicates lost most of their active silanol groups.[211] One of the methods used to regenerate these silanol groups was by boiling in water for two hours.[223] The IR spectra of Misi C400 and boiled Misi C400 were similar, while the Misi C600 and boiled C600 were markedly different at around 3485 cm^{-1} (Figure 3.16). The broad band around 3485 cm^{-1} for boiled Misi C600-A (boiled) suggested loosely held water rather than silanol group.
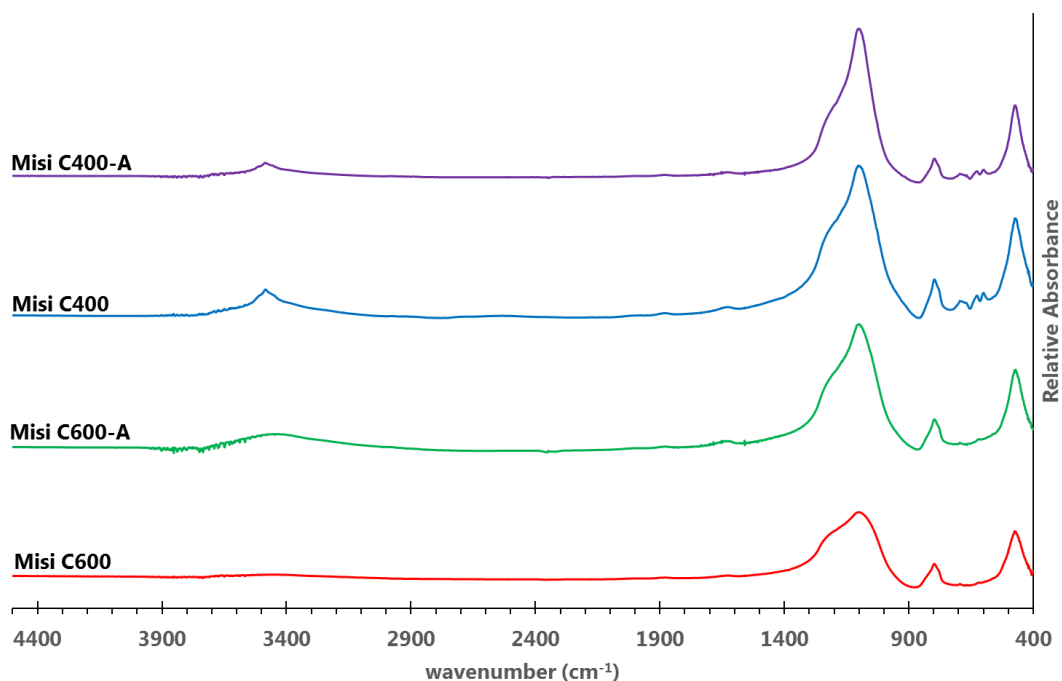
Figure 3.16. IR absorption spectra of Misi C400 and C600 before and after boiling (A)

3.3.4 FeOOH layer

Iron oxyhydroxide (FeOOH, or sometimes written as Fe(O)OH) had previously been used to chemically modify silicate surfaces to improve nZVI adsorption on the surface with some success.[223,224] FeOOH layers were usually synthesised from oxidation of Fe^{2+} salts in alkaline conditions, or hydrolisation of Fe^{3+} salts.[269–273] Upon heating in air (80 – 120 °C), $FeSO_4$ salts formed goethite (α-FeOOH) as long as there are no chloride ions present.[274,275] To help anchor FeOOH layer on mesoporous silica microspheres, polyethylene glycol (PEG) had been utilised. nZVI was then synthesised in the presence of the treated silica.[223] Using X-Ray photoelectron spectroscopy (XPS), it was reported that FeOOH surface had been created based on *2p* binding energy at 711.5 eV that indicated Fe existing as FeOOH.

In this research FeOOH was formed from soaking silicate in an iron sulfate solution, and heating the separated silicate in 120 °C oven for at least 3 hours. PEG was trialled but ultimately the synthesis proceeded without PEG due to lack of benefit, with full results and reasoning discussed in chapter 4.1.2. To determine the presence of FeOOH layer, three techniques were utilised: AAS, XRD and Raman spectroscopy.

In a typical synthesis, 100 mg of Fe in the form of $FeSO_4$ (0.5 g $FeSO_4 \cdot 7H_2O$, 98% purity) were added to each gram of Misi to form the FeOOH layer. The presence of extra iron after FeOOH layer formation was confirmed by AAS, with the increase in digestible iron from 620 μg in Misi-C600 to 7.02 mg in Misi-C600-AF.   This mean only 7% of Fe added were adsorbed onto the Misi surface prior to oxidation into FeOOH.

The XRD spectrum of Misi-C600-AF did not reveal any additional crystalline material compared to Misi C600 (Figure 3.17), Lepidocrocite (γ-FeOOH) and goethite (α-FeOOH) were shown as reference as goethite is the expected phase of FeOOH formed under this condition while lepidocrocite can often be formed from goethite under oxidation and with the presence of carbonate.[87]   The presence of either material could not be confirmed and this could be due to the relatively small amount of FeOOH compared to Misi.
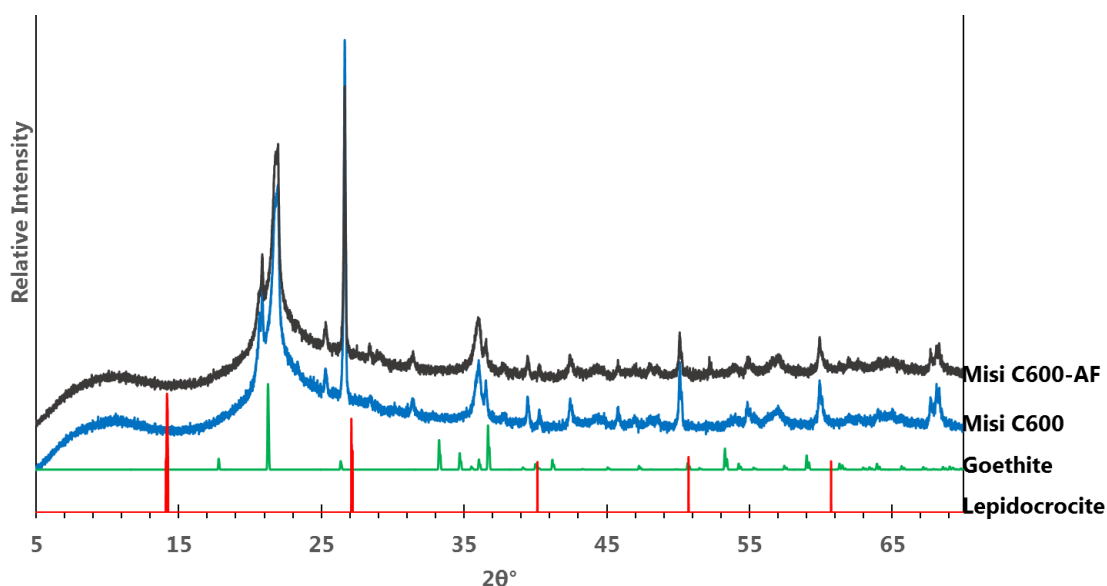
Figure 3.17. Powder X-Ray diffraction Misi C600 compared to Misi C600-AF with reference of goethite (RRUFF ID: R120086), and lepidocrocite (RRUFF ID:R050454)

As XRD could not confirm the form and phase of FeOOH present on Misi C600-AF, Raman spectroscopy was utilised for this purpose.[276–278]   Due to sample heterogeneity of Misi, a number of spots were investigated (A, B, C; Figure 3.18). The Raman spectra indicated the presence of quartz (465 cm^{-1}), and possibly goethite (387 cm^{-1}). Two major bands in Misi-C600-AF at 521 and 642 cm^{-1} had not been assigned. As the Raman spectra were too noisy

get a clear spectrum of Misi C600-AF, the form of Fe in our system could only be tentatively assigned as goethite (α-FeOOH).
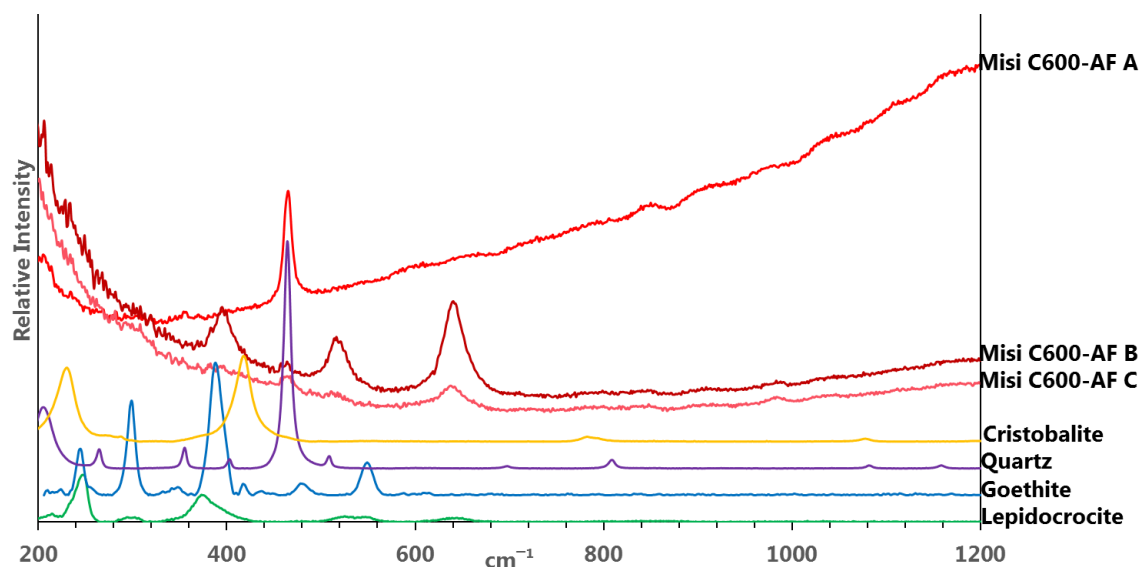
Figure 3.18. Raman spectra of Misi C600-AF with reference Raman spectra of cristobalite (RRUFF ID : R061107), quartz (RRUFF ID: R040031-M), goethite (RRUFF ID: R120086), and lepidocrocite (RRUFF ID:R050454)

Qiu *et al* stated that one of the aims of coating silica surface with FeOOH was to increase surface area of the silica to allow more nucleation sites.[223] The surface area of FeOOH-coated Misi was analysed and found to correlate with the order of treatment (Table 3.8). When the silicate had not been washed in acid, the surface area increased with FeOOH coating. However, washing in acid changed this relationship as the acid soak reduced surface area (entry 1 and 6). Calcination after acid washing increased the surface significantly (compare entry 7 and 9 to 2 and 4). The addition of FeOOH layer decreased surface area when the silica had been acid-washed. A plausible explanation was that acid washing allows access to the interior of the particles that were removed during calcination; and as silicate were coated with FeOOH the surface area was reduced due to the adsorption of FeOOH in the silicate interior.

77

Table 3.8. Surface area of treated and untreated Misi

Entry	Silicate	Surface Area (m^2/g)
1	Raw Misi	17.53 (± 0.04)
2	Misi C400	17.12 (± 0.03)
3	Misi C400-AF	17.28 (± 0.09)
4	Misi C600	16.66 (± 0.05)
5	Misi C600-AF	19.05 (± 0.04)
6	Misi 5	14.92 (± 0.07)
7	Misi 5-C400	18.9 (± 0.6)
8	Misi 5-C400-AF	17.4 (± 0.1)
9	Misi 5-C600	17.1 (± 0.2)
10	Misi 5-C600 AF	13.9 (± 0.03)
11	Misi C600-5-AF	17.36 (± 0.06)

To test the hypothesis that acid washing improved the adsorbance of Fe^{2+} prior to reduction, a known amount of Misi was washed in known concentration of Fe^{2+} **or** Fe^{3+} solutions, and left to equilibrate overnight utilising orbital shaking. A filtered aliquot was then quantified for iron content using AAS (Table 3.9). All Misi tested adsorbed more Fe^{3+} than Fe^{2+}, which was possibly due to increased preference of the silicates for the harder Fe^{3+}. Further treatments (acid washing and boiling) increased the amount of Fe^{2+} adsorbed, but no distinct trend could be observed.

Table 3.9. Percentage of Fe^{3+} and Fe^{2+} ions adsorbed by differently treated Misi using 175 ppm of Fe^{3+} and 120 ppm of Fe^{2+}.

Silica type	% of Fe^{3+} adsorbed	% of Fe^{2+} adsorbed
Raw Misi	34.4	9.9
Misi-C600	98.9	9.4
Misi-C600-A	76.2	20.2
Misi-C600-5	98.1	12.6
Misi-C600-5-A	94.5	14.5
Misi-5-C600	92.5	17.5
Misi-5-C600-A	81.3	16.4

3.4 Methods of adding nZVI to Misi

Two methods of adding nZVI to pre-treated Misi were trialled: physical adsorption and chemical reduction of Fe^{3+} or Fe^{2+} in the presence of Misi.

3.4.1 Physical adsorption

In this method, Misi was ground together with pre-synthesised nZVI. Figure 3.19 showed that the nZVI particles were unevenly dispersed on Misi particles, and the nZVI were in the form of short chains rather than discrete nano particles, indicating agglomeration. Interestingly, the XRD of the physical adsorption method (Misi-C600-FeOOH + nZVI) showed a strong Fe^0 peak at 44.55°, which were not seen when Fe^{2+} were reduced in the presence of Misi (Figure 3.20). This finding suggested that XRD analysis alone was not enough evidence of nZVI adsorption on support system. Furthermore, the lack of a strong peak suggested that nZVI adsorbed on silicate (Misi C600-AF-nZVI) had different phase or crystallinity to unsupported nZVI, although how and why it was different was unknown, possibly due the differ sizes of aggregates in the two materials. Attempts was made to calculate the full width at half maximum (FWHM) to estimate particle size; however, since the size of the identifying peak at 45° for Misi-C600-AF-nZVI was less than twice of the background noise, FWHM could not be calculated.[241]
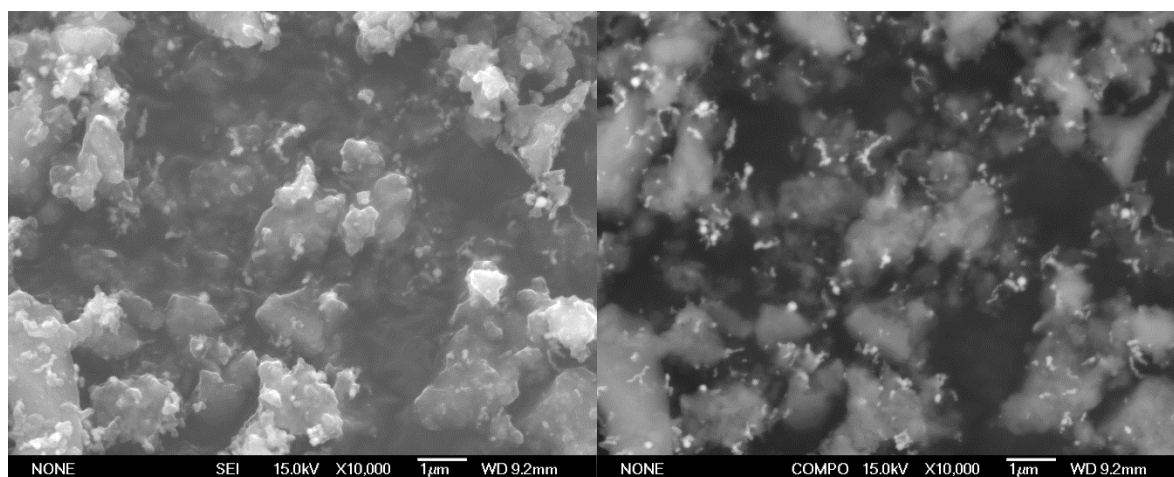

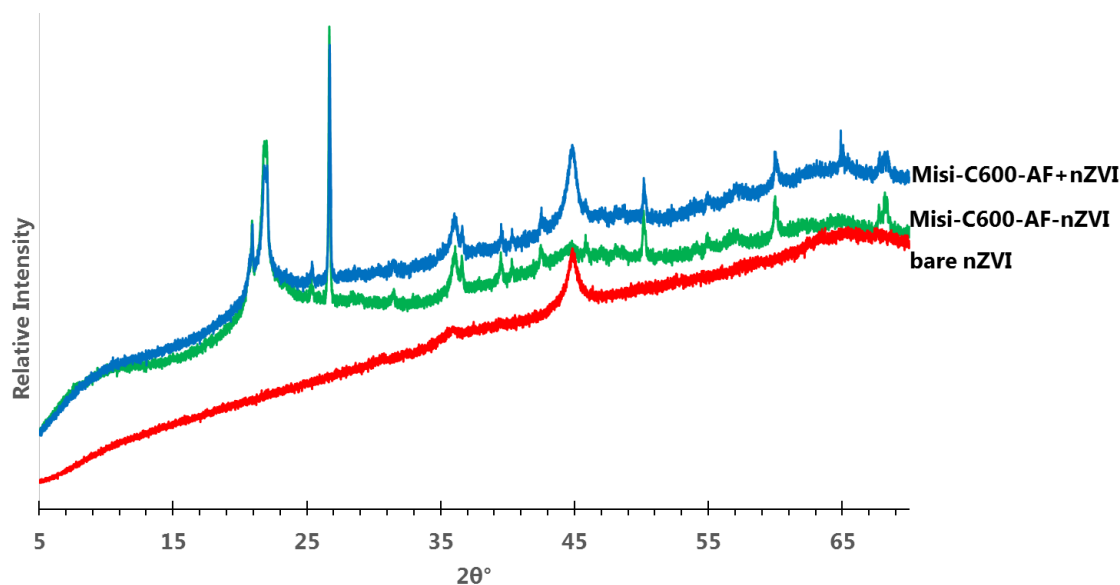*Figure 3.19. Misi-C600-FeOOH + nZVI. Left: SEI Image, Right: COMPO image*

Figure 3.20. XRD spectra of Misi C600-AF+nZVI (synthesised nZVI ground together with Misi C600-AF) and Misi C600-AF-nZVI (Fe^{2+} reduced in the presence of the support) with bare nZVI as reference

3.4.2 Reduction of adsorbed Fe^{2+} and Fe^{3+} in the presence of silicate

In this method, Fe^{2+} or Fe^{3+} were adsorbed onto Misi overnight, decanted and then re-dispersed in DI-H$_2$O. The suspension was then reduced using NaBH$_4$ solution as per normal method (section 2.3.1). Aside from trialling a new method of loading nZVI onto Misi, this method also allowed the investigation of mechanism of adsorption of nZVI onto Misi surface. There were two possible pathways: first, Fe^{2+}/Fe^{3+} in solution were reduced into nZVI and then adsorbed by silicate, or second, pre-adsorbed Fe^{2+}/Fe^{3+} was being reduced to nZVI. If the second pathway (adsorbed then reduced) was correct, then the dispersion of nZVI should be even and no agglomeration formed using this method. However, SEM images indicated that this was not the case as loose chains of nZVI could be seen from this method (Figure 3.21). For both Fe^{2+} and Fe^{3+} soaked Misi, loose chains dominated except for Misi-C600-5-A-Fe^{2+} where evenly dispersed nZVI could be seen on one of (but not all of) the Misi particles.

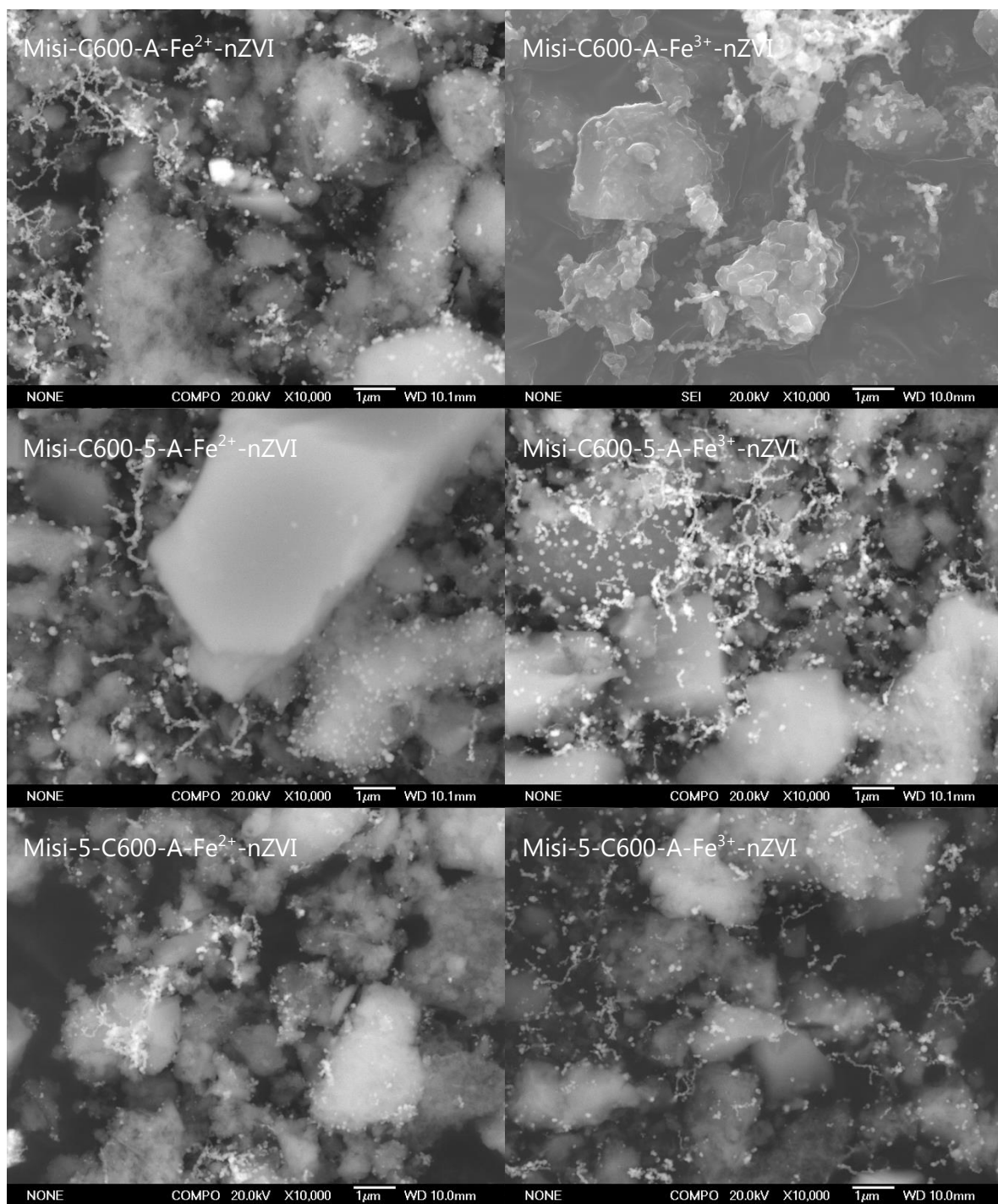*Figure 3.21. Adsorption of nZVI from adsorbed Fe^{2+} and Fe^{3+} onto different Misi surfaces.*

The result suggested that the adsorbed iron were held loosely by the silicate structure and therefore could leach out again once the silicate were dispersed in water. To eliminate the re-leaching problem, NaBH$_4$ solution was added to dry Misi C600-AF while mixing under N$_2$. SEM image showed that little to no nZVI were formed (Figure 3.22). This result might be due to the small amount of Fe^{2+} that could be adsorbed onto Misi C600-A surface (approximately 0.7 % $^w/_w$).
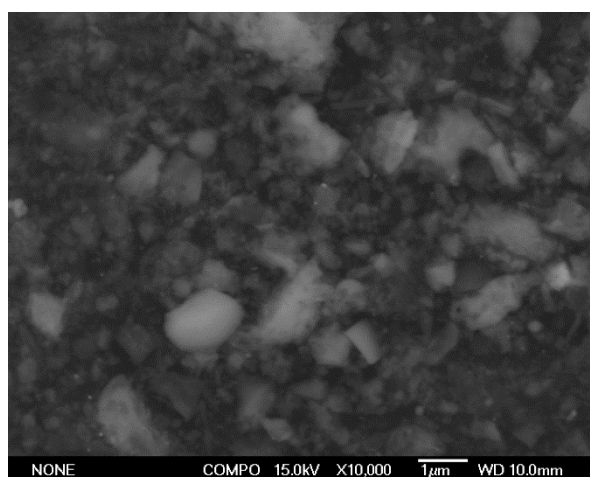
Figure 3.22. COMPO image of Misi-C600-AF-nZVI (borohydride added to dry Misi C600-AF).

3.4.3 Reduction of aqueous Fe^{2+} in the presence of silicate

The reduction of aqueous ferrous ion by a sodium borohydride solution (section 2.3.1) was the most successful method for adsorbing nZVI to silicate surface of all. The detailed result of this reduction method on nZVI adsorption on Misi described in the next section (3.5.2). All nZVI/Misi material formed by this method were typically black/dark grey (see Appendix C) except for Misi-5-uC-AF-nZVI (acid washed, uncalcined, boiled with FeOOH layer, (Appendix C, image C-a). As this method was the most successful, all nZVI-Misi mentioned after this section was made with this method.

3.5 Effect of Misi treatments on nZVI adsorption

3.5.1 Calculation of *A*-value

Several major variables were trialled to improve nZVI adsorption on Misi: calcination temperature, acid washing and strength of acid, order of calcination and acid washing, boiling, and FeOOH coating. Not all the combinations were investigated and decisions were made based on preliminary results. To analyse the adsorption of nZVI onto silicate surfaces, SEM images were taken of each sample. All of the SEM images showing nZVI adsorption were taken using the backscattered electron mode which showed heavier elements in lighter shade of grey (COMPO), unless otherwise stated. In these images, iron is white and silicon is grey. The label for each sample can found on the top corner of each images. In each figure, the difference in treatment between the images were printed in yellow or red depending on the background colour.

The measure for successful adsorption were twofold. First, a visual check that there was a good dispersion of nZVI particles on the surface of the silicates and minimal formation of nZVI aggregates that appear as chains, especially loose chains that were separate from silicate structure. Well dispersed nZVI particles indicated that nZVI had adsorbed onto the Misi surface, instead of aggregated. Second, the compo images (x10,000 magnification) were processed using Picasa and FIJI as detailed in section 2.3.3 and appendix A to yield an *A*-value (agglomeration value). The smaller *A*-value indicated small or almost no agglomeration and better dispersion of nZVI particles onto the surface of silicate.

Before the *A*-value could be calculated, a discriminant analysis was conducted with the guidance from Dr. Lisa Woods (School of Mathematics and Statistics, VUW). It should be noted that there might be an issue with the assumption of multivariate normality, but this analysis was included to illustrate how an image-classification procedure could be developed, given that the subjective nature of the image classification used in this thesis was one of the limitations of this research. A total of 65 FIJI-processed COMPO image were ranked on a scale from 1 to 5, with 1 being images where nZVI were very well dispersed with few chains, to 5 where chains dominates the image and nZVI particles were not well dispersed.   There were

four variables that were examined to determine their contribution to the agglomeration value: **Mean** (average size of particles in nm^2), **SD** (standard deviation of particle size in nm^2), **% under** (percentage of particles under 2000 nm^2, which was the observed maximum size of discrete iron nano particles in our samples), and **total count** (number of particles in each image). Many different combinations of these variables were examined in order to determine if they could predict the assigned ranking (SPSS, V.23 © IBM)

In order to be able to understand these results (Table 3.10), a brief explanation for each component is required.[279] **Wilks' λ** is a measure of how much of the variation in rating that cannot be predicted by the discriminant functions of the variables included, and hence the smaller Wilks' λ, the more accurate the prediction will be. **Chi-square** (χ^2) is a test statistic used to determine if the discriminant functions were better at predicting the image rating than chance alone. Since all of the discriminant analyses have a p of < 0.001, these variables can confidently be utilised in future research to develop a formal image classification method. **dF** refers to degree of Freedom. **Canonical correlation** is the correlation between the new canonical variables formed by the discriminant function and the dependent variable (rating). Therefore, the higher the canonical correlation the better the functions were at placing each image to the right group. With four predictor variables, three discriminant **functions** were created, each with different weighting of the predictor variables. On the last column, **% correctly classified** is the percent of images with an assigned rank matching that previously given by the researcher. A higher percentage in this column indicated high agreement between the ranking given prior to calculation and ranking given by the calculation.

Each of the entries represented the different combination of variables included in the discriminate analysis. For example, all 4 variables were included in entry 1, and only Mean and SD were included. Based on these indicators above, entry 1, 5 and 10 had the best Wilks' λ, canonical correlation and % correctly classified included in entry 6.

Entry 1 had much lower % correctly classified than Entry 5 and 10, and thus discarded. Entry 5 was slightly better on both Wilks' λ and canonical correlation, and thus used to calculate *A*-value, with the Mean variables not included in the analysis.

Table 3.10. Discriminate analysis by variables included

Entry	Variables included				Wilks' λ	Chi-Square	dF	Canonical correlation	p	% correctly classified
	Mean	SD	%under	Total Count						
1	✓	✓	✓	✓	0.326	66.767	16	0.802	<0.001	53.8
2	✓	✓	✓		0.379	58.194	12	0.778	<0.001	52.3
3	✓	✓		✓	0.347	63.586	12	0.795	<0.001	58.5
4	✓		✓	✓	0.479	44.117	12	0.698	<0.001	56.9
5		✓	✓	✓	0.350	62.926	12	0.792	<0.001	60.0
6	✓	✓			0.403	54.937	8	0.770	<0.001	43.1
7	✓		✓		0.564	34.698	8	0.651	<0.001	50.8
8	✓			✓	0.515	40.120	8	0.680	<0.001	58.5
9		✓	✓		0.407	54.390	8	0.767	<0.001	47.7
10		✓		✓	0.355	62.581	8	0.791	<0.001	60.0
11			✓	✓	0.594	31.548	8	0.619	<0.001	56.9

Table 3.11 presented the standardized discriminant function coefficients for the discriminant analysis including SD, %under and Total Count as predictors. Each discriminant function combined the different independent variables, with different loadings of each variables. For example, function 1 had a high positive loading of SD, and negative loading of Total Count.

Table 3.11. Standarised Canonical Discriminant Function Coefficients

	Function		
	1	2	3
% under	.089	.073	1.217
SD (nm²)	.978	.406	.610
Total Count	-.393	.918	-.072

Table 3.12 showed the three functions at the group centroids. Function 1 was able to clearly differentiate the different rankings, while the other functions, for example function 2 showed no discriminating ability between the different rankings (Figure 3.23). Reclassification of cases based on the new canonical variables was successful: 60.0 % of the cases were correctly reclassified into their original categories. As there were no samples excluded from the training data set, the effectiveness of this approach on new samples could not be investigated.

Table 3.12. Function at group centroids

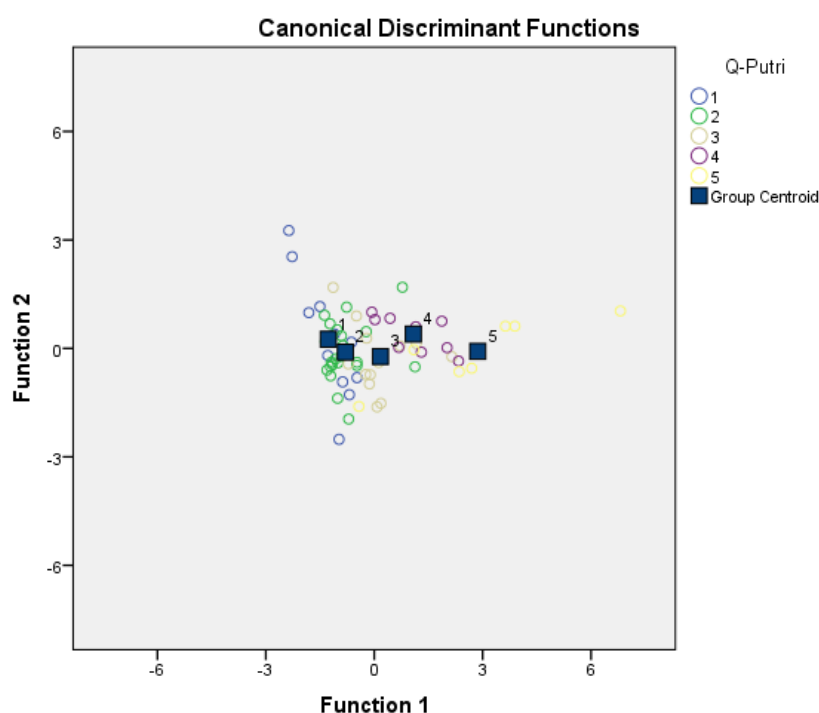| Ranking	Function		
	1	2	3
1.0	-1.271	.253	.087
2.0	-.799	-.104	.033
3.0	.172	-.226	-.116
4.0	1.081	.397	-.129
5.0	2.864	-.082	.169

Figure 3.23. Canonical discrimant functions

The formula of *A*-value was then developed based on Function 1, which yielded:

$$A\,value = \frac{(0.89 \times \%under) + (0.978 \times SD) - (0.393 * TC)}{1000}$$

The value for *A* in this project ranged from 0.28 – 5.07 with the smaller *A* number indicating better dispersity. Due to processing issues from both Picasa™ and FIJI, *A*-values could not be taken as an absolute quantitative value, but more as a relative qualitative value. These were classified in Table 3.13, and examples from each range can be found on Figure 3.24. The first

example, Misi C600-5-nAnF-nZVI (*a*) had a very even dispersion of nZVI with very minimal aggregation, and good dispersion. The next image, Misi 1-C600-nAF-nZVI (*b*) showed more aggregation (circled in yellow). Even more aggregation could be observed in the next image (Misi C400-nAF, *c*), and the particle size were more varied as well.   In the next two images, *d* and *e*, aggregation was more dominant, and more marked differences in particle sizes could also be observed.
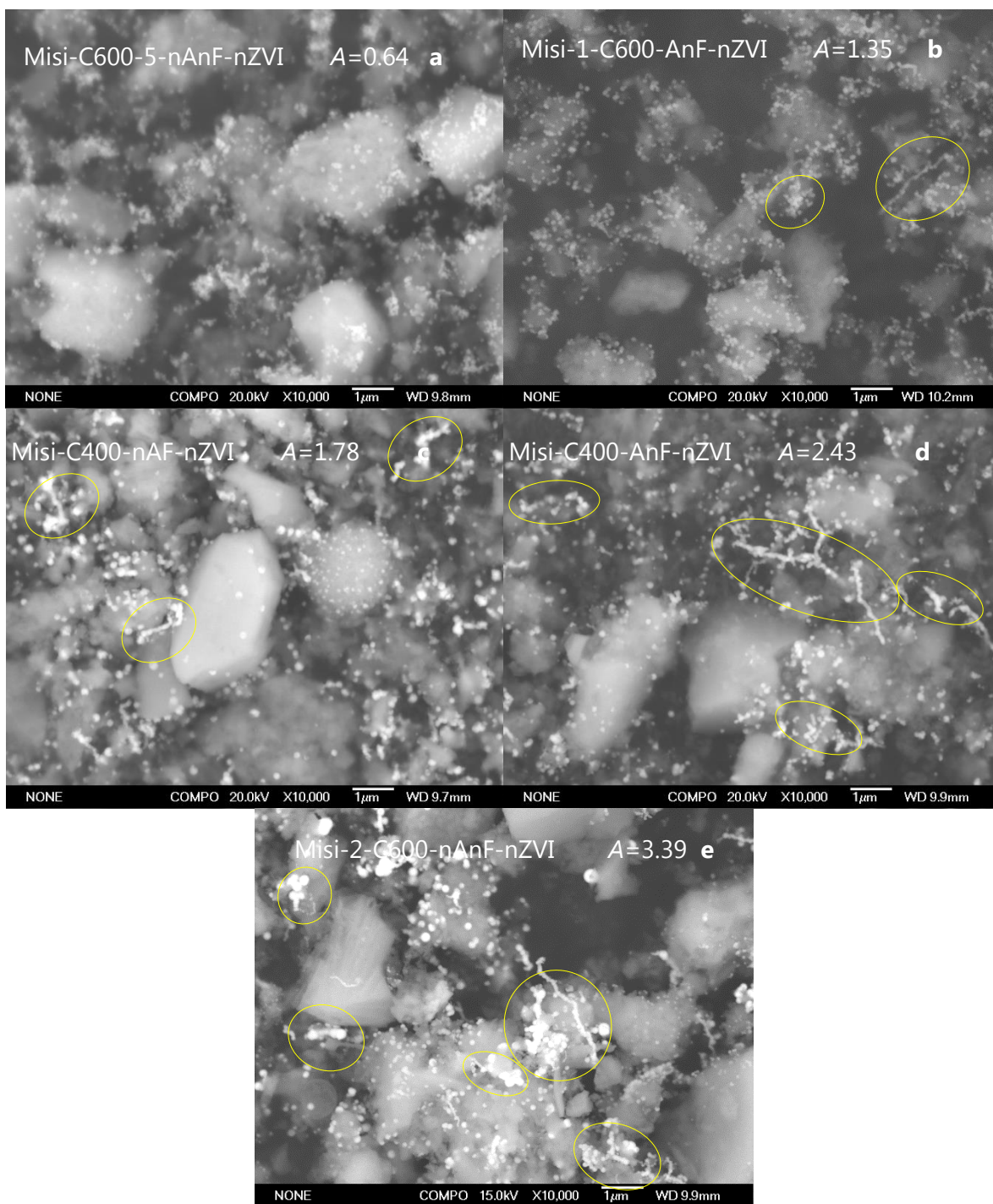
Figure 3.24. Sample image relating to each range of A-Value: a, Misi C600-nAnF-nZVII (entry 59); b, Misi 1-C600-AnF-nZVI (entry 3); c, Misi C400-nAF-nZVI (entry 50); d, Misi-C400-AnF-nZVI (entry 49); e, Misi 2-C600-nAnF-nZVI (entry 20). A-Value displayed on each image. Entry referred to Table 3.14 .

Table 3.13. Description of A-value range

Range of *A*-value	Description
<0.75	Well dispersed with minimal aggregation
0.76-1.50	Well dispersed with some chain
1.51-2.25	A mixture of well dispersed and obvious chains
2.25-3.00	Chains dominate the image
>3.01	Mostly chains

3.5.2 *A*-value assignments

The assignment of *A*-values revealed the heterogeneity of the system (Table 3.14). nZVI adsorption to the same system were often not reproducible as different batches sometimes showed different *A*-value, and sometimes they were similar (Figure 3.25). For instance, Misi-2-uC-nAF-nZVI (*a* and *b*) showed two similar *A*-value, at 0.73 and 0.54. On both materials, nZVI were well dispersed, and little agglomeration observed. On the other hand, Misi-2-C600-nAF-nZVI had two dissimilar *A*-values at 0.55 and 2.50 (*c* and *d*). One of the most extreme cases was between Misi C600-nAF-nZVI (*e* and *f*), where one batch was at 0.75 and the particles were well dispersed, while the next batch was one of the worst sample at 5.07, dominated by agglomeration and larger particles. This was possibly due to the heterogeneity of Misi itself, and even though all care had been taken to ensure homogeneity, batch to batch reproducibility was still an issue.

Table 3.14. List of A-Value for nZVI adsorbed on Misi surfaces. Items in blue were discussed in the text.

Entry	Name	Particle size average (nm²)	SD (nm²)	% < 2000 nm²	Total Count	*A*-value
1	1-C600-AF-nZVI	10641	10881	86.9	748	1.04
2	1-C600-AnF-nZVI 1	6314	8745	97.1	2382	0.77
3	1-C600-AnF-nZVI 2	10626	14175	87.9	1133	1.35
4	1-C600-nAF-nZVI 1	8286	10446	92.4	1190	0.98
5	1-C600-nAF-nZVI 2	7793	9581	93.4	894	0.91
6	1-C600-nAnF-nZVI 1	10236	16802	87.3	1309	1.60
7	1-C600-nAnF-nZVI 2	9820	25277	92.2	490	2.46
8	1-uC-AF-nZVI	8344	12168	92.2	708	1.17
9	1-uC-AnF-nZVI	7467	13763	92.7	1068	1.31
10	1-uC-nAF-nZVI 1	11752	22214	86.1	1001	2.14
11	1-uC-nAF-nZVI 2	7116	7903	95	988	0.74
12	1-uC-nAnF-nZVI	15593	36714	81.3	630	3.57
13	2-C600-AF-nZVI 1	10840	18782	88.7	1175	1.80
14	2-C600-AF-nZVI 2	8401	10109	92.2	1025	0.96
15	2-C600-AnF-nZVI 1	8946	10552	90	1271	0.99
16	2-C600-AnF-nZVI 2	6430	6819	95.8	1529	0.62
17	2-C600-nAF-nZVI 1	10605	25819	88.6	945	2.50
18	2-C600-nAF-nZVI 2	5650	5633	98.6	355	0.55
19	2-C600-nAnF-nZVI 1	7215	8976	94.8	1445	0.83
20	2-C600-nAnF-nZVI 2	13620	34855	85.2	656	3.39
21	2-uC-AF-nZVI 1	7500	9803	94.4	1086	0.92
22	2-uC-AF-nZVI 2	6325	6447	96.9	927	0.60
23	2-uC-AnF-nZVI	8714	13850	91.4	1322	1.31
24	2-uC-nAF-nZVI 1	7250	7646	94	744	0.73
25	2-uC-nAF-nZVI 2	4704	7869	98.2	435	0.76
26	2-uC-nAF-nZVI 3	6481	5793	96.8	910	0.54
27	2-uC-nAnF-nZVI	10090	12248	87.2	744	1.18
28	5-C600-AF-nZVI 1	5630	5457	97.7	597	0.52
29	5-C600-AF-nZVI 2	9434	14196	91.2	794	1.37
30	5-C600-AF-nZVI 3	10551	24693	91.6	559	2.40
31	5-C600-AF-nZVI-4	5262	7458	96.6	589	0.71
32	5-C600-AnF-nZVI 1	6798	9088	95.9	1339	0.84
33	5-C600-AnF-nZVI 2	7145	11911	94.3	1677	1.11
34	5-C600-AnF-nZVI 3	9044	13135	90.5	1447	1.24

Entry	Name	Particle size average (nm²)	SD (nm²)	% < 2000 nm²	Total Count	A-value
35	5-C600-nAF-nZVI 1	7063	9019	93.7	994	0.85
36	5-C600-nAF-nZVI 2	4842	5779	98	837	0.54
37	5-C600-nAF-nZVI 3	6871	6783	96.7	1045	0.63
38	5-C600-nAF-nZVI 4	5851	7305	96.4	1186	0.68
39	5-C600-nAnF-nZVI 1	6554	8895	94.6	1547	0.82
40	5-C600-nAnF-nZVI 2	4049	2890	100	196	0.28
41	5-uC-AF-nZVI	11819	27594	85.6	389	2.69
42	5-uC-AnF-nZVI	11563	21316	87.3	735	2.06
43	5-uC-nAF-nZVI	9688	12085	87.9	1103	1.15
44	5-uC-nAnF-nZVI	7042	9369	93.9	1231	0.88
45	C400-5-AF-nZVI	12463	20932	83.7	797	2.02
46	C400-5-nAF-nZVI	17336	21800	71.2	667	2.11
47	C400-5-nAnF-nZVI	7651	12026	91.6	1413	2.10
48	C400-AF-nZVI	8811	14249	92	847	1.37
49	C400-AnF-nZVI	11511	25005	88.4	673	2.43
50	C400-nAF-nZVI	9316	18475	89	875	1.78
51	C400-nAnF-nZVI	7190	6930	96.3	943	0.65
52	C600-5-AF-nZVI 1	12843	25492	86.8	403	2.49
53	C600-5-AF-nZVI 2	10320	12146	87.6	637	1.17
54	C600-5-AnF-nZVI	8645	16163	91.8	1214	1.54
55	C600-5-nAF-nZVI 1	9786	12476	88.4	406	1.21
56	C600-5-nAF-nZVI 2	5604	10679	95.9	366	1.04
57	C600-5-nAnF-nZVI 1	7906	10975	92.9	876	1.05
58	C600-5-nAnF-nZVI 2	6987	10638	93.8	844	1.02
59	C600-5-nAnF-nZVI 3	4555	6836	96.8	965	0.64
60	C600-AF-nZVI 1	9165	20776	92.7	918	2.00
61	C600-AF-nZVI 2	11421	21142	87.2	837	2.04
62	C600-AnF-nZVI	10623	18235	88.8	865	1.76
63	C600-nAF-nZVI 1	6445	7926	95.3	940	0.75
64	C600-nAF-nZVI 2	16797	51859	84.6	350	5.07
65	C600-nAnF-nZVI	5478	7655	97.1	2121	0.67

91

Figure 3.25. A-value of threesets of different batch of the same type Misi surface: a& b, Misi 2-uC-nAF-nZVI (entry 24 and 26); c & d, Misi 2-C500-nAF-nZVI (entry 18 and 17); e & f, Misi-C600-nAF-nZVI (entry 63 and 64).

Discussion

Calcination is an important step in modifying Misi surface for nZVI adsorbance. Uncalcined Misi did not adsorb nZVI when other treatment, including acid washing or addition of FeOOH coating, were applied (Figure 3.26 *a* & *b*; entry 41 and 29). However, washing Misi in more concentrated acid (5.6 M) allowed better surfaces for nZVI adsorption as long as there were no other treatments performed (Figure 3.27). Aside from generating silanols, acid washing might also create pitting on the surface of Misi that could be utilised to nucleate nZVI. However, SEI and the related COMPO image of Misi (Figure 3.28) suggested that this was not the case as an increased nZVI adsorption on the edges of the Misi surface, especially on Misi-C600-5-nAnF-nZVI was not observed.

Calcination either at 400 °C or 600 °C had similar effects on nZVI adsorption by Misi, while holding the other treatments the same (Figure 3.26 *c - f*; entry 51, 65, 45 and 53 respectively). From this, it seemed that the adsorption of Misi was not related to the presence of greigite, although it might be related to the isolated silanol groups that were generated at 400° and 600°C. Acid washing might generate weakly acidic functional groups, while calcination created isolated silanols, thus this suggested that adsorption of nZVI onto Misi surfaces was enhanced by the presence of these functional groups.

For the Misi 5-C600 series, comparison between Misi 5-C600-AF-nZVI (Figure 3.26*b*, entry 29), Misi 5-C600-nAnF (Figure 3.27 *f*, entry 40), Misi-5-C600-AnF-nZVI (Figure 3.29 *c*, entry 32), and Misi-5-C600-nAF-nZVI (Figure 3.29 *d*, entry 38) showed that in this series, boiling and FeOOH layer were not necessary for good adsorption of nZVI. For the Misi C600-5 series (entry 52-59), a similar trend could be found, as the Misi C600-5-nAnF-nZVI had much better adsorption of nZVI compared to the AF, and AnF treated Misi C600-5 (Figure 3.24*a*, Figure 3.26*f*, and Figure 3.29*a* respectively). The nAF treatment however resulted in worse adsorption in some cases (see entry 55 and 56). It was plausible that the combination of acid wash and calcination was enough to create good adsorption sites through the creation of isolated silanol sites.
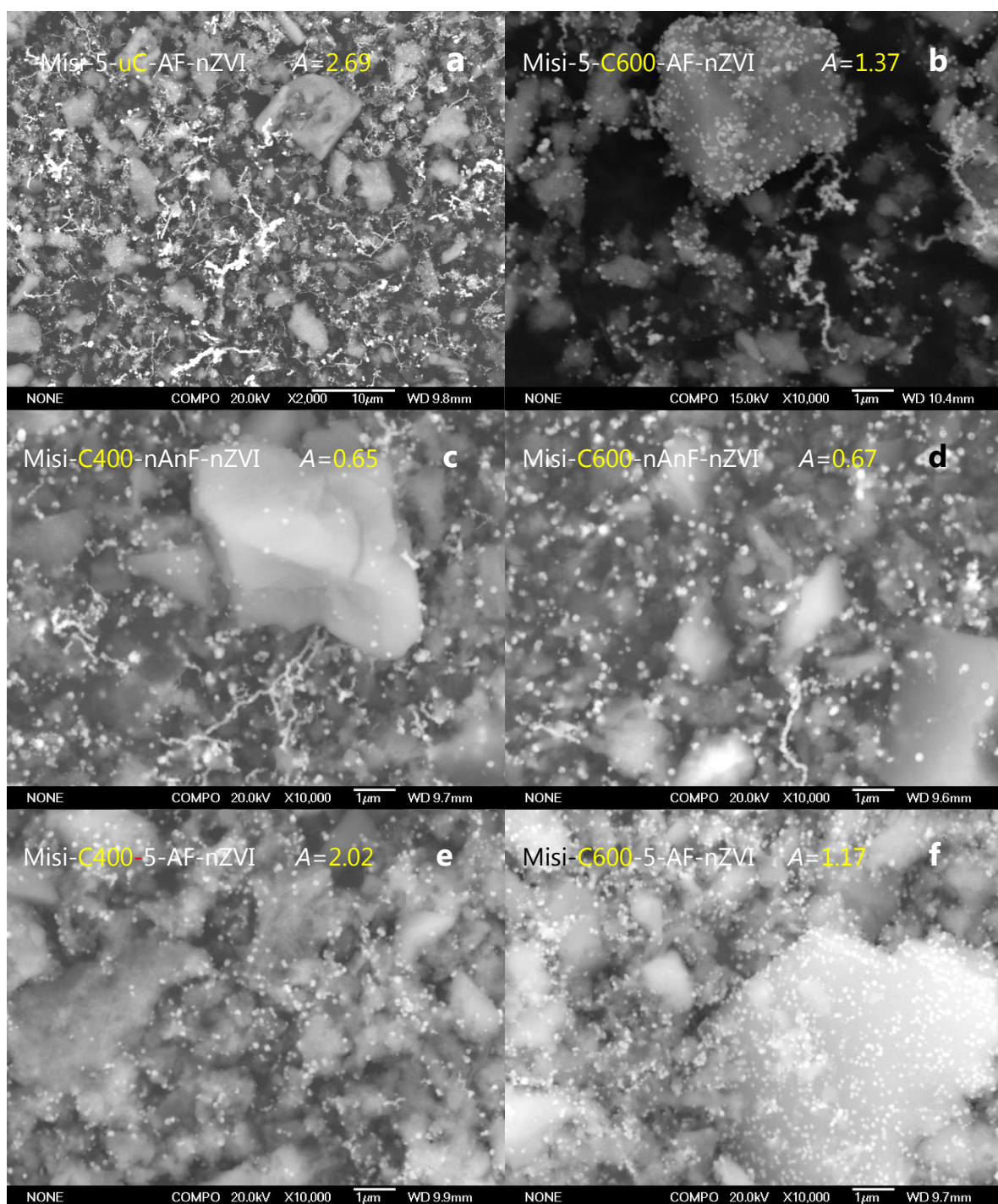
Figure 3.26. Effect of calcination and calcination temperature on adsorption of nZVI on Misi 5-AF and nAnF: a, Misi-5-uC-AF-nZVI (entry 41); b, Misi-5-C600-AF-nZVI (entry 29); c, Misi C400-nAnF-nZVI (entry 51); d, Misi-C600-nAnF-nZVI (entry 65); e, Misi C400-5-AF-nZVI (entry 45); f, Misi-C600-5-AF-nZVI (entry 53)
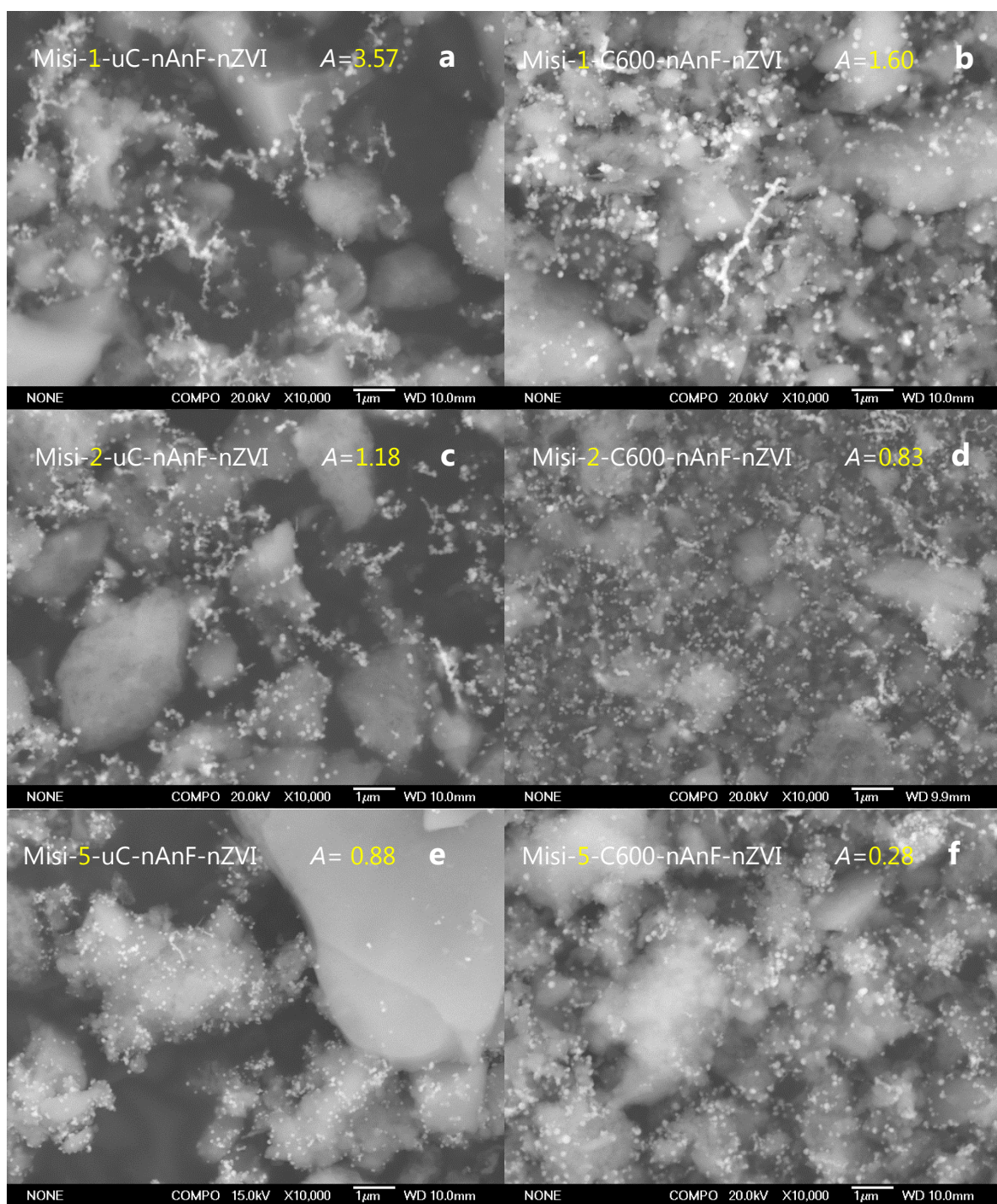
Figure 3.27. Effect of concentration of acid on adsorption of nZVI on Misi C600-nAnF and uC-nAnF, a, Misi-1-uC-nAnF-nZVI (entry 12); b, Misi-1-C600-nAnF-nZVI (entry 6); c, Misi-2-uC-nAnF-nZVI (entry 27); d, Misi-2-C600-nAnF-nZVI (entry 19); e, Misi-5-uC-nAnF-nZVI (entry 44); f, Misi-5-C600-nAnF-nZVI (entry 40).

Misi-5-C600-nAnF-nZVI

Misi-5-C600-nAnF-nZVI

Misi-C600-5-AnF-nZVI

Misi-C600-5-AnF-nZVI

Misi-C600-5-nAnF-nZVI

Misi-C600-5-nAnF-nZVI
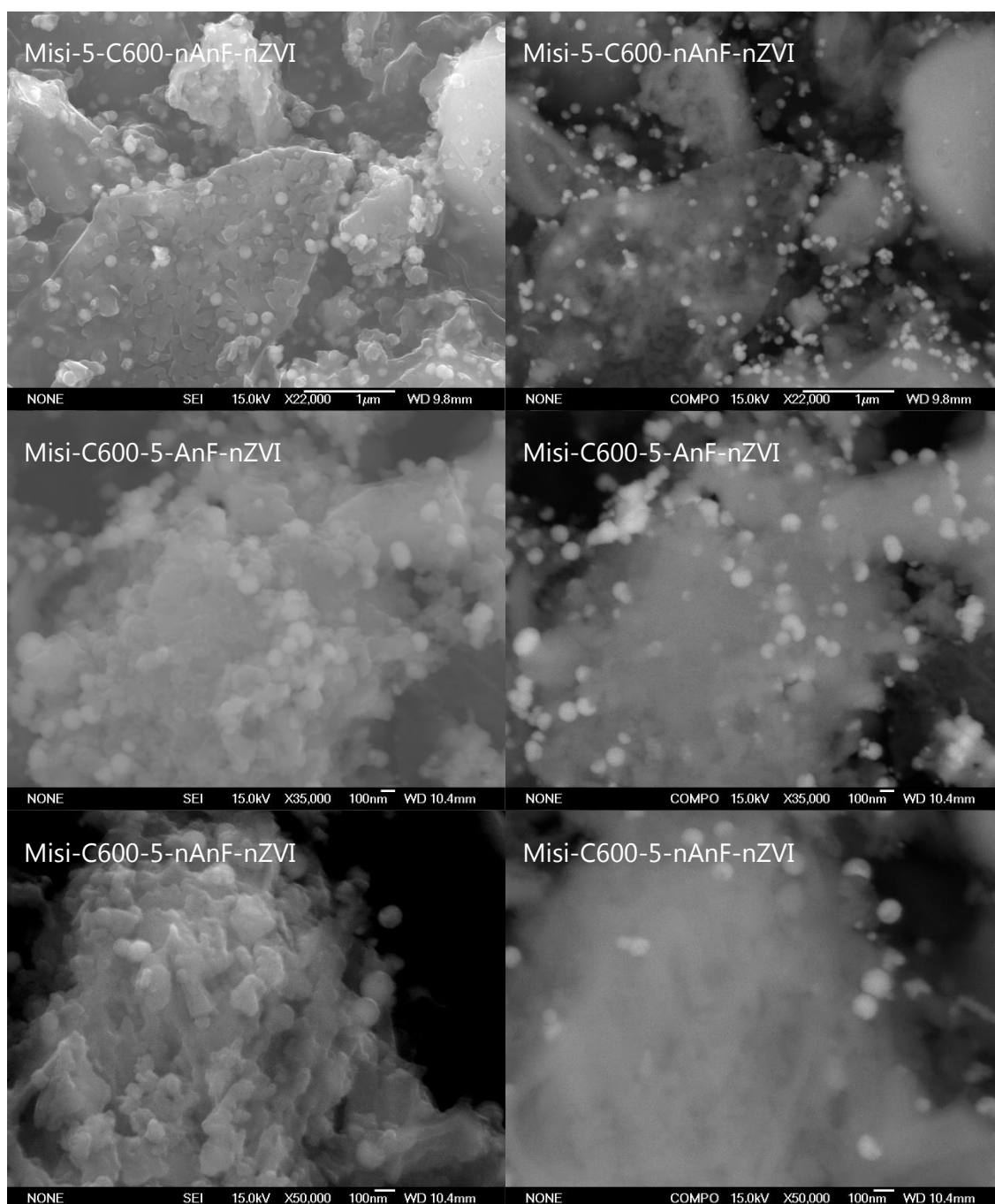
Figure 3.28. SEI images (left column) and COMPO images (right column) of different acid washed system

96
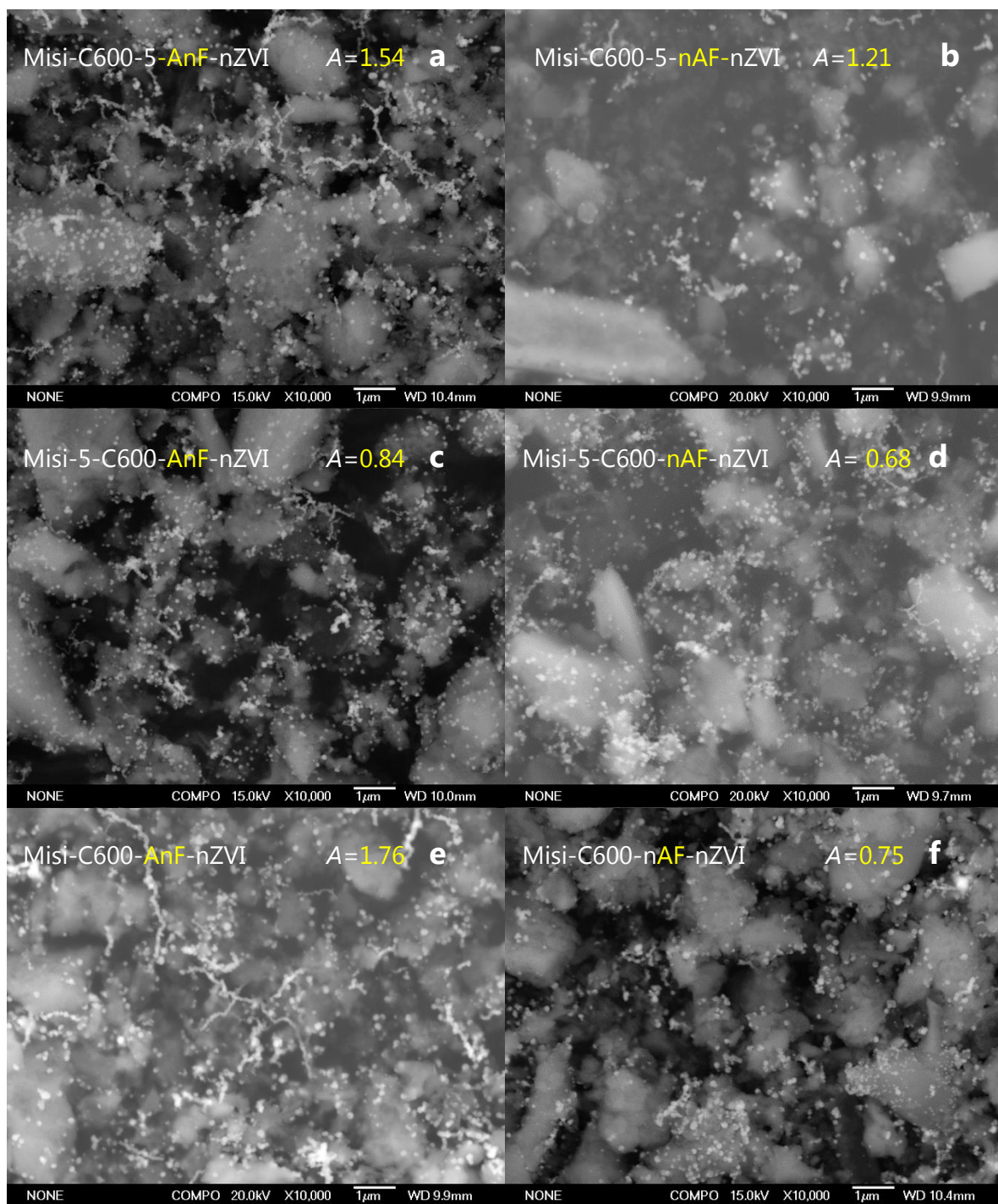
Figure 3.29. Effect of activation (left column) and FeOOH layer (right column) on adsorption of nZVI on Misi 5-C600, C600-5, and C600; a, Misi-C600-5-AnF-nZVI (entry 54); b, Misi-C600-5-nAF-nZVI (entry 55); c, Misi-5-C600-AnF-nZVI (entry 32); d, Misi 5-C600-nAF-nZVI (entry 38); e, Misi-C600-AnF-nZVI (entry 62); f, Misi-C600-nAF-nZVI (entry 63)

Based on the average *A*-value for each type of treatments, the best overall surface modification was AnF, when Misi had been acid washed and calcined, and nAnF if they had only been calcined (Table 3.15). The best overall acid/calcination Misi surface modifier was 5-C600. The better nZVI adsorption afforded by the combination of acid wash/calcination and AnF suggested nZVI adsorption depended on having isolated silanol and not FeOOH linkage. Acid washing, calcination and also activation by boiling all contributed to the formation of silanol groups. Once these were created, then FeOOH coating could hinder the adsorption of nZVI due to competition of active sites.

Table 3.15. Summary of result for adsorbtion of nZVI on treated Misi surfaces (average of A-*value) Items in blue indicates the lowest average for each section.*

Acid washed						
Calcination/acid	**AF**	**AnF**	**nAF**	**nAnF**	***Average***	**SD**
1-C600	1.04	1.06	0.95	2.03	*1.27*	*0.44*
2-C600	1.38	0.80	1.52	2.11	*1.45*	*0.47*
5-C600	1.25	1.06	0.67	0.55	*0.88*	*0.28*
C600-5	1.83	1.54	1.13	0.90	*1.35*	*0.36*
C400-5	2.02		2.11	2.10	*2.08*	*0.04*
Average	*1.50*	*1.12*	*1.28*	*1.54*	*1.36*	
SD	*0.37*	*0.27*	*0.50*	*0.67*	*0.39*	
Acid washed, uncalcined						
1-uncalcined	1.17	1.31	1.44	3.57	*1.87*	*0.99*
2-uncalcined	0.76	1.31	0.68	1.18	*0.98*	*0.27*
5-uncalcined	2.69	2.06	1.15	0.88	*1.69*	*0.72*
Average	*1.54*	*1.56*	*1.09*	*1.88*	*1.52*	*0.28*
SD	*0.83*	*0.35*	*0.32*	*1.21*		
Not acid washed						
C600	2.02	1.76	2.91	0.67	*1.84*	*0.80*
C400	1.37	2.43	1.78	0.65	*1.56*	*0.65*
Average	*1.70*	*2.09*	*2.34*	*0.66*	*1.70*	*0.64*
SD	*0.33*	*0.33*	*0.56*	*0.01*		
Total Average	*1.55*	*1.48*	*1.43*	*1.46*		
total SD	*0.55*	*0.49*	*0.66*	*0.92*		

ANOVA analysis was performed on the data using a general linear model. Investigation of the main effects and combination of each treatment showed that the interaction between acid wash and activation had the smallest p ($p= 0.105$; Table 3.16), but there were no main effects or interactions that were statistically significant. The statistically relevant interaction suggested that activation was required when washed with the 1.2 M and 2.6M HCl, but not with 5.6 M HCl acid washing or when not acid washed (Figure 3.30). Even though there were 65 different samples, the number of independent variables (5) and the variety in the independent variables (40 different possible combinations in total) meant that a larger sample pool was required to tease out statistically significant differences.
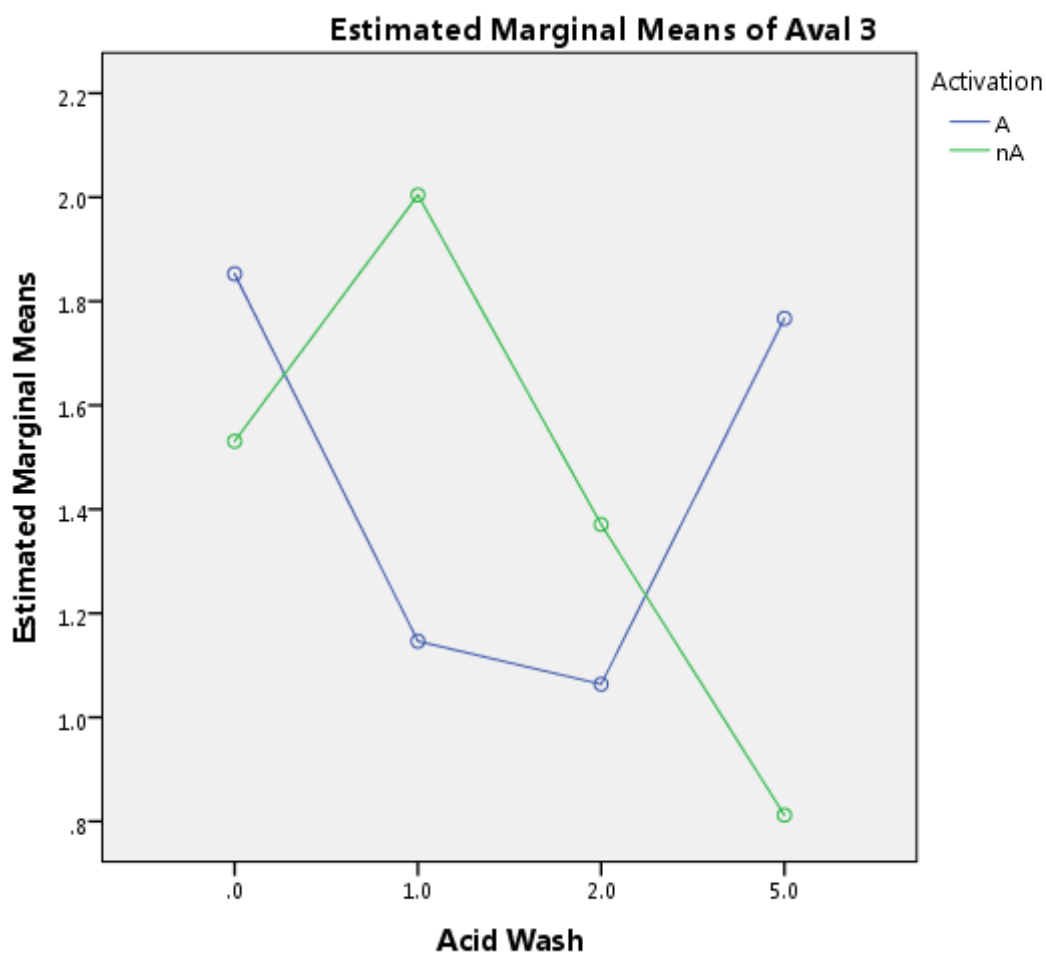
Figure 3.30. Profile Plots of Acid Wash, Activation and A-Value. For acid wash 0= no washing, 1= 1.2 M HCl, 2.0 = 2.8 M HCl, and 5.0 = 5.6 M HCl.

Table 3.16. Test of between-subjects effects, A-value as dependent variable

Source	Type III Sum of Squares	df	Mean Square	F	Sig.
Corrected Model	27.700[a]	39	.710	.907	.616
Intercept	68.928	1	68.928	88.028	.000
AcidWash	2.827	3	.942	1.204	.329
Calcination	2.282	2	1.141	1.457	.252
AcidWash2	.071	1	.071	.090	.767
Activation	.260	1	.260	.332	.570
FeOOH	.396	1	.396	.506	.483
AcidWash * Calcination	3.291	3	1.097	1.401	.266
AcidWash * Activation	5.326	3	1.775	2.267	.105
AcidWash * FeOOH	4.070	3	1.357	1.733	.186
Calcination * AcidWash2	1.383	1	1.383	1.766	.196
Calcination * Activation	.093	2	.046	.059	.943
Calcination * FeOOH	.618	2	.309	.395	.678
AcidWash2 * Activation	.058	1	.058	.074	.788
AcidWash2 * FeOOH	.582	1	.582	.744	.397
Activation * FeOOH	.117	1	.117	.150	.702
AcidWash * Calcination * Activation	.922	2	.461	.589	.562
AcidWash * Calcination * FeOOH	.283	2	.142	.181	.836
AcidWash * Activation * FeOOH	2.878	3	.959	1.225	.321
Calcination * AcidWash2 * Activation	.266	1	.266	.339	.566
Calcination * AcidWash2 * FeOOH	.125	1	.125	.160	.693
Calcination * Activation * FeOOH	.018	2	.009	.011	.989
AcidWash2 * Activation * FeOOH	.771	1	.771	.985	.330
AcidWash * Calcination * Activation * FeOOH	.331	2	.165	.211	.811
Error	19.576	25	.783		
Total	170.195	65			
Corrected Total	47.275	64			

a. R Squared = .586 (Adjusted R Squared = -.060)

3.6 Conclusion

The most important modification step for Misi surface was calcination, followed closely by acid washing. The generation of active silanol functional groups with either calcination or acid washing was the key in improving adsorption of nZVI onto Misi surface, although the reason was still unclear. Once the surface had been activated with acid, calcination, or boiling, the presence of FeOOH coating seemed to hinder nZVI adsorption on Misi surface. This suggested that the adsorption of nZVI onto Misi surface depended more on availability of silanol sites rather than roughness of surface or FeOOH-based anchoring sites.

4 Adsorption of nZVI onto pure and functionalised silica surfaces

4.1 Introduction

In order to understand factors controlling the adsorption of nZVI on silicate surfaces without interferences from other elements, nZVI was adsorbed on pure silica and functionalised silica surfaces. Two types of silica were used: commercially available silica gel, typically used in this research for chromatography, and silica synthesised via the Stöber method. The silica was used both with and without further surface functionalisation. The variety of treatments conducted including those previously performed on Misi, as well as other treatments such as pore enlargements, dilute acid and base wash. These treatments will be described in more detail within each relevant chapter section.

4.2 Silica Gel

Silica gel (SG) is a vitreous granular form of SiO_2, typically synthesised from sodium silicate.[251] SG is commonly used as a desiccant or as the stationary phase in column chromatography. The silica gel used in these experiments were rated 60 mesh, which corresponds to beads 40-63 micron in size. There had only been one report on the use of SG as a support for nZVI. Arain *et al* (2014) reported adsorbing pre-synthesised nZVI onto SG without prior treatment, and utilised the system to adsorb As^{3+}.[280] However, there was no evidence that nZVI was dispersed evenly onto the SG surface as the low resolution SEM image provided did not include EDS mapping. The SEI images from SEM analysis showed only the morphology of the surface, and did not indicate which elements were present. To be able to show the adsorption of nZVI on a silica surface, COMPO images supported by EDS mapping was required. Furthermore, there was no indication that nZVI was synthesised under N_2 atmosphere, which was important as nZVI is prone to oxidation when in water.

4.2.1 Activation

Four types of activation were trialled on SG including dilute acid (dA: ~0.1M H_2SO_4, 2 hours),[147] dilute base (dB: ~0.1M NaOH, 2 hours), boiling for 2 hours (A: 2 g SG in 100 mL DI-H_2O), and strong acid on reflux (Ar: 4 g of SG in 200 mL of 5 M HCl, overnight).[223] Dilute acid, acid reflux and boiling were used to generate silanol sites on the silica surface, while weak base was used

to deprotonate silanol sites to form silanoxy sites. nZVI was then synthesised in the presence of these four activated SG materials by reducing a ferrous solution with sodium borohydride. These four activation methods were not successful in helping adsorption of nZVI onto SG surface (Figure 4.1). In all experiments, nZVI was observed, some of which were adsorbed on the SG surface, but the majority of nZVI formed agglomerates. When SG was only activated by boiling (SG-A-nZVI, Figure 4.1*a*), there was almost no adsorption of nZVI onto the surface of the SG. Similarly, SG washed in dilute acid (SG-dA-nZVI, Figure 4.1*b*) and base (SG-dB-nZVI, Figure 4.1*c*) also resulted in agglomerates of nZVI with only a small amount of nZVI adsorbed on the SG surface. Refluxing silica gel in concentrated acid (SG-Ar-nZVI, Figure 4.1*d*) showed the least amount of agglomeration, and more nZVI adsorbed on the silica surface, however the particles were mostly chains instead of discrete spheres. *A*-values were not calculated for these images as the high level of agglomeration would put the mean particle size outside a normal distribution of mean and render the normality assumption for discriminate analysis erroneous.

4.2.2 FeOOH coating

The role of PEG (P*) and FeOOH (F) linkage and coating as described by Qiu *et al* had been explored fully.[223] Qiu *et al* stated that PEG forms a link between the silica surface and FeOOH layer. PEG was adsorbed on SG following procedure from Qiu *et al*. Briefly, 1 g of activated silica gel was soaked with 100 mL DI-H_2O containing 1g of PEG and 1 g of $FeSO_4 \cdot 7H_2O$ for 30 minutes before being centrifuged, decanted, and placed in a 110 °C oven overnight. The nZVI was generated *in situ* by adding a sodium borohydride solution to a suspension of the silica gel in an iron sulfate solution. After a standard workup involving washing with water then ethanol, the new material was isolated. All of the SG-F-nZVI materials were dark grey in colour and magnetic, indicating the presence of iron nanoparticles.
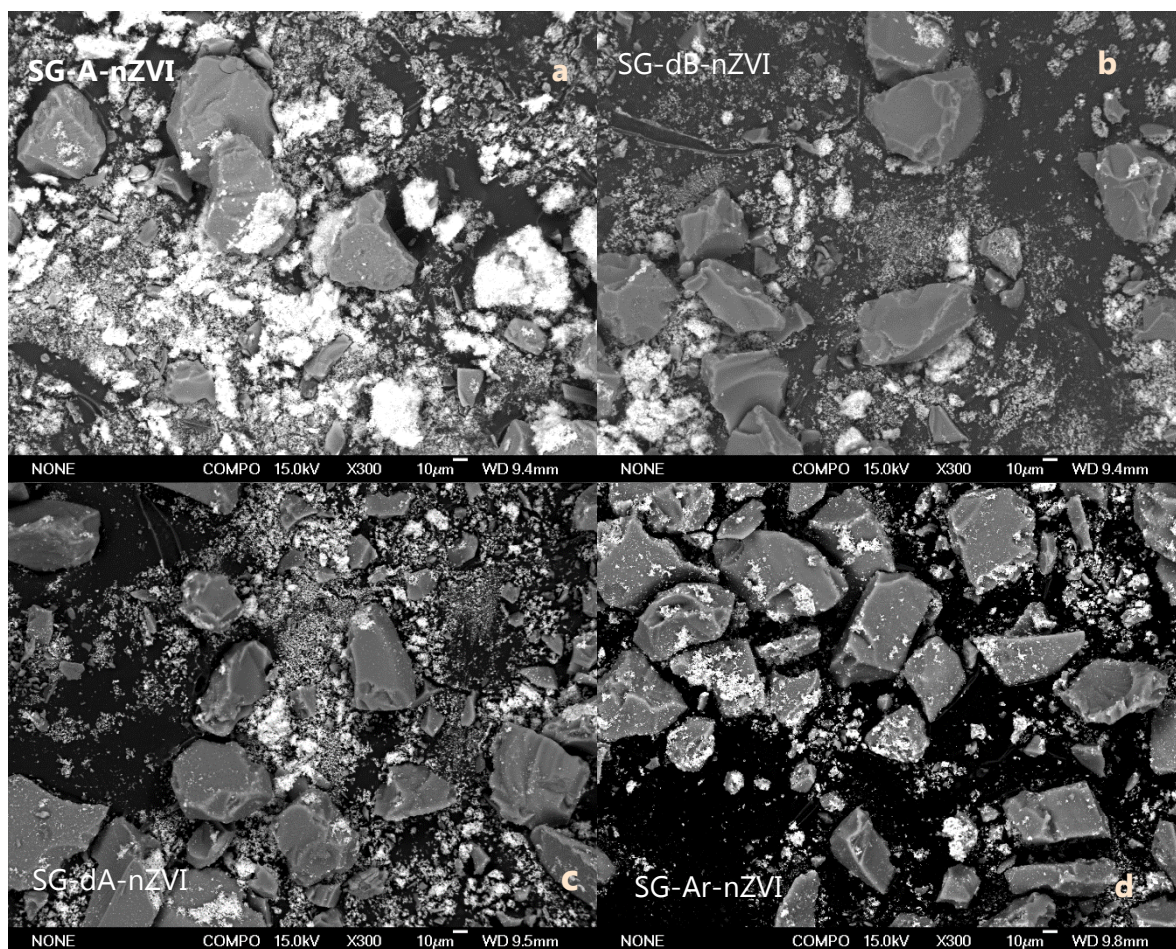
Figure 4.1. nZVI adsorbed on activated silica gel: a, SG-A-nZVI; b, SG-dB-nZVI; c, SG-dA-nZVI; d, SG-Ar-nZVI

The SEM analysis of nZVI adsorbed on SG with and without PEG linkage showed that PEG did not improve the adsorption of nZVI on FeOOH coated SG (*vis-à-vis* Figure 4.2 *b*, *d*, *f* and *a*, *c*, *e*). The combination of different activation methods (dilute acid, base and boiling) and FeOOH/PEG layer did not show any improvement on nZVI adsorption on the SG surface compared to the SG without the FeOOH/PEG layer. From both Figure 4.1 and Figure 4.2, SG-A-F-nZVI (Figure 4.2*e*) had the best distribution of nZVI adsorbed on the surface, however dispersion was still minimal.
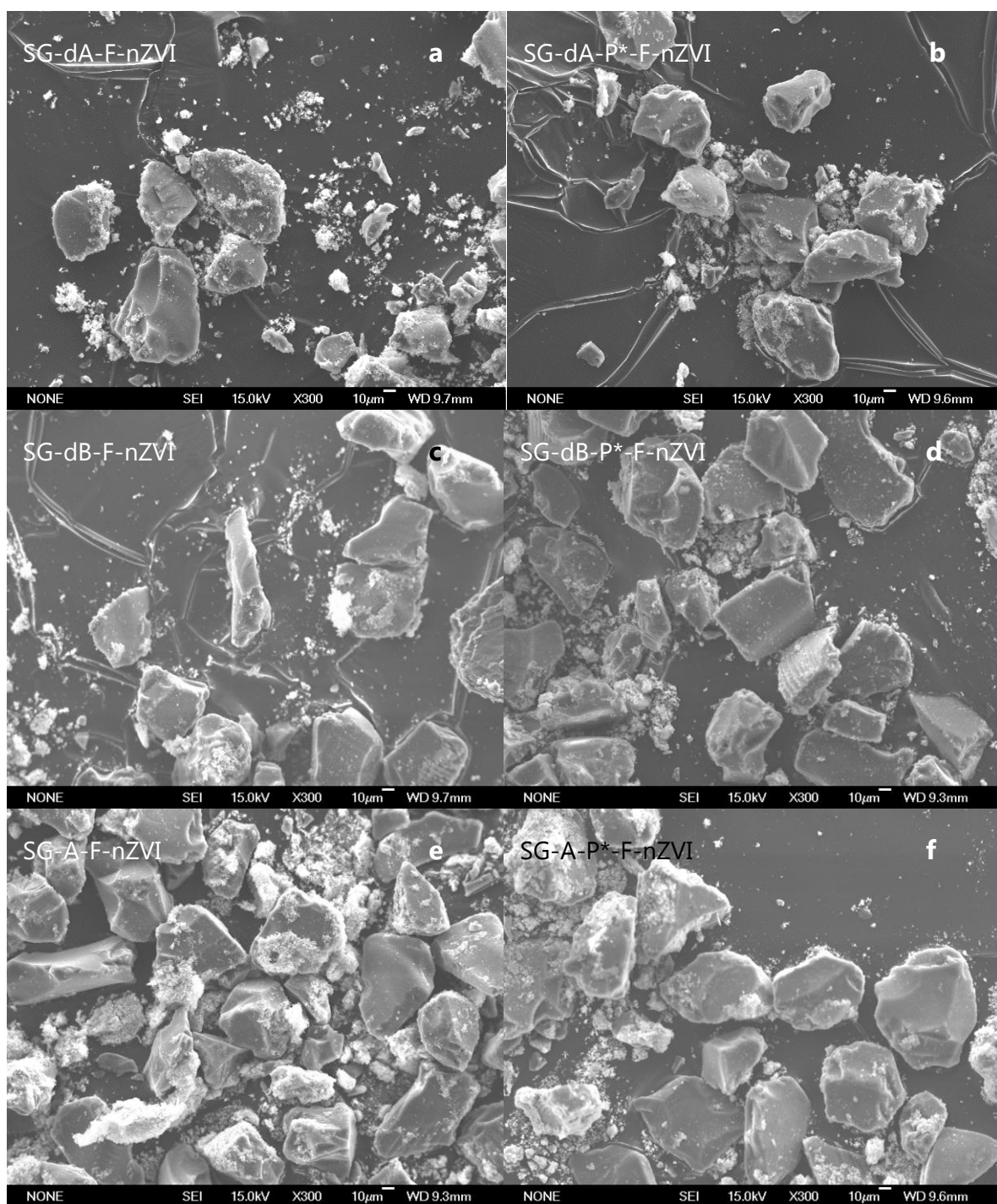
Figure 4.2. Adsorption of nZVI on treated Silica Gel (SG) with and without PEG link: a, SG-dA-F-nZVI; b, SG-dA-P*-F-nZVI; c, SGpdB-F-nZVI; d, SG-dB-P*-F-nZVI; e, SG-A-F-nZVI; f, SG-A-P*-nZVI. dA: dilute Acid wash, dB: dilute base wash, A: boiling for 2 h, P*: PEG linkage, F: FeOOH layer:

As calcination had been proven to be useful in Misi, SG was calcined at 600 °C (C600) prior to activation by dilute acid, dilute base, boiling and FeOOH coating (Figure 4.3). Calcination seems to improve the adsorption of nZVI on SG but only if it was then activated by boiling and had a FeOOH layer (SG-C600-A-F-nZVI, Figure 4.3*a*). Adsorption of nZVI was not improved when the calcined silica was activated by either dilute acid or dilute base as indicated by the lack of nZVI particles on the surfaces of the treated silica (SG-C600-dA-F-nZVI and SG-C600-dB-F-nZVI; Figure 4.3 *b* and *c* respectively).
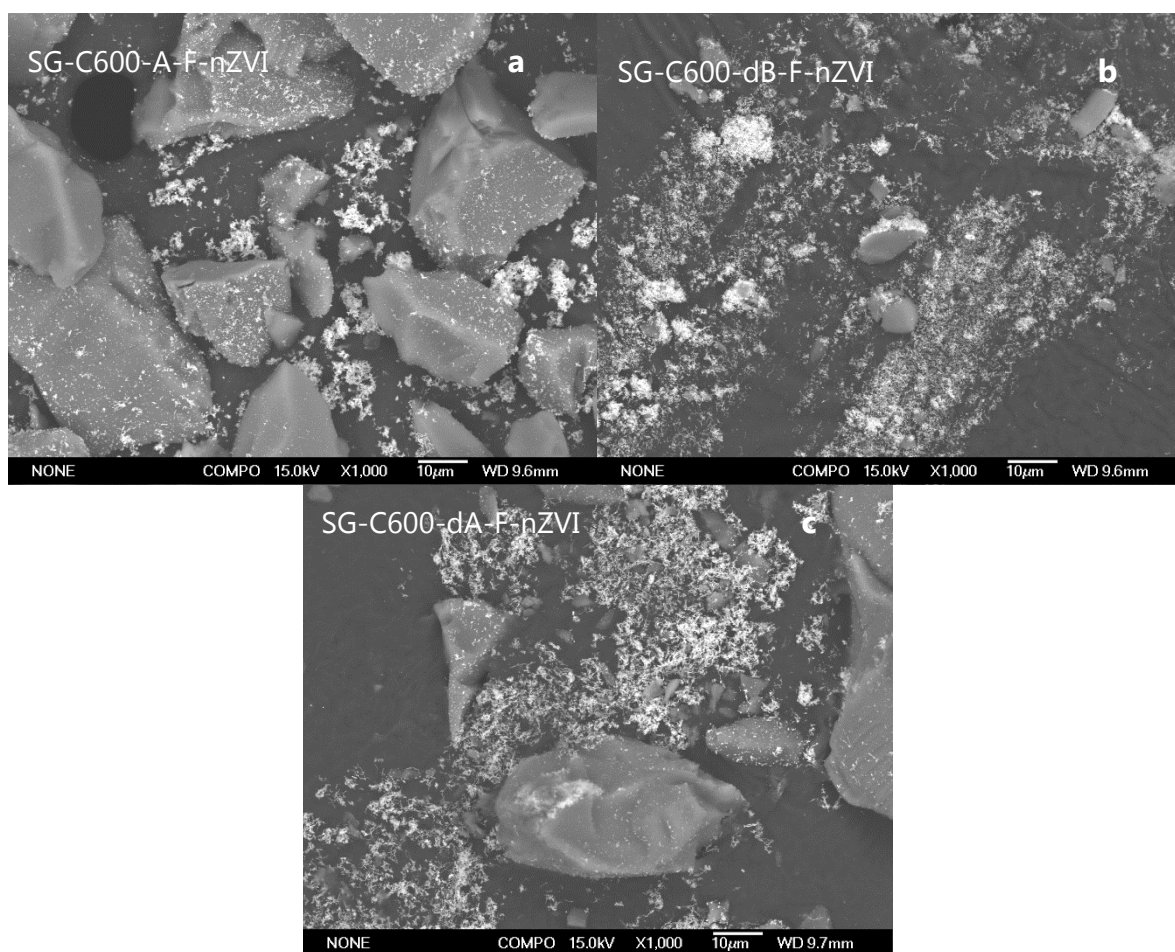
Figure 4.3. Adsoprtion of nZVI on calcined SG: a, SG-C600-AF-nZVI; b, SG-C600-dB-F-nZVI; c, SG-C600-dA-F-nZVI.

4.2.3 Ligand functionalisation

In silica chromatography, ligands and chelating agents such as carboxyhyrdozide,[281] 3-thiopropyl-trimethoxysilane (3-TPTMS),[220] 3-aminopropyl-triethoxysilane (3-APTES),[214] had

been used to improve the adsorption of Hg^{2+}, Pd^{2+} and CO_2 onto silica gel respectively (Figure 4.4). A number of ligands had been used to adsorb Fe^{3+} over Fe^{2+} selectively, such as 2-benzimidasolethiol, but no ligand had been reported to adsorbed Fe^{2+} selectively.[282] In our research, two ligands were used to functionalise SG surfaces: 3-APTES and 3-TPTMS. 3-APTES had been used to synthesise organosilicas that can bind to Fe^{3+},[283] while 3-TPTMS had also been used in conjunction with resacetophenone (2',4'-dihydroxyacetophenone) to adsorb Fe^{3+}.[219] The ligands were attached to the silica surface by reflux in toluene overnight following methods by Goswami and Singh (section 2.2.3.2).[219]

| Carboxyhydrozide | 3-thiopropyltrimethylsilane (3-TPTMS) | 2-benzimidasolethiol |

3-aminopropyltriethylsilane (3-APTES)   2',4'-dihydroxyacetophenone
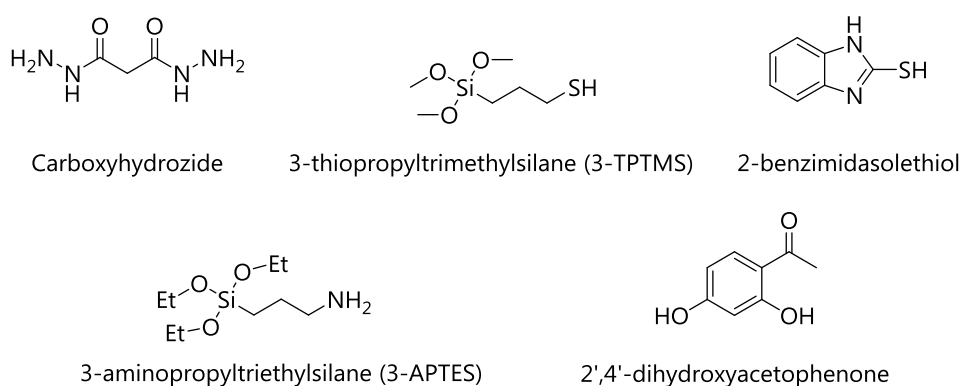
Figure 4.4. Example of ligands that had been used with silica gel

Three methods of nZVI adsorption onto ligand functionalised SG were trialled. The first method involves the reduction of Fe^{2+} in the presence of the functionalised silica using $NaBH_4$ following the standard procedure (Section 2.3.1). In this method, it was observed that silica gel functionalised with 3-APTES turned light grey green, indicative of the presence of sulfate green rust, a mixture of Fe^{2+}, Fe^{3+}, sulfate and hydroxy ions, upon the addition of $FeSO_4$.[284] This was in contrast to the light yellow/cream colour observed when $FeSO_4$ was added to other silica. Upon addition of $NaBH_4$, the mixture turned black, which was indicative of the presence of nZVI. After the standard washing and drying procedure, the silica was observed to be to white with uneven dark green/grey areas. In contrast, 3-TPTMS functionalised silica did not turn green upon the addition of $FeSO_4$, and the final product was a grey/white powder similar to other SG-nZVI products.
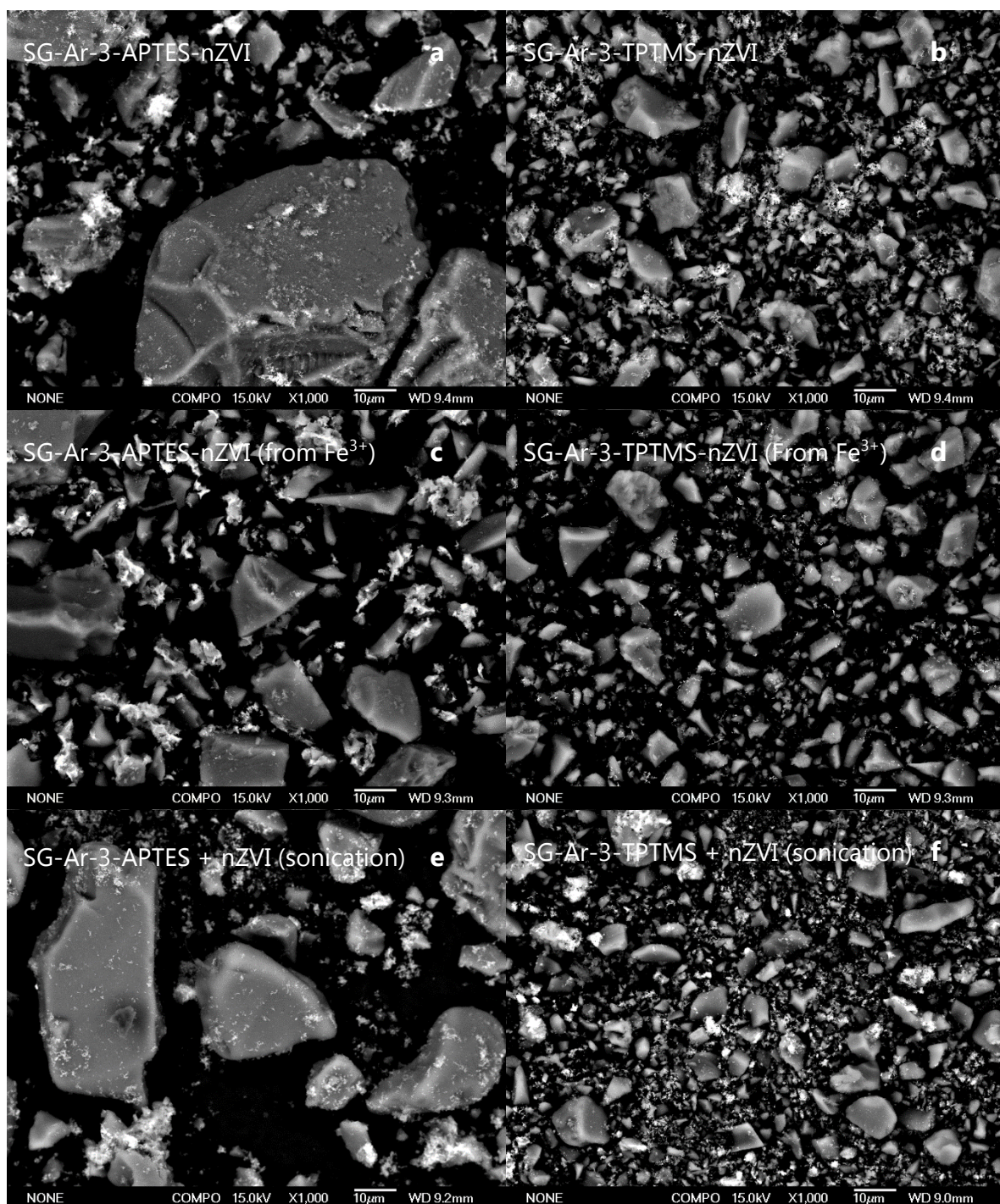
Figure 4.5. Adsorption of nZVI on functionalised silica gel: a, SG-Ar-3-APTES-nZVI; b, SG-Ar-3-TPTMS-nZVI; c, SG-Ar-3-APTES-nZVI (Fe^{3+}); d, SG-Ar-3-TPTMS-nZVI (Fe^{3+}); e, SG-Ar-3-APTES + nZVI (sonication); f, SG-Ar-3-TPTMS + nZVI (sonication). Ligand loading: 10%mol. Ar = acid refluxed.

109

The second method of nZVI adsorption utilised $FeCl_3$ as a source of Fe^{3+} instead of Fe^{2+} from $FeSO_4$.[219] The two oxidation states of iron were tested. Both 3-APTES and 3-TMTPS had been used to pre-concentrate Fe^{3+} and thus binding of the ligands to Fe^{3+} might increase the number of nucleation sites.   The third method was sonication of silica with pre-synthesized nZVI dispersed in ethanol following the method described by Arain *et al*.[285]

The adsorption of nZVI on all silica surfaces was examined using SEM analysis. In all gases, uneven adsorption was observed as evidenced by the loose nZVI chains surrounding the silica gel (Figure 4.5). SG functionalised with APTES (Figure 4.5*a*, *c*, *e*) showed the best adsorption, especially when used in conjunction with Fe^{2+} (SG-Ar-3-APTES-nZVI, Figure 4.5*a*).   The sonication loading method was more successful with the APTES ligand compared to the TPTMS ligand, as there were more nZVI particles on the SG-Ar-3-APTES surfaces compared to those of SG-AR-3-TPTMS (Figure 4.5*e* and *f* respectively). Based on the oxidation states of Fe, nZVI synthesised from Fe^{2+} was better dispersed compared to nZVI from Fe^{3+} in APTES (*vis-à-vis* Figure 4.5*a* and *c*), but the reverse was true for TPTMS ligand (Figure 4.5*b* and *d*). However, all of these differences were trivial as overall, as the adsorption of nZVI on all these ligand functionalised surfaces were poor. As observed in the SEM images, adsorption was not a function of particle size. As with other SG-nZVI products, *A*-value were not calculated as the value of mean, SD and % under was outside a normal distribution and thus violate the assumptions of discriminate analysis.

4.3 Synthetic silica

Since the adsorption of nZVI on silica gel was not successful, the attention turned to synthetic silica (SS) as these can be made in high purity in a range of sizes.   The synthesis of the silica was based on the Stöber process with dodecyl amine as both the base and reductant, and TEOS as the source of silicon (Section 2.1.2) .[221]   It is important to emphasize that the final step of SS synthesis was calcination at 600 °C to remove the amine template, as calcination had also been shown to be an effective surface treatment for nZVI adsorption. The spherical silica diameter was around 1μm (Figure 4.6), and although there was a variation of size, these were not as large as SG.   The pH of SS in DI-H_2O was 2.7, with zeta potential of -12 mV.
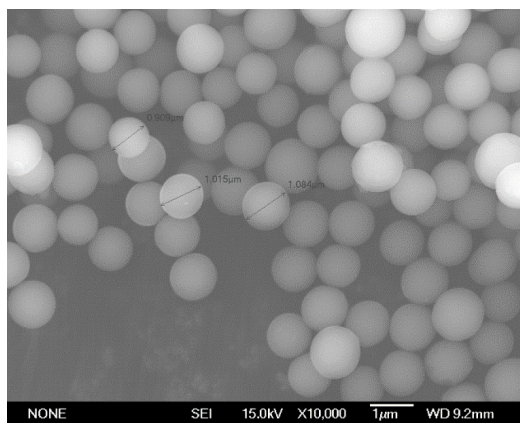
Figure 4.6. SEM image of Synthetic Silica (SS)

4.3.1 C600-AF system with acid washing

The surface of SS was modified using three different modifications: acid washing with 5.6 M HCl (5), boiling (A) and FeOOH coating (F).   For the acid washed silica, calcined silica was washed with 5.6 M HCl, and then either re-calcined or not re-calcined. (SS1-5-C600 and SS1-5-uC respectively).   The nZVI was generated *in situ* by adding a sodium borohydride solution to a suspension of the SS support in an iron sulfate solution. After standard workup involving washing with water then ethanol, the new material was isolated. All of the nZVI-SS materials were dark grey in colour and magnetic, indicating the presence of iron nanoparticles, although the SS-5-uC and SS-CAF were noticeably more grey than black (Figure 4.7).

The presence of a FeOOH layer assisted with the adsorption of nZVI (*vis à vis* SS-A-F-nZVI and SSA-nF-nZVI, Figure 4.8*a* and *b* respectively) however adsorption was uneven, with some silica adsorbing more nZVI than others and loose aggregates of nZVI still present.   Acid washing did not improve the adsorption of nZVI onto SS surfaces even if followed by other treatments (SS5-C600-AF-nZVI and SS-5-uC-nAnF-nZVI, Figure 4.8*c* and *d* respectively).

One unanticipated issue was the uneven adsorption of nZVI on a SS surface of the same batch. As these silica were synthetically produced under a controlled environment, it was assumed that the surface chemistry of all the silica surfaces would be similar. SEM images did not support this assumption as some of the silica spheres had multiple nZVI particles adsorbed on them while some spheres had none at all. As it was difficult to separate out the particles with and without nZVI, no studies were conducted to investigate this issue.
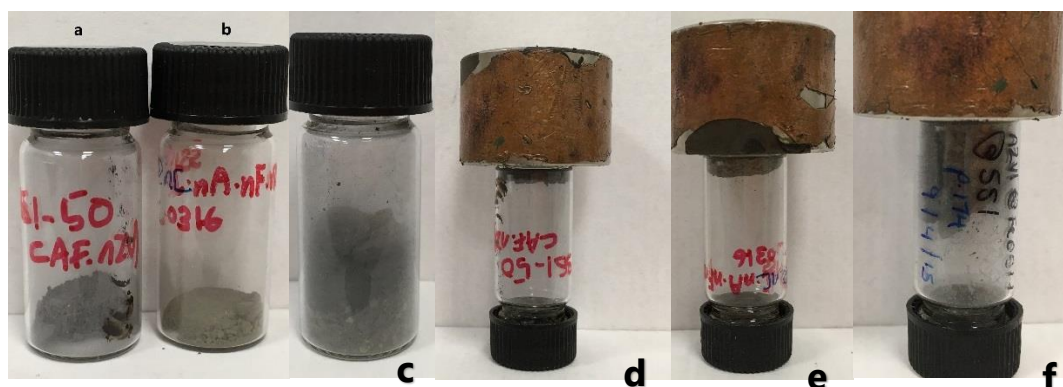
Figure 4.7. nZVI supported on SS: a, SS-5-C600-AF-nZVI; b, SS-5-uC-nAnF-nZVI; c, SS-C600-AF-nZVI; and magnetism of the particles: d, SS-5-C600-AF-nZVI; e, SS-5-uC-nAnF-nZVI; f, SS-C600-AF-nZVI.
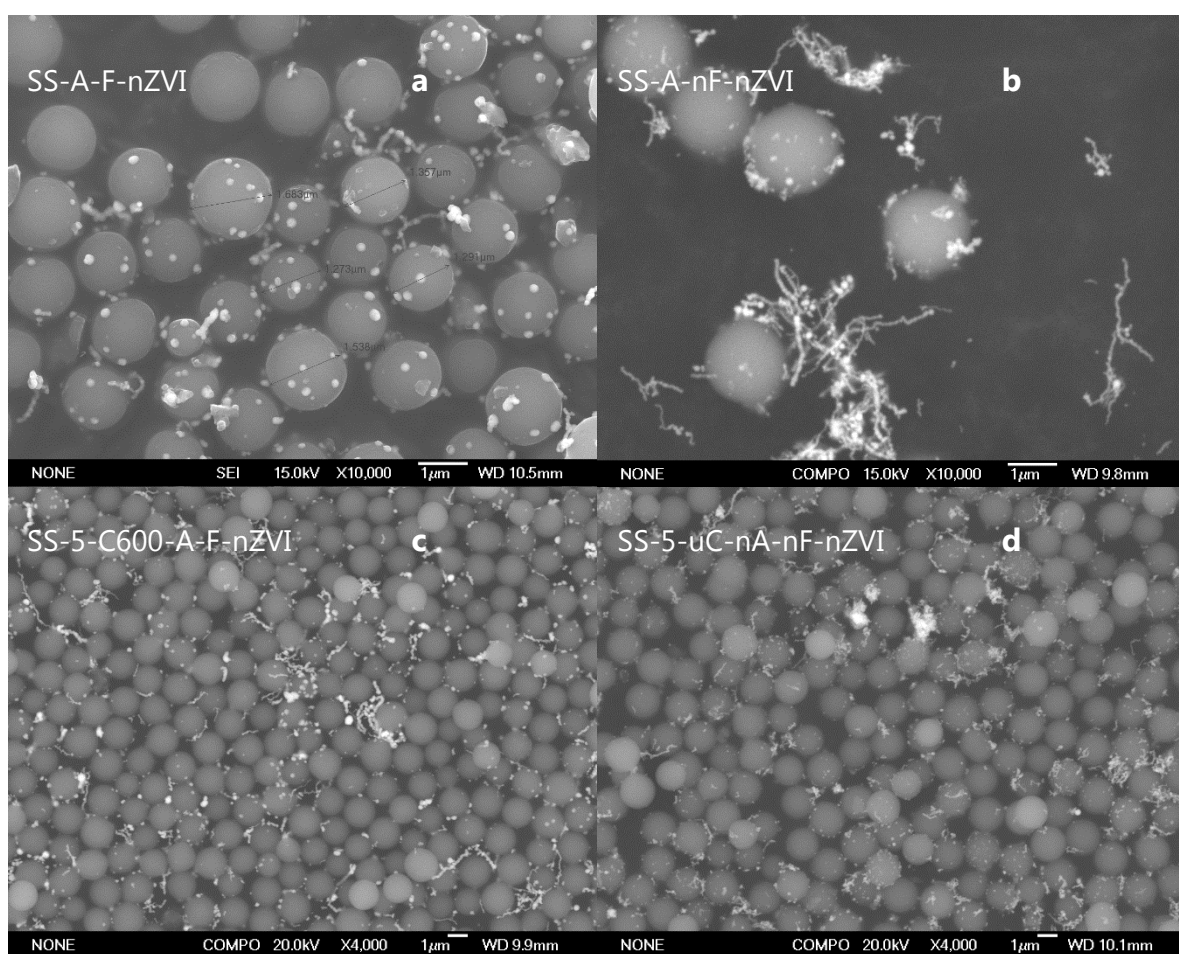
Figure 4.8. Adsorption of nZVI on SS surfaces: a, SS-AF-nZVI; b, SS-AnF-nZVI; c, SS-5-C600-AF-nZVI; d. SS-5-uC-nAnF-nZVI. A=boiled for 2 hours. F= FeOOH coating, nF=no FeOOH coating, 5=acid washed in 5.6 M HCl, C600=calcined at 600 °C for 6 hours

4.3.2 Pore enlargement

As the surface of SS was smooth, it was thought that generating a rough surface could potentially create nucleation sites for nZVI particles. Li described a process of soaking silica spheres in a mixture of salt followed by sonication and calcination at 300 °C to enlarge pores on the silica surface.[286] The method however did not describe whether the spheres were washed before or after calcination. Therefore, in attempt to enlarge pores, SS spheres were soaked in a mixture of NaCl, LiCl and KNO_3, sonicated, and calcined either before or after they were washed, or with no washing, denoted as WbC, WaC and uW respectively (Section 2.2.4). The nZVI was generated *in situ* by adding a sodium borohydride solution to a suspension of the SS support in an iron sulfate solution. After standard workup involving washing with water then ethanol, the new material was isolated. All of the nZVI-SS materials were dark grey in colour and magnetic, indicating the presence of iron nanoparticles. When the pore enlarged silica were washed either before or after calcination (WbC and WaC respectively), the surface of the spheres were noticeably rougher (Figure 4.9). However, this roughness did not translate to being a better surface for nZVI to adsorb on, as all three pore-enlarged silica in conjunction with FeOOH layer did not provide adsorbing surfaces for nZVI. Comparing Figure 4.8 and Figure 4.9, it could be surmised that this pore enlargement attempt, especially WbC, had failed to provide an adsorbent surface for nZVI.

113
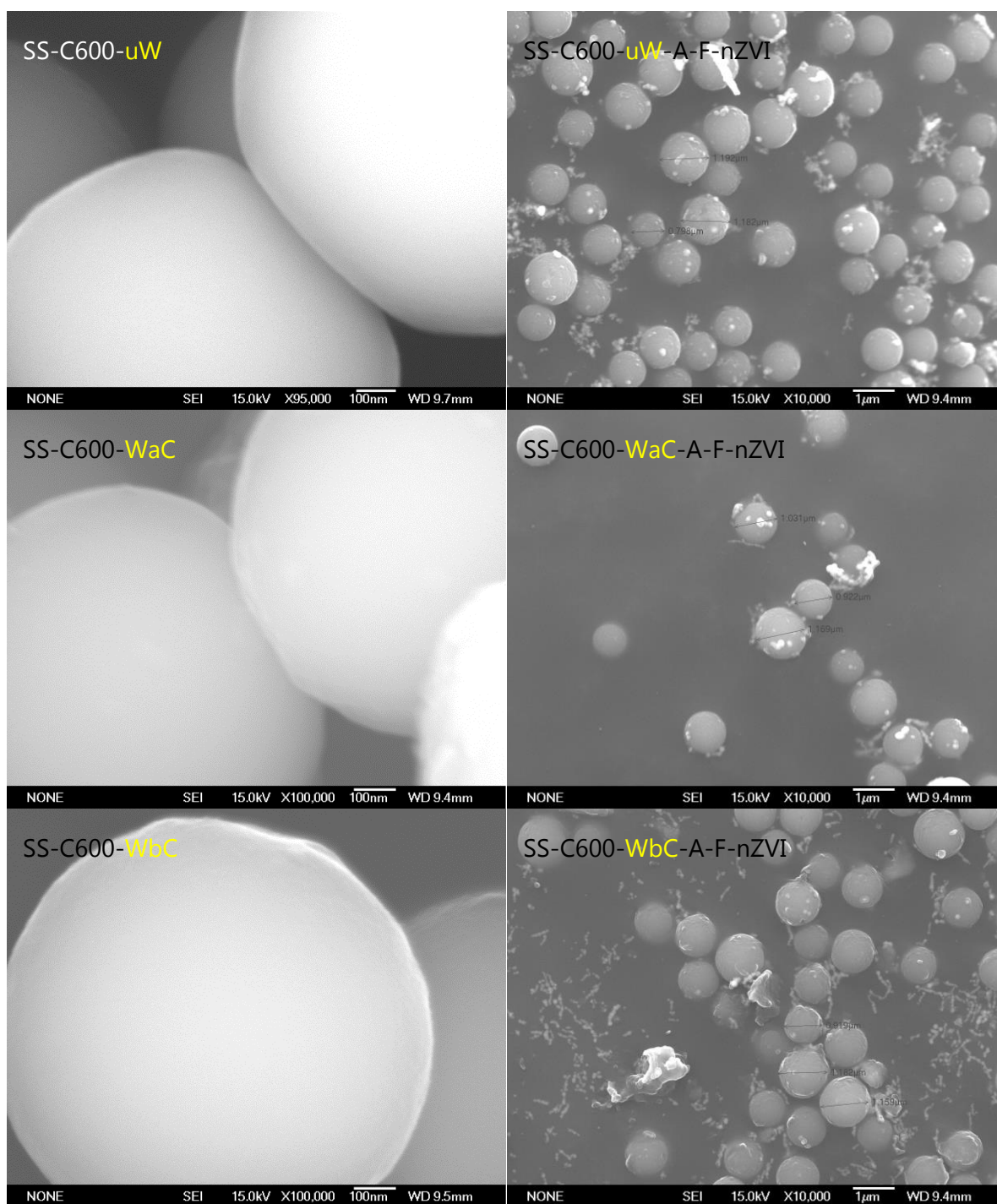
Figure 4.9. Pore enlargement experiment. Top row: unwashed (uW); middle row, washed after calcination (WaC); bottom row washed before calcination (WbC). Left column: silica after pore enlargement process; right column, nZVI adsorption with FeOOH layer.

114

4.3.3 Zeta potential adjustment

The zeta potential difference between silica spheres and nZVI were adjusted to see whether the difference between a positive and negative zeta potential would allow for adsorption of nZVI onto SS surfaces. The pH of the silica suspension was adjusted so there was a maximum opposite charge between the silica and pre-synthesised nZVI. nZVI has a positive zeta potential at around pH 5.9 (~+20 mV),[254] while SS has negative zeta potential (-35 mV) at the same pH. Pre-synthesised nZVI was sonicated along with a number of pore-enlarged SS in pH-adjusted deoxygenated DI-H_2O, but this method did not help adsorption of nZVI to SS surface (Figure 4.10).
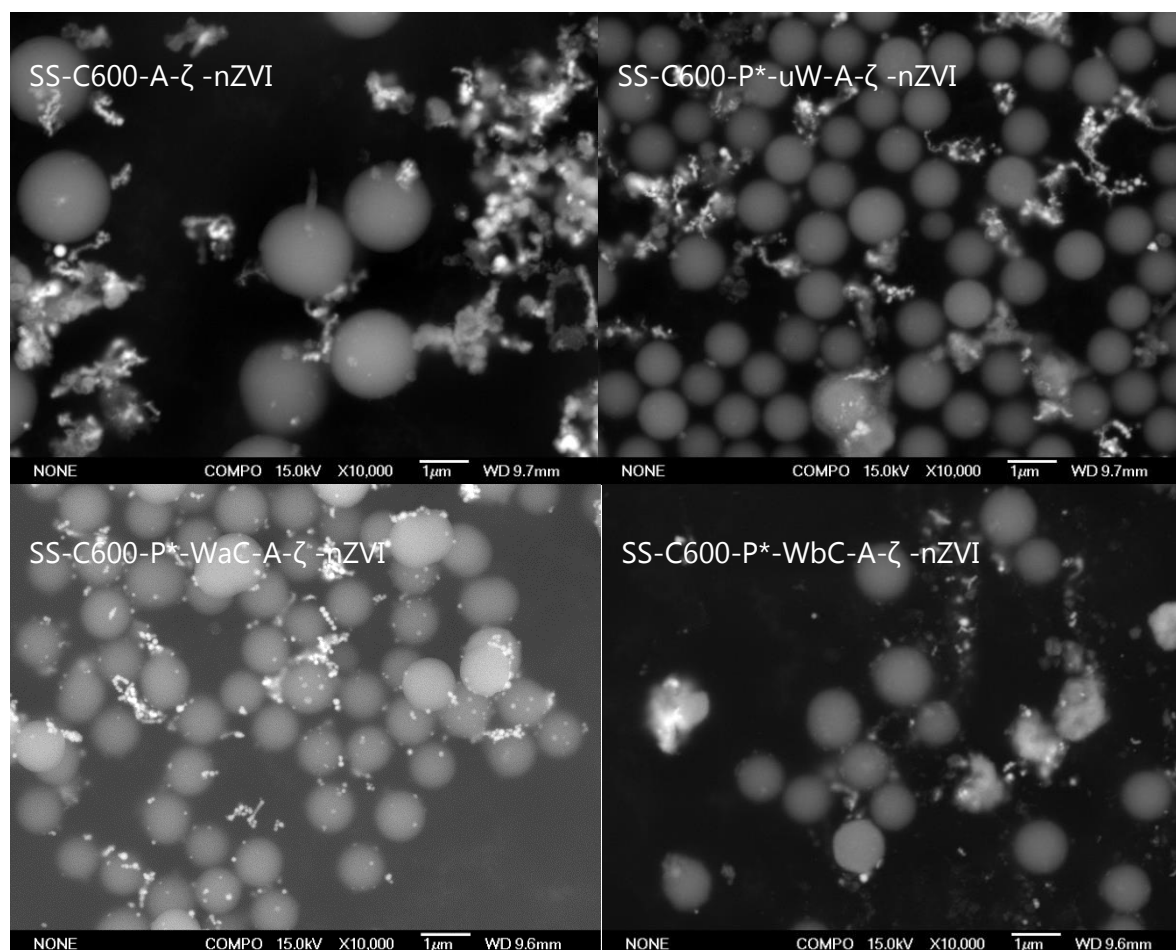
Figure 4.10. nZVI adsorption utilising zeta potential (ζ).

115

4.3.4 Physical method

As all chemisorption methods investigated had been ineffective, silica spheres were also ground together with nZVI. The adsorption of nZVI onto silica surface by grinding was not successful as very little nZVI was adhered to the silica surface (Figure 4.11).
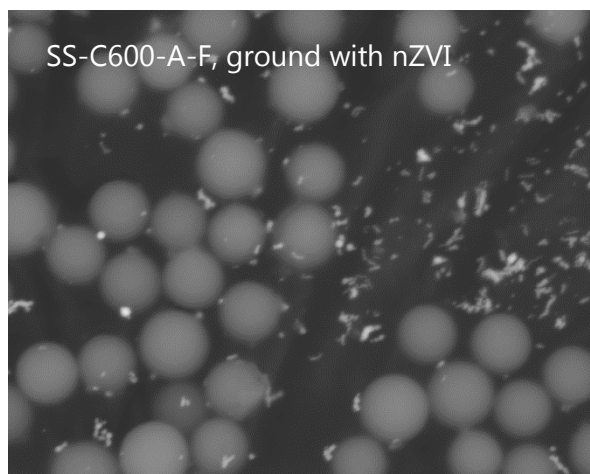
Figure 4.11. COMPO image of silica and nZVI ground together

4.4 Functionalised silica

As pure silica was not successful in adsorbing nZVI, functionalised silica was synthesised as a support. In this method, amino functional groups were added during synthesis of the spheres through the use of 3-APTES. There was no advantage of using 3-TPTMS compared to 3-APTES as suggested in the SG series. As 3-TPTMS is hazardous to the aquatic environment,[287,288] it was decided to continue the project with only 3-APTES. Amino-functionalised silica (AS) was synthesised following the protocol from Araki *et al* (section 2.1.2.).[214]   Different percentages of 3-APTES to TEOS were used (3 mol%, 5 mol% and 10 mol%) to form AS-3%, AS-5%, and AS-10% respectively. The nZVI was generated *in situ* by adding a sodium borohydride solution to a suspension of the AS support in an iron sulfate solution. After standard workup involving washing with water then ethanol, the new material was isolated. All of the AS-nZVI materials were dark grey in colour and magnetic, indicating the presence of iron nanoparticles. The resulting functionalised silica was not calcined as calcination remove the functional group.

Attempts to adsorb nZVI onto these surfaces were not very successful, whether an FeOOH coating was used or not. As with pure silica, some of the silica sphere were almost covered fully with nZVI particles, while others had none or very few (Figure 4.13).

According to Vacassy *et al*,[233] the amine group in 3-APTES/TEOS system acted as porogen (source of pores). Calcination at 500 °C removed the amine group, leaving pores behind. In this project, the AS series were calcined at 600 °C to ensure complete removal of the amine group. nZVI adsorbed on AS-5%-C600 were dark grey and magnetic (Figure 4.12). The surface of the silica was not noticeably rougher on the SEM (Figure 4.14), however the calcined AS series were noticeably better at adsorption of nZVI compared to the uncalcined series, even though the dispersion was uneven.
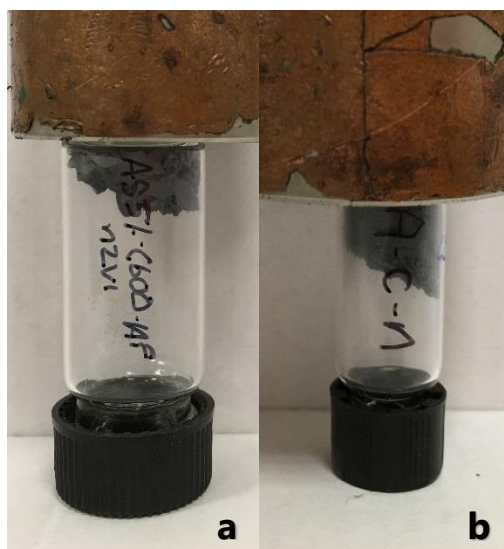
Figure 4.12. Magnetism of nZVI adsorbed on two AS-5%-C600 silica: a, AS-5%-C600-AF-nZVI; b, AS-5%-C600-AnF-nZVI.
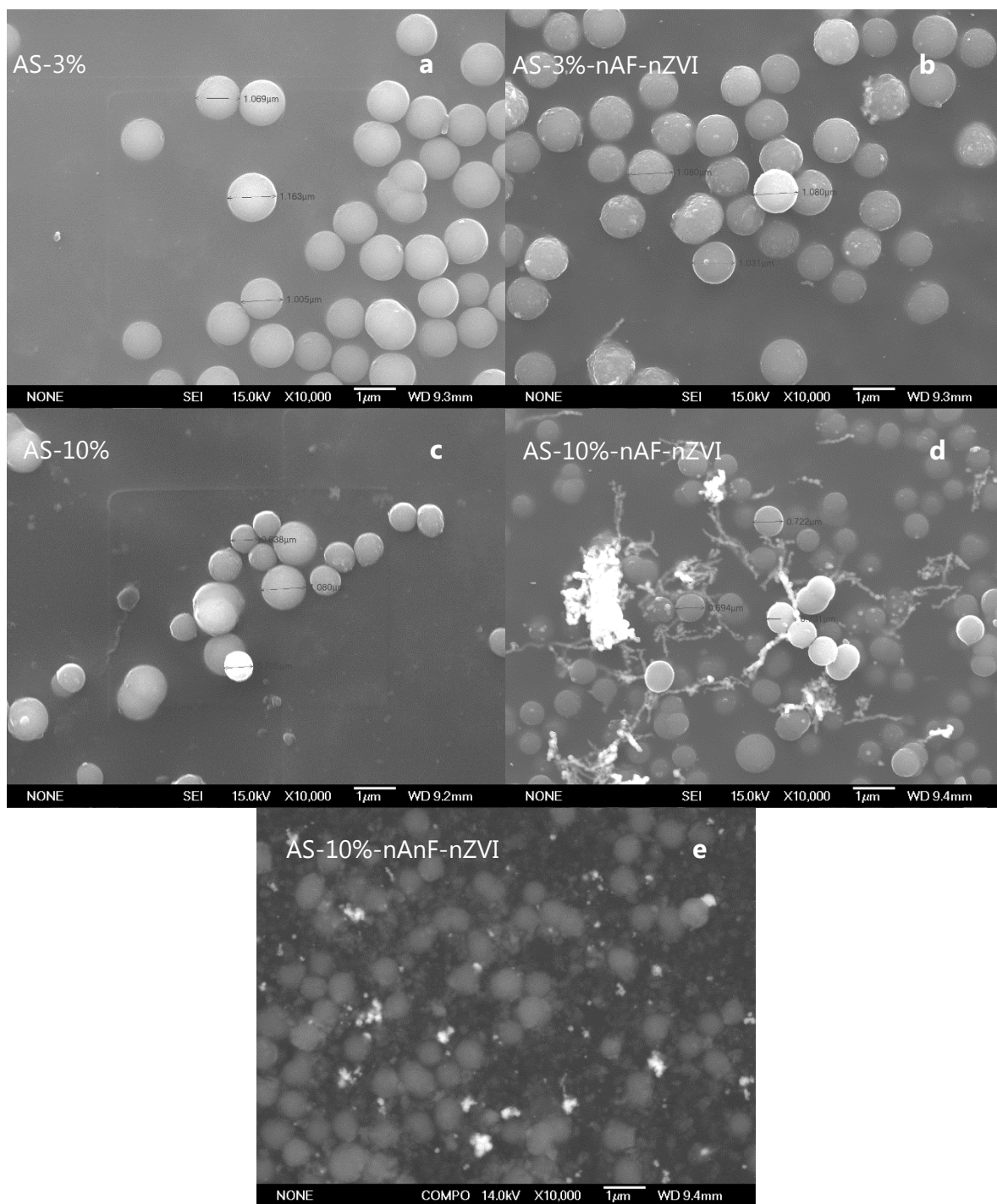
Figure 4.13. Amino-functionalised silica with nZVI: a, AS-3%; b, AS-3%-nAF-nZVI; c, AS-10%; d, AS-10%-nAF-nZVI; e, AS-10%-nAnF-nZVI.
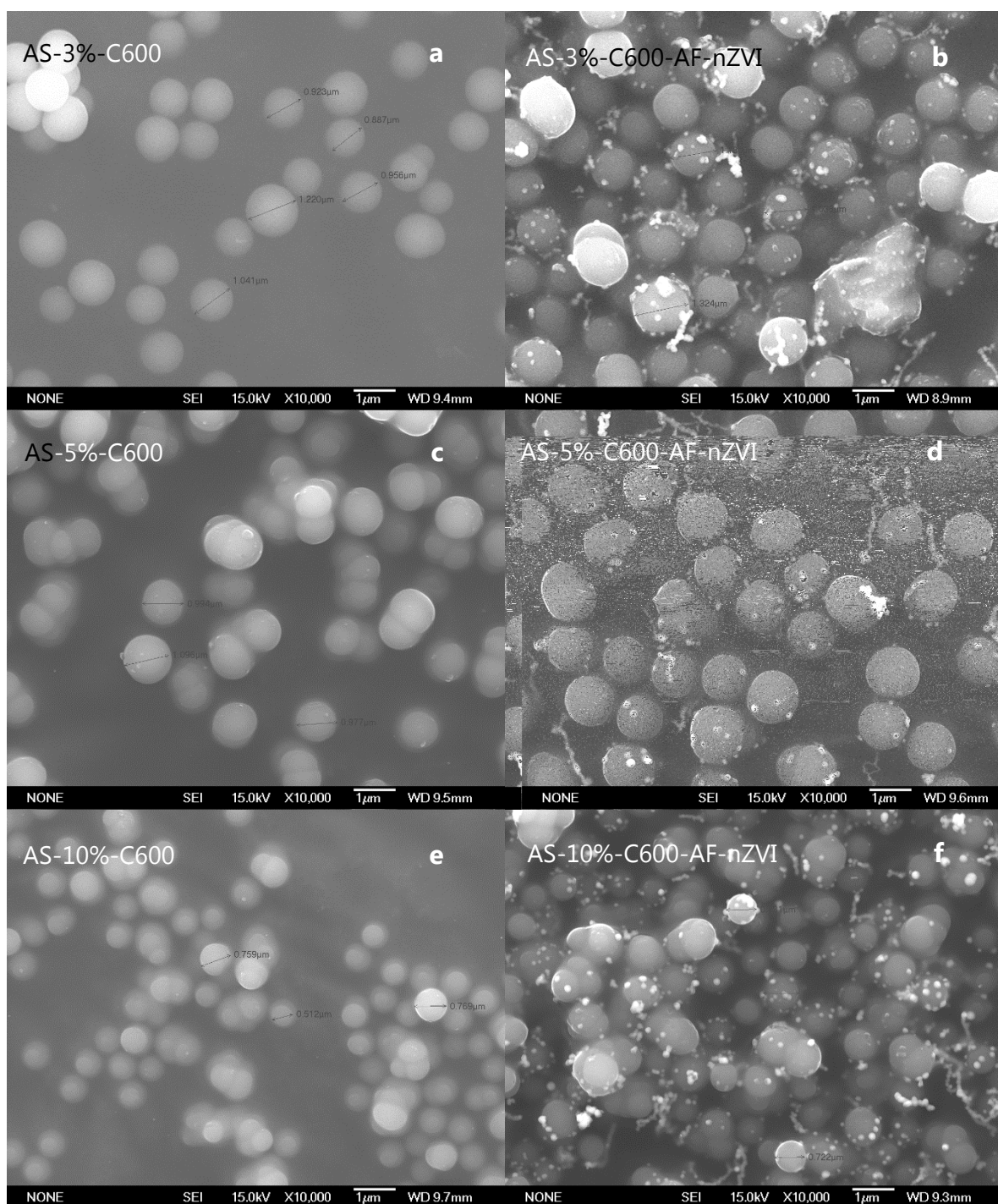
Figure 4.14. Calcined amino-functionalised silica with and without nZVI: a, AS-3%-C600; b, AS-3%-C600-AF-nZVI; c, AS-5%-C600; d, AS-5%-C600-AF-nZVI; e, AS-10%-C600; f, AS-10%-C600-AF-nZVI.

4.5 Nitrate reduction

Although the adsorption of nZVI onto SG/SS surface was not optimal, a number of these materials were tested for their nitrate reduction capabilities (Table 4.1). The ratio of nZVI to NO_3^- was kept at 50:1 for all the experiments. All of these materials were only capable of reducing a maximum of 13% NO_3^- at the end of 30 minutes. All of these systems contained nZVI as shown in their SEM images and therefore their inability to reduce nitrate was surprising.

Table 4.1. List of SG, SS and AS-nZVI system tested for nitrate reduction

Silica/nZVI	%Nitrate removed (30 minutes)
SG-AF-nZVI	12
SG-dA-F-nZVI	8
SG-dB-F-nZVI	11
SG-Ar-3-APTES-F-nZVI	13
SG-Ar-3-APTES-F-nZVI (Fe^{3+})	8
SG-Ar-3-TPTMS-F-nZVI	3
SG-Ar-3-TPTMS-F-nZVI (Fe^{3+})	0
SS-C600-AF-nZVI	0
SS-C600-AnF-nZVI	10
AS-5%-C600-AF-nZVI	1
AS-5%-C600-AnF-nZVI	0

Some studies,[289,290] but not all,[291] had shown that nZVI-induced nitrate reduction was faster on lower pH. The pH of AS-5%-C600-AF-nZVI was adjusted to see whether the inability to reduce nitrate was related to the pH of the solution. When the pH was lowered to acidic condition, nitrate reduction was successful (Table 4.2). Unfortunately, the acidic conditions destabilise the adsorption of nZVI onto AS, and more loose aggregated nZVI could be observed on systems with lower pH (*vis-à-vis* Figure 4.15*a*, *b*, *c* with *d*).

Table 4.2. Relationship between pH and % nitrate removed after 30 minutes.

pH	%Nitrate removed (30 minutes)
1.75	94
1.8	95
6.7	86
8.1	6
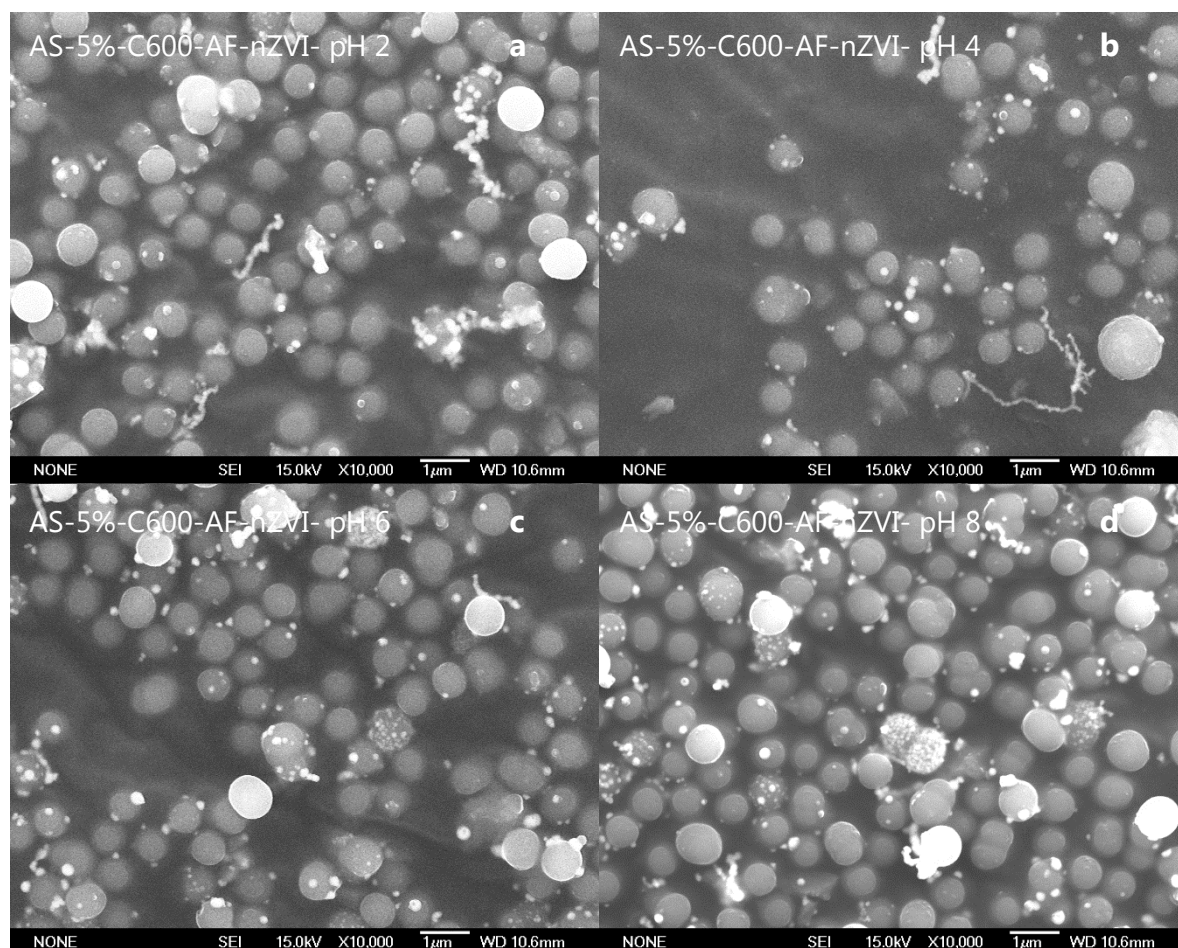
Figure 4.15. Stability of AS-5%-C600-AF-nZVI at different pH: a, pH 2; b, pH 4; c, pH 6; d, pH 8.

4.6 Conclusion

Despite many attempts at repeating these experiments under a variety of different conditions, the pure silica proved to be an ineffective support for nZVI. These results indicated that it was the presence of impurities in Misi that aids in the adsorption of nZVI. Calcined functionalised silica, AS-3%-C600-AF, AS-5%-C600-AF and AS-10%-C600-AF, were marginally better at adsorbing nZVI; however nZVI aggregates were still observed and adsorption was uneven.

These materials showed limited ability to reduce nitrate. Nitrate reduction was only observed for AS-5%-C600-AF-nZVI when the pH of the system was manually lowered. This was in sharp contrast to the nitrate results observed for nZVI supported on Misi (section 6.2.1) in which no pH adjustment was required. As such, the use of these silica-supported nZVI materials was not investigated further.

5 Adsorption of nZVI on waste and precipitated silicate surfaces

5.1 Introduction

In this chapter, the adsorption of nZVI on other types of silicates were investigated. The first three types of silicates can be categorised as by-product silicates: from rice production (rice husk ash), silicon smelter (Western Australia silica fume), and power generation (Mt Piper fly ash) and their compositions were listed in Table 5.1. Precipitated aluminium silicate, which is a condensation product of sodium silicate and aluminium sulfate, was also examined as an example of a pure aluminosilicate system. From these four waste products, rice husk ash (RHA) has the highest silica content at 95% and very low alumina at 0.4%. Western Australia silica fume (WA) and Mt. Piper fly ash (PFA) has a similar profile with ~60% silica and 20 – 30% alumina and ~1% iron oxide. The silica, alumina, and iron oxide content of Misi were approximately between RHA and WA/PFA.

Table 5.1. Composition of 4 by-products Silicates, expressed as % of their oxide

By-product Silicate	SiO_2	Al_2O_3	Fe_2O_3	CaO	Na_2O	K_2O	MnO	TiO_2	MgO	P_2O_5	SO_3
Misi[292]	86	5	0.46	0.3	0.19	0.66	0.02	0.69	0.08	0.04	0.03
Rice Husk Ash[293]	95	0.4	0.26	0.54	0.25	0.94	0.16	0.02	0.90	0.74	-
Western Australia Silica Fume	61.4	33	1.1	0.6	0.1	0.1	2	-	-	-	-
Mt Piper Fly Ash[294]	67	23.8	1.72	0.31	0.25	2.46	0.03	0.99	0.27	0.11	<0.01

5.2 Rice husk ash

Rice husk is the outer layer and the stalk of harvested rice that is collected after threshing.[279] For each ton of rice produced, approximately 0.23 ton of RHA is created.[295] Annually, 700 million tonnes of rice is produced worldwide, producing 160 million tonnes of RHA. Traditionally, rice husk is burned to provide energy for further processing of the grain. In Indonesia, RHA has many traditional uses, such as household abrasives, to prevent bricks sticking to each other during brick making, and along with crushed brick and salt, as a coating to make salted duck eggs.[280] Household demand for RHA is very low compared to its

production rate as these traditional usages, though varied, are not enough to utilise all the RHA produced. Hence, the drive to utilise this by-product in other way is very high.[298]

In the 1990s, it was observed that RHA is high in silica. This allowed RHA to be used as a source of pure silica for various applications including silicon wafer and silicon nitride production.[299] RHA was typically treated with base and calcined at high temperatures when used as a source of silica. When calcined below 700 °C, amorphous silica was produced, while above 700 °C, various crystalline phases of silica such as quartz and cristobalite are formed. RHA had also been used in the building industry to replace concrete due to its pozzolanic and concrete-strengthening properties.[299–303] The low alumina content of RHA made RHA a good candidate for exploring the role of alumina in nZVI adsorption on silica surfaces.

The RHA used in this research was mostly crystalline, with cristobalite as the major component (Figure 5.1). The XRD spectrum of RHA also showed diffraction peaks at 20.9°, 36.6° and 39.2° which were consistent with quartz, however the major quartz peak at 26.7° was not present. Therefore, the presence of quartz could not be confirmed.
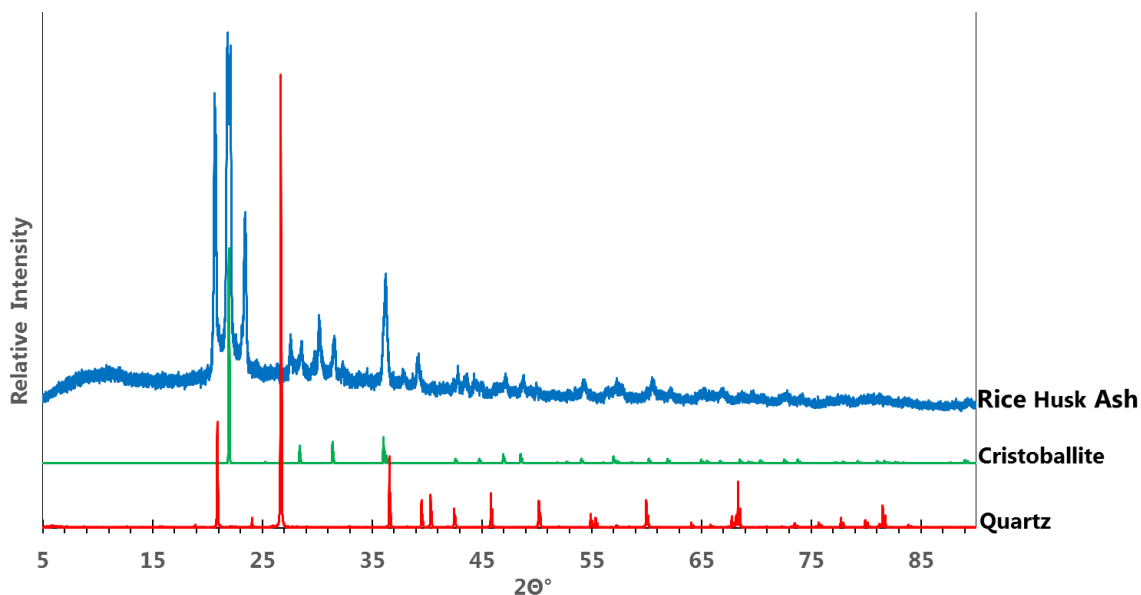
Figure 5.1. Powder X-Ray diffraction of RHA overlaid with Quartz (RRUFF ID#R040031) and Cristobalite (RRUFF ID#061107)

125
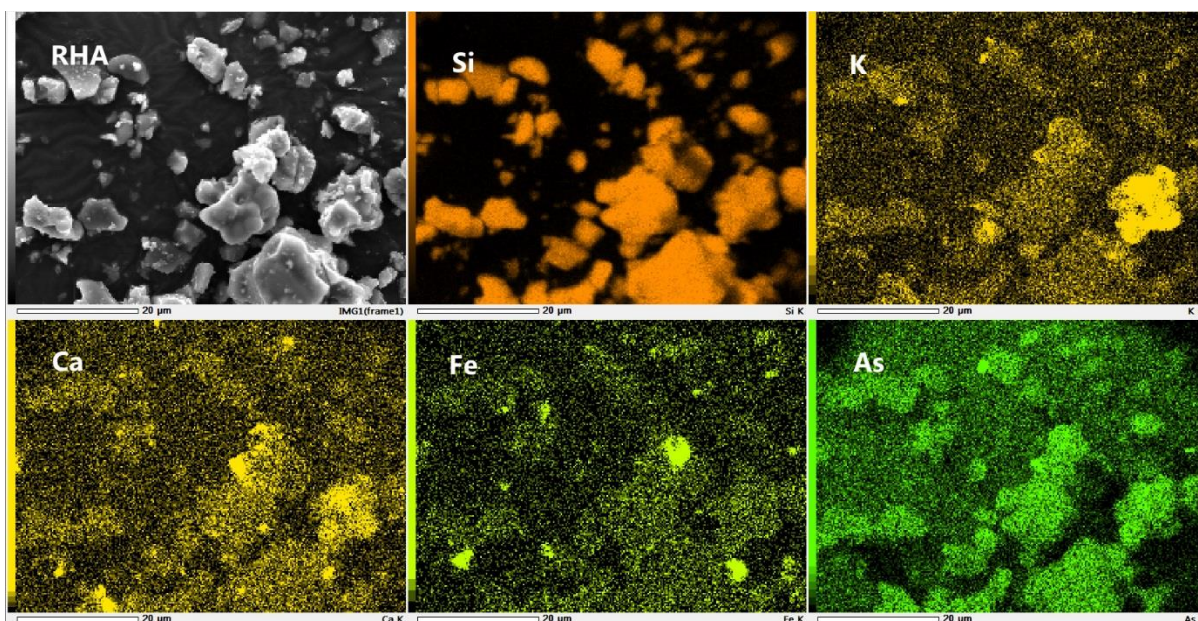
Figure 5.2. EDS mapping of RHA, showing distribution of Si, K, Ca, Fe and As.

EDS mapping of RHA showed that calcium, potassium and iron were not evenly distributed in the sample (Figure 5.2). RHA also contains trace amounts of arsenic, titanium, aluminium and sodium. Arsenic was more evenly distributed on the ash compared to other metals, but the amount present was very small. The presence of arsenic was expected in RHA as roots of rice uptake arsenic as arsenates in soil or water that contains arsenate or arsenite.[304–306] Arsenic contamination came from water that naturally contains arsenic (e.g. in Bangladesh), pollution from metal mining (e.g. in Thailand and China), and soil that had been treated with arsenic-containing pesticides (e.g. in South Central USA).[307]

RHA as Support for nZVI

To determine if RHA was suitable as a support for nZVI, it was exposed to some of the same treatments that maximised adsorption of nZVI onto Misi. This included calcination at 600 °C in all cases as well as:

1. boiling (RHA-C600-AnF),
2. boiling followed by coating with an FeOOH layer (RHA-C600-AF),
3. acid washing with 5.6 M HCl followed by calcination, boiling and coating with an FeOOH layer (RHA-5-C600-AF).

126

The nZVI was generated *in situ* by adding a sodium borohydride solution to a suspension of the RHA support in an iron sulfate solution. After a standard workup involving washing with water followed by ethanol, the new material was isolated. All of the nZVI-RHA materials were dark grey in colour and magnetic, indicating the presence of iron nanoparticles (Figure 5.3). However, SEM images of the materials indicated only minimal adsorption of nZVI onto RHA (Figure 5.4).   In all cases, the majority of the nZVI agglomerated, although some adsorption was observed.
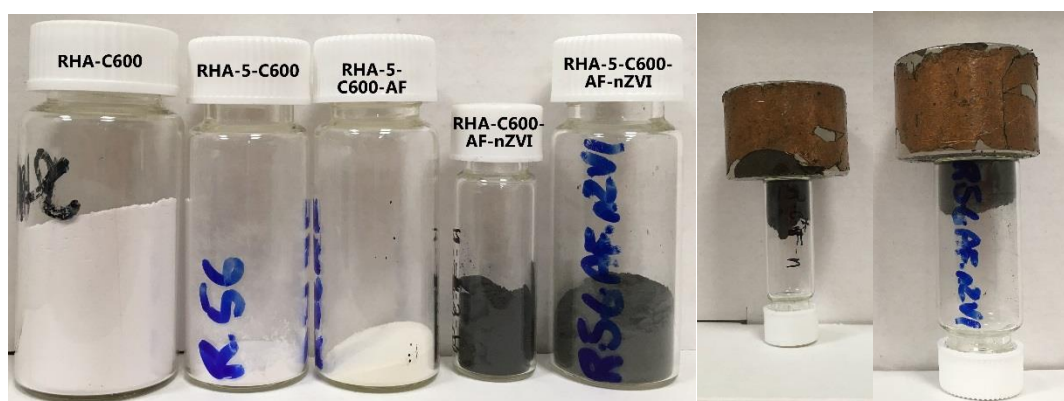
Figure 5.3. RHA at various stage of treatments: RHA-C600, RHA-5-C600, RHA-5-C600-AF, RHA-C600-AF-nZVI and RHA-5-C600-AF-nZVI, and showing the magnetism of RHA-C600 AF-nZVI and RHA-5-C600-AF-nZVI

These results were similar to that of untreated RHA and highlight how seemingly minor changes in the composition of the silicate had major implications towards the adsorption of nZVI. The major differences between RHA and Misi was the smaller alumina content in RHA over Misi and the pre-dominance of the cristobalite in RHA versus quartz in Misi. In addition, the RHA particles were larger than that of Misi, although it was unclear if that was a factor in their relative capability of adsorbing nZVI.
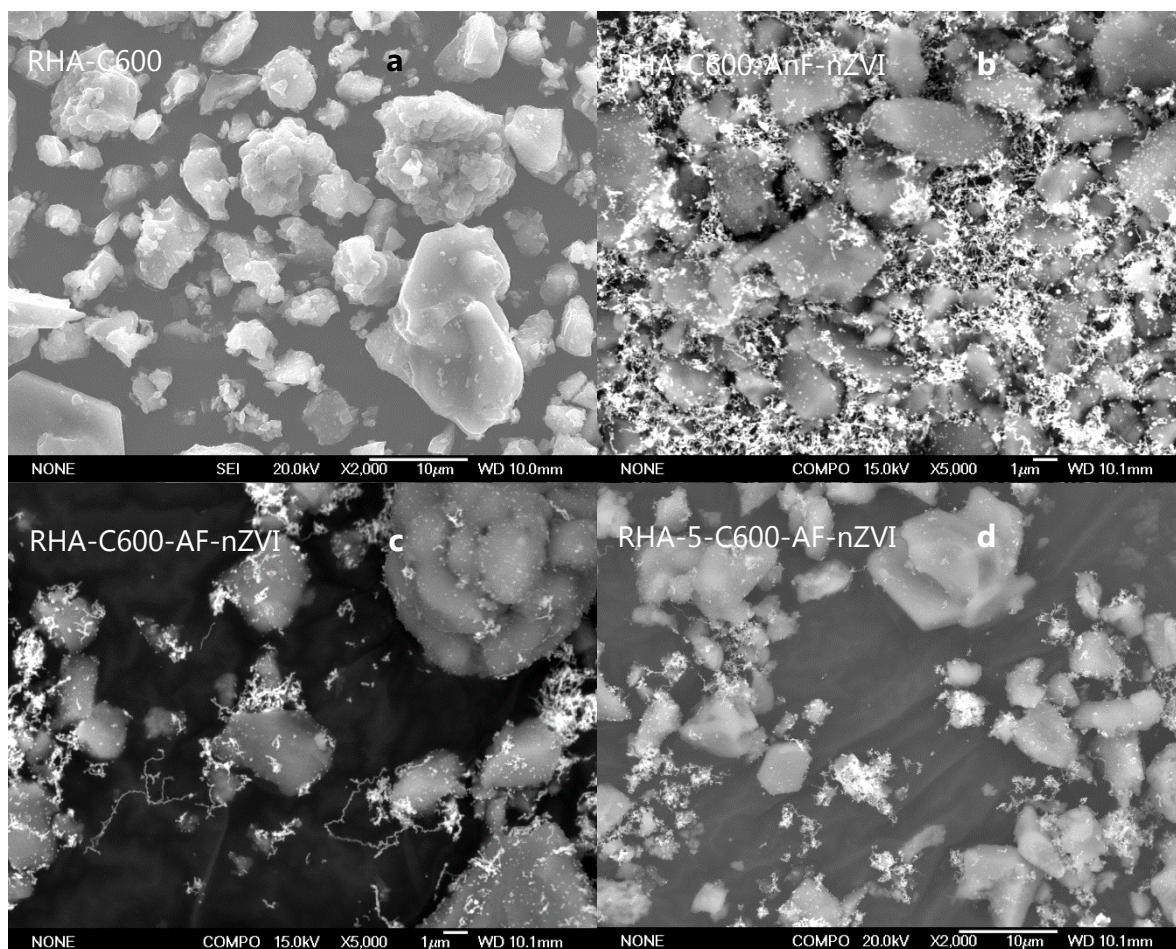
Figure 5.4. SEM images of a, RHA-C600; b, RHA-C600-AnF-nZVI; c, RHA-C600-AF-nZVI and d, RHA-5-C600-AF-nZVI

5.3 Western Australia silica fume

Western Australia silica fume (WA) is a by-product of silicon smelters in Australia. In a silicon smelter, raw material such as sand or quartzite (metamorphic rock composed of quartz) are mixed with a reductive carbon source such as charcoal and coal, and heated using electric arc furnaces to 3000 °C. Quartz is reduced by carbon to silicon and CO via SiO intermediates (eq. 29). The SiO intermediates reacts with C to form solid silicon carbide in the furnace (eq. 30), which reacts with more silica to form silicon and silicon monoxide (eq. 31). Unreacted SiO is oxidised by O_2 in the atmosphere to make SiO_2 silica fume particles (eq. 32), which can be collected in filtration facilities.[308]

128

$$SiO_2 + C \longrightarrow SiO + C \qquad (29)$$

$$SiO + 2C \longrightarrow SiC + CO \qquad (30)$$

$$SiC + SiO_2 \longrightarrow Si + SiO + CO \qquad (31)$$

$$2SiO + O_2 \longrightarrow 2SiO_2 \qquad (32)$$
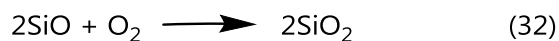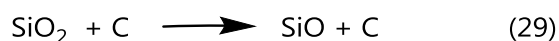
WA silica fume is commonly used as an additive in cement similar to Misi. WA silica fume has a much higher content of alumina, but lower content of silica. WA is mostly amorphous, although it did have some unidentified crystalline phase (Figure 5.5). WA can be used to see whether crystallinity is important for nZVI adsorption on silicate surfaces. The alumina content of WA is higher than Misi (33% and 5% respectively).
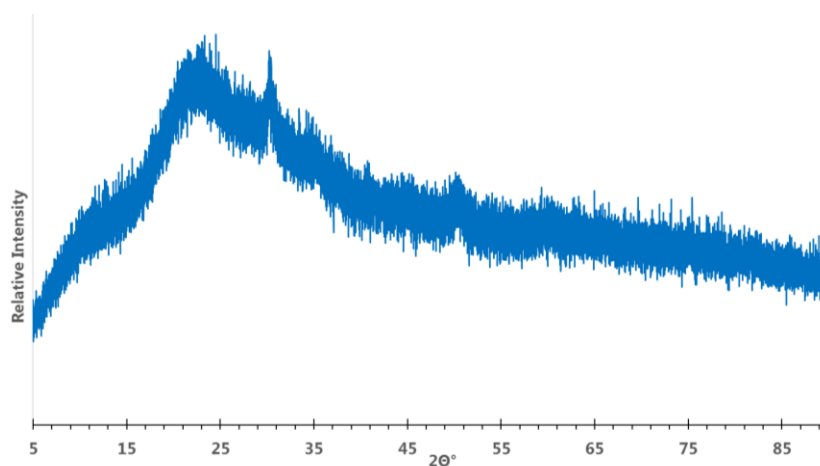
Figure 5.5. Powder X-Ray Diffraction of Western Australia silica fume.

WA as support for nZVI

Initial studies showed that raw WA was not a good support for nZVI as evidenced by the loose agglomerates of nZVI (Figure 5.6). WA was then exposed to two sets of treatments. The first one was calcination at 600 °C, boiling and coating with an FeOOH layer (WA-C600-AF) and the second was calcination, acid wash with 5.6 M HCl, boiling and coating with an FeOOH layer (WA-C600-5-AF). The nZVI was generated in situ by adding a sodium borohydride solution to a suspension of WA support in an iron sulfate solution. After a standard workup involving washing with water and then ethanol, the new material was isolated. The resulting materials were mostly dark grey and magnetic (Figure 5.7).

129
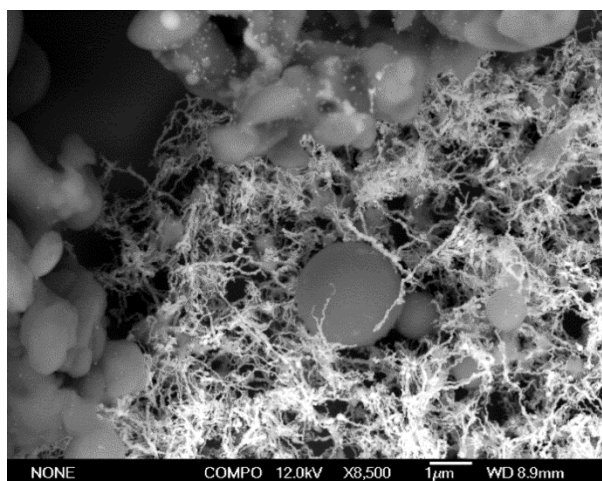
Figure 5.6. COMPO image of WA-nZVI, showing Si (gray) and Fe (white).
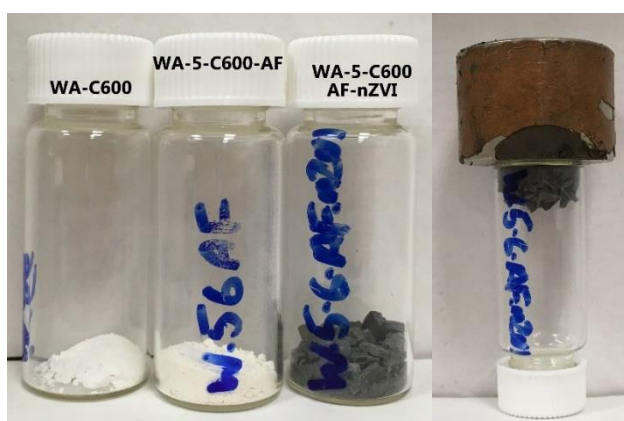
Figure 5.7. WA silica fume at various stage of treatments: WA-C600, WA-5-C600-AF, WA-5-C600-AF-nZVI, and showing the magnetic nature of WA-%-C600-AF-nZVI.

SEM images showed that nZVI was dispersed almost evenly on non-acid washed WA (WA-C600-AF), although chains of nZVI could still be observed (Figure 5.8). Some of the spherical particles acted as a good host for nZVI though more were dispersed on the smaller and more irregular particles. However, all acid washed WA samples showed poor adsorption of nZVI (Figure 5.9) with the majority of nZVI agglomerated. There was no observable surface difference between WA subjected to the different treatments of calcination, acid wash, activation, and FeOOH layer.

These results were the opposite of Misi, where acid washed Misi acted as a better support for nZVI compared to the non-acid washed Misi. Furthermore, nZVI adsorption on WA surfaces showed that the alumina content was very important (WA at 33%), while the crystallinity of the substrate was not as important.
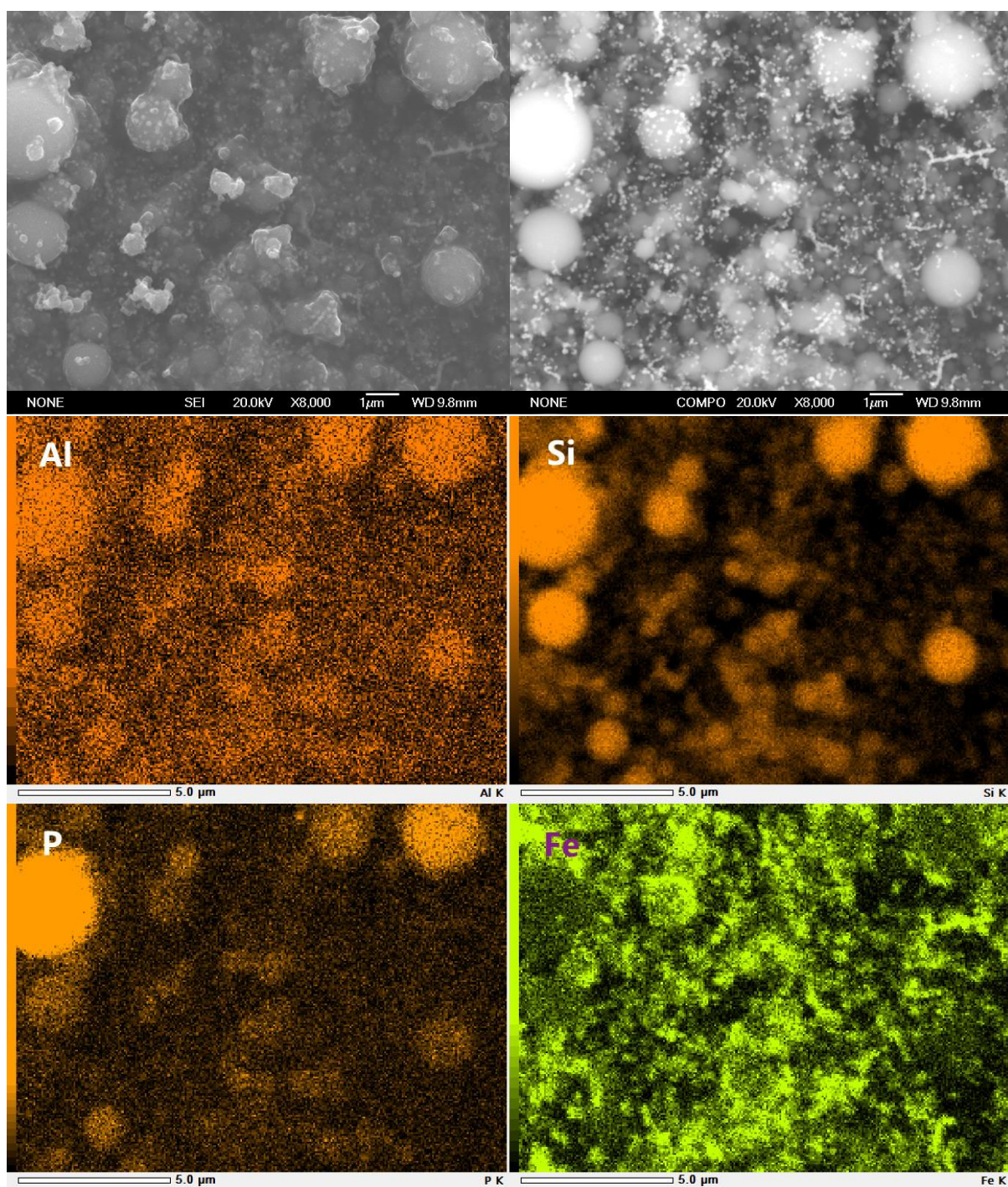
Figure 5.8. SEM, COMPO and EDS mapping of WA-C600-AF-nZVI. EDS maps showed the distribution of aluminium, silicon, phosphorus and iron.
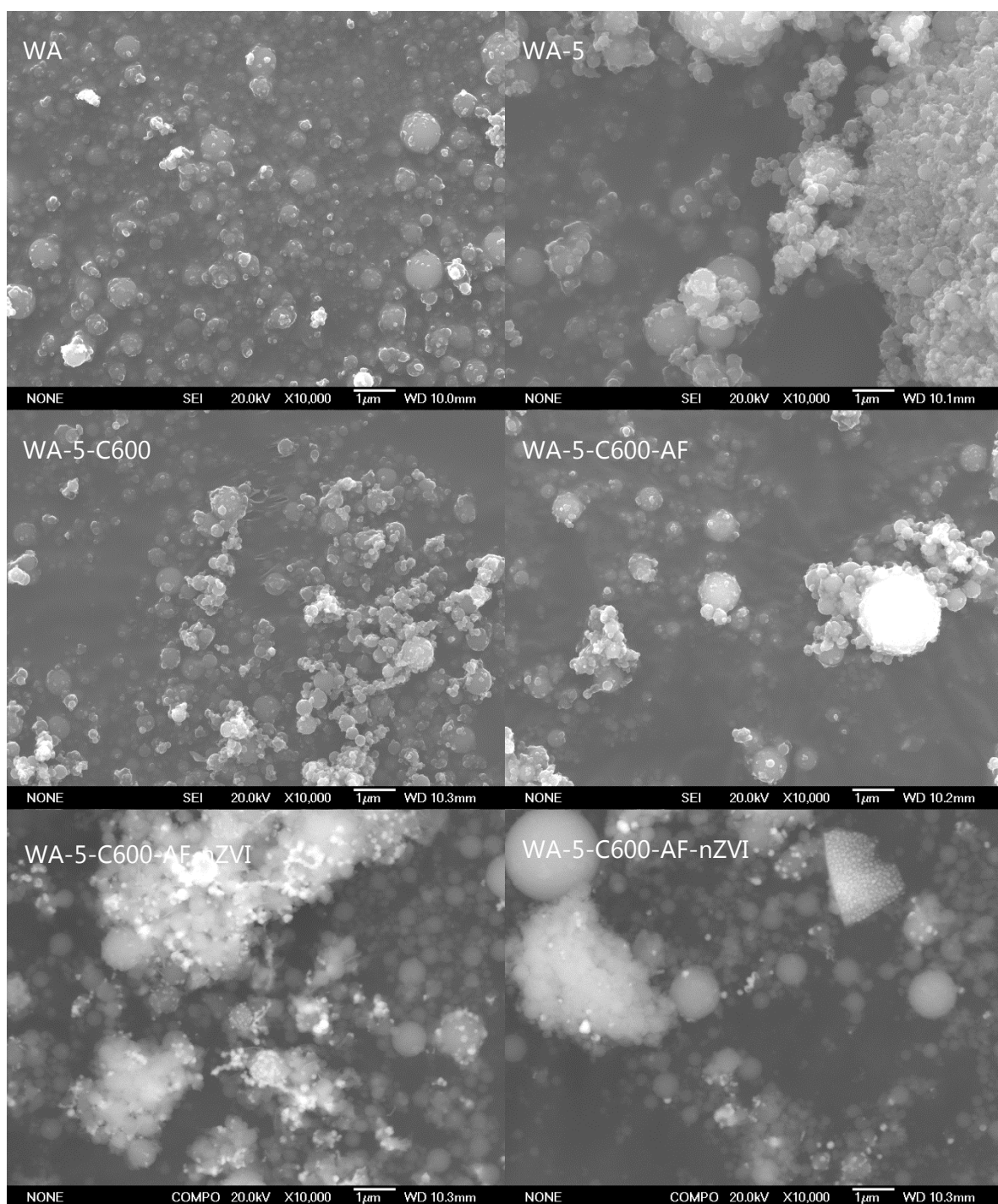
Figure 5.9. WA silica fume, and after acid wash, calcination, AF and with nZVI adsorbed on them

5.4 Mt. Piper fly ash

Fly ash is a by-product of coal burning. [309] In a coal-powered electricity plant, fly ash can be collected electrostatically from exhaust gas. The gaseous oxides (e.g. silicon, aluminium, iron, and titanium) condense into micro-sized spheres as it rapidly cool down while suspended in the exhaust gas. The rapid cooling of the exhaust gas means that most of the particles are amorphous, although some crystalline quartz phase can be detected on fly ash (Figure 5.10). Fly ash can also be used as a cement replacement like silica fume as it is pozzolanic. Mt Piper fly ash (PFA) used in this research came from Mt Piper Coal Power Plant near Portland in New South Wales, Australia.
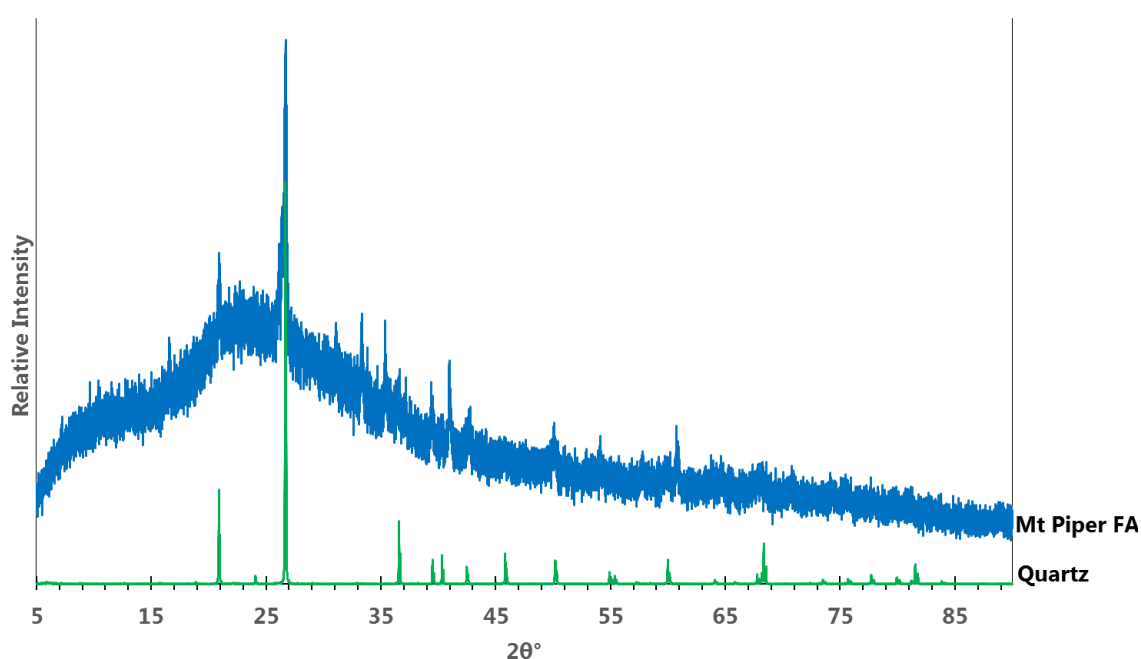
Figure 5.10. Powder X-Ray Diffraction of Mt Piper fly ash overlaid Quartz (RRUFF ID#R040031)

The composition of fly ash varies depending on the coal source. The PFA particles are spherical with a large variation in size (Figure 5.11). The EDS map showed that the dispersion of elements was uneven. Some spheres had more aluminium than silicon, and vice versa, and some were enriched with iron. Titanium overlapped more with aluminium than silicon.
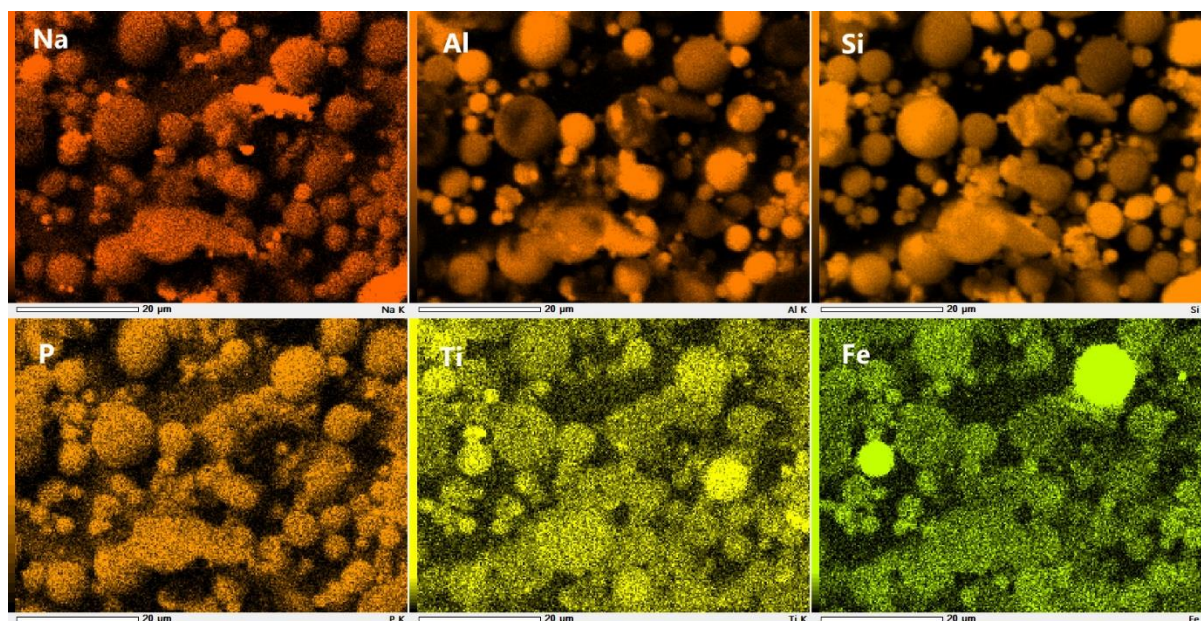
Figure 5.11. EDS mapping of PFA, showing the distribution of Na, Al, Si, P, Ti and Fe.

PFA as support for nZVI

Four different types of PFA were examined, including untreated PFA and three different types of treated PFA. For the latter, all of them were calcined at 600 °C, then:

1. boiled with no FeOOH coating (PFA-C600-A-nF),
2. not boiled but with FeOOH layer (PFA-C600-nAF)
3. acid washed with 5.6 M HCl followed by calcination, boiling and coating with an FeOOH layer (PHA-5-C600-AF.

The nZVI was generated *in situ* by adding a sodium borohydride solution to the suspension of the PFA support in an iron sulfate solution. After standard workup involving washing with water followed by ethanol, the new material was isolated. The PFA/nZVI materials were dark grey in colour and magnetic, indicating the presence of iron nanoparticles (Figure 5.12).
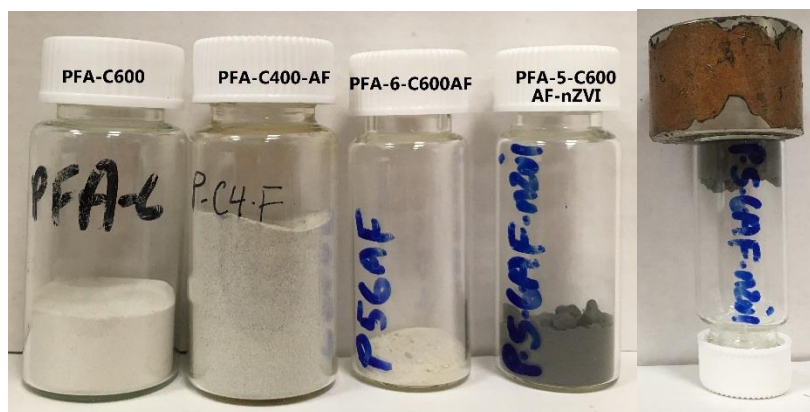
Figure 5.12. PFA at various stages of treatments: PFA-C600, PFA-C400-AF, PFA-5-C600-AF-nZVI and the magnetism of PFA-5-C600-AF-nZVI

Figure 5.13 showed the adsorption of nZVI on the four Mt Piper fly ash (PFA) surfaces. The adsorption of nZVI was most successful on the PFA-5-C600-AF and PFA-C600-nAF, whilst PFA-C600-A-nF and PFA-nZVI were the least successful as indicated by the loose agglomerates of nZVI. These results suggested that the acid wash improved the adsorption of nZVI onto the PFA surface. Furthermore, adsorption of nZVI to PFA surfaces required the FeOOH layer, but not the activation step. FeOOH layer aided the adsorption of nZVI to PFA surfaces although the role and mechanism was unclear.

Compared to PFA, WA was a better support for nZVI (*vis-à-vis* Figure 5.9 and Figure 5.13). WA-C600-AF-nZVI showed an even distribution of nZVI while none of the PFA was effective as a support. The major differences between PFA and WA was that PFA was more amorphous than WA. PFA has slightly more iron and titanium, however there was an even distribution of aluminium and silica in WA but not in PFA. (Figure 5.14). The nZVI adsorption results seemed to suggest that silicon and aluminium had to be on the same structure to afford adsorption of nZVI. Other groups had been unable to create an even dispersion of nZVI on pure ground alumina. [310] Chapter 4 showed that nZVI also did not adsorb on pure silica surfaces. This might explain why nZVI was poorly adsorbed on PFA surfaces that were mostly silica or mostly alumina.
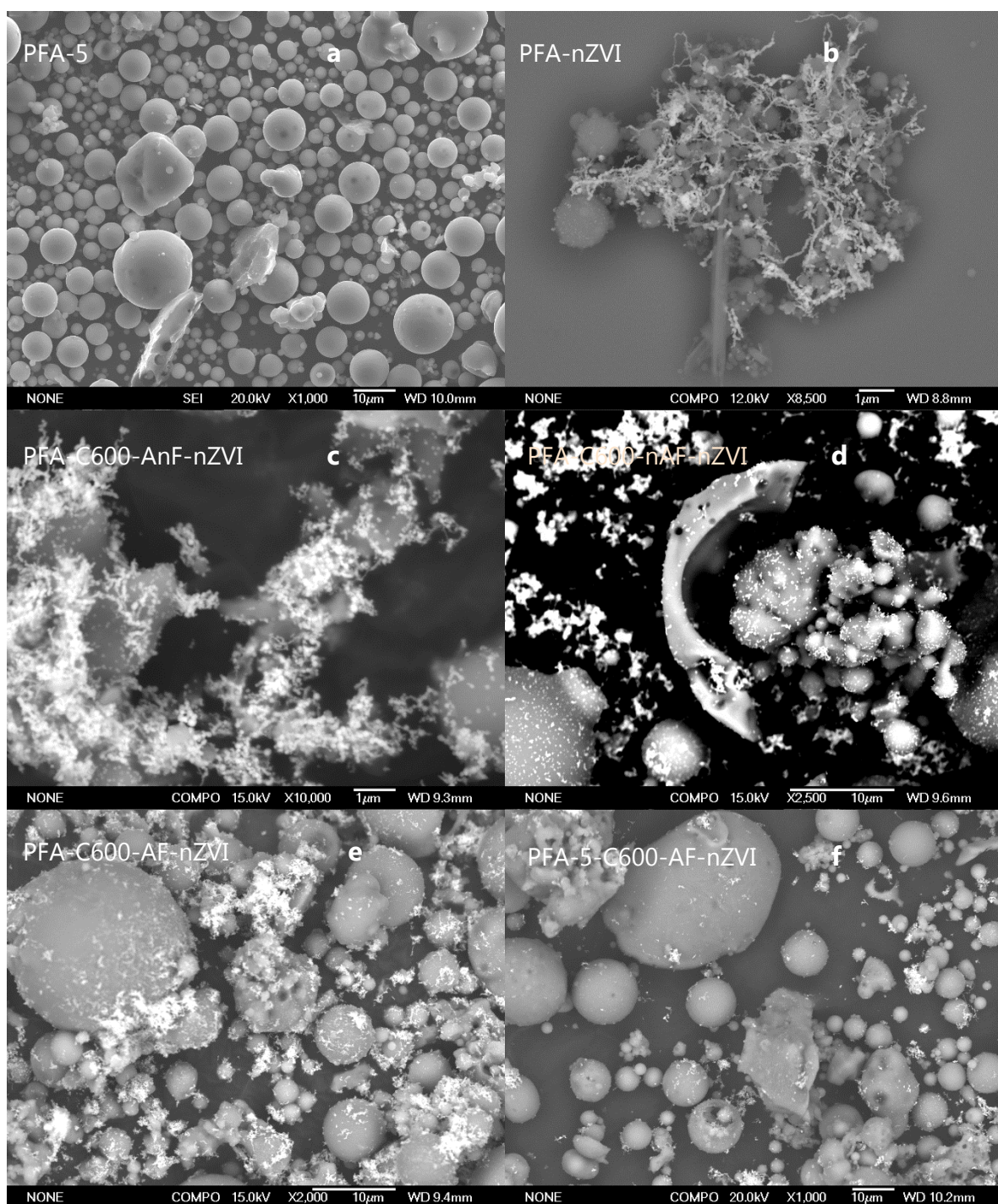
Figure 5.13. Mt Piper fly ash surfaces and nZVI adsorption on PFA: a, PFA-C600; b, PFA-nZVI; c, PFA-C600-A-nF-nZVI; d, PFA-C600-nAF-nZVI; e, PFA C600-AF-nZVI and f, PFA-5-C600-AF-nZVI.
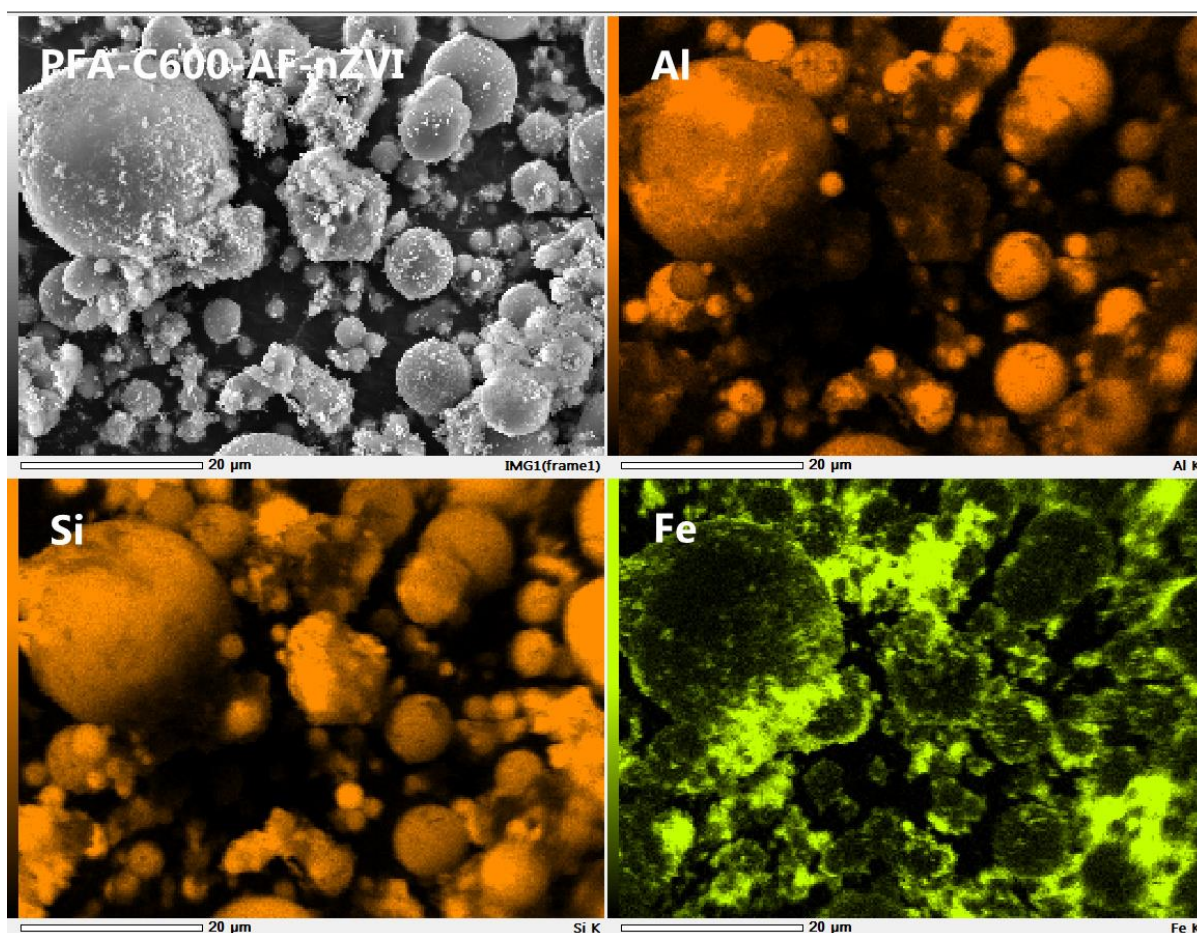
Figure 5.14. EDS mapping of PFA-C600-AF-nZVI.

Nitrate reduction

PFA-C600-AnF-nZVI and PFA-C600-AF-nZVI were tested for nitrate reduction. Both materials were able to reduce 25% of nitrate after 60 minutes. In both of these system, nZVI were not adsorbed fully on the surface of both PFA and the images were dominated by agglomerated nZVI, and yet the reduction of nitrate was minimal.

5.5 Precipitated aluminium silicate

The results from the four silicates that had been tested so far (Misi, RHA, WA and PFA) suggested that for nZVI to adsorb successfully on to silica/silicate surface, the surface must contain aluminium. To test this hypothesis, nZVI was adsorbed on precipitated aluminium silicate (**AlSi**). Precipitated aluminium silicate is typically synthesised from sodium silicate and aluminium sulfate. The AlSi used in this experiment was an amorphous white powder (Figure

137

5.15). EDS mapping for AlSi showed an overlay of sodium, silicon and aluminium, the only three elements present aside from oxygen (Figure 5.16).
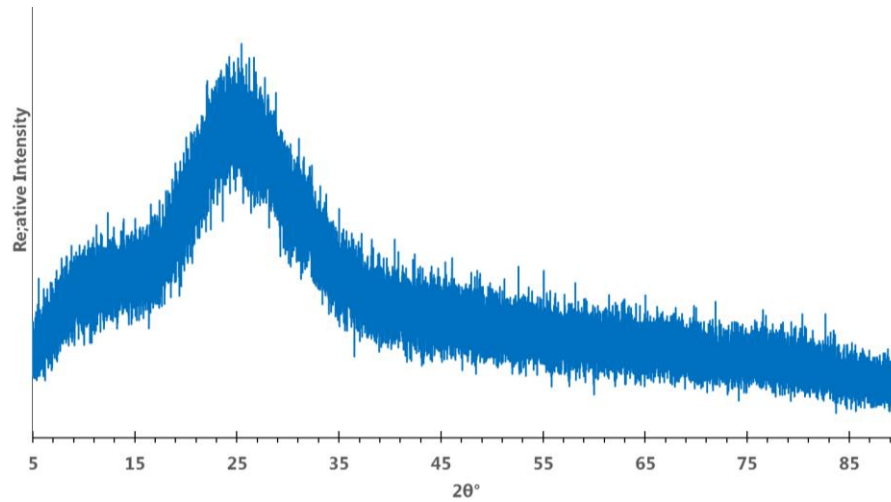
Figure 5.15. X-Ray Diffraction of precipitated aluminium silicate.
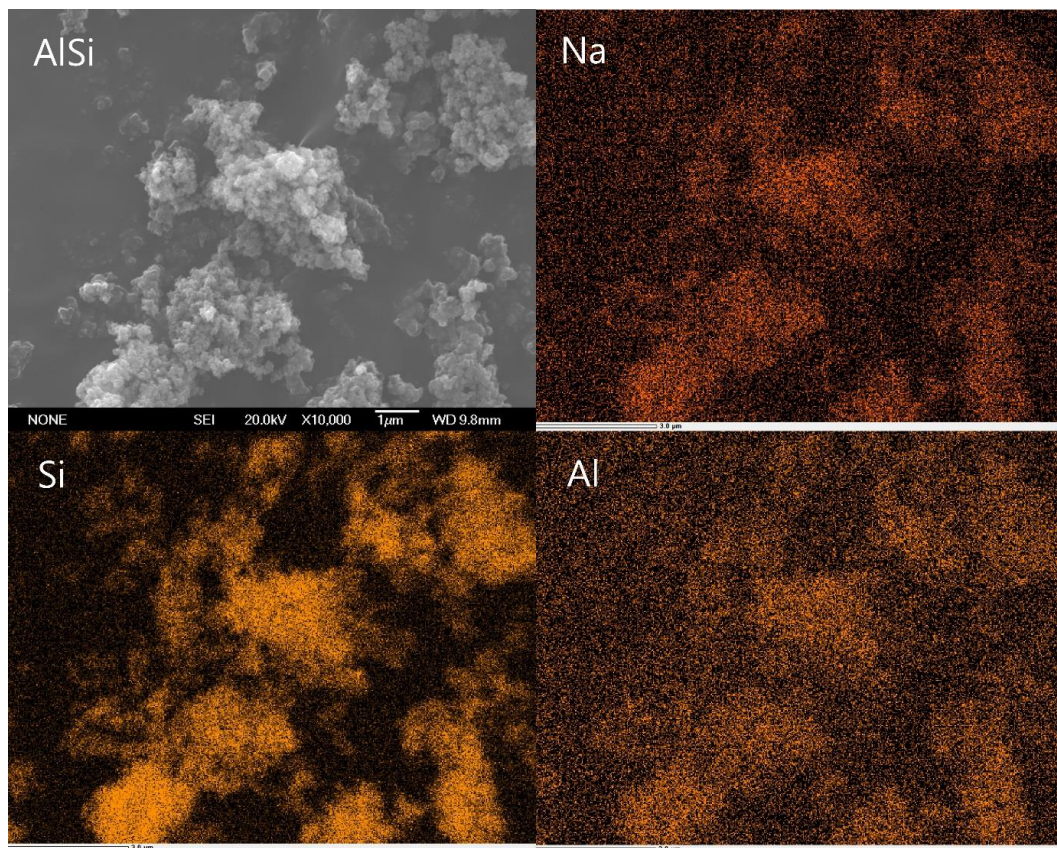
Figure 5.16. EDS mapping of raw precipitated aluminium silicate.

nZVI was synthesised in the presence of raw AlSi (without any treatment) and AlSi that had been calcined, boiled and coated with a FeOOH layer (AlSi-C600-AF). Upon addition of aqueous $FeSO_4$ to raw AlSi, the solution turned dark green. The dark green was consistent with sulfate green rust. This observation was similar to that observed with 3-APTES functionalised SG.[284] After the addition of borohydride solution, a standard workup of washing with water and ethanol was performed. It was noted that compared to all of the other materials previously synthesised, both of the AlSi materials took longer to dry under vacuum, requiring the application of heat before dryness was achieved. This might be due to the fineness of the AlSi powder. The AlSi-nZVI material was dark grey in colour and magnetic, indicating the presence of iron nanoparticles. In contrast, AlSi-C600-AF-nZVI was a lighter grey and not fully magnetic (Figure 5.17).
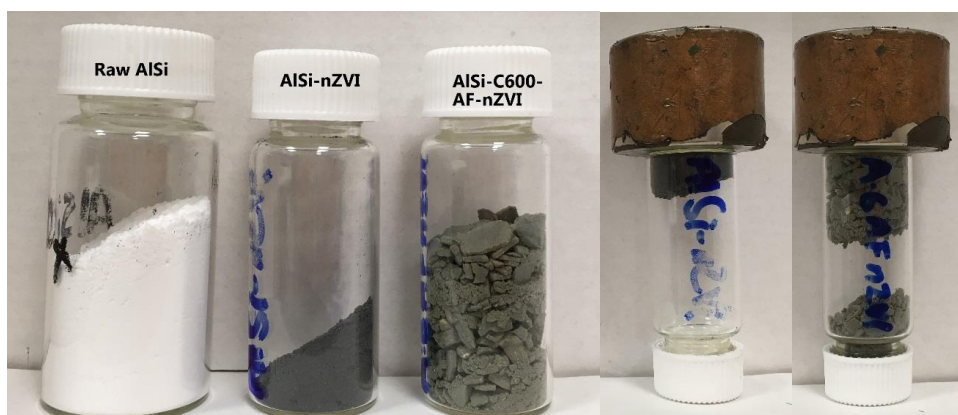
Figure 5.17. From left to right: Raw AlSi, AlSi-nZVI, AlSi-C600-AF-nZVI, magnetic properties of AlSi-nZVI and AlSi-C600-AF-nZVI.

SEM images of the materials showed that the adsorption of nZVI was much better on raw AlSi compared to AlSi-C600-AF (Figure 5.18).   AlSi-C600-AF-nZVI did not show discrete nZVI particles adsorbing onto the surface, even though the EDS mapping showed the presence of iron (Figure 5.19). nZVI were evenly dispersed on raw AlSi. This result seems to support the hypothesis that for successful adsorption, an aluminium silicate surface was needed, and crystallinity was not important.
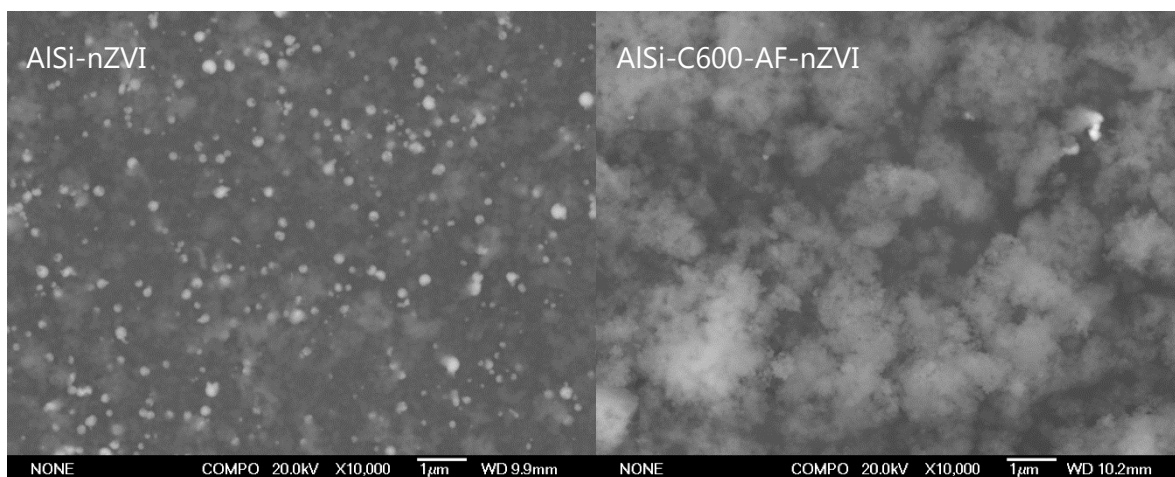
Figure 5.18. Comparison between AlSi-nZVI and AlSi-C600-AF-nZVI
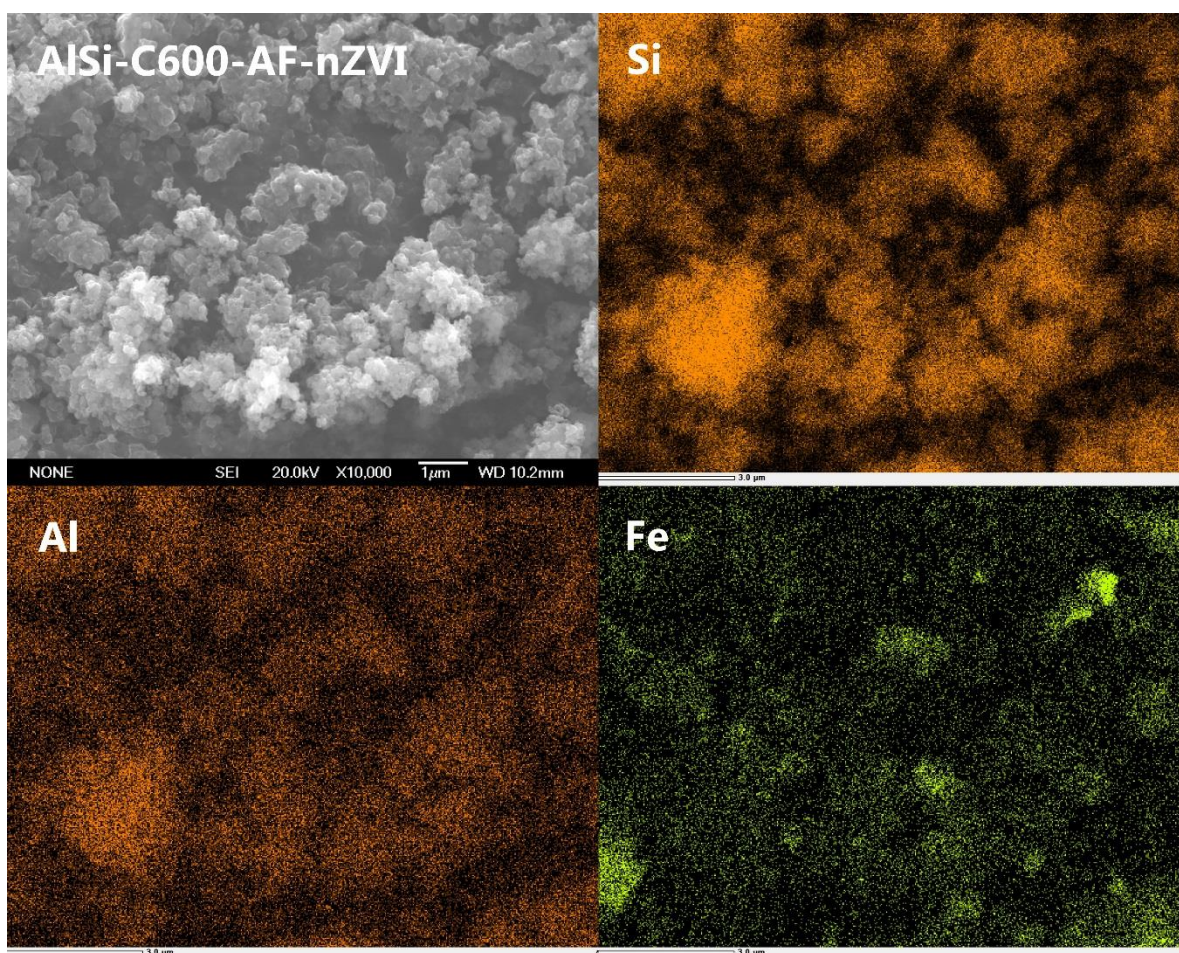
Figure 5.19. SEM images and EDS mapping of AlS-C600-AF-nZVI

From EDS mapping, the atomic percentage for each element present on the surface can also be calculated (Table 5.2). The percentages reported from EDS were not absolute value, as the amount of carbon tape exposed at any given area will greatly influence the percentage of other elements. Hence all the percentage were normalised against percentage of the total silicon. Furthermore, it can be assumed that during the processing, the amount of Si stays relatively constant as calcination, activation or layering with FeOOH did not change the amount of silicon.

As all of these measurements were taken of only one sample, uncertainties could be reported. AlSi were more homogenous than the other silicates tested so far, as evident from the EDS mapping (Figure 5.16). The trend that could be discerned from this table was worth noting. The ratio of Al to Si stayed relatively constant, however the fluctuation of atomic percentage of sodium and oxygen were much greater. The ratio of O to Si decreased greatly as AlSi was calcined (entry 1 and 3), while the ratio of both Al and Na to Si increased. These changes were consistent with removal of OH group from aluminosilicate during calcination.

Table 5.2. Ratio of O, Na, Al, Fe, S and K to Si of different AlSi surfaces from EDS-mapping

Entry	AlSi surfaces	Si	O	Na	Al	Fe	S	K
1	Raw AlSi	1.000	23.278	0.367	0.139		0.013	0.013
2	AlSi-nZVI	1.000	19.545	0.325	0.154	0.268		
3	AlSi-C600	1.000	20.960	0.416	0.149			
4	AlSi-C600-AF	1.000	23.627	0.269	0.149	0.045	0.015	
5	AlSi-C600-AF-nZVI	1.000	14.223	0.376	0.134	0.079	0.025	

Sodium ions were typically exchangeable in silicate structure with other cations.[263,311] As the iron sulfate solution for the iron oxyhydroxide layer was added, sodium ions were exchanged with iron, as shown by the decrease of sodium (entry 4). As the iron layer was oxidised, the percentage of oxygen atom also increased.   Formation of nZVI requires $NaBH_4$, and the data suggested that boron from $NaBH_4$ was removed during washing while sodium was reintroduced back to the system (entry 2 and 5).

The decrease of oxygen as nZVI was adsorbed onto the surface of AlSi-nZVI and AlSi-C600-AF-nZVI (entry 2 and 5 respectively) was more perplexing. It would make more sense for the amount of oxygen to increase as nZVI had a layer of FeO on its surface. As AlSi-nZVI (entry 2) had no FeOOH layer, the lost oxygen cannot come from FeOOH, although it was possible for this oxygen to come from FeOOH for AlSi-C600-AF-nZVI (entry 5). The only other plausible source of oxygen for AlSi-nZVI (entry 2) was the OH from silicate structure, however confirmation of this hypothesis was not yet attempted. Furthermore, AlSi-nZVI showed elevated amounts of aluminium and higher content of iron compared to entry 5. It can be postulated that for AlSi-nZVI, the addition of $FeSO_4$ allowed exchange between oxygen based molecule, possibly bound OH_3^+ and Fe^{2+}. This explained the formation of green sulfate rust, although why the green rust was not formed with AlSi-C600-AF was unclear.[284]

Nitrate reduction

AlSi-nZVI was tested for nitrate reduction. Unfortunately, it was unable to reduce nitrate with only less than 10% of nitrate removed after 60 minutes.

5.6 Conclusion

From the four silicates trialled in this chapter, raw AlSi provided the best adsorption surface for nZVI, followed by WA-C600-AF. The results suggested that nZVI would readily adsorbed on an aluminosilicate surface with a relatively large amount of alumina, but not on an aluminosilicate with low alumina content. Even though PFA was classified as an aluminosilicate, EDS mapping suggested that the alumina surfaces were different to silica surfaces, and this might lend to the minimal adsorption of nZVI on PFA. RHA consists of mostly silica, and hence the adsorption of nZVI onto RHA surfaces was not successful.

6 Application of nZVI-Misi

6.1 Introduction

The dispersion of nZVI onto supports was linked with various measurements such as efficiency in environmental remediation capabilities, transport ability and reduction in potential harm in terms of leaching nZVI to the environment.[206,312–314] In this chapter, the nitrate reduction capabilities of several nZVI/Misi system were investigated, first in connection to their surface treatment, and later, with A-value. The transport ability and leaching of nZVI particles in a column set up will also be examined.

6.2 Nitrate reduction

6.2.1 Effect of surface treatment and relationship of A-Value with nitrate reduction

nZVI-Misi systems that scored well on the A-scale were tested for their ability to reduce nitrate. In a typical test, 0.1 g nZVI/silicate (approximately equivalent to 0.02 g of nZVI) was used to reduce 10 mL of a 10 ppm NO_3^- -N solution, which was approximately equal to 50:1 Fe:NO_3^- molar loading. As a comparison, based on the candidate's honour project, bare nZVI can reduce 100% of nitrate within 15 minutes with the same molar ratio. Overall, 12 different nZVI/Misi systems were tested for nitrate reduction, including calcination temperature (C400 or C600), acid wash (5), boiling (A and nA), and FeOOH layer (nF and F). To make the graphs easier to analyse, a combination of patterns and colours were used as described in Table 6.1. For example, Misi C600-5-AF was represented by purple vertical lines, Misi 5-C600-nAnF by green horizontal lines.

Table 6.1. Combination of pattern and colour to denote different modifications to Misi

5-C600	C600-5	5-C400	C600	C400
AF	AnF	nAF	nAnF	

The reproducibility of nitrate reduction was probed, both in terms of the comparisons of the same Misi batch, and by comparing different batches of Misi that have undergone the same treatment. The number of replicates for each sample and number of different batches tested for each one was listed in Table 6.2. The reproducibility of nitrate reduction was typically consistent when comparing the same batch; however different batches of the same type of Misi were less reproducible. For instance, for C600-AF-nZVI (entry 11), the first batch with 3 samples had an uncertainty of 2% (from percentage removed of 85%). Between batches however, the range of nitrate removal varies from 43 % to 86 %.

As shown in Chapter 3, the calcination of Misi was an important step for maximizing the adsorption of nZVI onto its surface. Although only minor changes in adsorption of nZVI onto Misi were observed when Misi was calcined at 400 °C versus 600 °C, the samples calcined at 600 °C were consistently able to reduce nitrate more than the samples calcined at 400 °C when comparing similar additional treatments. For instance, after 60 minutes, C400-AF-nZVI removed 39 ± 5% of nitrate whereas C600-AF-nZVI removed 62 ± 9 % (Figure 6.1). A greater difference was observed with 5-C400-AnF-nZVI and 5-C600-AnF-nZVI, with the former removing 33% after 60 minutes and the later 65 ± 8% in the same time frame. As the nZVI adsorbed on Misi calcined at 600 °C was consistently better than the nZVI adsorbed on Misi calcined 400 °C, the rest of the nitrate reduction studies were performed on nZVI adsorbed on Misi calcined at 600 °C. One major difference between Misi C400 and Misi C600 was the presence of greigite (section 2.2.1). Hence, it was possible that greigite hindered the reduction of nitrate by nZVI, but the reason and mechanism for this inhibition was unclear.

Figure 6.1 also revealed that additional surface treatment steps might also be important in maximizing the nitrate reduction rate of nZVI. This was more notable in the Misi samples that were not boiled or possess a FeOOH coating (green bars). These results were explored further by comparing the difference in the nitrate reduction rates in the 5-C600 series (Figure 6.2). The nZVI adsorbed on Misi that had undergone the most treatment reduced nitrate faster than all other samples, with 90 ± 14% reduced after 60 minutes. The FeOOH coating had a greater effect on nitrate reduction than boiling (74 ± 12 % and 65 ± 8 % after 60 minutes, respectively).

Table 6.2. Variability of nitrate reduction by different batches of nZVI. Data in red was obtained via UV-Vis, black via IC.

Entry	Sample	Batch #	# of replicates	%NO$_3^-$ removed at 60 mins	SD
1	5-C600-nAnF-nZVI	1	3	36	4
		2	1	40	
		Average		36	4
2	5-C600-nAF-nZVI	1	3	66	3
		2	1	88	
		3	1	69	
		Average		74	12
3	5-C600-AnF-nZVI	1	3	60	2
		2	1	79	
		Average		65	8
4	5-C600-AF-nZVI	1	1	89	
		2	1	74	
		3	1	85	
		4	1	95	
		Average		90	6
5	C600-5-nAnF-nZVI	1	3	18	1
		1	1	78	
		Average		33	26
6	C600-5-AnF-nZVI	1	2	86	0.8
		2	1	80	
		3	1	88	
		4	1	59	
		Average		80	12
7	C600-5-AF-nZVI	1	2	78	13
		2	2	98	
		Average		85	14
8	5-C400-nAnF-nZVI	1	3	49	28
9	5-C400-AnF-nZVI	1	1	33	
10	C600-nAF-nZVI	1	2	62	3
		2	1	85	
		Average		70	11
11	C600-AF-nZVI	1	3	86	2
		2	1	50	
		3	1	51	
		4	1	43	
		5	1	86	
		6	1	70	
		7	1	53	
		Average		62	9
12	C400-AF-nZVI	1	3	44	5
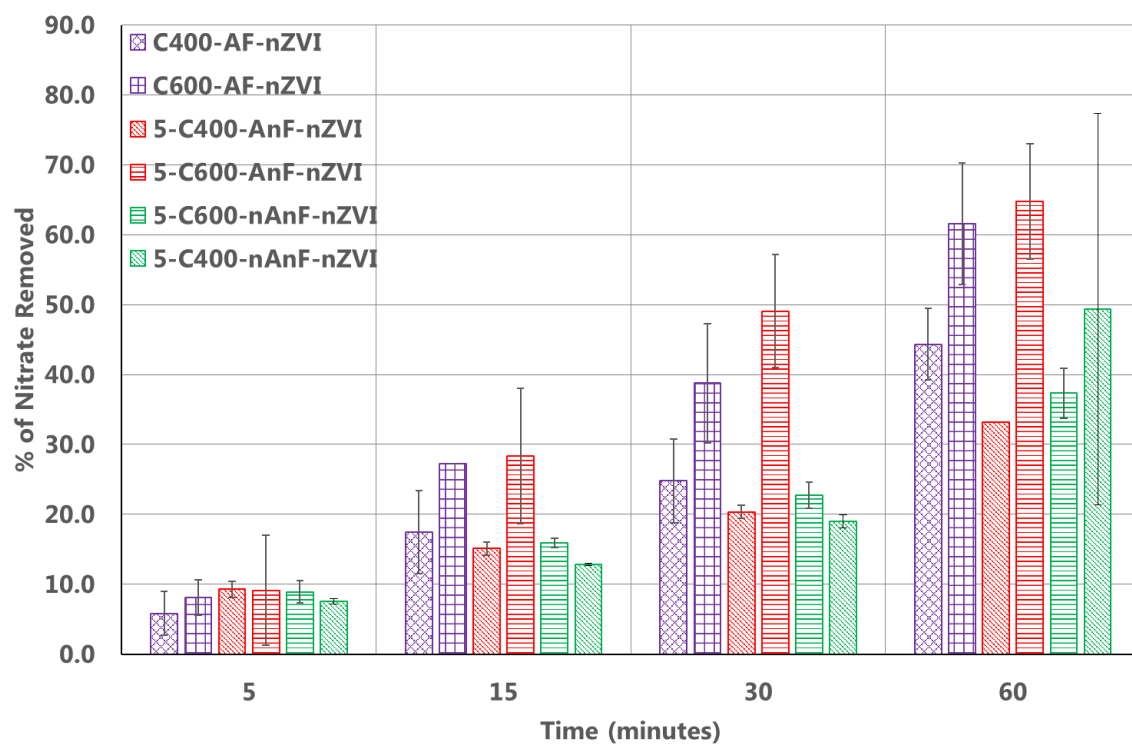
Figure 6.1. Effect of calcination temperature on nitrate reduction.
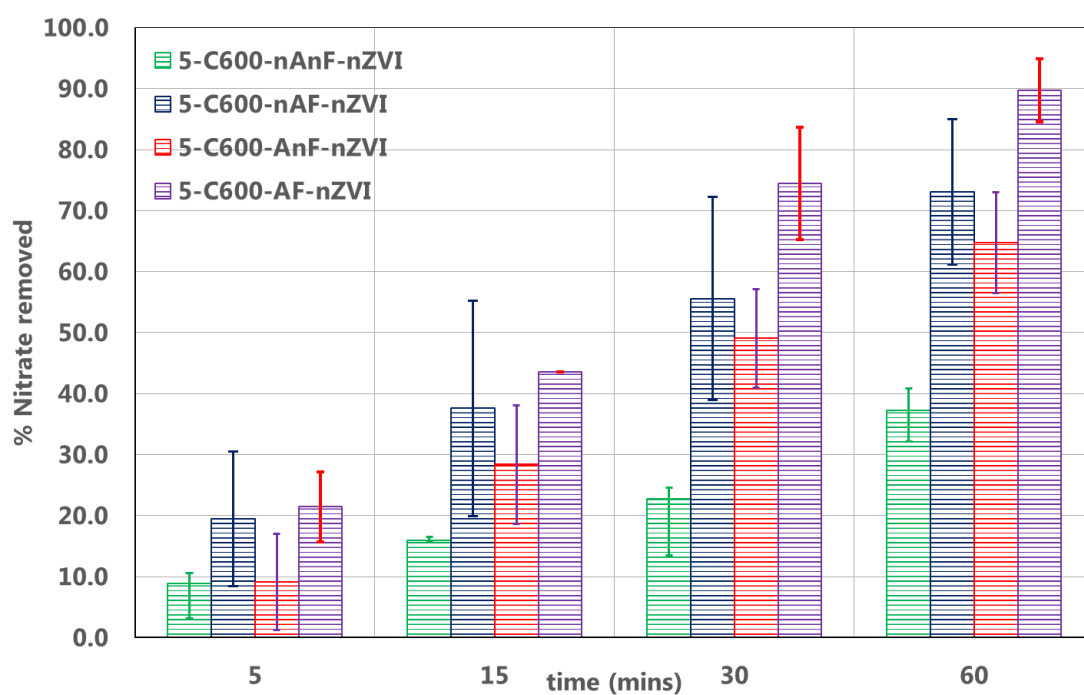
Figure 6.2. Nitrate reduction by the 5-C600 series.

147

A similar trend can also be observed in the C600-5 series where Misi was washed with 5.6 M HCl after calcination (Figure 6.3). nZVI adsorbed on nAnF Misi had a low average with large variability in its nitrate reduction capability (33 ± 26 %). nZVI adsorbed on C600-5-AnF and C-5-AF had similar nitrate reduction capabilities of 80 ± 12% and 85 ± 14 % at 60 minutes, respectively. Whilst the C600-5 series showed the full AF treatment trending to be higher in its nitrate reduction capability, for the C600 series, the reverse was observed. C600-AF-nZVI showed a lower percentage of nitrate removed in 60 minutes compared to C600-nAF-nZVI, though the average was still within the uncertainty limit (62 ± 9% and 70 ± 11 % respectively).
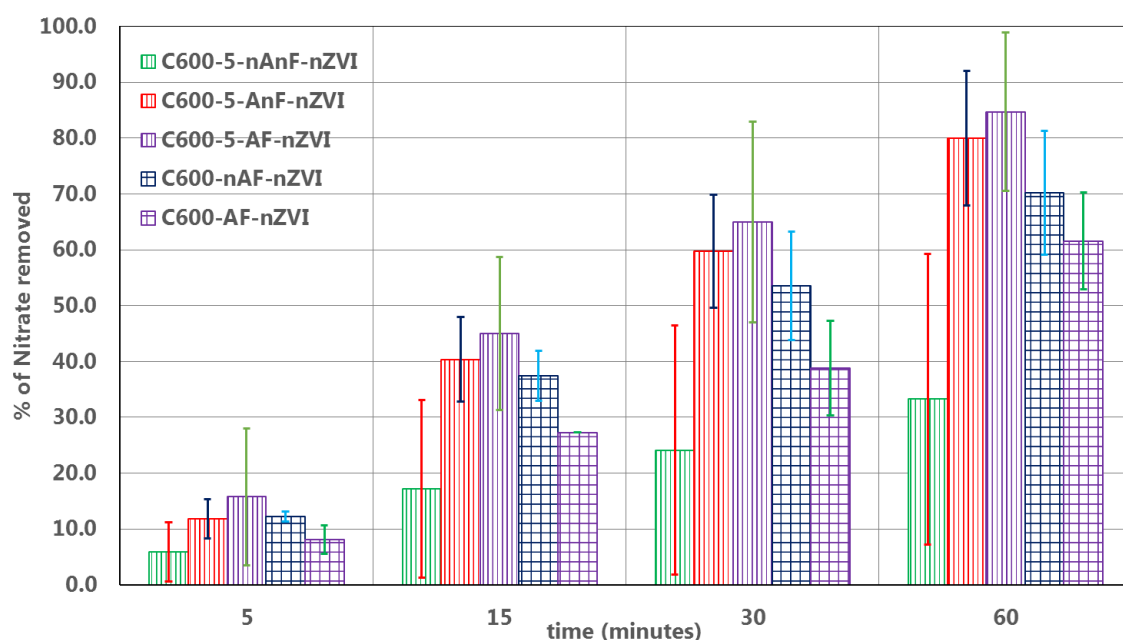
Figure 6.3. Nitrate reduction by nZVI adsorbed on Misi C600 and C600-5 series.
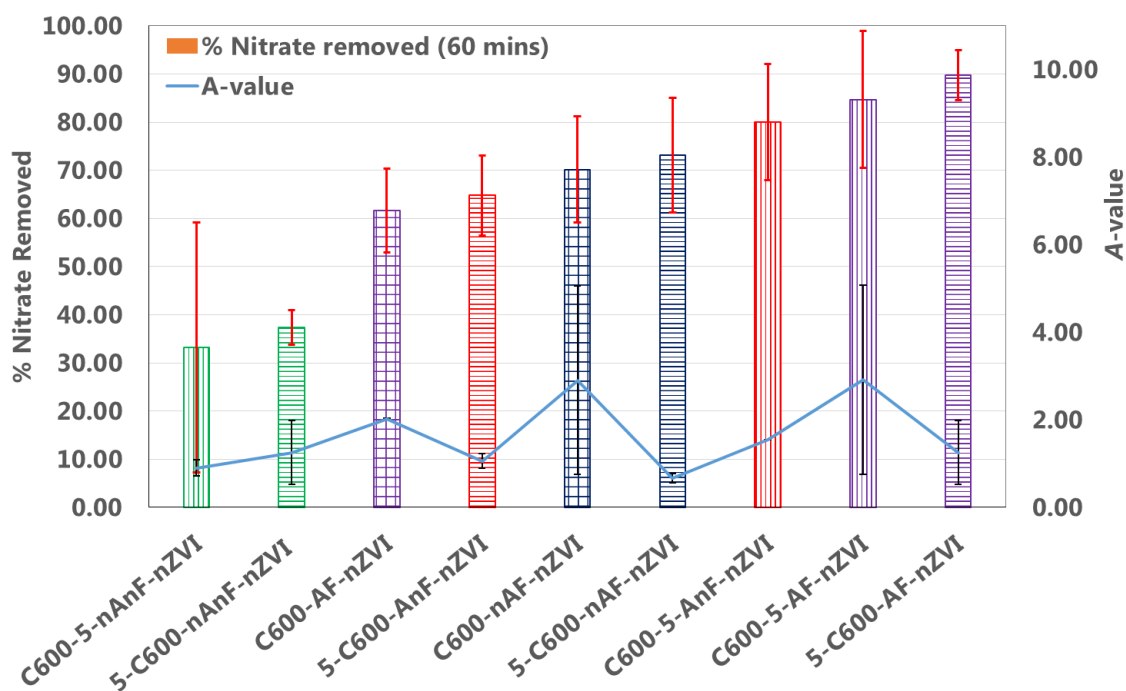
Figure 6.4. Relationship between A-*value and nitrate reduction.*

Figure 6.4 showed the relationship between percentage of nitrate removed after 60 minutes and *A*-value from section 3.5 In all series, nZVI adsorbed on the nAnF-treated Misi (green columns) was the lowest performing system in reducing nitrate. nZVI adsorbed on the AF-treated Misi (purple columns) was better in reducing nitrate when the silica had been acid washed, either before or after calcination. Indeed, the pattern seems to suggest that the order of acid washing and calcination was not important, as long as both were performed. There was however, no correlation between *A*-value and nitrate reduction.

The role of FeOOH layer on nitrate reduction

The FeOOH layer had little effect on nZVI adsorption, however, the presence of FeOOH seemed to improve nitrate reduction. This result could also be seen in AlSi-nZVI, with only 10% nitrate reduced in 60 minutes despite a very good dispersion of nZVI (section 5.5). This improved ability might be explained by the interplay between the FeOOH layer, the oxidation product of nZVI (Fe^{2+}) and Fe_3O_4. In a study by Klausen *et al*, it was found that Fe^{2+} did not have a strong reductive capability, but in the presence of Fe^{3+} containing minerals such as magnetite,

149

lepidocrocite or goethite, the Fe^{2+} reductive capability was increased. This was possibly due to the regenerative ability of the Fe^{3+} containing mineral in providing more Fe^{2+}.[315]

In another study by Gorski *et al*, it was found that that in the presence of iron oxides (e.g. goethite and hematite), the redox couple of Fe^{3+}/Fe^{2+} had a lower standard reduction potential, especially at higher pH.[316] A 'normal' standard reduction potential of Fe^{3+}/Fe^{2+} was 771 mV. In the presence of goethite the reduction potential was 768 ± 1 mV, while in the presence of hematite, the reduction potential was 739 ± 16 mV, thus indicating a stronger reducing power of Fe^{2+} in the presence of these minerals.

In the presence of nZVI, Fe^{2+} promoted the reduction of nitrate through the formation of Fe_3O_4.[317] While Fe^0 served as electron donors to reduce nitrate (eq. 33), the reduction of Fe^0 and Fe^{2+} to Fe_3O_4 also provided both electron and protons that acted as a buffer for the reaction and maintain the pH at 7 (eq. 34 and 35). Furthermore, Fe_3O_4 is a good electrical conductor, effectively lowering the electrical resistance and assisting with electron transfer from the Fe^0 to nitrate.

$$Fe^0 \longrightarrow Fe^{2+} + 2e^- \qquad (33)$$

$$3Fe^0 + 4H_2O \longrightarrow Fe_3O_4 + 8H^+ + 8e^- \qquad (34)$$

$$3Fe^{2+} + 4H_2O \longrightarrow Fe_3O_4 + 8H^+ + 2e^- \qquad (35)$$

Therefore, it could be postulated that as nZVI was oxidised to Fe^{2+}, the FeOOH layer acted as a catalyst to reduce the standard reduction potential, allowing Fe^{2+} to react as a reductant. Furthermore, Fe_3O_4, a possible oxidation product of Fe^{2+}, could assist with the electron transfer, and provided protons as a buffer, increasing the nitrate reduction capabilities of these materials.

The role of acid washing on nitrate reduction

As mentioned in section 3.2.2., acid washing reduced the surface area of Misi (Table 3.6), even though on SEM it showed a more pitted and rougher surface (Figure 3.15). Upon calcination

however, the surface area of Misi increased again. The role of acid washing and calcination on nitrate reduction was not clear, however there were some possible explanations. First, the acid washing removes metal impurities, which allows FeOOH to form on all available surfaces. This increase in FeOOH formation allows improved reduction of nitrate. Second, the acid washing along with activation, allowed the formation of more reactive silanol sites. This allowed better dispersion of nZVI (as shown from their A-value), and hence better reduction. As all of the nZVI system tested here were those with good A-value, the first explanation was more likely.

6.2.2 Effect of other ions in nitrate reduction

The presence of other anions in solution were examined for their effect on nitrate reduction by nZVI. In a test utilising Misi C600-AF-nZVI it was found that sulfate and bicarbonate interfere with nitrate reduction, while chloride had a very small effect on nitrate reduction (Figure 6.5). This result was contrary to research by Tang et al that showed all anions, except for phosphate, enhanced nZVI reduction of nitrate.[175] nZVI was not known to reduce sulfate or bicarbonate, and hence the reduced reduction capacity might be due to competition of adsorption sites. The effect of phosphate was not examined, as in the candidate's previous Honour' report, phosphate was shown to inhibit nitrate reduction by nZVI.
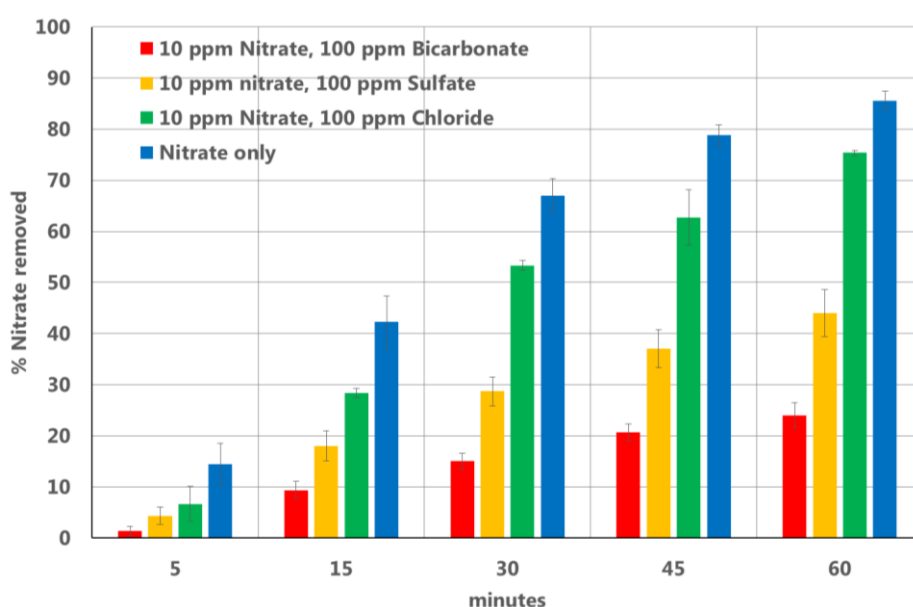
Figure 6.5. Effect of interfering ions on nitrate reduction by Misi-C600-AF-nZVI

6.3 Stability of dispersion and mobility of particles

To examine the mobility of the particles, a column with sea sand was set up. The particles (0.1 g for nZVI/silicate system and 0.02 g for bare nZVI) were placed on top of the column and the images were taken after all the eluent (100 mL 10 ppm KNO_3) had been flushed from the column (Figure 6.6). Columns *a* (bare nZVI), *b* (Misi 5-C600-nAnF-nZVI), *c* (Misi C600-5-nAnF-nZVI), *f* (AlSi-C600-AF-nZVI), and *g* (PFA-5-C600-AF-nZVI) showed no spreading of black particles in the sand, while column *d* (Misi-5-C600-AF-nZVI), and *e* (Misi C600-AF-nZVI) showed approximately 3 and 8 cm of black particles in the sand below, respectively. The lack of mobility of the nZVI/Misi materials through sand could partially be due to the pozzolanic properties of Misi; that is, Misi started to behave as a clay-like material upon compression in water. These results were consistent with the work of Bright-Young, who found that nZVI/Misi became clay-like when the reduction of nitrate was carried out in the absence of efficient stirring.[318] In his studies, the nZVI/Misi was used as a column material through which a nitrate solution was forced through. When only nZVI/Misi was used, the material became clay-like, dramatically reducing the flow-rate of the system. However, if the nZVI/material was mixed with an additional support such as silica gel, a good flow rate was maintained. In these studies, there was no mention of the mobility of nZVI/Misi through the pure silica.

The only two samples that had discernible mobility was Misi-5-C600-AF-nZVI and Misi C600-AF-nZVI. Both of these materials had been boiled and contained a layer of FeOOH which suggested that the AF layer increases mobility of nZVI/Misi, but not in the other silicates (PFA or AlSi). Misi that had not been acid washed however (Misi C600-AF-nZVI) showed a much greater mobility compared to the acid washed material (Misi 5-C600-AF-nZVI). It was possible that the acid washed Misi had a relatively more positive charge than non-acid washed Misi, thus was unable to be transported through the positively charged sand due to charge repulsion.
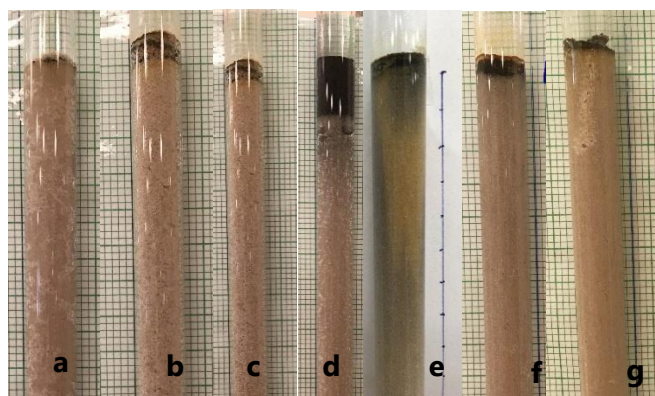
Figure 6.6. Mobility of nZVI on sea sand column (30 g) after 100 mL 10 ppm KNO$_3$ eleuent: (a) bare nZVI, (b) Misi-5-C600-nAnF-nZVI, (c) Misi C600-5-nAnF-nZVI, (d) Misi-5-C600-AF-nZVI, (e)Misi C600-AF-nZVI, (f) AlSi-C600-AF-nZVI (g) PFA-5-C600-AFnZVI. All nZVI/silicate 0.1 g, bare nZVI 0.02 g.

The eluent from these columns were then analysed with AAS to investigate iron leaching. From the 7 columns examined, only three columns: Misi 5-C600-AF-nZVI, Misi C600-5-nAnF-nZVI and AlSi-C600-AF-nZVI showed the presence of iron ions in the first 20 mL of eluent at 0.5, 1.7, and 1.7 ppm respectively. No iron were detected beyond the first 20 mL of eluent for all the systems. The maximum amount of iron leached was approximately 0.034 mg. Given that there was approximately 20 mg of Fe in each material, the leached amount represented 0.05 to 0.17% of available iron. Bare nZVI did not leach, however the column experiment showed that it also had no transport ability, and hence its soil-based application was limited. Misi C600-AF-nZVI had the best mobility with no iron leaching. However, results from nitrate reduction suggested that this material was only average in its capability in reducing nitrate. Misi 5-C600-AF-nZVI was shown to be the best overall, with high nitrate reduction capability, low leaching, and medium transport capability.

The stability of particles toward dispersion was important as more dispersed particles were easier to apply and can treat a larger area with the same amount of particles. Seven different nZVI-Misi systems (0.1 g) were dispersed in 10 mL of deoxygenated DI-H$_2$O (Vial 2-8) and left overnight (Figure 6.7). As a comparison, 0.02 g of nZVI (vial 1) and 0.1 g trimetallic system (Pd/Ni/nZVI on Misi C600-AF, vial 9) were also dispersed in 10 mL of deoxygenated DI-H$_2$O. Bare nZVI could not be dispersed by shaking, and remained as an agglomerate. All of the supported nZVI dispersed in water. After 45 minutes, most of the particles had settled, though a suspension of fine particles could still be observed.

153

The aging of the particles could be observed from the colour of the solution once the particle settled. A yellow solution indicated the presence of Fe2+/Fe3+. From the Misi-nZVI range, solution 3, 4, 7 which correspond to Misi 5-C600-nAF-nZVI, Misi 5-C600-AnF-nZVI and Misi 5-C600-nAnF-nZVI respectively, showed a more yellow solution. A layer of oxidised iron could also be seen on top of the sediments in all systems.
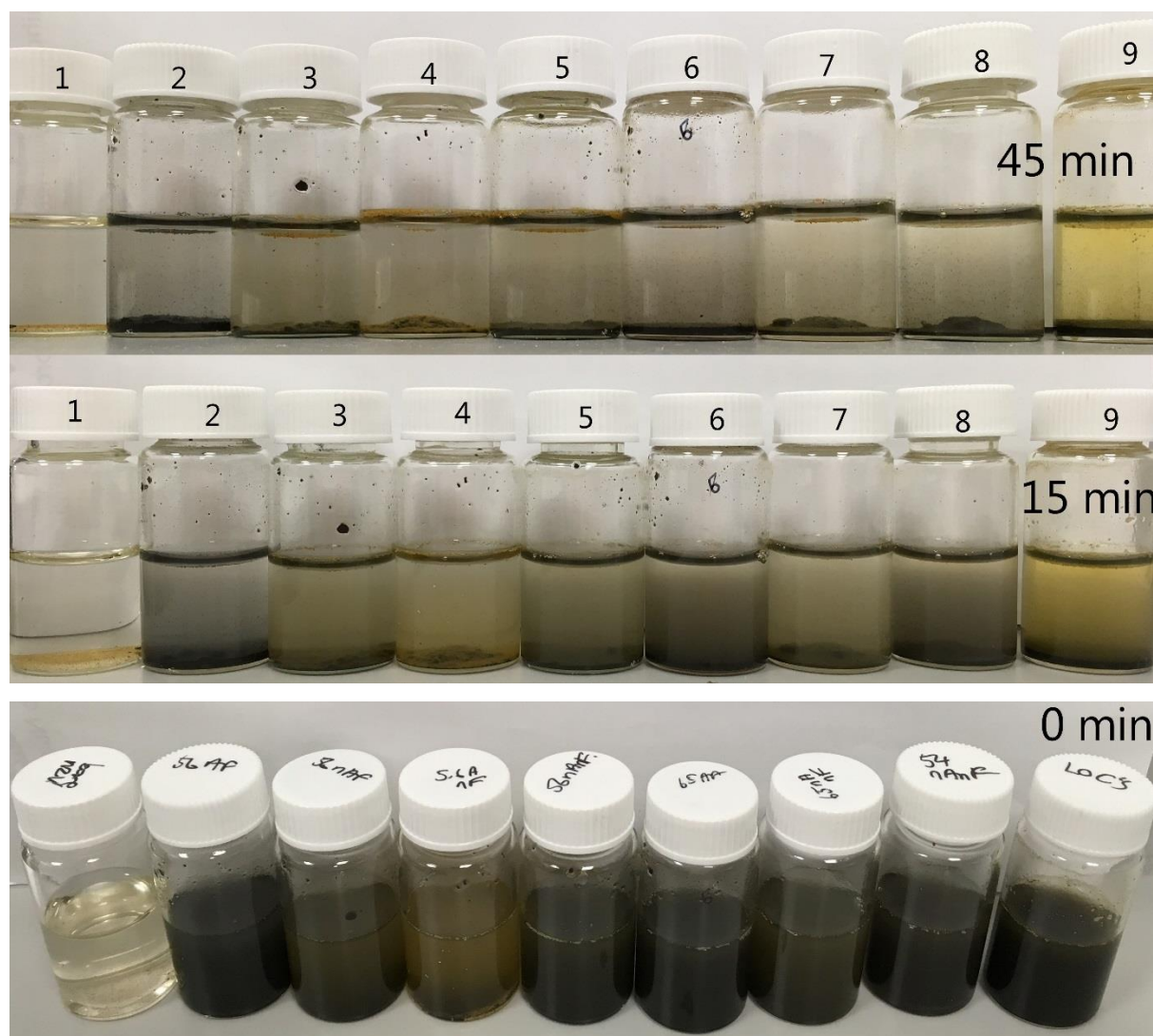
Figure 6.7. Stability of dispersion. Picture taken after particles were left in the vial overnight. Minutes indicate time from shaking the vial. 1: bare nZVI; 2: Misi 5-C600-AF-nZVI, 3: Misi 5-C600-nAF-nZVI; 4: Misi 5-C600-AnF-nZVI, 5: Misi 5-C600-nAnF-nZVI, 6: Misi C600-5-AF-nZVI, 7: Misi C600-5-nAnF-ZVI, 8: Mis 5-C400-nAnF-nZVI, 9: Misi C600-AF-Pd/Ni/nZVI (supplied by Loc Tran)

6.4 Conclusion

All of the Misi-supported nZVI material were able to reduce nitrate, although none were as effective as bare nZVI. The reduction rate was fastest when Misi had undergone all of the surface modifications investigated, including calcination, acid washing, boiling and coating with FeOOH. There was no correlation between the nitrate reduction rate and the A-value, indicating that nZVI adsorption alone was not the determining factor in the reduction of nitrate. Instead, it was the cumulative effect of all the treatments that work together to generate a reactive system.

The role of interfering ions was also explored with carbonate ions giving the strongest negative influence in nitrate reduction. This could be due to the carbonate binding to the iron surface, thus inhibiting the reaction.

Misi-supported nZVI material, especially Misi C600-AF-nZVI, was superior to bare nZVI with respect to mobility of particles and stability of dispersion. Bare nZVI agglomerate very readily and did not disperse in sand or aqueous media, limiting its practical use.

7 Summary and outlook for future research

7.1. Summary

7.2. Future direction

7.1 Summary

There are a number of conclusion that can be drawn from this research.

1. *For their use as support for nZVI, the type of silicates matter.* Pure or surface functionalised silica were not an effective support for nZVI. Silicates with an uneven distribution of aluminium were also ineffective. The presence of aluminosilicate, and therefore exchangeable cations, allowed successful adsorption of nZVI.

2. *Depending on what type of silicate was used, surface modifications were often necessary to ensure better adsorption.* Misi required acid washing and calcination for effective adsorption of nZVI. Western Australia silica fume required calcination, activation and iron oxyhydroxide coating, while precipitated aluminium silicate did not require any modification to make them a successful support for nZVI.

3. *The surface modification requirement for adsorbing nZVI and successful reduction of nitrate were different.* While Misi only required acid washing and calcination to adsorb nZVI successfully, it required activation and FeOOH coating for the fastest nitrate reduction. For pure and functionalised silica, surface modification did not significantly improved nitrate reduction. Despite the presence of nZVI on the surface of silica, the reduction of nitrate in these materials was minimal, unless the pH was manually lowered. Unfortunately, lowering pH also lead to desorption of nZVI from the surface of silica.

4. *In order to confirm the presence of nZVI on the surface of silicates, SEM with EDS mapping or at least COMPO mode was required.* While XRD can detect the presence of nZVI, it was unable to confirm adsorption of nZVI to any surface.

5. *nZVI supported on Misi C600-AF and Misi 5-C600-AF had improved dispersion and mobility compared to bare nZVI or nZVI supported on Misi that had not been activated and had FeOOH surface.* Furthermore, the amount of iron leached from the material in a sand column set-up was minimal.

Overall, this research had created a new nZVI/support material in Misi 5-C600-AF-nZVI. This magnetic material achieved good dispersion in water, and had good mobility in soil.

Furthermore, this material can be reproduced reliably, and had a consistent nitrate reduction performance across different batch.

7.2 Future Direction

The future explorations for this material lies in two different directions, first was in its application towards other contaminants, in organic pollutants such as TCE and heavy metal such as arsenic and lead. The second direction was to see the effect of surface modification on more materials which can lend us to understanding how nZVI interacts with its support material. Furthermore, the modified Misi should be examined for its use as support for other nano materials or nano bimetallic or tri-metallic composites such as Fe/Pd, Fe/Ni and Fe/Cu/Pd.

8 References

(1)   Statistics NZ. Fertiliser Use and the Environment http://www3.stats.govt.nz/environment/Fertiliser_use_and_the_environment_Aug06.pdf (accessed Feb 18, 2015).

(2)   Moir, J. .; Cameron, K. C.; Di, H. .; Ferstak, U. *J. Agric. Sci.* **2010**, 1–13.

(3)   Di, H. J.; Cameron, K. C. *Nutr. Cycl. Agroecosystems* **2002**, *64* (3), 237–256.

(4)   Di, H. J.; Cameron, K. C. *Soil Res.* **2002**, *40* (2), 317–334.

(5)   Anderson, D. M.; Glibert, P. M.; Burkholder, J. M. *Estuaries* **2002**, *25* (4), 704–726.

(6)   Chorus, I.; Bartram, J. *Toxic cyanobacteria in water: A guide to their public health consequences, monitoring and management*; Spon Press, 1999.

(7)   Biggs, B. J. F. *New Zealand Periphyton Guideline: Detecting, Monitoring and Managing Enrichment of Streams*; National Institute of Water and Atmospheric Research, 2000.

(8)   Rosemond, A. D.; Benstead, J. P.; Bumpers, P. M.; Gulis, V.; Kominoski, J. S.; Manning, D. W. P.; Suberkropp, K.; Wallace, J. B. *Science (80-.).* **2015**, *347* (6226), 1142–1145.

(9)   Sharma, S. B.; Sayyed, R. Z.; Trivedi, M. H.; Gobi, T. A. *Springerplus* **2013**, *2*, 587.

(10)   Stewart, J. W. B.; Tiessen, H. *Biogeochemistry* **1987**, *4*, 41–60.

(11)   Zou, X.; Binkley, D.; Doxtader, K. G. *Plant Soil* **1992**, *147* (2), 243–250.

(12)   Elliott, A. H.; Alexander, R. B.; Schwarz, G. E.; Shankar, U.; Sukias, J. P. S.; McBride, G. B. *J. Hydrol. (New Zealand)* **2005**, *44* (1), 1–27.

(13)   Bennett, E. M.; Carpenter, S. R.; Caraco, N. F. *Bioscience* **2001**, *51* (3), 227.

(14)   Waikato Regional Council. Water quality glossary http://www.waikatoregion.govt.nz/Environment/Natural-resources/Water/Rivers/healthyrivers/Water-quality-glossary/ (accessed Feb 20, 2015).

(15)   Schröder, J. J.; Smit, A. L.; Cordell, D.; Rosemarin, A. *Chemosphere* **2011**, *84* (6), 822–831.

(16)   Chang, S. C.; Chu, W. K. *J. Soil Sci.* **1961**, *12* (2), 286–293.

(17)   Baken, S.; Salaets, P.; Desmet, N.; Seuntjens, P.; Vanlierde, E.; Smolders, E. *Environ. Sci.*

Technol. **2015**, *49* (5), 2886–2894.

(18)   Correll, D. L. *J. Environ. Qual.* **1998**, *27* (2), 261–266.

(19)   Carpenter, S. R. *Proc. Natl. Acad. Sci. U. S. A.* **2005**, *102* (29), 10002–10005.

(20)   Childers, D. L.; Corman, J.; Edwards, M.; Elser, J. J. *Bioscience* **2011**, *61* (2), 117–124.

(21)   Wright, J. 2012.

(22)   He, L. M.; Zelazny, L. W.; Martens, D. C.; Baligar, V. C.; Ritchey, K. D. *Soil Sci. Soc. Am. J.* **1997**, *61* (3), 784–793.

(23)   Chen, J.; Kong, H.; Wu, D.; Hu, Z.; Wang, Z.; Wang, Y. *J. Colloid Interface Sci.* **2006**, *300* (2), 491–497.

(24)   Ning, P.; Bart, H.-J.; Li, B.; Lu, X.; Zhang, Y. *J. Environ. Sci.* **2008**, *20* (6), 670–674.

(25)   Sakadevan, K.; Bavor, H. J. *Water Res.* **1998**, *32* (2), 393–399.

(26)   Ugurlu, A. *Environ. Int.* **1998**, *24* (8), 911–918.

(27)   Agyei, N. M.; Strydom, C. A.; Potgieter, J. H. *Cem. Concr. Res.* **2002**, *32* (12), 1889–1897.

(28)   Johnston, T. B.; Cairns, M. J.; Anderson, B. G.; Holl, W. H.; James, H. *Int. J. Environ. Waste Manag.* **2011**, *8* (3), 383–403.

(29)   Southam, D. C.; Lewis, T. W.; McFarlane, A. J.; Borrmann, T.; Johnston, J. H. *J. Colloid Interface Sci.* **2008**, *319* (2), 489–497.

(30)   Johnston, J. H.; Borrmann, T.; Rankin, D.; Cairns, M.; Grindrod, J. E.; Mcfarlane, A. *Curr. Appl. Phys.* **2008**, *8* (3), 504–507.

(31)   Wilfert, P.; Kumar, P. S.; Korving, L.; Witkamp, G.-J.; van Loosdrecht, M. C. M. *Environ. Sci. Technol.* **2015**, *49*, 9400–9414.

(32)   Fewtrell, L. *Environ. Health Perspect.* **2004**, *112* (14), 1371.

(33)   Ministry of Health. *Drinking-water Standards for New Zealand 2005 (Revised 2008)*; 2008.

(34)   Ministry for the Environment. Environmental indicator for fresh water: river condition http://www.mfe.govt.nz/environmental-reporting/fresh-water/river-condition-indicator/index.html.

(35)   Uexküll, H. R.; Mutert, E. *Plant Soil* **1995**, *171* (1), 1–15.

(36)   DairyNZ.   Sustainable   Dairy   Water   Accord http://www.dairynz.co.nz/media/209792/Sustainable-Dairying-Water-Accord.pdf (accessed Feb 23, 2015).

(37)   Overseer.   OVERSEER   Model   http://www.overseer.org.nz/OVERSEERModel.aspx (accessed Feb 23, 2015).

(38)   GrazingSystemLimited. Grazing Systems The Usefulness and Efficacy of Linear Programming   Models   as   Farm   Management   Tools»   Grazing   Systems http://www.grazingsystems.co.nz/the-usefulness-and-efficacy-of-linear-programming-models-as-farm-management-tools/ (accessed Feb 23, 2015).

(39) DairyNZ.   Sustainable   Dairying-Water   Accord: One   Year   On http://www.dairynz.co.nz/media/1346370/water-accord-progress-report-dnz.pdf (accessed Feb 23, 2015).

(40) Edmeades, D. C. *Nitrification and Urease Inhibitor*; Hamilton, Waikato, 2004.

(41) Turley,   A.   DCD   in   New   Zealand   milk | Chemistry   World http://www.rsc.org/chemistryworld/2013/01/dcd-milk-new-zealand-fonterra (accessed Feb 23, 2015).

(42) Bhatnagar, A.; Kumar, E.; Sillanpää, M. *Chem. Eng. J.* **2010**, *163* (3), 317–323.

(43) Mizuta, K.; Matsumoto, T.; Hatate, Y.; Nishihara, K.; Nakanishi, T. *Bioresour. Technol.* **2004**, *95* (3), 255–257.

(44) Teimouri, A.; Nasab, S. G.; Vahdatpoor, N.; Habibollahi, S.; Salavati, H.; Chermahini, A. N. *Int. J. Biol. Macromol.* **2016**, *93*, 254–266.

(45) Öztürk, N.; Bektaş, T. E. *J. Hazard. Mater.* **2004**, *112* (1), 155–162.

(46) Bae, B.-U.; Jung, Y.-H.; Han, W.-W.; Shin, H.-S. *Water Res.* **2002**, *36* (13), 3330–3340.

(47) An, B.; Liang, Q.; Zhao, D. *Water Res.* **2011**, *45* (5), 1961–1972.

(48) Schoeman, J. J.; Steyn, A. *Desalination* **2003**, *155* (1), 15–26.

(49) Elmidaoui, A.; Elhannouni, F.; Sahli, M. A. M.; Chay, L.; Elabbassi, H.; Hafsi, M.; Largeteau, D. *Desalination* **2001**, *136*, 325–332.

(50) Hell, F.; Lahnsteiner, J.; Frischherz, H.; Baumgartner, G. *Desalination* **1998**, *117* (1), 173–180.

(51) Soares, M. I. M. *Water. Air. Soil Pollut.* **2000**, *123* (1–4), 183–193.

(52) Wasik, E. *Sep. Purif. Technol.* **2001**, *22–23* (1–2), 383–392.

(53) Volokita, M.; Belkin, S.; Abeliovich, A.; Soares, M. I. M. *Water Res.* **1996**, *30* (4), 965–971.

(54) Volokita, M.; Abehovich, A.; Soares, M. I. M.; Abeliovich, A.; Inesmsoares, M. *Water Sci. Technol.* **1996**, *34* (1–2), 379–385.

(55) Moorman, T. B.; Parkin, T. B.; Kaspar, T. C.; Jaynes, D. B. *Ecol. Eng.* **2010**, *36* (11), 1567–1574.

(56) Shutt, P. *The Timaru Herald*. Fairfax Media: Timaru 2013.

(57) Schipper, L. A.; Vojvodić-Vuković, M. *Water Res.* **2001**, *35* (14), 3473–3477.

(58) Shrimali, M.; Singh, K. . *Environ. Pollut.* **2001**, *112* (3), 351–359.

(59) Fanning, J. C. *Coord. Chem. Rev.* **2000**, *199* (1), 159–179.

(60) Shand, M.; Anderson, J. A. *Catal. Sci. Technol.* **2013**, *3* (4), 879.

(61) Cox, J. L.; Hallen, R. T.; Lilga, M. A.; Lllga, M. A. *Environ. Sci. Technol.* **1994**, *28* (3), 423–428.

(62) Chen, Y.-X.; Zhang, Y.; Chen, G.-H. *Water Res.* **2003**, *37* (10), 2489–2495.

(63)   Pintar, A.; Batista, J.; Levec, J. *Chem. Eng. Sci.* **2001**, *56* (4), 1551–1559.

(64)   Longstaff, J. V. L.; Singer, K. *J. Chem. Soc.* **1954**, No. 0, 2604.

(65)   Longstaff, J. V. L. *J. Chem. Soc.* **1957**, No. 0, 3488.

(66)   Nakamura, H.; Yamaguchi, I.; Kubota, M. *J. Nucl. Sci. Technol.* **1978**, *15* (10), 760–764.

(67)   Kubota, M.; Yamaguchi, I.; Nakamura, H. *J. Nucl. Sci. Technol.* **1979**, *16* (6), 426–433.

(68)   Garron, A.; Epron, F. *Water Res.* **2005**, *39* (13), 3073–3081.

(69)   Gaugush, R. F.; Heath, R. T. *Water Res.* **1984**, *18* (4), 449–450.

(70)   Jones, M. N. *Water Res.* **1984**, *18* (5), 643–646.

(71)   Soares, O. S. G. P.; Pereira, M. F. R.; Órfão, J. J. M.; Faria, J. L.; Silva, C. G. *Chem. Eng. J.* **2014**, *251*, 123–130.

(72)   Hirayama, J.; Kamiya, Y. *ACS Catal.* **2014**, *4* (7), 2207–2215.

(73)   Pan, J. R.; Huang, C.; Hsieh, W.-P.; Wu, B.-J. *Sep. Purif. Technol.* **2012**, *84*, 52–55.

(74)   Liu, G.; You, S.; Ma, M.; Huang, H.; Ren, N. *Environ. Sci. Technol.* **2016**, *50*, 11218–11225.

(75)   Mook, W. T.; Chakrabarti, M. H.; Aroua, M. K.; Khan, G. M. A.; Ali, B. S.; Islam, M. S.; Abu Hassan, M. A. *Desalination* **2012**, *285*, 1–13.

(76)   Li, M.; Feng, C.; Zhang, Z.; Shen, Z.; Sugiura, N. *Electrochem. commun.* **2009**, *11* (10), 1853–1856.

(77)   Rutten, O. W. J. S.; Sandwijk, A. Van; Weert, G. Van. *J. Appl. Electrochem.* **1999**, *29* (1), 87–92.

(78)   Li, M.; Feng, C.; Zhang, Z.; Lei, X.; Chen, R.; Yang, Y.; Sugiura, N. *J. Hazard. Mater.* **2009**, *171* (1), 724–730.

(79)   Da Cunha, M. C. P. M.; De Souza, J. P. I.; Nart, F. C. *Langmuir* **2000**, *16*, 771–777.

(80)   Freeman, E. S. *J. Phys. Chem.* **1956**, *60* (11), 1487–1493.

(81)   Karn, B.; Kuiken, T.; Otto, M. *Environ. Health Perspect.* **2009**, *117* (12), 1823–1831.

(82)   Henderson, A. D.; Demond, A. H. *Environ. Eng. Sci.* **2007**, *24* (4), 401–423.

(83)   Gandhi, S.; Oh, B.-T.; Schnoor, J. L.; Alvarez, P. J. J. *Water Res.* **2002**, *36* (8), 1973–1982.

(84)   Cundy, A. B.; Hopkinson, L.; Whitby, R. L. D. *Sci. Total Environ.* **2008**, *400* (1), 42–51.

(85)   US-EPA. .

(86)   US-EPA. US EPA.

(87)   Schwertmann, U.; Cornell, R. M. In *Iron Oxides in the Laboratary*; Wiley-VCH Verlag GmbH: Weinheim, Germany; pp 5–18.

(88)   Anthony, J. W., Bideaux, R. A., Bladh, K. W., Nicholds, M. C., Eds.; Mineralogical Society of America: Chantilly, VA, 1990.

(89)   Siantar, D. P.; Schreier, C. G.; Chou, C.-S.; Reinhard, M. *Water Res.* **1996**, *30* (10), 2315–

162

2322.

(90) Wilkin, R. T.; McNeil, M. S. *Chemosphere* **2003**, *53* (7), 715–725.

(91) Ritter, K.; Odziemkowski, M. .; Simpgraga, R.; Gillham, R. .; Irish, D. . *J. Contam. Hydrol.* **2003**, *65* (1), 121–136.

(92) Su, C.; Puls, R. W. *Environ. Sci. Technol.* **2004**, *38* (9), 2715–2720.

(93) Huang, Y. H.; Zhang, T. C. *Water Res.* **2004**, *38* (11), 2631–2642.

(94) Huang, C.-P.; Wang, H.-W.; Chiu, P.-C. *Water Res.* **1998**, *32* (8), 2257–2264.

(95) Neyens, E.; Baeyens, J. *J. Hazard. Mater.* **2003**, *98* (1), 33–50.

(96) Wei, X.; Wu, H.; He, G.; Guan, Y. *J. Hazard. Mater.* **2017**, *321*, 408–416.

(97) Zheng, P.; Bai, B.; Guan, W.; Wang, H.; Suo, Y. *RSC Adv.* **2016**, *6* (5), 4101–4107.

(98) Shahwan, T.; Abu Sirriah, S.; Nairat, M.; Boyacı, E.; Eroğlu, A. E.; Scott, T. B.; Hallam, K. R. *Chem. Eng. J.* **2011**, *172* (1), 258–266.

(99) Maharaja, P.; E, G.; N, P.; K, P.; Karthikeyan, S.; Boopathy, R.; S, S.; Sekaran, G. *RSC Adv.* **2015**, *6* (5), 4250–4261.

(100) Silbeberg, M. S. *Chemistry: The Molecular Nature of Matter and Change*, 5th ed.; McGraw-Hill: New York, 2009.

(101) Nowack, B.; Bucheli, T. D. *Environ. Pollut.* **2007**, *150* (1), 5–22.

(102) Johnston, J. H.; Lucas, K. A. *Gold Bull.* **2011**, *44* (2), 85–89.

(103) Borrmann, T.; Lim, T. H.; Cope, H.; Lucas, K.; Lorden, M. *Gold Bull.* **2013**, *46* (1), 13–18.

(104) Herzog, M. B.; Johnston, J. H. *Surf. Innov.* **2014**, *2* (2), 127–134.

(105) Ashok Kumar, S.; Cheng, H.-W.; Chen, S.-M. *React. Funct. Polym.* **2009**, *69* (6), 364–370.

(106) Yang, P.; Wei, W.; Tao, C.; Xie, B.; Chen, X. *Microchim. Acta* **2008**, *162* (1–2), 51–56.

(107) Fang, B.; Zhang, C.; Zhang, W.; Wang, G. *Electrochim. Acta* **2009**, *55* (1), 178–182.

(108) Basu, M.; Seggerson, S.; Henshaw, J.; Jiang, J.; del A Cordona, R.; Lefave, C.; Boyle, P. J.; Miller, A.; Pugia, M.; Basu, S. *Glycoconj. J.* **2004**, *21* (8–9), 487–496.

(109) Kumar, S. A.; Tang, C.-F.; Chen, S.-M. *Talanta* **2008**, *76* (5), 997–1005.

(110) Vamvakaki, V.; Chaniotakis, N. A. *Biosens. Bioelectron.* **2007**, *22* (12), 2848–2853.

(111) Vamvakaki, V.; Fournier, D.; Chaniotakis, N. A. *Fluorescence detection of enzymatic activity within a liposome based nano-biosensor*; 2005; Vol. 21.

(112) Price, M. B.; Butkus, J.; Jellicoe, T. C.; Sadhanala, A.; Briane, A.; Halpert, J. E.; Broch, K.; Hodgkiss, J. M.; Friend, R. H.; Deschler, F. *Nat. Commun.* **2015**, *6*, 8420.

(113) Halpert, J. E.; Morgenstern, F. S. F.; Ehrler, B.; Vaynzof, Y.; Credgington, D.; Greenham, N. C. *ACS Nano* **2015**, *9* (6), 5857–5867.

(114) Macdonald, T. J.; Tune, D. D.; Dewi, M. R.; Gibson, C. T.; Shapter, J. G.; Nann, T.

ChemSusChem **2015**, *8* (20), 3396–3400.

(115)   Macdonald, T. J.; Tune, D. D.; Dewi, M. R.; Bear, J. C.; McNaughter, P. D.; Mayes, A. G.; Skinner, W. M.; Parkin, I. P.; Shapter, J. G.; Nann, T. *J. Mater. Chem. C* **2016**, *4* (16), 3379–3384.

(116)   Macdonald, T. J.; Mange, Y. J.; Dewi, M. R.; Islam, H. U.; Parkin, I. P.; Skinner, W. M.; Nann, T. *J. Mater. Chem. A* **2015**, *3* (25), 13324–13331.

(117)   Wu, Z.-S.; Zhou, G.; Yin, L.-C.; Ren, W.; Li, F.; Cheng, H.-M. *Nano Energy* **2012**, *1* (1), 107–131.

(118)   Candelaria, S. L.; Shao, Y.; Zhou, W.; Li, X.; Xiao, J.; Zhang, J.-G.; Wang, Y.; Liu, J.; Li, J.; Cao, G. *Nano Energy* **2012**, *1* (2), 195–220.

(119)   Nann, T.; Ibrahim, S. K.; Woi, P.-M.; Xu, S.; Ziegler, J.; Pickett, C. J. *Angew. Chemie Int. Ed.* **2010**, *49* (9), 1574–1577.

(120)   Chandrasekaran, S.; Vijayakumar, S.; Nann, T.; Voelcker, N. H. *Int. J. Hydrogen Energy* **2016**, *41* (44), 19915–19920.

(121)   Cousins, A.; Howard, D.; Henning, A. M.; Nelson, M. R. M.; Tilley, R. D.; Thierry, B. In *Proceedings Volume 9668, Micro+Nano Materials, Devices, and Systems*; Eggleton, B. J., Palomba, S., Eds.; International Society for Optics and Photonics, 2015; p 96685Q.

(122)   Cheong, S.; Ferguson, P.; Hermans, I. F.; Jameson, G. N. L.; Prabakar, S.; Herman, D. A. J.; Tilley, R. D. *Chempluschem* **2012**, *77* (2), 135–140.

(123)   Ferguson, P. M.; Feindel, K. W.; Slocombe, A.; MacKay, M.; Wignall, T.; Delahunt, B.; Tilley, R. D.; Hermans, I. F. *PLoS One* **2013**, *8* (2), e56572.

(124)   Cheong, S.; Graham, L.; Brett, G. L.; Henning, A. M.; Watt, J.; Miedziak, P. J.; Song, M.; Takeda, Y.; Taylor, S. H.; Tilley, R. D. *ChemSusChem* **2013**, *6* (10), 1858–1862.

(125)   McGrath, A. J.; Chien, Y.-H.; Cheong, S.; Herman, D. A. J.; Watt, J.; Henning, A. M.; Gloag, L.; Yeh, C.-S.; Tilley, R. D. *ACS Nano* **2015**, *9* (12), 12283–12291.

(126)   Saha, S.; Sarkar, P. *J. Hazard. Mater.* **2012**, *227*, 68–78.

(127)   Afkhami, A.; Saber-Tehrani, M.; Bagheri, H. *J. Hazard. Mater.* **2010**, *181* (1), 836–844.

(128)   Jain, P.; Pradeep, T. *Biotechnol. Bioeng.* **2005**, *90* (1), 59–63.

(129)   Bao, Q.; Zhang, D.; Qi, P. *J. Colloid Interface Sci.* **2011**, *360* (2), 463–470.

(130)   Gunawan, P.; Guan, C.; Song, X.; Zhang, Q.; Leong, S. S. J.; Tang, C.; Chen, Y.; Chan-Park, M. B.; Chang, M. W.; Wang, K.; Xu, R. *ACS Nano* **2011**, *5* (12), 10033–10040.

(131)   Rodriguez, J. A.; Liu, G.; Jirsak, T.; Chang, Z.; Dvorak, J.; Maiti, A. *J. Am. Chem. Soc* **2002**, *124*, 5242–5250.

(132)   Zhang, L. Z.; Mu, Y.; Jia, F.; Ai, Z. *Environ. Sci. Nano* **2016**.

(133)   Kharisov, B. I.; Rasika Dias, H. V; Kharissova, O. V; Manuel Jimenez-Perez, V.; Olvera Perez, B.; Munoz Flores, B. *RSC Adv.* **2012**, *2* (25), 9325–9358.

164

(134) Li, S.; Yan, W.; Zhang, W. *Green Chem.* **2009**, *11* (10), 1618.

(135) Pineda, A.; Balu, A. M.; Campelo, J. M.; Romero, A. A.; Carmona, D.; Balas, F.; Santamaria, J.; Luque, R. *ChemSusChem* **2011**, *4* (11), 1561–1565.

(136) Petr, M.; Machalova Siskova, K.; Machala, L.; Zboril, R. In *NanoCon*; Brno, 2013.

(137) Hahn, H. *Nanostructured Mater.* **1997**, *9* (1–8), 3–12.

(138) Yan, W.; Lien, H.-L.; Koel, B. E.; Zhang, W.-X. *Environ. Sci. Process. Impacts* **2013**, *15*, 63–77.

(139) Glavee, G. N.; Kenneth Klabunde, la J.; Christopher Sorensen, J. M.; Hadjipanayisld, G. C. *Inorg. Chem* **1995**, *34*, 28–35.

(140) Hoag, G. E.; Collins, J. B.; Holcomb, J. L.; Hoag, J. R.; Nadagouda, M. N.; Varma, R. S. *J. Mater. Chem.* **2009**, *19* (45), 8671–8677.

(141) Nadagouda, M. N.; Castle, A. B.; Murdock, R. C.; Hussain, S. M.; Varma, R. S. *Green Chem.* **2010**, *12* (1), 114–122.

(142) Machado, S.; Pinto, S. L.; Grosso, J. P.; Nouws, H. P. A.; Albergaria, J. T.; Delerue-Matos, C. *Sci. Total Environ.* **2013**, *445–446* (0), 1–8.

(143) Varma, R. S. *Curr. Opin. Chem. Eng.* **2012**, *1* (2), 123–128.

(144) Prasad, K. S.; Gandhi, P.; Selvaraj, K. *Appl. Surf. Sci.* **2014**, *317*, 1052–1059.

(145) Crane, R. A.; Scott, T. B. *J. Hazard. Mater.* **2012**, *211–212* (0), 112–125.

(146) Yin, L.; Li, Y.; Zhang, L.; Peng, Y.; Ying, Z. *Environ. Sci.* **2009**, *4*, 21.

(147) Li, Y.; Li, T.; Jin, Z. *J. Environ. Sci.* **2011**, *23* (7), 1211–1218.

(148) Dries, J.; Bastiaens, L.; Springael, D.; Kuypers, S.; Agathos, S. N.; Diels, L. *Water Res.* **2005**, *39* (15), 3531–3540.

(149) Yan, W.; Herzing, A. A.; Kiely, C. J.; Zhang, W.-X. *J. Contam. Hydrol.* **2010**, *118* (3–4), 96–104.

(150) Moraci, N.; Calabrò, P. S. *J. Environ. Manage.* **2010**, *91* (11), 2336–2341.

(151) Afkhami, A.; Saber-Tehrani, M.; Bagheri, H.; Madrakian, T. *Microchim. Acta* **2011**, *172* (1–2), 125–136.

(152) Benjamin, M. M.; Leckie, J. O. *J. Colloid Interface Sci.* **1981**, *79* (1), 209–221.

(153) Boparai, H. K.; Joseph, M.; O'Carroll, D. M. *J. Hazard. Mater.* **2011**, *186* (1), 458–465.

(154) Boparai, H. K.; Joseph, M.; O'Carroll, D. M. *Environ. Sci. Pollut. Res. Int.* **2013**, *20* (9), 6210–6221.

(155) Kanel, S. R.; Manning, B.; Charlet, L.; Choi, H. *Environ. Sci. Technol.* **2005**, *39* (5), 1291–1298.

(156) Zhu, H.; Jia, Y.; Wu, X.; Wang, H. *J. Hazard. Mater.* **2009**, *172* (2–3), 1591–1596.

(157) Yan, W.; Ramos, M. A. V.; Koel, B. E.; Zhang, W. *J. Phys. Chem. C* **2012**, *116* (9), 5303–

165

5311.

(158) Kim, H.; Hong, H.-J.; Jung, J.; Kim, S.-H.; Yang, J.-W. *J. Hazard. Mater.* **2010**, *176* (1–3), 1038–1043.

(159) Kim, J. H.; Tratnyek, P. G.; Chang, Y. S. *Environ. Sci. Technol.* **2008**, *42* (11), 4106–4112.

(160) Darko-Kagya, K.; Khodadoust, A. P.; Reddy, K. R. *J. Hazard. Mater.* **2010**, *182* (1–3), 177–183.

(161) Liu, H. B. B.; Chen, T. H. H.; Chang, D. Y. Y.; Chen, D.; Liu, Y.; He, H. P. P.; Yuan, P.; Frost, R. *Mater. Chem. Phys.* **2012**, *133* (1), 205–211.

(162) Ziajahromi, S.; Zand, A. D.; Khanizadeh, M. *International Conference on Applied Life Sciences (ICALS2012)*. Turkey 2012.

(163) Huang, Y. H.; Zhang, T. C.; Shea, P. J.; Comfort, S. D. *J. Environ. Eng.* **2014**, *140* (8), 4014029-1–7.

(164) Almeelbi, T.; Bezbaruah, A. *J. Nanoparticle Res.* **2012**, *14* (7), 1–14.

(165) Miao, Z.; Brusseau, M. L.; Carroll, K. C.; Carreón-Diazconti, C.; Johnson, B. *Environ. Geochem. Health* **2012**, *34* (4), 539–550.

(166) Bilek, F. *Environ. Geol.* **2005**, *49* (5), 674–683.

(167) Babuponnusami, A.; Muthukumar, K. *Environ. Sci. Pollut. Res.* **2013**, *20* (3), 1596–1605.

(168) Wang, J. B. L.; Wan, Z.; Wang, J. B. L.; Wang, J. B. L.; Wang, S. Z.; Koyuncu, I.; Arikan, O. A.; Wiesner, M. R.; Rice, C.; Putra, E. K.; Pranowo, R.; Sunarso, J.; Indraswati, N.; Ismadji, S.; Wang, J. B. L.; Xu, L. J.; Cruz, N. D. la; Esquius, L.; Grandjean, D.; Magnet, A.; Tungler, A.; Alencastro, L. F. De; Pulgarín, C.; Prieto-Rodríguez, L.; Oller, I.; Klamerth, N.; Agüera, A.; Rodríguez, E. M.; Malato, S.; El-Ghenymy, A.; Rodríguez, R. M.; Arias, C.; Centellas, F.; Garrido, J. A.; Cabot, P. L.; Brillas, E.; Wang, J. B. L.; Chu, L. B.; Orbeci, C.; Untea, I.; Nechifor, G.; Segneanu, A. E.; Craciun, M. E.; Zou, X. L.; Zhou, T.; Mao, J.; Wu, X. H.; Ryu, A.; Jeong, S.; Jang, A.; Choi, H.; Li, A.; Tai, C.; Zhao, Z. S.; Wang, Y. W.; Zhang, Q. H.; Jiang, G. B.; Hu, J. T.; Wang, X. Y.; Chen, C.; Liu, H. L.; Ma, J.; Zheng, T. H.; Zhan, J. J.; He, J. B.; Day, C.; Lu, Y. F.; McPherson, G. L.; Piringer, G.; John, V. T.; Zhang, Y.; Yang, M. X.; Dou, X. M.; He, H.; Wang, D. S.; Heckert, E. G.; Seal, S.; Self, W. T.; Xu, L. J.; Wang, J. B. L.; Li, H. L.; Wu, C. Y.; Li, Y.; Zhang, J. Y.; Danilczuk, M.; Schlick, S.; Coms, F. D.; Gubler, L.; Koppenol, W. H.; Xu, L. J.; Wang, J. B. L.; Ling, Q.; Yang, M. X.; Li, C. S.; Zhang, A. M.; Xu, L. J.; Wang, J. B. L.; Ni, Y. H.; Ge, X. W.; Zhang, Z. C.; Ye, Q.; Yan, W. L.; Herzing, A. A.; Li, X. Q.; Kiely, C. J.; Zhang, W. X.; Grosvenor, A. P.; Kobe, B. A.; Biesinger, M. C.; McIntyre, N. S.; Burroughs, P.; Hamnett, A.; Orchard, A. F.; Thornton, G.; Yang, S. X.; Zhu, W. P.; Jiang, Z. P.; Chen, Z. X. L.; Wang, J. B. L.; Russell, J. D.; Tian, B. Z.; Tang, H. X.; Zolin, V. F.; Kudryashova, V. A.; Kuznetsova, V. V.; Razvina, T. I.; Turković, A.; Dubček, P.; Bernstorff, S.; Ohtsuka, T.; Kubo, K.; Sato, N.; Reddy, B. M.; Khan, A.; Yamada, Y.; Kobayashi, T.; Loridant, S.; Volta, J.; Lin, X. M.; Li, L. P.; Li, G. S.; Su, W. H.; Nolas, G. S.; Tsoukala, V. G.; Gayen, S. K.; Slack, G. A.; Jabeen, H.; Chandra, V.; Jung, S.; Lee, J. W.; Kim, K. S.; Kim, S. B.; Fang, Z. Q.; Chen, J. H.; Qiu, X. Q. H.; Qiu, X. Q. H.; Cheng, W.; Zhu, L. C.; Chen, J. H.; Qiu, X. Q. H.; Fang, Z. Q.; Yang, M. X.; Pokeung, T.; Gu, F. L.; Cheng, W.; Lan, B. Y.; Zha, S. X.; Cheng, Y.; Gao, Y.;

Chen, Z. X. L.; Megharaj, M.; Naidu, R.; Ma, J.; Yang, M. X.; Yu, F.; Chen, J. H.; Liu, Y. K.; Hu, J. T.; Wang, J. B. L.; Wan, Z.; Wang, J. B. L.; Wan, Z.; Wang, J. B. L.; Wan, Z.; Hu, J. T.; Wang, J. B. L.; Wan, Z.; Wang, J. B. L.; Moreira, F. C.; Boaventura, R. A. R.; Brillas, E.; Vilar, V. J. P.; Ghandi, H. S.; Piken, A. G.; Shelef, M.; Deloch, R. G.; Bielski, B. H.; Cabelli, D. E.; Arudi, R. L.; Ross, A. B. *RSC Adv.* **2016**, *6* (105), 103523–103531.

(169) Gavaskar, A.; Tatar, L.; Condit, W. *Cost and Performance Report Nanoscale Zero-Valent Iron Technologies for Source Remediation*; Port Hueneme, California, 2005.

(170) Mueller, N. C.; Braun, J.; Bruns, J.; Černík, M.; Rissing, P.; Rickerby, D.; Nowack, B. *Environ. Sci. Pollut. Res.* **2012**, *19* (2), 550–558.

(171) US EPA. *Selected Sites Using or Testing Nanoparticles for Remediation*.

(172) *Emulsified Zero-Valent Iron (EZVI) Treatment of Chlorinated Solvent*; 2009.

(173) Cheng, I. F.; Muftikian, R.; Fernando, Q.; Korte, N. *Chemosphere* **1997**, *35* (11), 2689–2695.

(174) Hwang, Y.-H.; Kim, D.-G.; Shin, H.-S. *J. Hazard. Mater.* **2011**, *185* (2–3), 1513–1521.

(175) Tang, C.; Zhang, Z.; Sun, X. *J. Hazard. Mater.* **2012**, *231–232* (0), 114–119.

(176) US EPA. Wastewater Technology Fact Sheet: Ammonia Stripping http://water.epa.gov/scitech/wastetech/upload/2002_06_28_mtb_ammonia_stripping.pdf (accessed Mar 6, 2015).

(177) Ahn, S. C.; Oh, S.-Y.; Cha, D. K. *J. Hazard. Mater.* **2008**, *156* (1–3), 17–22.

(178) Liou, Y. H.; Lo, S.-L.; Lin, C.-J.; Kuan, W. H.; Weng, S. C. *J. Hazard. Mater.* **2005**, *127* (1–3), 102–110.

(179) Yang, G. C. C. C.; Lee, H.-L. *Water Res.* **2005**, *39* (5), 884–894.

(180) Li, Y.; Jin, Z.; Li, T. *J. Chinese Ceram. Soc.* **2011**, *39* (7), 1211–1217.

(181) Greenlee, L. F.; Hooker, S. A. *Desalin. Water Treat.* **2012**, *37* (1–3), 114–121.

(182) Zhang, W.; Elliott, D. W. *Remediat. J.* **2006**, *16* (2), 7–21.

(183) Li, H.; Zhou, Q.; Wu, Y.; Fu, J.; Wang, T.; Jiang, G. *Ecotoxicol. Environ. Saf.* **2009**, *72* (3), 684–692.

(184) Keller, A. A.; Garner, K.; Miller, R. J.; Lenihan, H. S. *PLoS One* **2012**, *7* (8), e43983.

(185) Chen, P.-J.; Su, C.-H.; Tseng, C.-Y.; Tan, S.-W.; Cheng, C.-H. *Mar. Pollut. Bull.* **2011**, *63* (5–12), 339–346.

(186) Chen, P.-J.; Tan, S.-W.; Wu, W.-L. *Environ. Sci. Technol.* **2012**, *46* (15), 8431–8439.

(187) Álvarez-Manzaneda, I.; Ramos-Rodríguez, E.; López-Rodríguez, M. J.; Parra, G.; Funes, A.; de Vicente, I. *J. Hazard. Mater.* **2017**, *322*, 437–444.

(188) Ayoub, S. R. A.; Uchiyama, H.; Iwasaki, K.; Doi, T.; Inaba, K. *Environ. Technol.* **2008**, *29* (4), 363–373.

(189) Zhang, M.; He, F.; Zhao, D.; Hao, X. *Water Res.* **2011**, *45* (7), 2401–2414.

(190) Cirtiu, C. M.; Raychoudhury, T.; Ghoshal, S.; Moores, A. *Colloids Surfaces A Physicochem. Eng. Asp.* **2011**, *390* (1–3), 95–104.

(191) Johnson, R. L.; Johnson, G. O.; Nurmi, J. T.; Tratnyek, P. G. *Environ. Sci. Technol.* **2009**, *43* (14), 5455–5460.

(192) Peng, S.; Wang, C.; Xie, J.; Sun, S. H. *J. Am. Chem. Soc.* **2006**, *128* (33), 10676–10677.

(193) An, Y.; Li, T.; Jin, Z.; Dong, M.; Xia, H.; Wang, X. *Bioresour. Technol.* **2010**, *101* (24), 9825–9828.

(194) Jiang, F.; Fu, Y.; Zhu, Y.; Tang, Z.; Sheng, P. *J. Alloys Compd.* **2012**, *543* (0), 43–48.

(195) Zhang, D.; Wei, S.; Kaila, C.; Su, X.; Wu, J.; Karki, A. B.; Young, D. P.; Guo, Z. *Nanoscale* **2010**, *2* (6), 917–919.

(196) Li, Y.; Jin, Z.; Li, T.; Xiu, Z. *Sci. Total Environ.* **2012**, *421–422*, 260–266.

(197) Meeks, N. D.; Smuleac, V.; Stevens, C.; Bhattacharyya, D. *Ind. Eng. Chem. Res.* **2012**, *51* (28), 9581–9590.

(198) Haugstad, M.; Almeelbi, T.; Bezbaruah, A. In *World Environmental and Water Resources Congress 2011*; pp 1733–1740.

(199) Shi, L.; Zhang, X.; Chen, Z. *Water Res.* **2011**, *45* (2), 886–892.

(200) Chen, Z.; Jin, X.; Chen, Z.; Megharaj, M.; Naidu, R. *J. Colloid Interface Sci.* **2011**, *363* (2), 601–607.

(201) Zhang, Y.; Li, Y.; Li, J.; Hu, L.; Zheng, X. *Chem. Eng. J.* **2011**, *171* (2), 526–531.

(202) Jiang, Z.; Lv, L.; Zhang, W.; Du, Q.; Pan, B.; Yang, L.; Zhang, Q. *Water Res.* **2011**, *45* (6), 2191–2198.

(203) Shi, J.; He, H.; Long, C.; Li, A. *J. Chem. Technol. Biotechnol.* **2014**, n/a-n/a.

(204) Dorathi, P. J.; Kandasamy, P. *J. Environ. Sci.* **2012**, *24* (4), 765–773.

(205) Zhang, R.; Li, J.; Liu, C.; Shen, J.; Sun, X.; Han, W.; Wang, L. *Colloids Surfaces A Physicochem. Eng. Asp.* **2013**, *425*, 108–114.

(206) Petala, E.; Dimos, K.; Douvalis, A.; Bakas, T.; Tucek, J.; Zbořil, R.; Karakassides, M. A. *J. Hazard. Mater.* **2013**, *261*, 295–306.

(207) Park, H.; Yeon, K.-H.; Park, Y.-M.; Lee, S.-J.; Lee, S.-H.; Choi, Y.-S.; Chung, Y. *J. Water Environ. Technol.* **2008**, *6* (1), 35–42.

(208) Li, F. *Microporous Mesoporous Mater.* **2013**, *171* (0), 139–146.

(209) Rudnick, R. L.; Gao, S. *Treatise on Geochemistry*; Elsevier, 2003.

(210) Housecroft, C. E.; Sharpe, A. G. *Inorganic Chemistry*, 4th Ed.; Pearson: Harlow, England, 2012.

(211) Iler, R. *The Chemistry of Silica*; John Wiley & Sons, Inc., 1979.

(212) Stöber, W.; Fink, A.; Bohn, E. *J. Colloid Interface Sci.* **1968**, *26* (1), 62–69.

(213) Bogush, G. H.; Tracy, M. A.; Zukoski, C. F. *J. Non. Cryst. Solids* **1988**, *104* (1), 95–106.

(214) Araki, S.; Doi, H.; Sano, Y.; Tanaka, S.; Miyake, Y. *J. Colloid Interface Sci.* **2009**, *339* (2), 382–389.

(215) Belmabkhout, Y.; Sayari, A. *Adsorption* **2009**, *15* (3), 318–328.

(216) Jal, P. K.; Patel, S.; Mishra, B. K. *Talanta* **2004**, *62* (5), 1005–1028.

(217) Morrow, B. A.; McFarlan, A. J. *J. Non. Cryst. Solids* **1990**, *120* (1), 61–71.

(218) Nawrocki, J. *Chromatographia* **1991**, *31* (3–4), 177–192.

(219) Goswami, A.; Singh, A. K. *Anal. Chim. Acta* **2002**, *454* (2), 229–240.

(220) Hernández, G.; Rodríguez, R. *J. Non. Cryst. Solids* **1999**, *246* (3), 209–215.

(221) Miyake, Y.; Yosuke, M.; Azechi, E.; Araki, S.; Tanaka, S. *Ind. Eng. Chem. Res.* **2009**, *48* (2), 938–943.

(222) Silcates | Article about Silcates by The Free Dictionary http://encyclopedia2.thefreedictionary.com/Silcates (accessed Aug 9, 2017).

(223) Qiu, X.; Fang, Z.; Liang, B.; Gu, F.; Xu, Z. *J. Hazard. Mater.* **2011**, *193*, 70–81.

(224) Ensie, B.; Samad, S. *Desalination* **2014**, *347*, 1–9.

(225) Hu, B.; Ye, F.; Ren, X.; Zhao, D.; Sheng, G.; Li, H.; Ma, J.; Wang, X.; Huang, Y. *Environ. Sci. Nano* **2016**, *3*, 1460–1472.

(226) Ren, C.; Li, Y.; Li, J.; Sheng, G.; Hu, L.; Zheng, X. *J Chem Technol Biotechnol* **2013**, *89*, 1961–1966.

(227) Üzüm, Ç.; Shahwan, T.; Eroğlu, A. E.; Hallam, K. R.; Scott, T. B.; Lieberwirth, I. *Appl. Clay Sci.* **2009**, *43* (2), 172–181.

(228) Cho, D.-W.; Chon, C.-M.; Jeon, B.-H.; Kim, Y.; Khan, M. A.; Song, H. *Chemosphere* **2010**, *81* (5), 611–616.

(229) Ji, M.-K.; Park, W.-B.; Khan, M. A.; Abou-Shanab, R. A. I.; Kim, Y.; Cho, Y.; Choi, J.; Song, H.; Jeon, B.-H.; Huang, H. C.; Lee, S. D. *J. Environ. Monit.* **2012**, *14* (4), 1153.

(230) Fraser, H. P. Silica and Silicate Supported nZVI for the Reduction of Nitrate, Victoria University of Wellington, 2013.

(231) Walker, R.; Pavía, S. *Mater. Struct.* **2011**, *44* (6), 1139–1150.

(232) Rahman, I. A.; Vejayakumaran, P.; Sipaut, C. S.; Ismail, J.; Chee, C. K. *Ceram. Int.* **2008**, *34* (8), 2059–2066.

(233) Vacassy, R.; Flatt, R.; Hofmann, H.; Choi, K.; Singh, R. *J. Colloid Interface Sci.* **2000**, *227* (2), 302–315.

(234) Wang, P.; Zhu, Y.; Yang, X.; Chen, A. *Flavour Fragr. J.* **2008**, *23* (1), 29–34.

(235) ImageJ https://imagej.net/Welcome (accessed Jul 3, 2017).

(236) Atkins, P.; de Paula, J. *Physical Chemistry*, 8th Editio.; Oxford University Press: Oxford,

2006.

(237) Clogston, J. D.; Patri, A. K. *Methods Mol. Biol.* **2011**, *697*, 63–70.

(238) Myers, D. *Surfaces, Interfaces and Colloids: Principles and Applications*; VCH Publishers, 1991.

(239) Armarego, W. L. .; Perrin, D. D. *Purification of Laboratory Chemical*, 4th Editio.; Butterworth Heinemann: Bath, 1998.

(240) JEOL. *Invitation to the SEM World*.

(241) Jenkins, R.; de Vries, J. L. *An Introduction to X-ray Powder Diffractometry*; N. V. Philips Gloeilampenfabrieken: Eindhoven.

(242) *Powder Diffraction: Theory and Practice*; Dinnebier, R. E., Billinge, S. J. ., Eds.; Royal Society of Chemistry, 2008.

(243) Lafuente, B.; Downs, R. T.; Yang, H.; Stone, N. In *Highlights in Mineralogical crystallography*; Armbruster, T., Danisi, R. M., Eds.; W. De Gruyter: Berlin, 2015; pp 1–30.

(244) PerkinElmer. .

(245) *General Guide to Microsilica*; Auckland.

(246) Ribeiro, J.; Taffarel, S. R.; Sampaio, C. H.; Flores, D.; Silva, L. F. O. *Int. J. Coal Geol.* **2013**, *109–110*, 15–23.

(247) Grangeon, S.; Claret, F.; Linard, Y.; Chiaberge, C. *Acta Crystallogr. B. Struct. Sci. Cryst. Eng. Mater.* **2013**, *69* (Pt 5), 465–473.

(248) Launer, P. J. *Infrared Analysis of Organosilicon Compounds: Spectra-Structure Correlations*; New York, 1987.

(249) Hair, M. L. *J. Non. Cryst. Solids* **1975**, *19*, 299–309.

(250) Li, X.; King, T. A. *J. Non. Cryst. Solids* **1996**, *204* (3), 235–242.

(251) Nawrocki, J. *J. Chromatogr. A* **1997**, *779*, 29–71.

(252) Rouquerol, J.; Rouquerol, F.; Llewellyn, P. *Adsorption by Powders and Porous Solids: Principles, Methodology and Applications (2)*; Academic Press: Oxford, GB, 2013.

(253) *IUPAC Compendium of Chemical Terminology*; Nič, M., Jirát, J., Košata, B., Jenkins, A., McNaught, A., Eds.; IUPAC: Research Triangle Park, NC, 2009.

(254) Sun, Y.-P.; Li, X.-Q.; Zhang, W.-X.; Wang, H. P. *Colloids Surfaces A Physicochem. Eng. Asp.* **2007**, *308* (1–3), 60–66.

(255) Zeng, L. *Water Res.* **2003**, *37* (18), 4351–4358.

(256) Mueller, P. *Synthesis of silica based porous nanomaterials*; 2014.

(257) Sabir, B. .; Wild, S.; Bai, J. *Cem. Concr. Compos.* **2001**, *23* (6), 441–454.

(258) Heaney, P. J.; Prewitt, C. T.; Gibbs, G. V. *Geochemistry Mater. Appl.* **1994**, 1–40.

(259) Skinner, B. J.; Erd, R. C.; Grimaldi, F. S. *Am. Mineral.* **1964**, *49* (5–6), 543–555.

(260) Krs, M.; Krsová, M.; Pruner, P.; Zeman, A.; Novák, F.; Jansa, J. *Phys. Earth Planet. Inter.* **1990**, *63* (1), 98–112.

(261) Dekkers, M. J.; Passier, H. F.; Schoonen, M. A. A. *Geophys. J. Int.* **2000**, *141* (3), 809–819.

(262) Vlisidis, A. C. *Geol. Surv. Bull.* **1966**, *1214–D*.

(263) Bhattacharyya, K. G.; Gupta, S. Sen. *Adv. Colloid Interface Sci.* **2008**, *140* (2), 114–131.

(264) Jozefaciuk, G. *Clays Clay Miner.* **2002**, *50* (5).

(265) Hodder, A. P. W. In *Chemical Processes in New Zealand*; NZIC, 1998.

(266) Technologies, A. Agilent Technologies 2015.

(267) Unger, K. K.; Lork, K. D.; Pfleiderer, B.; Albert, K.; Bayer, E. *J. Chromatogr. A* **1991**, *556* (1–2), 395–406.

(268) Jozefaciuk, G.; Bowanko, G. *Clays Clay Miner.* **2002**, *50* (6), 771–783.

(269) Kanie, K.; Muramatsu, A.; Suzuki, S.; Waseda, Y. *Mater. Trans.* **2004**, *45* (3), 968–971.

(270) Tang, B.; Wang, G.; Zhuo, L.; Ge, J.; Cui, L. *Inorg. Chem.* **2006**, *45*, 5196–5200.

(271) Bottero, J.-Y.; Manceau, A.; Villieras, F.; Tchoubars, D. *Langmuir* **1994**, *10*, 316–319.

(272) Blgham, J. M.; Schwertmann, U.; Carlson, L.; Murad, E. *Geochim. Cosmochim. Acta* **1990**, *54* (10), 2743–2758.

(273) Kandori, K.; Uchida, S.; Kataoka, S.; Ishikawa, T. *J. Mater. Sci.* **1992**, *27* (3), 719–728.

(274) Detournay, J.; Ghodsi, M.; Derie, R. *Zeitschrift f�r Anorg. und Allg. Chemie* **1975**, *412* (2), 184–192.

(275) Detournay, P. J.; Derie, R.; Ghodsi, M. *Zeitschrift für Anorg. und Allg. Chemie* **1976**, *427* (3), 265–273.

(276) Liu, A.; Liu, J.; Pan, B.; Zhang, W. *RSC Adv.* **2014**, *4*, 57377–57382.

(277) Liu, A.; Liu, J.; Zhang, W.-X. *Chemosphere* **2015**, *119*, 1068–1074.

(278) Liu, A.; Liu, J.; Han, J.; Zhang, W. *J. Hazard. Mater.* **2017**, *322*, 129–135.

(279) Agresti, A. *Categorical data analysis*; Wiley-Interscience, 2013.

(280) Ahmad, H. B.; Yasmin, G. E.; Arain, S. A.; Bhatti, I. A.; Hussain, M. *Korean J. Chem. Eng* **2015**, *32* (4), 661–666.

(281) Jal, P. *Talanta* **2001**, *55* (2), 233–240.

(282) Bagheri, H.; Gholami, A.; Najafi, A. *Anal. Chim. Acta* **2000**, *424* (2), 233–242.

(283) Gu, E.; Zhong, W.; Liu, X. *RSC Adv.* **2016**, *6* (100), 98406–98412.

(284) Bernal, J. D.; Dasgupta, D. R.; Mackay, A. L. **1958**, 15–31.

(285) Ben Haddada, M.; Blanchard, J.; Casale, S.; Krafft, J.-M.; Vall?e, A.; M?thivier, C.; Boujday, S. *Gold Bull.* **2013**, *46* (4), 335–341.

(286) Li, Y.; Zhu, Y.; Yang, X.; Li, C. *Cryst. Growth Des.* **2008**, *8* (12), 4494–4498.

(287) (3-Mercaptopropyl)trimethoxysilane 95% | Sigma-Aldrich http://www.sigmaaldrich.com/catalog/product/aldrich/175617?lang=en&region=NZ (accessed Jun 30, 2017).

(288) (3-Aminopropyl)triethoxysilane 99% | Sigma-Aldrich http://www.sigmaaldrich.com/catalog/product/aldrich/440140?lang=en&region=NZ (accessed Jun 30, 2017).

(289) Guo, X.; Yang, Z.; Liu, H.; Lv, X.; Tu, Q.; Ren, Q.; Xia, X.; Jing, C. *Sep. Purif. Technol.* **2015**, *146*, 227–234.

(290) Kim, D.-G.; Hwang, Y.-H.; Shin, H.-S.; Ko, S.-O. *KSCE J. Civ. Eng.* **2015**, *20* (1), 175–187.

(291) Bae, S.; Hanna, K. *Environ. Sci. Technol.* **2015**, *49* (17), 10536–10543.

(292) Fraser, C. *Chemical Analysis for all RMs*; Lower Hutt, 2011.

(293) Della, V. .; Kühn, I.; Hotza, D. *Rice husk ash as an alternate source for active silica production*; 2002; Vol. 57.

(294) *Blue Circle (r) Fly Ash: Product Data Sheet*; Prospect, New South Wales.

(295) Chandrasekhar, S.; Satyanarayana, K. G.; Pramada, P. N.; Raghavan, P.; Gupta, T. N. *J. Mater. Sci.* **2003**, *38* (15), 3159–3168.

(296) Lesmayati, S.; Rohaeni, E. S. In *Prosiding Seminar Nasional "Inovasi Teknologi Pertanian Spesifik Lokasi*; 2014; pp 601–695.

(297) Soeswanto, B.; Lintang, N. *J. Fluida* **2016**, *VII* (1), 18–22.

(298) Rice productivity - Ricepedia http://ricepedia.org/rice-as-a-crop/rice-productivity (accessed May 29, 2017).

(299) Yalcin, N.; Sevinc, V. *Ceram. Int.* **2001**, *27* (2), 219–224.

(300) Sakr, K. *J. Mater. Civ. Eng.* **2006**, *18* (3), 367–376.

(301) Gogoi, N.; Dutta, S.; Begum, T.; Bora, U.; Gogoi, P. K. *RSC Adv.* **2015**, *5*, 95344–95352.

(302) Zhang, S.; Gao, H.; Li, J.; Huang, Y.; Alsaedi, A.; Hayat, T.; Xu, X.; Wang, X. *J. Hazard. Mater.* **2017**, *321*, 92–102.

(303) Kalapathy, U.; Proctor, A.; Shultz, J. *Bioresour. Technol.* **2000**, *73* (3), 257–262.

(304) Meharg, A. A. *Trends Plant Sci.* **2004**, *9* (9), 415–417.

(305) Zhu, Y.-G.; Williams, P. N.; Meharg, A. A. *Exposure to inorganic arsenic from rice: A global health issue?*; 2008; Vol. 154.

(306) Stone, R. *Science (80-.).* **2008**, *321* (5886).

(307) Meharg, A. A.; Zhao, F. J. *Arsenic & rice*; Springer, 2012.

(308) Simcoa http://www.simcoa.com.au/company-2.html (accessed Jun 5, 2017).

(309) Blissett, R. S.; Rowson, N. A. *Fuel* **2012**, *97*, 1–23.

(310) Karabelli, D.; Ünal, S.; Shahwan, T.; Eroğlu, A. E. *Preparation and characterization of*

alumina-supported iron nanoparticles and its application for the removal of aqueous Cu2+ ions; 2011; Vol. 168.

(311) Yang, J.; Yu, K.; Liu, C. *J. Hazard. Mater.* **2017**, *321*, 73–80.

(312) Datta, K. K.; Petala, E.; Datta, K. J.; Perman, J. A.; Tucek, J.; Bartak, P.; Otyepka, M.; Zoppellaro, G.; Zboril, R. *Chem. Commun.* **2014**, *50*, 15673–15676.

(313) Diao, Z.-H.; Xu, X.-R.; Jiang, D.; Kong, L.-J.; Sun, Y.-X.; Hu, Y.-X.; Hao, Q.-W.; Chen, H. *Chem. Eng. J.* **2016**, *302*, 213–222.

(314) Ezzatahmadi, N.; Ayoko, G. A.; Millar, G. J.; Speight, R.; Yan, C.; Li, J.; Li, S.; Zhu, J.; Xi, Y. *Chem. Eng. J.* **2017**, *312*, 336–350.

(315) Klausen, J.; Troeber, S. P.; Haderlein, S. B.; Schwarzenbach, R. P. *Environ. Sci. Technol.* **1995**, *29* (9), 2396–2404.

(316) Gorski, C. A.; Edwards, R.; Sander, M.; Hofstetter, T. B.; Stewart, S. M. *Environ. Sci. Technol.* **2016**, *50* (16), 8538–8547.

(317) Xu, J.; Hao, Z.; Xie, C.; Lv, X.; Yang, Y.; Xu, X. *Desalination* **2012**, *284*, 9–13.

(318) Bright-Young, J.; Fulton, J. R. *unpublished result*; 2016.

Appendix

A. DETAILED INSTRUCTION ON IMAGE PROCESSING IN PICASA™ AND FIJI

The steps are as follow:

1. Open the image in Picasa3™ →<Edit> → <more fun and useful image processing> (paintbrush with green box) → <HDR-ish>

2. Change the setting to approximately 1/5 radius, almost maximum strength, and <Apply>. The aim was a picture like this, where the white dots of the iron was over-exaggerated and 'pops out'.
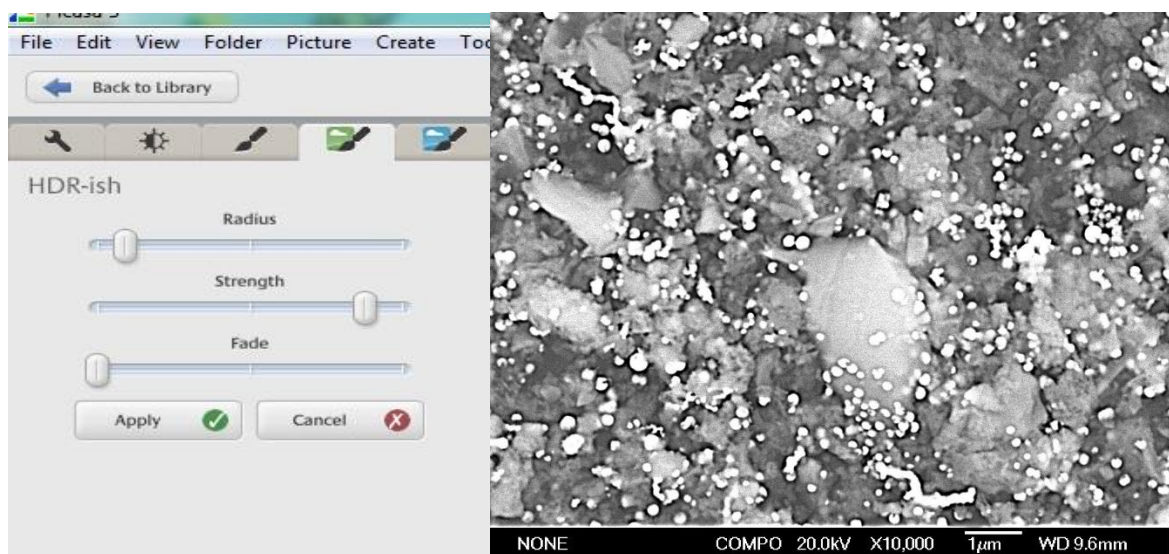
3. Save the image, and then open FIJI software. And open saved file in FIJI File→Open→

4. Change the image into 8 Bit: <Image>→<Type>→<8 Bit>

5. Set the scale by drawing a line over the scale on the image and then <Analyze>→<Set Scale>. Change the known distance and unit of length as necessary and <OK>. If all the pictures being processed had the same scale, click <Global>.
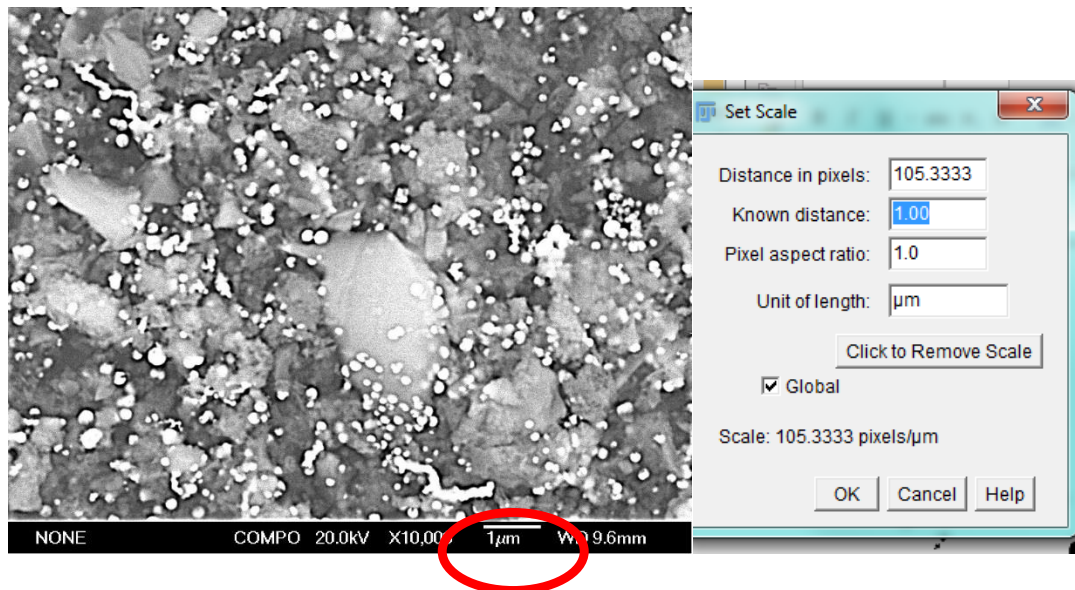
6. Delete the label box (picture information) by draw a box over it, including any white line on top of the box, then <Edit>→ <clear>.

7. Run Threshold (Ctrl+Shift+T). Adjust the scale until the 'red' only cover the white dots, at between 235-255. Click <Apply> to get the black and white image.
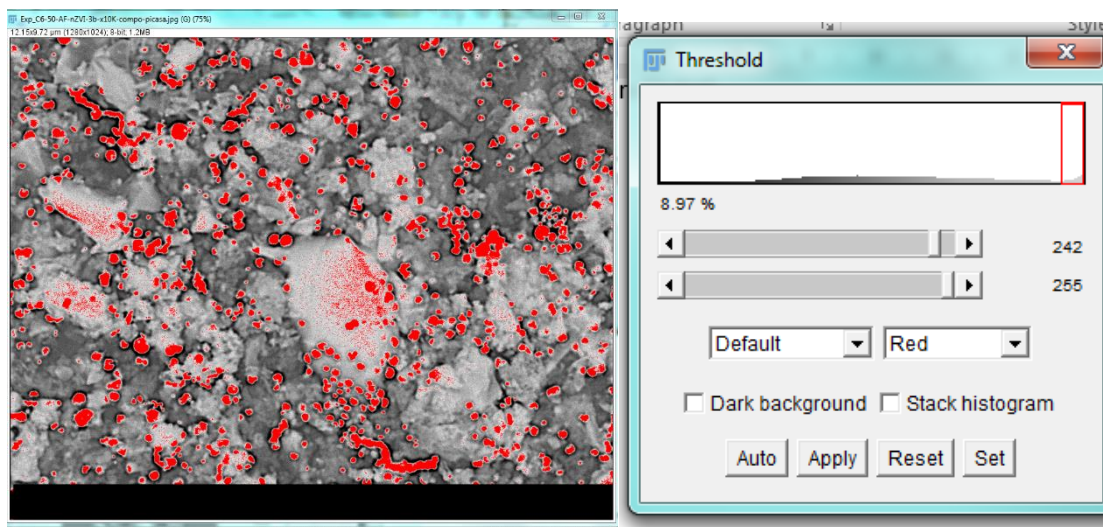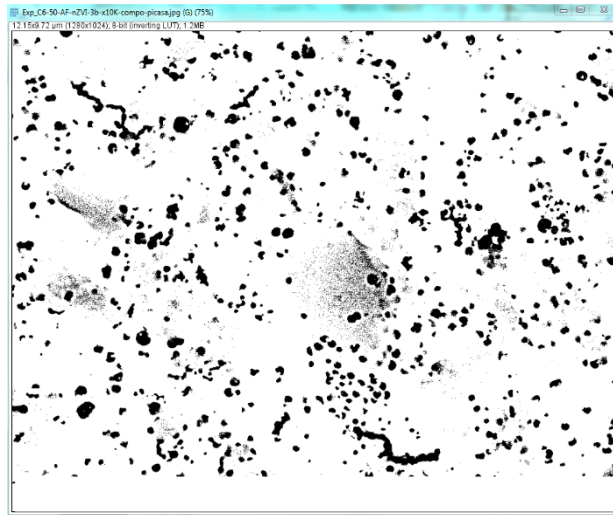
8. Now particle size can be analysed, <Analyze>→<Analyze Particles>. Put minimum size which in this case was 0.0009 to exclude noise. The smallest iron particles were around 0.001 µm^2, so not a lot of data was going to be lost by setting minimum size.
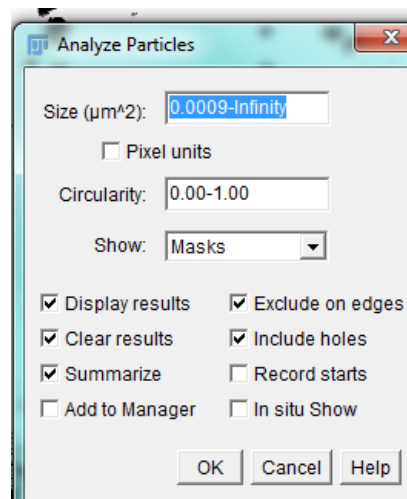
9. On this window, the image showed which sites calculated as area, and also the result box. Copy all these data and paste to Excel spreadsheet for further processing
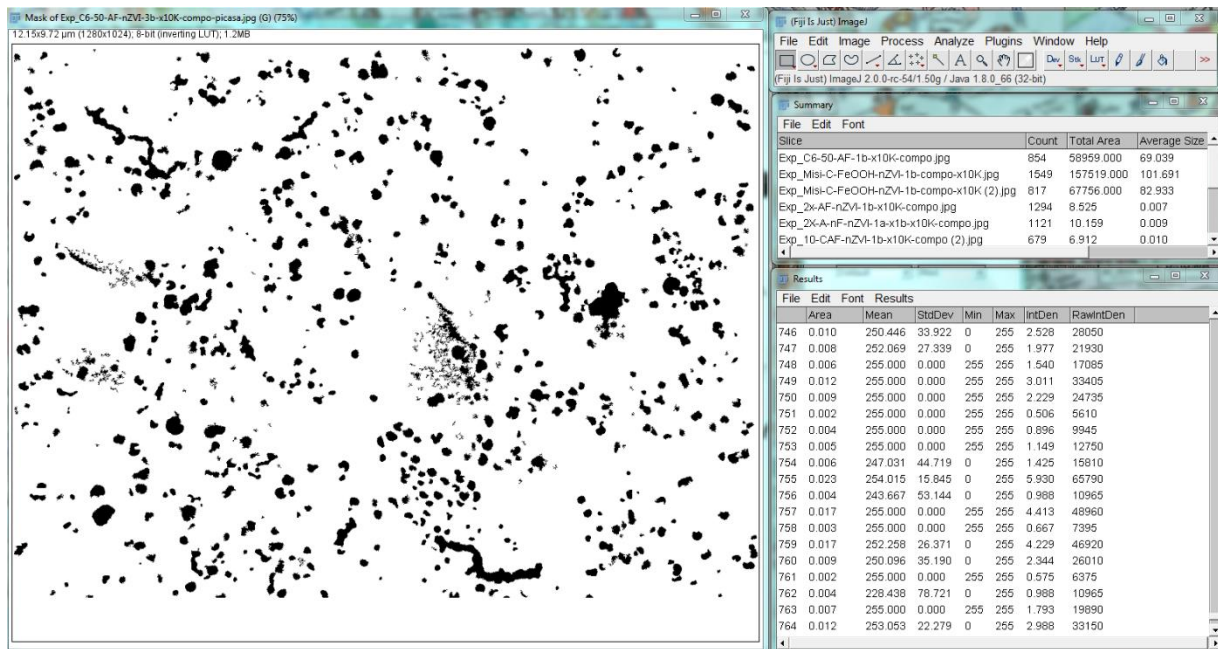
10. Area indicates the size of each black area as indicated by the result picture. A histogram of the area data should be constructed to indicate the distribution of particle size. The decision to discard outlier(s) should be made in conjunction with the image. Some outlier indicates the size of nZVI chain, while the others picking up area of silica which had a high brightness and therefore picked up during thresholding.

B. LIST OF CHEMICALS USED

Name	Source	Purity
3-Aminopropyl triethylsilane (3-APTES)	Sigma Aldrich (Germany)	97%
3-thiopropyl trimethylsilane (3-TPTMS)	Sigma Aldrich (USA)	95%
Diethyl ether	LabServe	99.0%
Dodecyl amine (DDA)	Sigma	
Ethanol (absolute)	Fisher Chemical	AR Grade
$FeCl_3$	Sigma Aldrich	99%
$FeSO_4 \cdot 7H_2O$	Riedel-deHaën	99.5%
HCl (Conc)	Merck	37%
Iron standard AAS	Sigma Aldrich (Switzerland)	
KNO_3	Vickers Lab Ltd	99.5%
LiCl Anyhdrous	BDH	
Microsilica 600	Golden Bay	
$NaBH_4$ (powder)	Sigma Aldrich	96%
NaOH	Pure Science	90%
Precipitated Aluminium silicate	BDH	
Sea Sand (acidified, calcined)	ChemSolute	
Silica Gel 60	Pure Science	
Tetraethyl orthosilicate (TEOS)	Sigma Aldrich (Germany)	>99%
Toluene	Pure Science	99.9%

179

C. Misi/nZVI products

A., a, Misi-C600-5-AF-nZVI; b, Misi-C600-5-AnF-nZVI; c, Misi-C600-5-nAF-nZVI;d, Misi-C600-5-nAnF-nZVI; e, Misi C600-AF-nZVI; f, Misi C600-AnF-nZVI; g, Misi C600-nAF-nZVI; h, Misi C600-nAnF-nZVI;
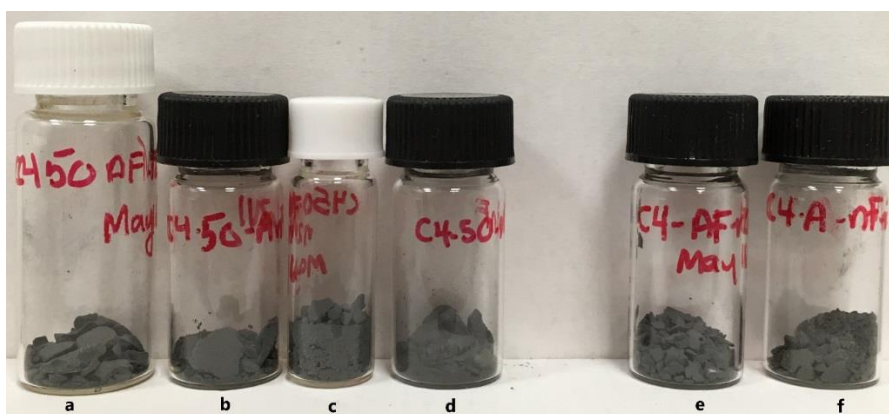
B., a, Misi C400-5-AF-nZVI; b, Misi C400-5-AnF-nZVI; c, Misi C400-5-nAF-nZVI; d,Misi C400-5-nAnF-nZVI; e, Misi-C400-AF-nZVI; e, Misi-C400-AnF-nZVI
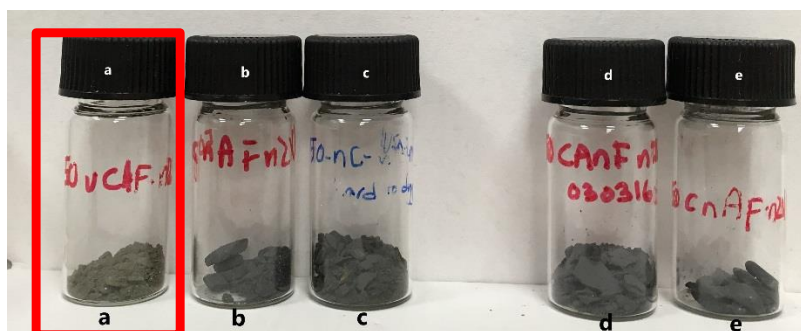
C., a, Misi-5-uC-AF-nZVI; b, Misi-5-uC-AnF-nZVI; c, Misi-5-uC-nAnF-nZVI; d, Misi-5-C600-AnF-nZVI; e, Misi-5-C600-nAF-nZVI;
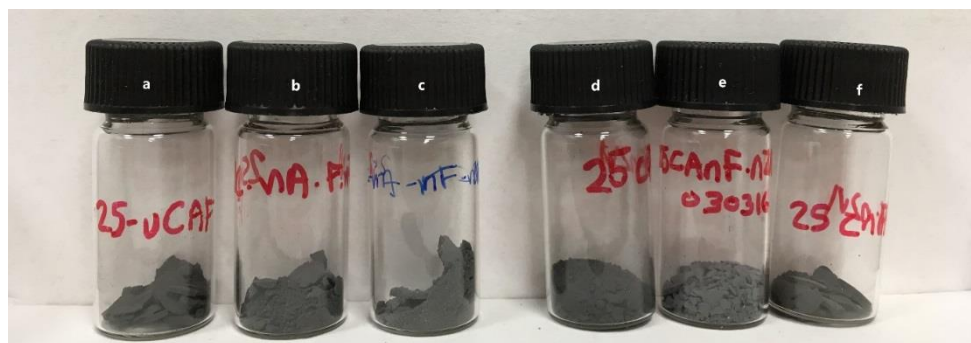
D., a, Misi-2-uC-AF-nZVI; b, Misi-2-uC-nAF-nZVI; c, Misi-2-uC-nAnF-nZVI; d, Misi-2-C600-AF-nZVI; e, Misi-2-C600-AnF-nZVI;f, Misi 2-C600-nAnF-nZVI
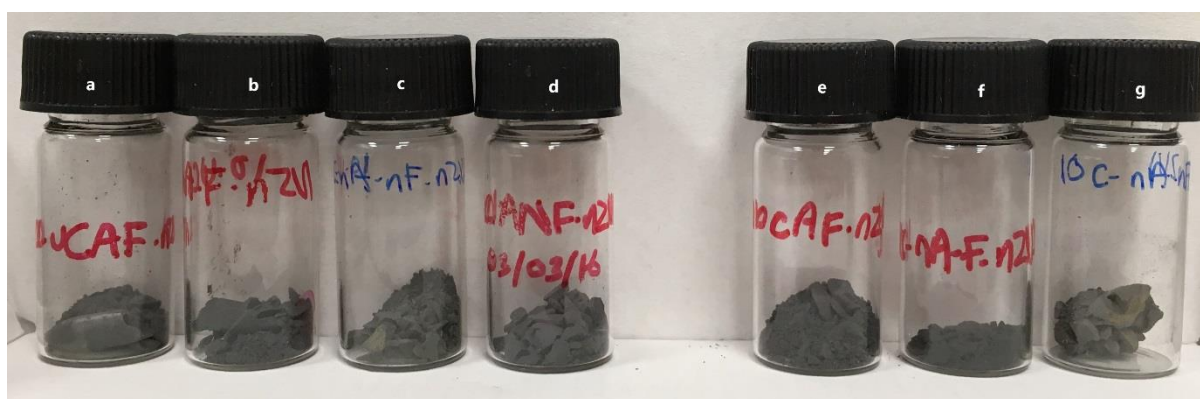
E., a, Misi 1-uC-AF-nZVI; b, Misi 1 uC-AnF-nZVI; c, Misi 1-uC-nAF-nZVI; d, Misi-1-uC-nAnF-nZVI; e, Misi 1-C600-AF-nZVI; f, Misi 1-C600-nAF-nZVI g, Misi 1-C600-nAnF-nZVI

181

D. List of Misi-nZVI images

Entry	Name	Particle size average (nm^2)	SD (nm^2)	% < 2000 nm^2	Total Count	*A*-value
1	1-C600-AF-nZVI	10641	10881	86.9	748	1.04
2	1-C600-AnF-nZVI 1	6314	8745	97.1	2382	0.77
3	1-C600-AnF-nZVI 2	10626	14175	87.9	1133	1.35
4	1-C600-nAF-nZVI 1	8286	10446	92.4	1190	0.98
5	1-C600-nAF-nZVI 2	7793	9581	93.4	894	0.91
6	1-C600-nAnF-nZVI 1	10236	16802	87.3	1309	1.60
7	1-C600-nAnF-nZVI 2	9820	25277	92.2	490	2.46
8	1-uC-AF-nZVI	8344	12168	92.2	708	1.17
9	1-uC-AnF-nZVI	7467	13763	92.7	1068	1.31
10	1-uC-nAF-nZVI 1	11752	22214	86.1	1001	2.14
11	1-uC-nAF-nZVI 2	7116	7903	95	988	0.74
12	1-uC-nAnF-nZVI	15593	36714	81.3	630	3.57
13	2-C600-AF-nZVI 1	10840	18782	88.7	1175	1.80
14	2-C600-AF-nZVI 2	8401	10109	92.2	1025	0.96
15	2-C600-AnF-nZVI 1	8946	10552	90	1271	0.99
16	2-C600-AnF-nZVI 2	6430	6819	95.8	1529	0.62
17	2-C600-nAF-nZVI 1	10605	25819	88.6	945	2.50
18	2-C600-nAF-nZVI 2	5650	5633	98.6	355	0.55
19	2-C600-nAnF-nZVI 1	7215	8976	94.8	1445	0.83
20	2-C600-nAnF-nZVI 2	13620	34855	85.2	656	3.39
21	2-uC-AF-nZVI 1	7500	9803	94.4	1086	0.92
22	2-uC-AF-nZVI 2	6325	6447	96.9	927	0.60
23	2-uC-AnF-nZVI	8714	13850	91.4	1322	1.31
24	2-uC-nAF-nZVI 1	7250	7646	94	744	0.73
25	2-uC-nAF-nZVI 2	4704	7869	98.2	435	0.76
26	2-uC-nAF-nZVI 3	6481	5793	96.8	910	0.54
27	2-uC-nAnF-nZVI	10090	12248	87.2	744	1.18
28	5-C600-AF-nZVI 1	5630	5457	97.7	597	0.52
29	5-C600-AF-nZVI 2	9434	14196	91.2	794	1.37
30	5-C600-AF-nZVI 3	10551	24693	91.6	559	2.40
31	5-C600-AF-nZVI-4	5262	7458	96.6	589	0.71
32	5-C600-AnF-nZVI 1	6798	9088	95.9	1339	0.84
33	5-C600-AnF-nZVI 2	7145	11911	94.3	1677	1.11
34	5-C600-AnF-nZVI 3	9044	13135	90.5	1447	1.24

Entry	Name	Particle size average (nm²)	SD (nm²)	% < 2000 nm²	Total Count	*D*-value
35	5-C600-nAF-nZVI 1	7063	9019	93.7	994	0.85
36	5-C600-nAF-nZVI 2	4842	5779	98	837	0.54
37	5-C600-nAF-nZVI 3	6871	6783	96.7	1045	0.63
38	5-C600-nAF-nZVI 4	5851	7305	96.4	1186	0.68
39	5-C600-nAnF-nZVI 1	6554	8895	94.6	1547	0.82
40	5-C600-nAnF-nZVI 2	4049	2890	100	196	0.28
41	5-uC-AF-nZVI	11819	27594	85.6	389	2.69
42	5-uC-AnF-nZVI	11563	21316	87.3	735	2.06
43	5-uC-nAF-nZVI	9688	12085	87.9	1103	1.15
44	5-uC-nAnF-nZVI	7042	9369	93.9	1231	0.88
45	C400-5-AF-nZVI	12463	20932	83.7	797	2.02
46	C400-5-nAF-nZVI	17336	21800	71.2	667	2.11
47	C400-5-nAnF-nZVI	7651	12026	91.6	1413	2.10
48	C400-AF-nZVI	8811	14249	92	847	1.37
49	C400-AnF-nZVI	11511	25005	88.4	673	2.43
50	C400-nAF-nZVI	9316	18475	89	875	1.78
51	C400-nAnF-nZVI	7190	6930	96.3	943	0.65
52	C600-5-AF-nZVI 1	12843	25492	86.8	403	2.49
53	C600-5-AF-nZVI 2	10320	12146	87.6	637	1.17
54	C600-5-AnF-nZVI	8645	16163	91.8	1214	1.54
55	C600-5-nAF-nZVI 1	9786	12476	88.4	406	1.21
56	C600-5-nAF-nZVI 2	5604	10679	95.9	366	1.04
57	C600-5-nAnF-nZVI 1	7906	10975	92.9	876	1.05
58	C600-5-nAnF-nZVI 2	6987	10638	93.8	844	1.02
59	C600-5-nAnF-nZVI 3	4555	6836	96.8	965	0.64
60	C600-AF-nZVI 1	9165	20776	92.7	918	2.00
61	C600-AF-nZVI 2	11421	21142	87.2	837	2.04
62	C600-AnF-nZVI	10623	18235	88.8	865	1.76
63	C600-nAF-nZVI 1	6445	7926	95.3	940	0.75
64	C600-nAF-nZVI 2	16797	51859	84.6	350	5.07
65	C600-nAnF-nZVI	5478	7655	97.1	2121	0.67

1-C600-AF-nZVI *A*= 1.04   Entry 1
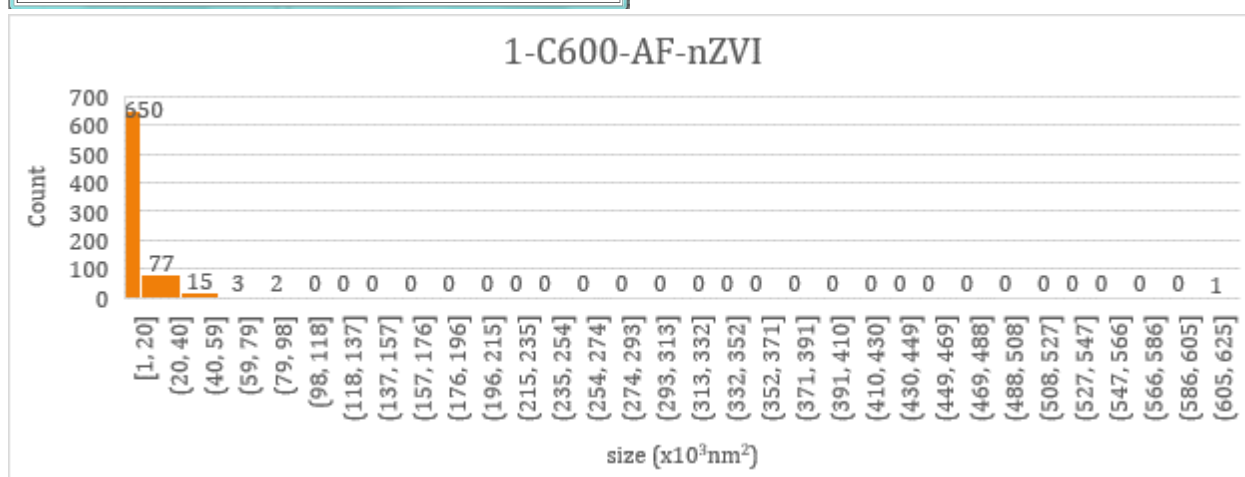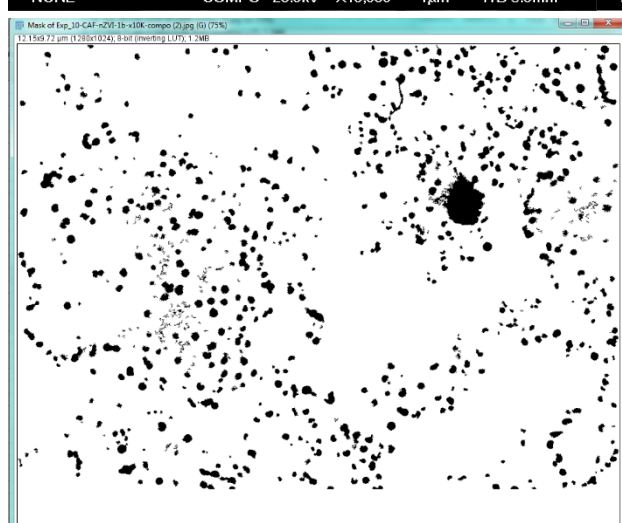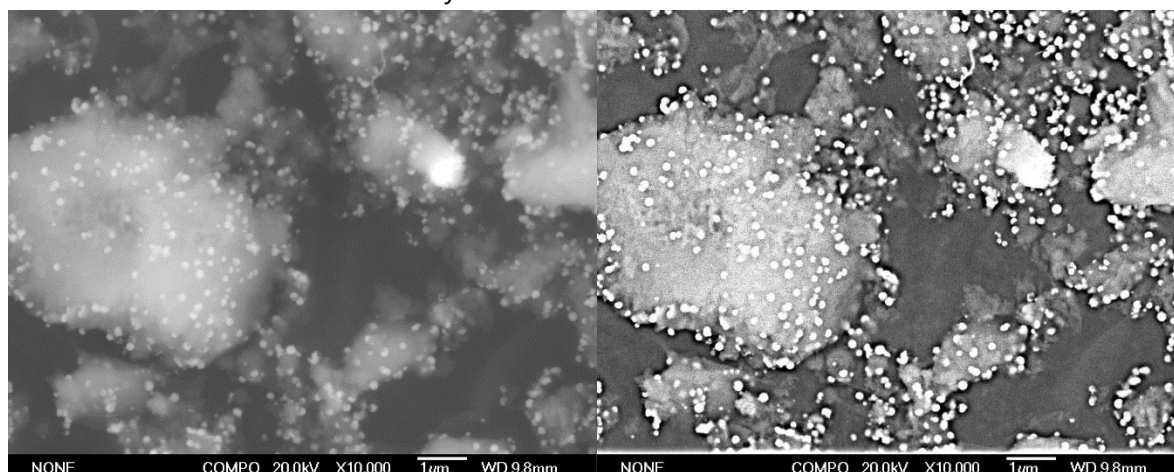
	With outlier	Without outlier (611)
Mean (nm2)	11444	10641
SD (nm2)	24484	10881
% of particles under 2000 nm2	86.9	86.9

184

1-C600-AnF-nZVI *A*= 0.77   Entry 2
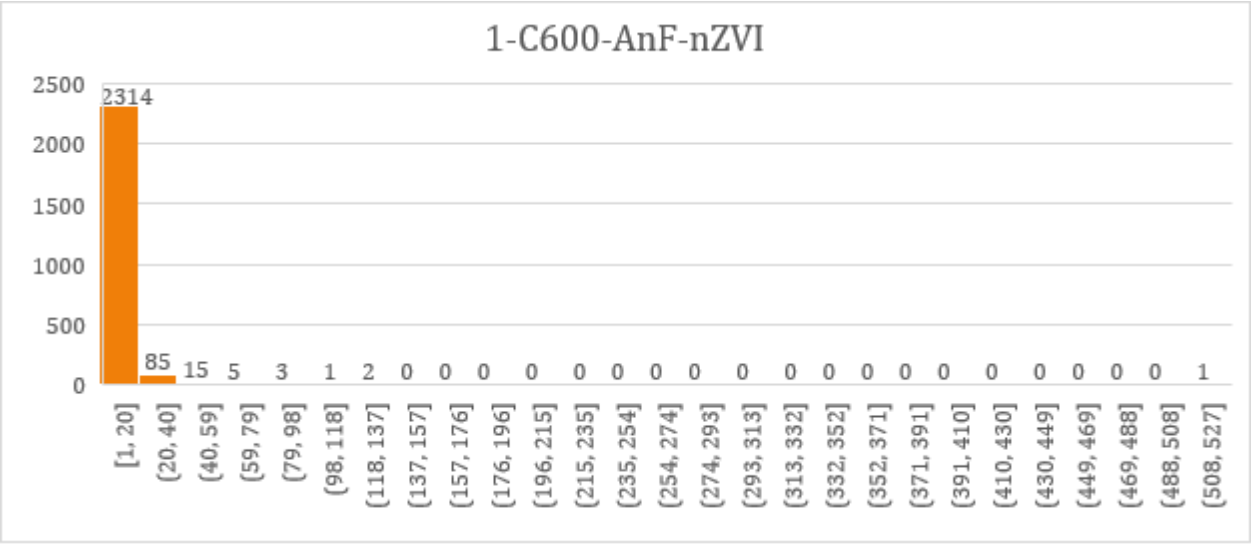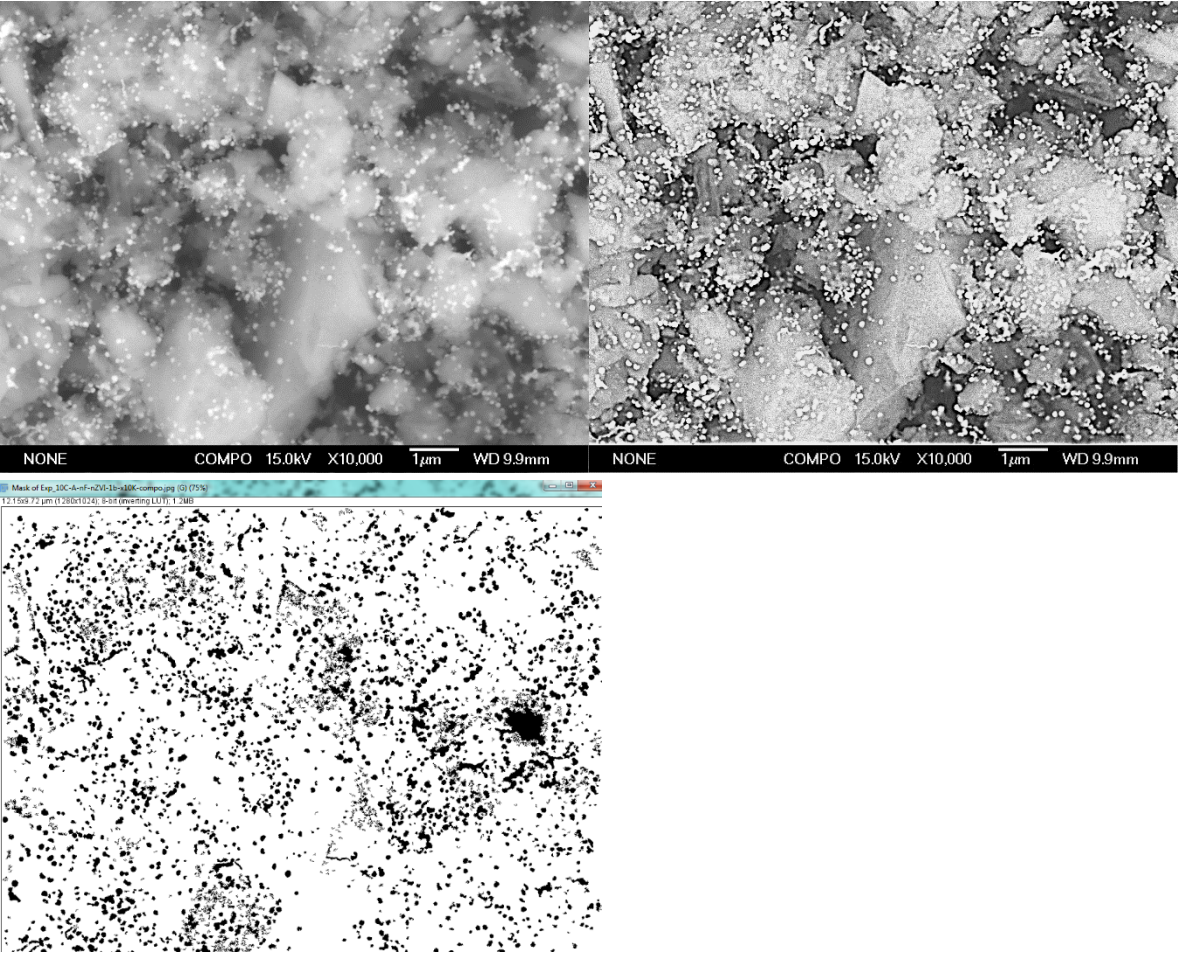
	With outlier	Without outlier (511)
Mean (nm^2)	6522	6314
SD (nm^2)	13468	8745
% of particles under 2000 nm^2	97.1	97.1

185

1-C600-AnF-nZVI 2 *A*=1.35   Entry 3
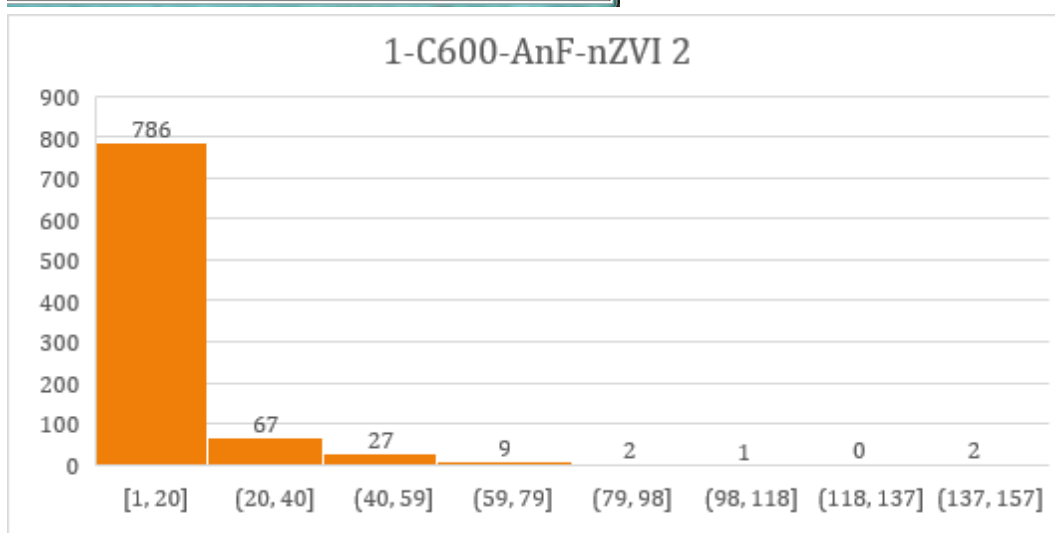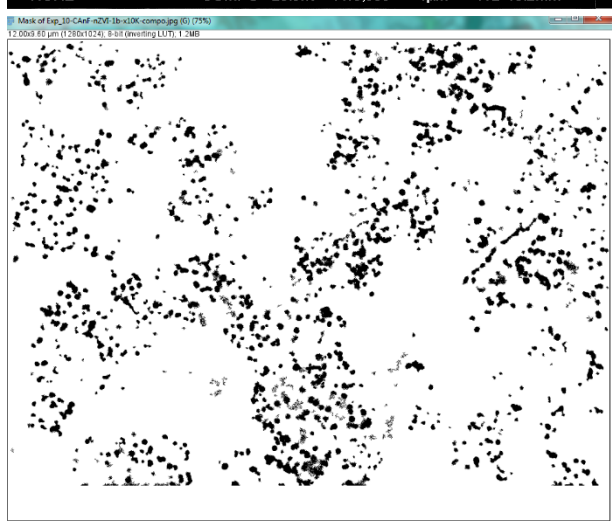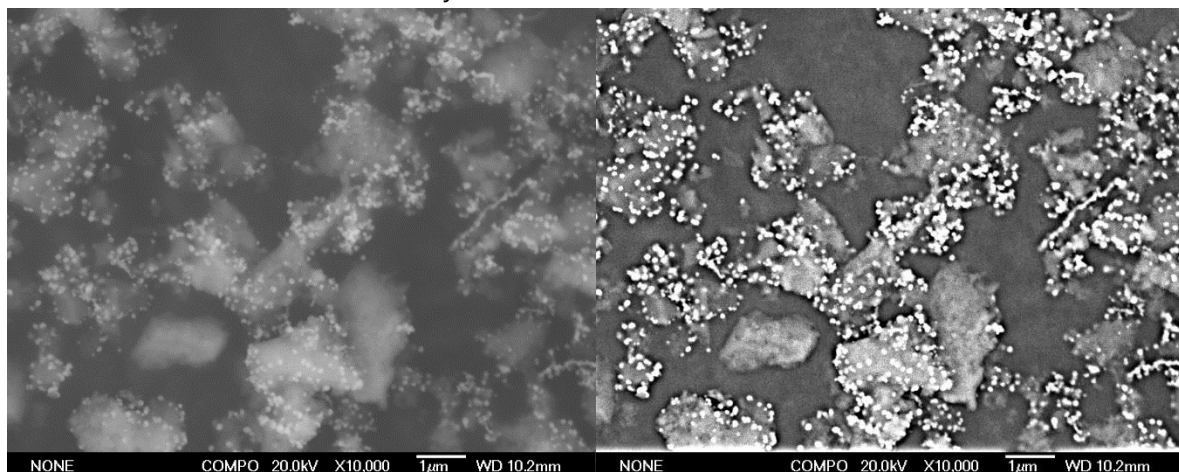
Mean = 10626nm^2

SD= 14175nm^2

% <2000 nm^2 : 92.2%

186

1-C600-nAF-nZVI *A* = 0.98   Entry 4
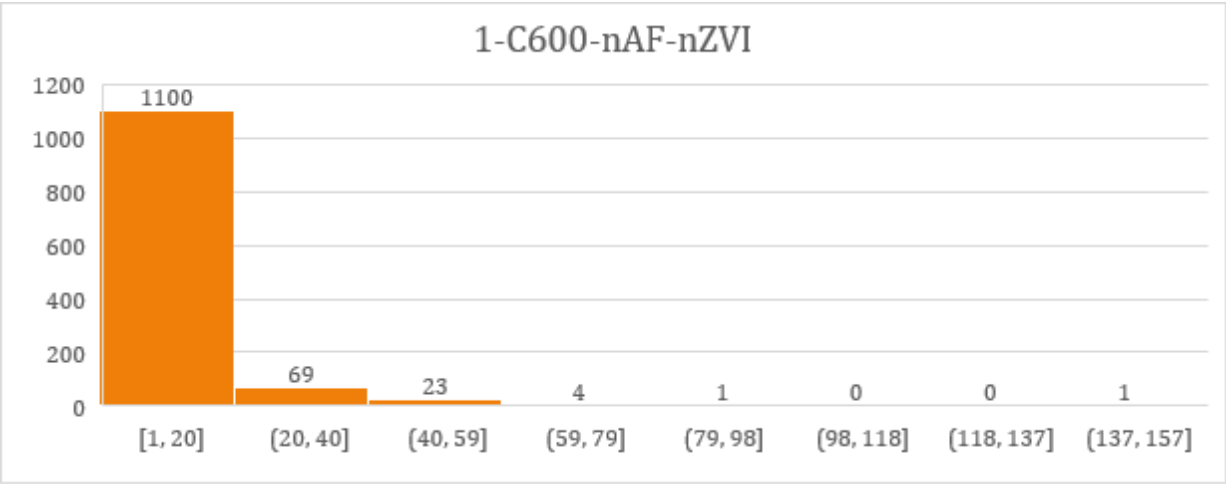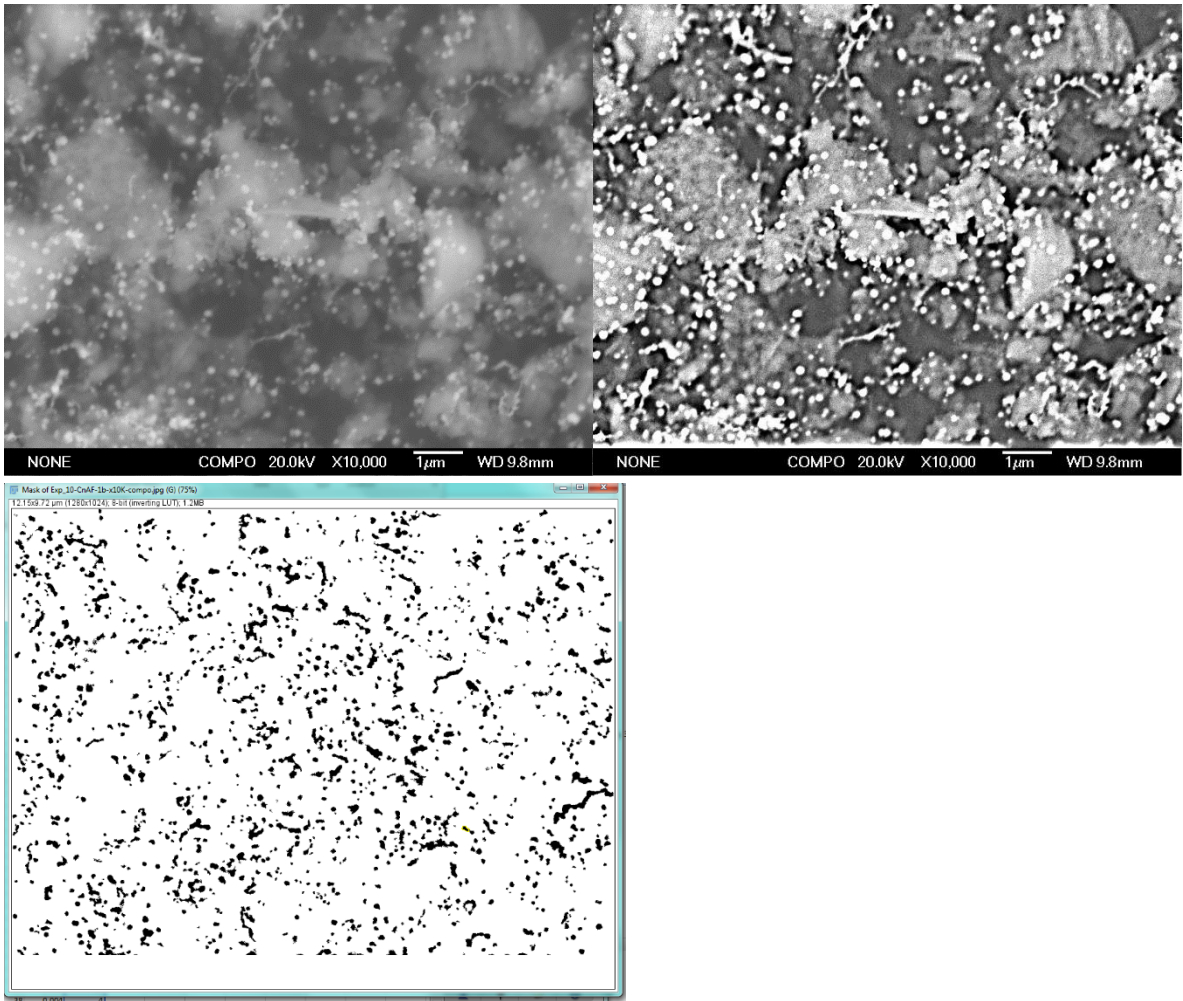
Mean = 8286 nm^2
SD= 10446 nm^2
% <2000 nm^2 : 92.4%

1-C600-nAF-nZVI 2   *A*= 0.91   Entry 5
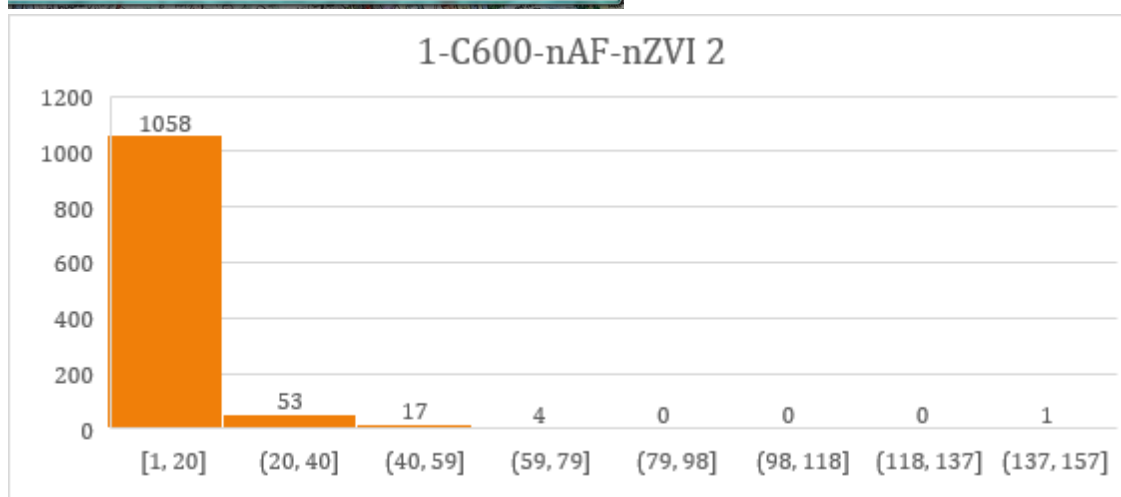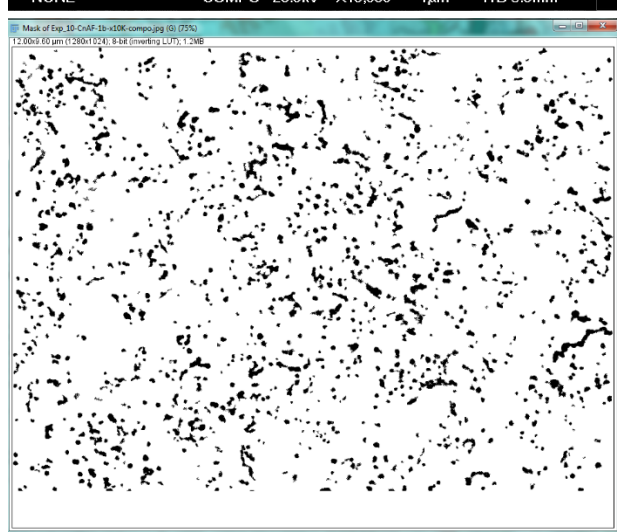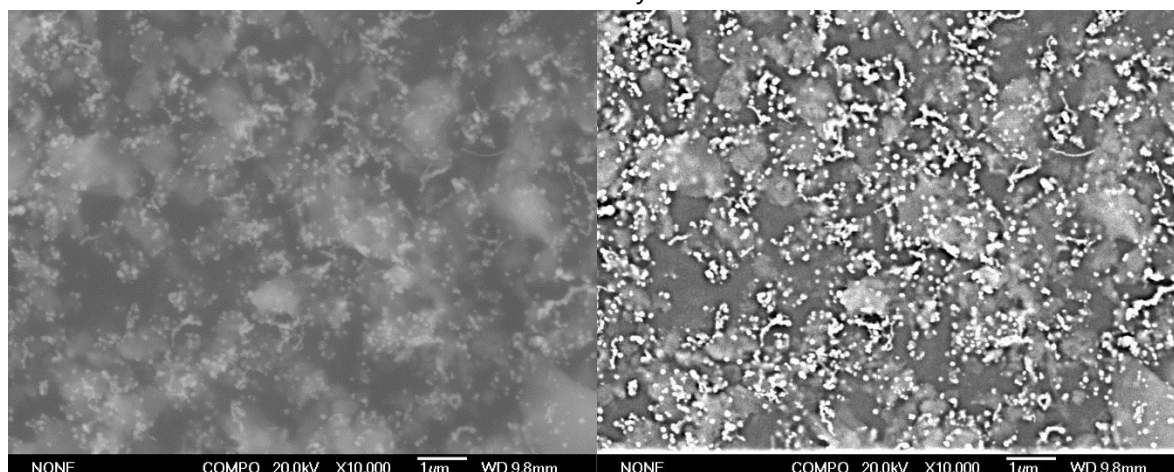
Mean = 7793 nm^2
SD= 9581 nm^2
% <20000 nm^2 : 93.4%

1-C600-nAnF-nZVI 1   *A*=1.60   Entry 6
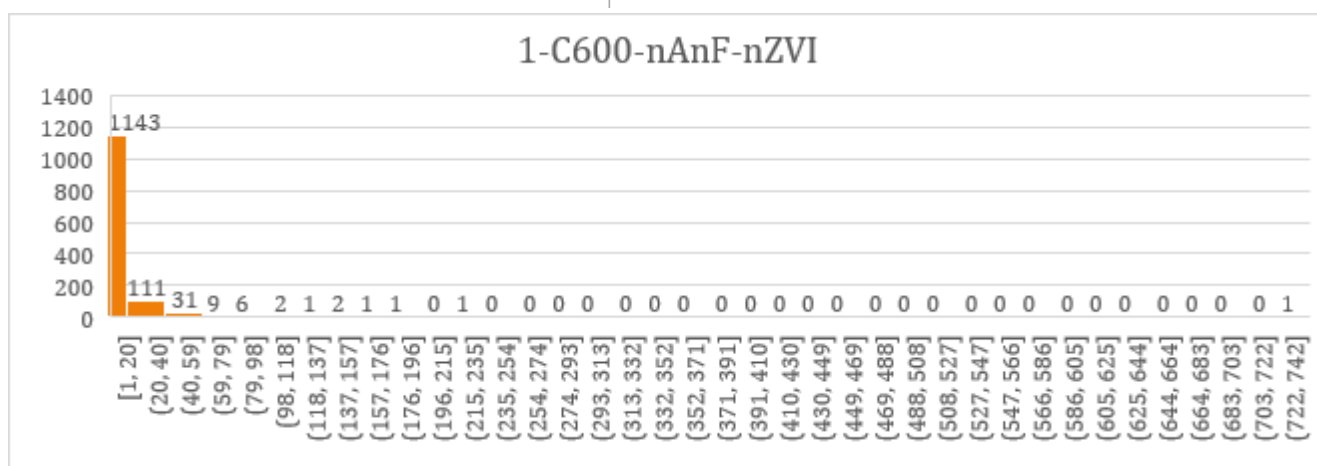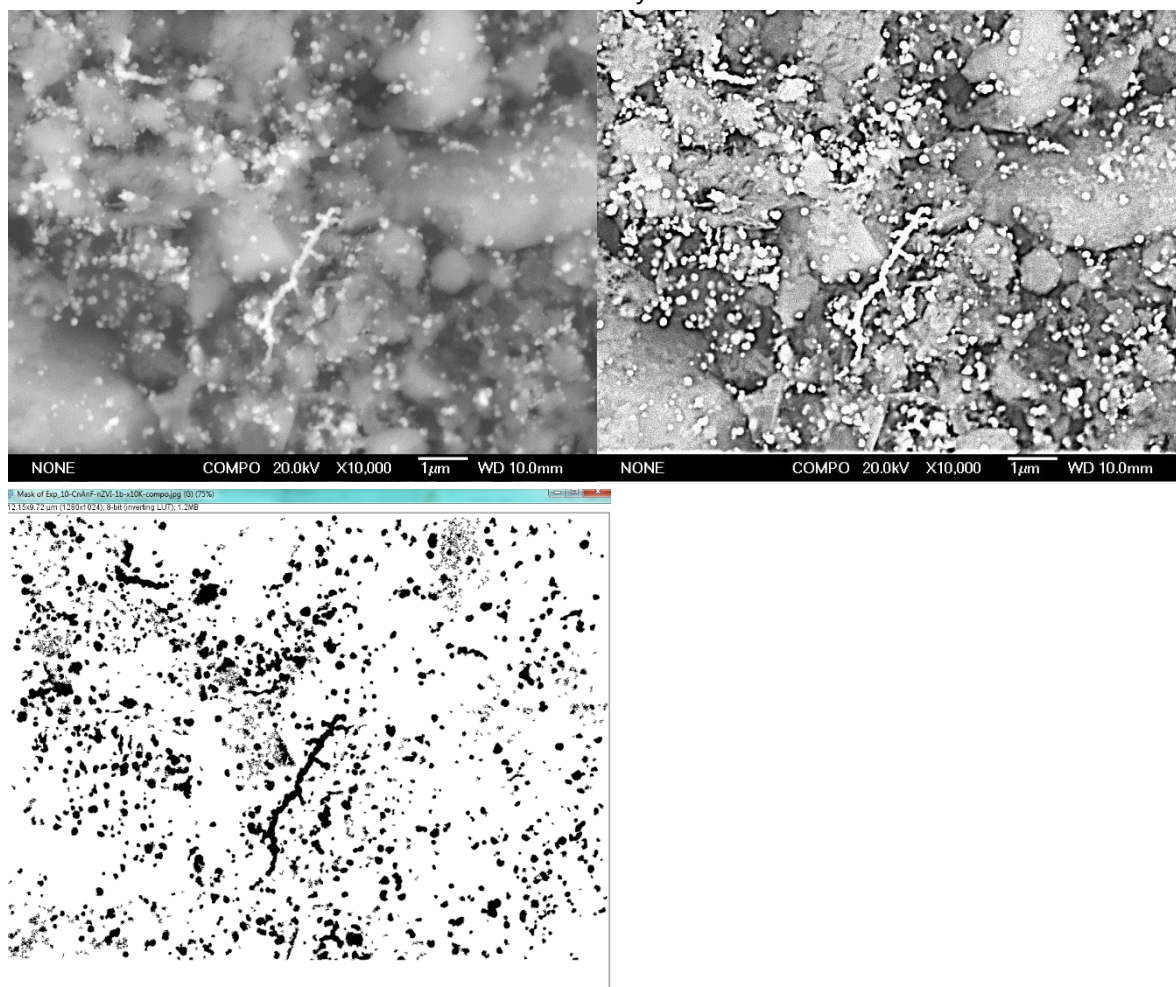
	With outlier	**Without outlier (741)**
Mean (nm^2)	10794	10236
SD (nm^2)	26263	16802
% of particles under 2000 nm^2	87.3	87.3

1-C600-nAnF-nZVI 2 *A*=2.46   Entry 7
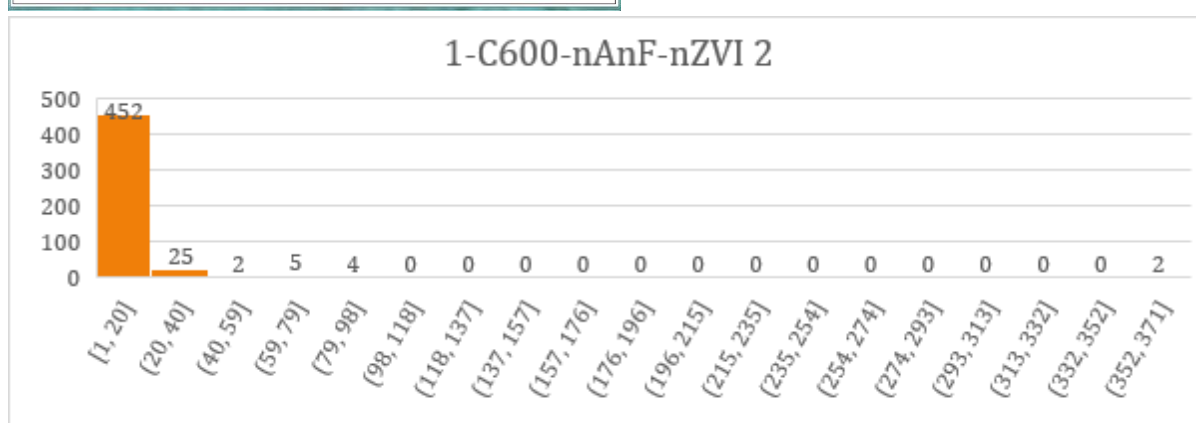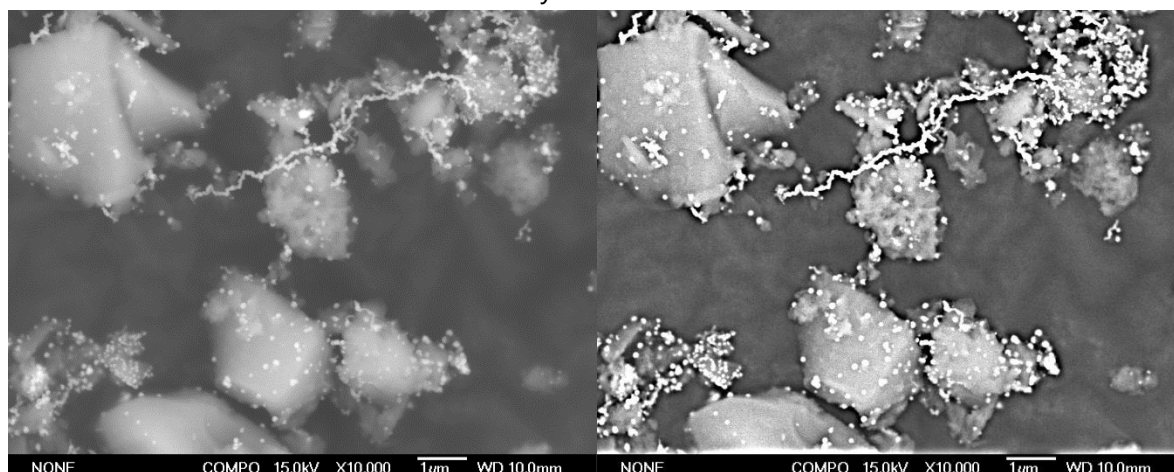
Mean = 9820 nm^2

SD= 25277 nm^2

% <2000 nm$^{2.}$: 92.2%

1-uC-AF-nZVI   *A* = 1.17   Entry 8
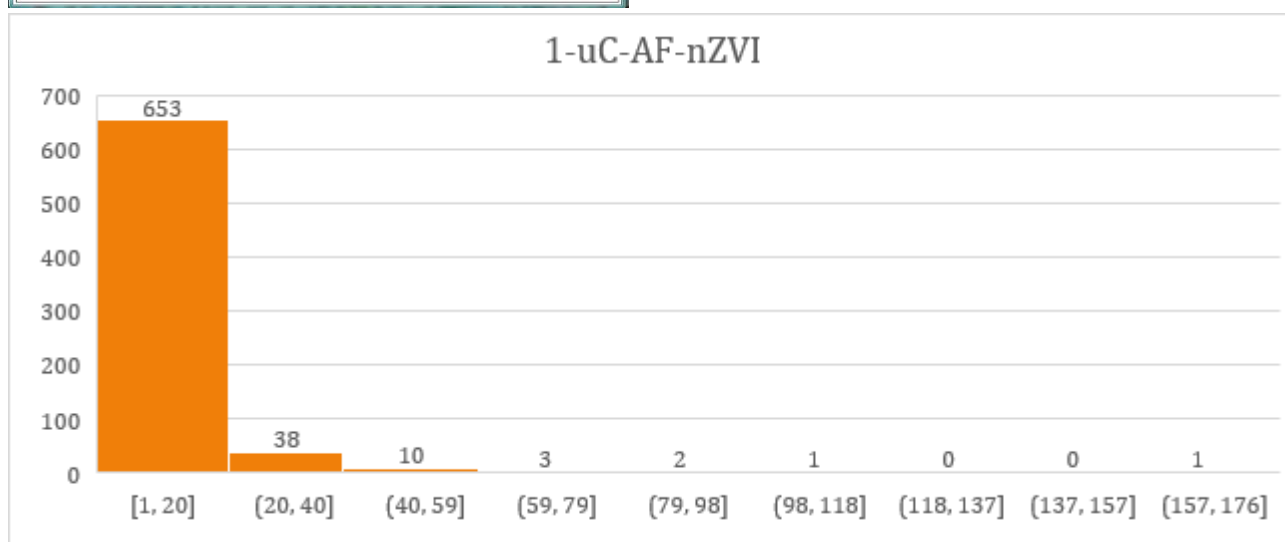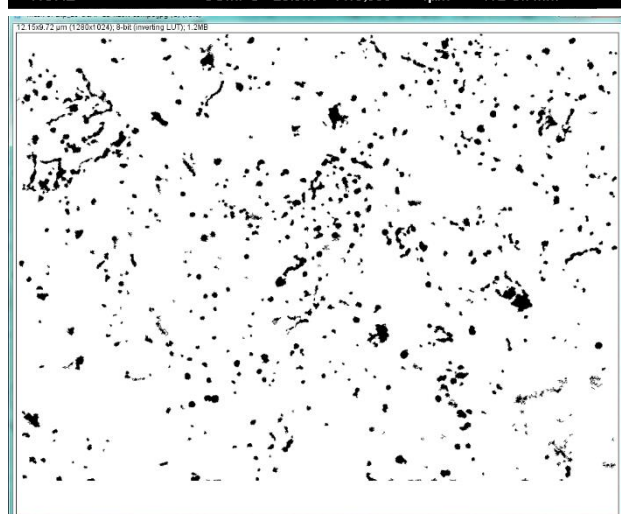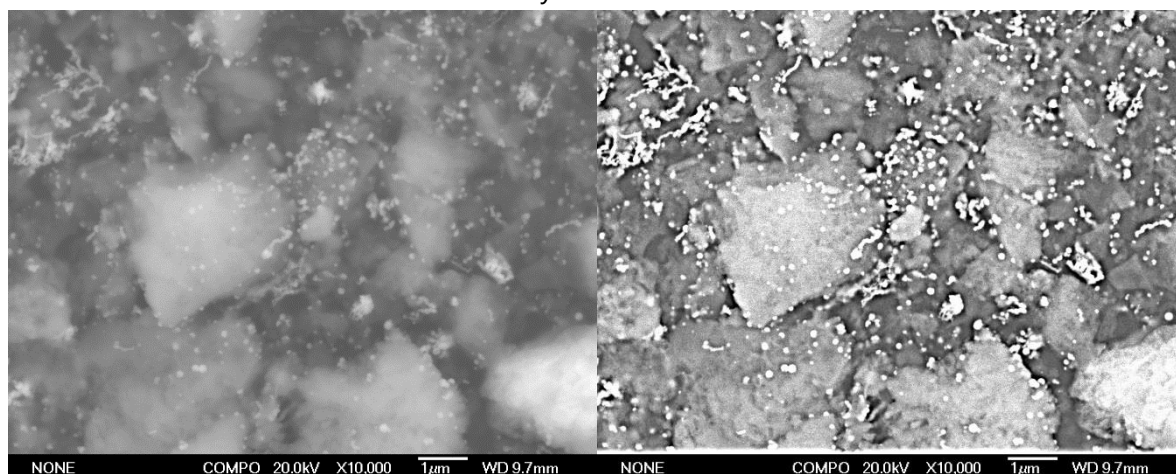
Mean = 8344 nm^2
SD = 121168 nm^2
% < 2000 nm^2 : 92.2%

1-uC-AnF-nZVI   *A*=1.31   Entry 9
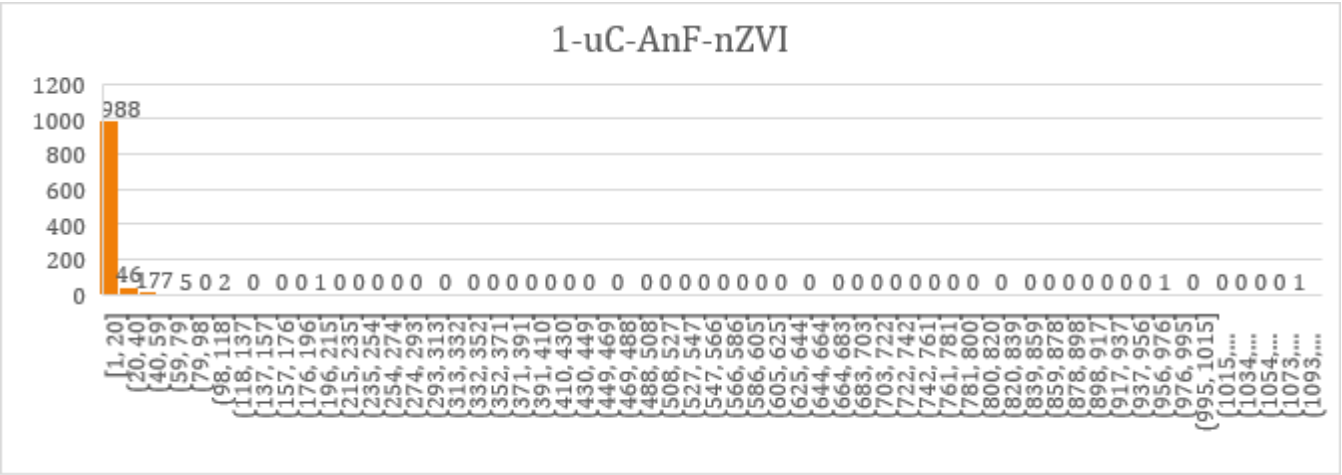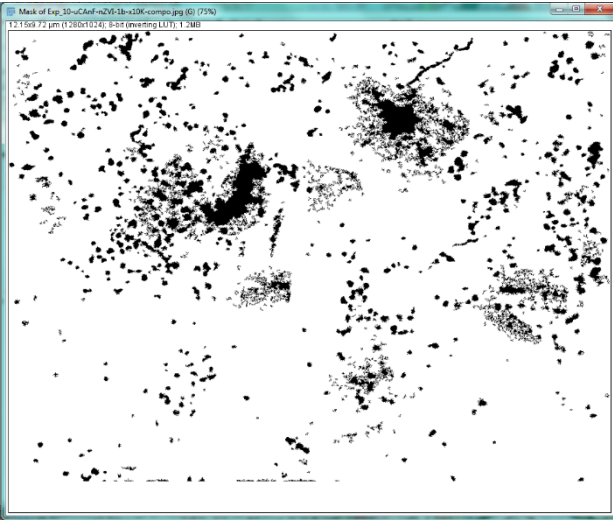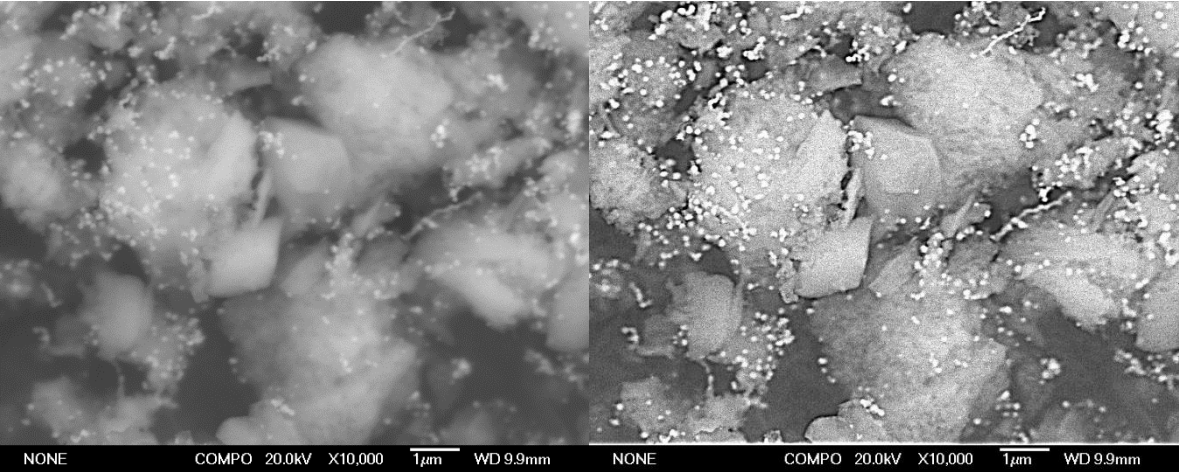
	With outlier	Without outliers (988 & 1096)
Mean (nm^2)	9401	7467
SD (nm^2)	46811	13763
% of particles under 2000 nm^2	92.7	92.7

1-uC-nAF-nZVI   *A*=2.14   Entry 10
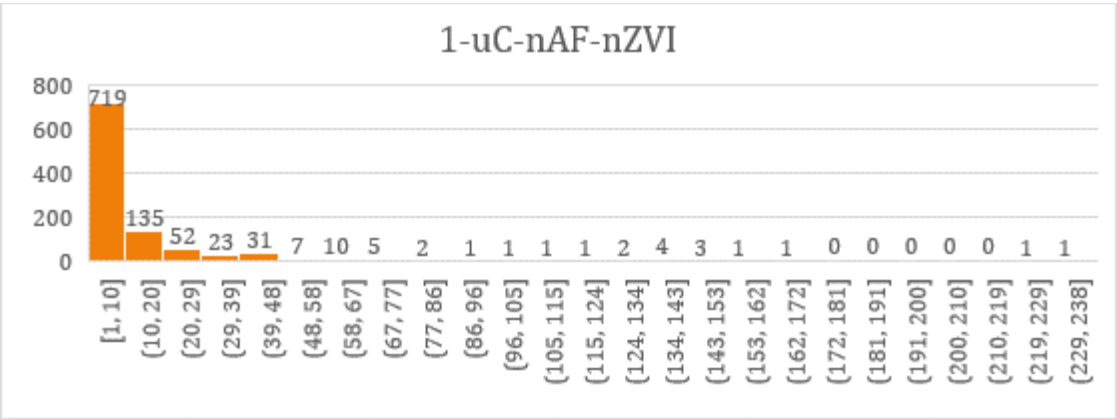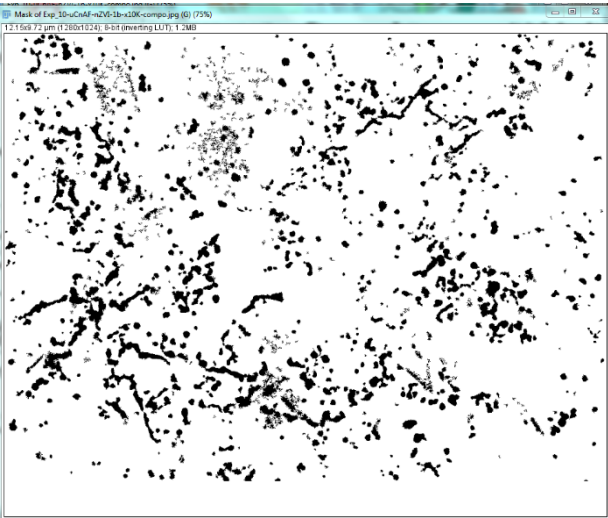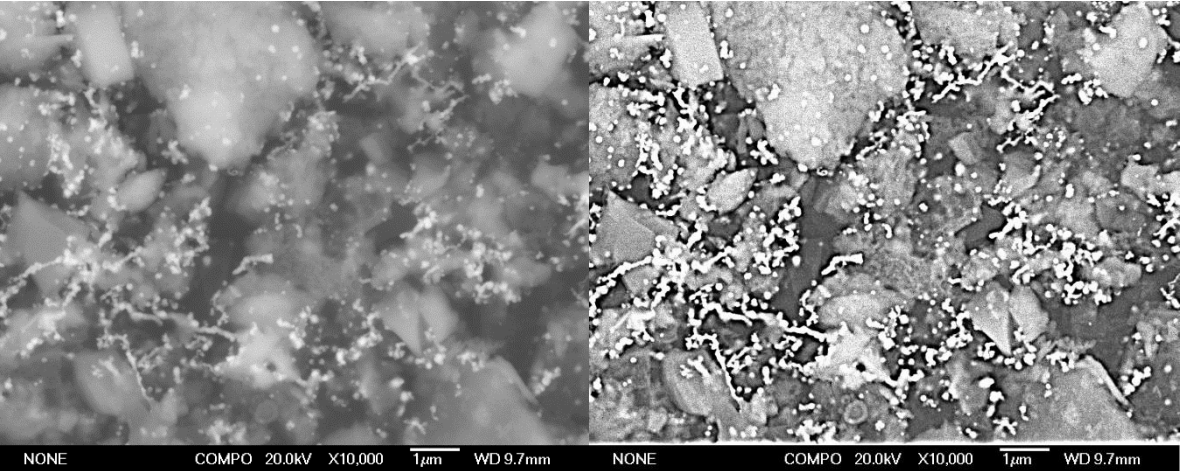
Mean = 11752 nm^2
SD= 22214 nm^2
% <2000 nm^2 : 86.1%

1-uC-nAF-nZVI 2   *A*=0.74   Entry 11

1-uC-nAF-nZVI 2
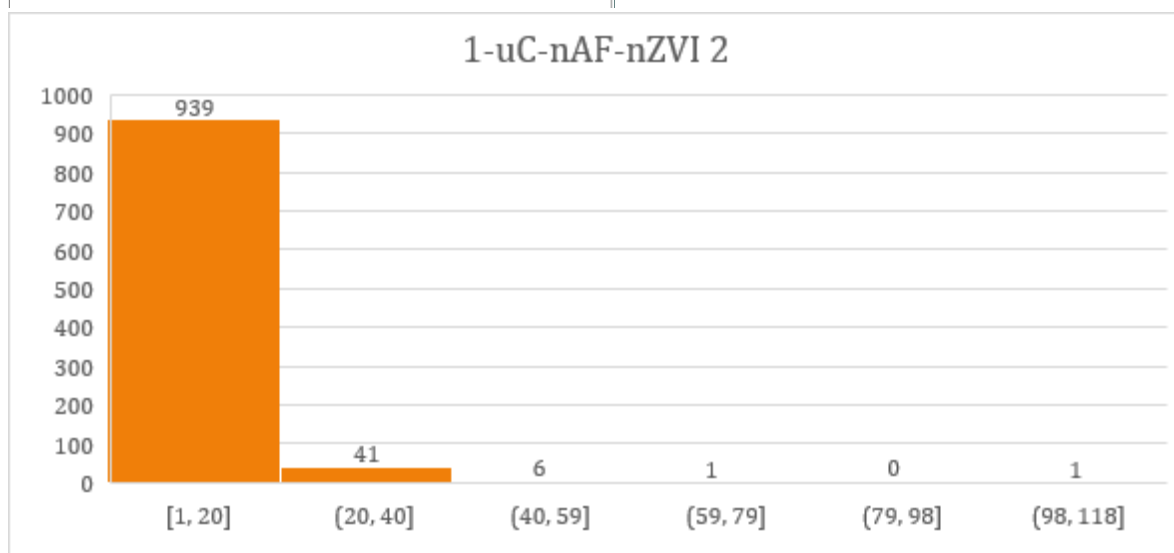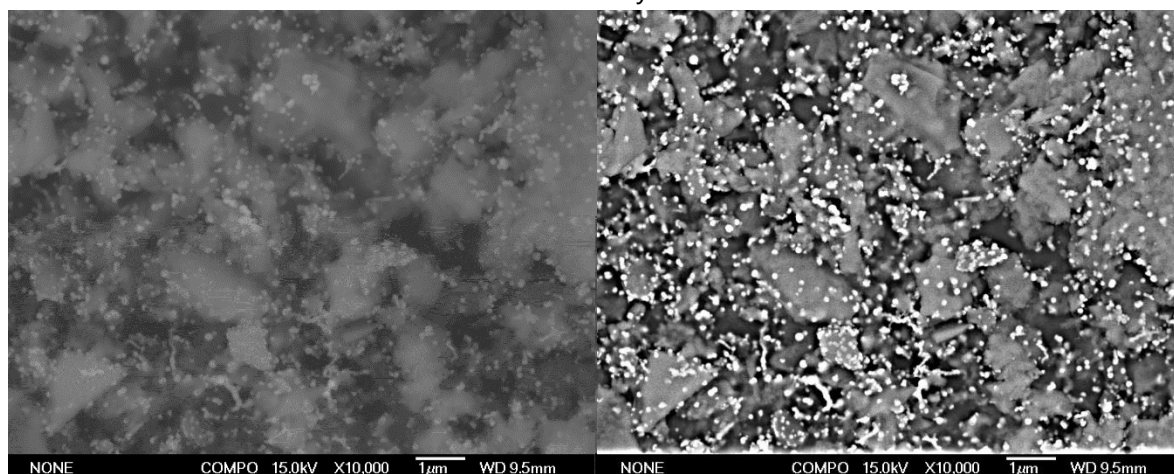
Mean = 7116 nm^2
SD= 7903 nm^2
% <2000 nm^2 : 95.0%

195

1-uC-nAnF-nZVI   *A*=3.57   Entry 12
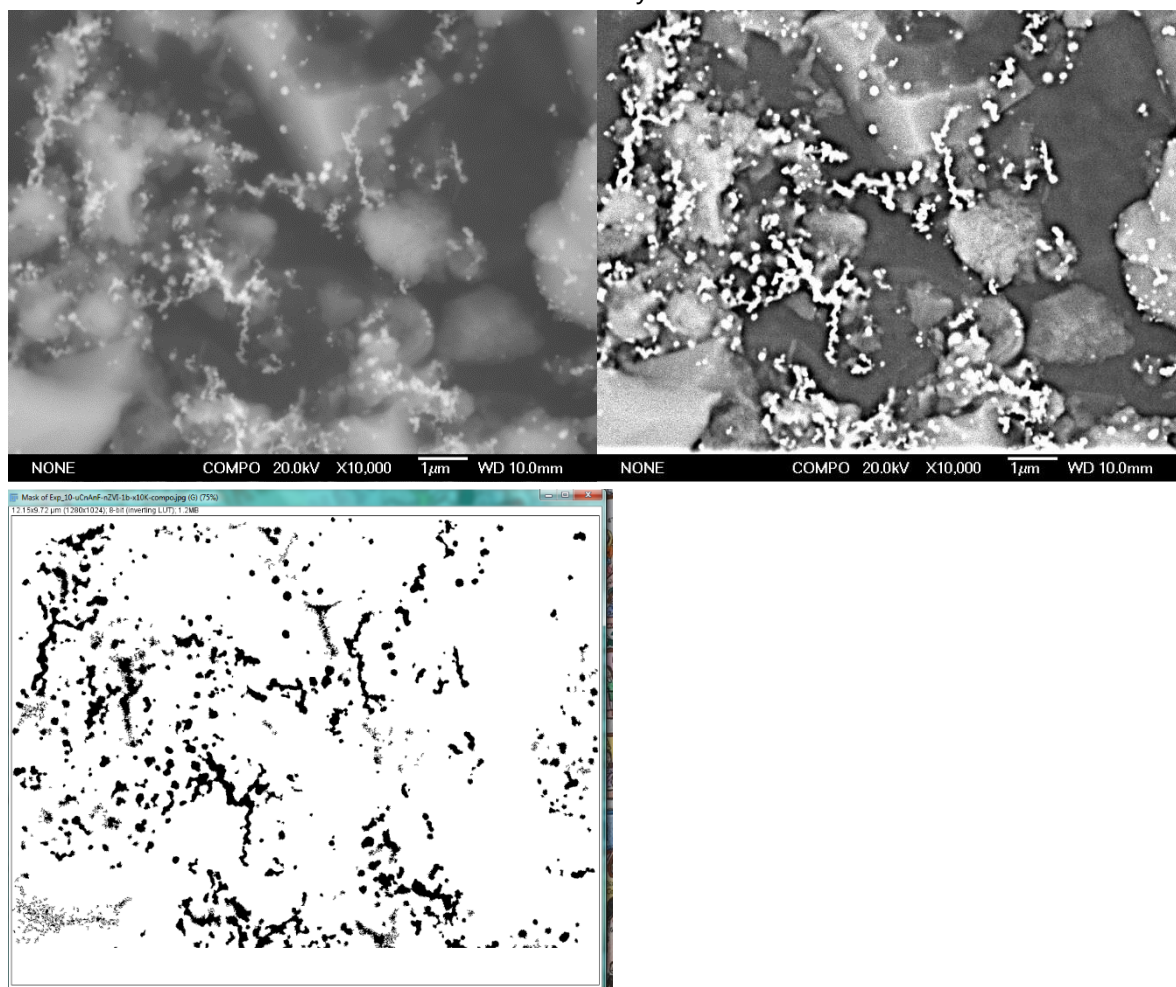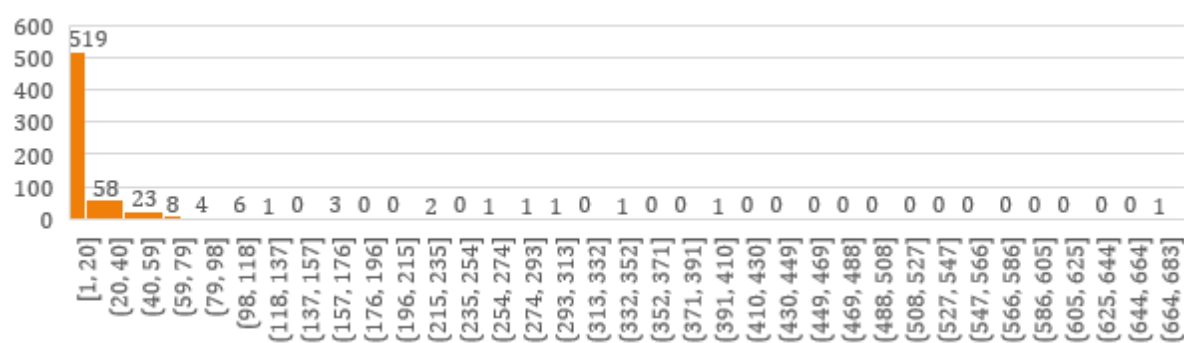
	With outlier	Without outlier (664)
Mean (nm^2)	16622	15593
SD (nm^2)	44856	36714
% of particles under 2000 nm^2	81.3	81.3

2-C600-AF-nZVI 1   *A*=1.80   Entry 13
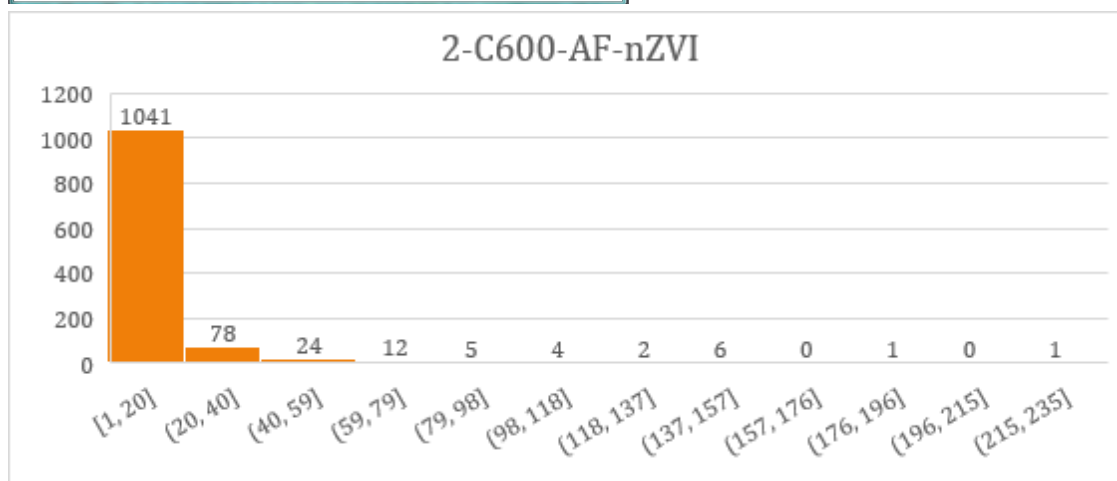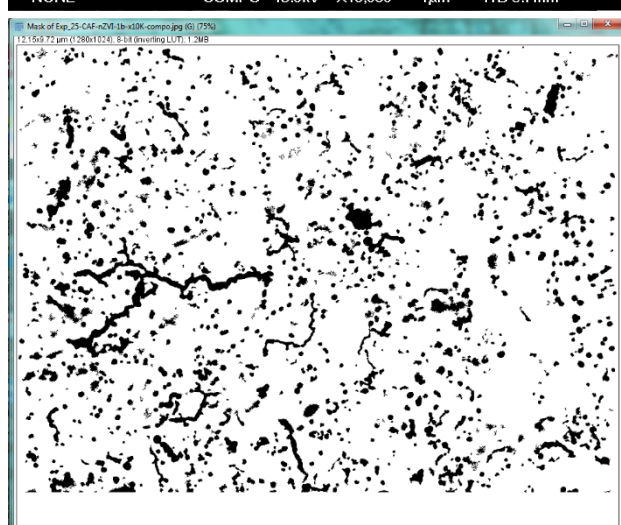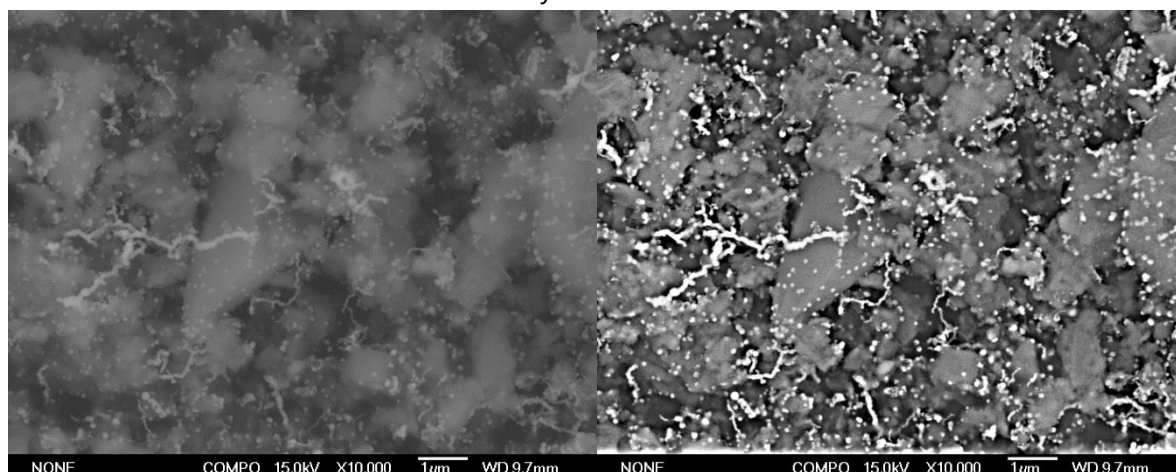
Mean = 10840 nm^2
SD= 18782 nm^2
% < 2000 nm^2 : 88.7%

2-C600-AF-nZVI 2   *A*=0.96   Entry 14
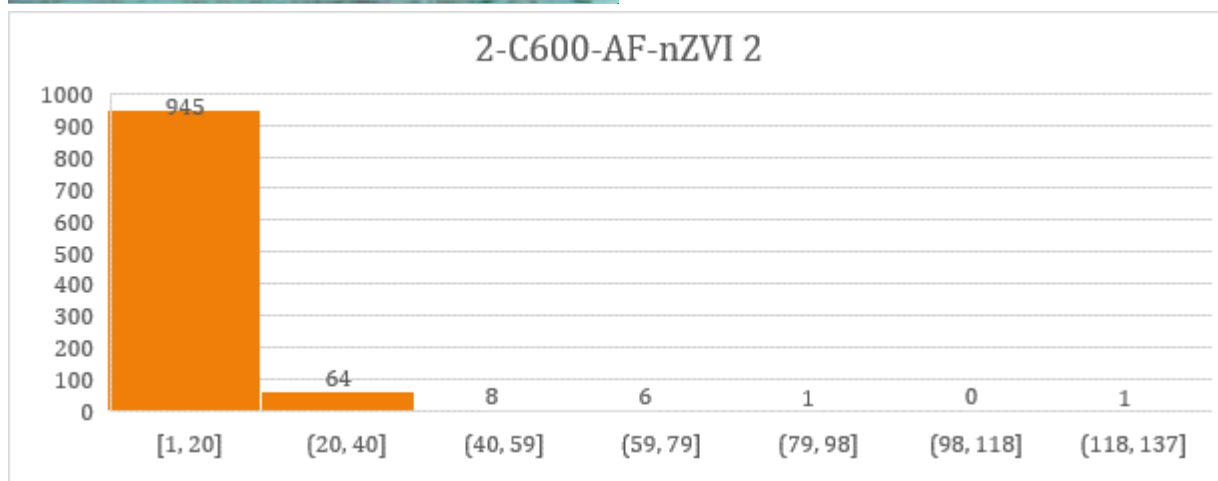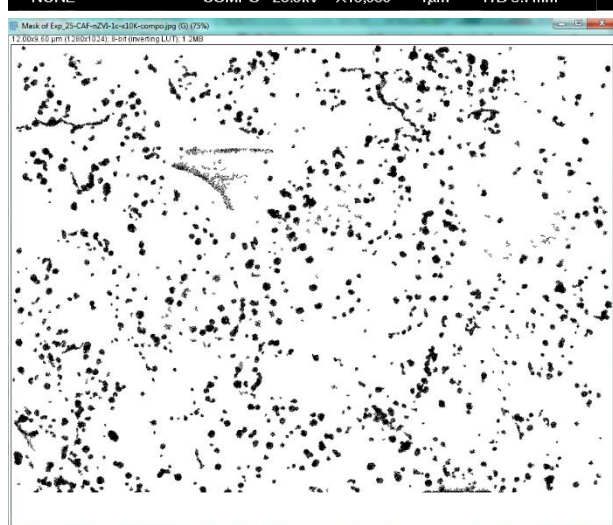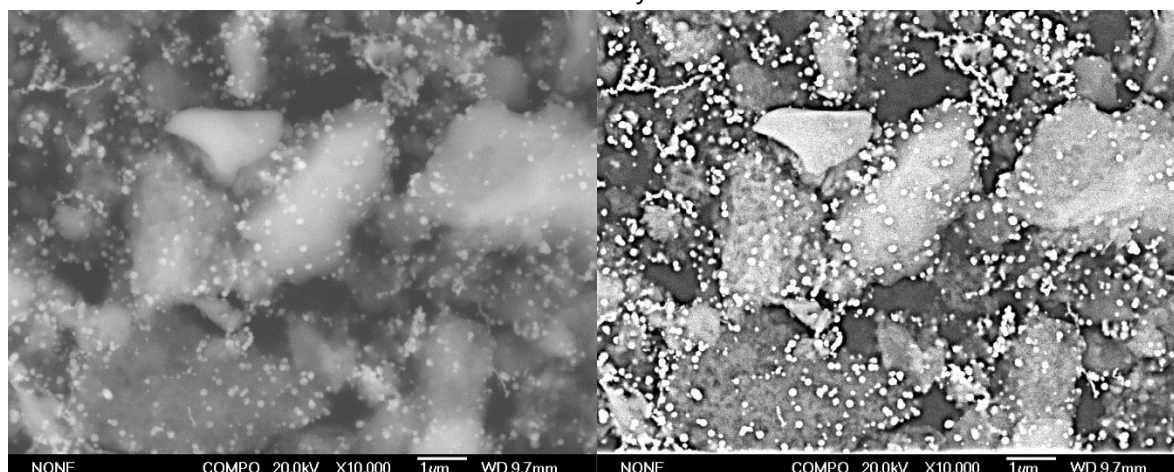
Mean = 8401 nm^2
SD= 10109 nm^2
% <2000 nm^2 : 92.2%

2-C600-AnF-nZVI 1   *A*=0.99   Entry 15
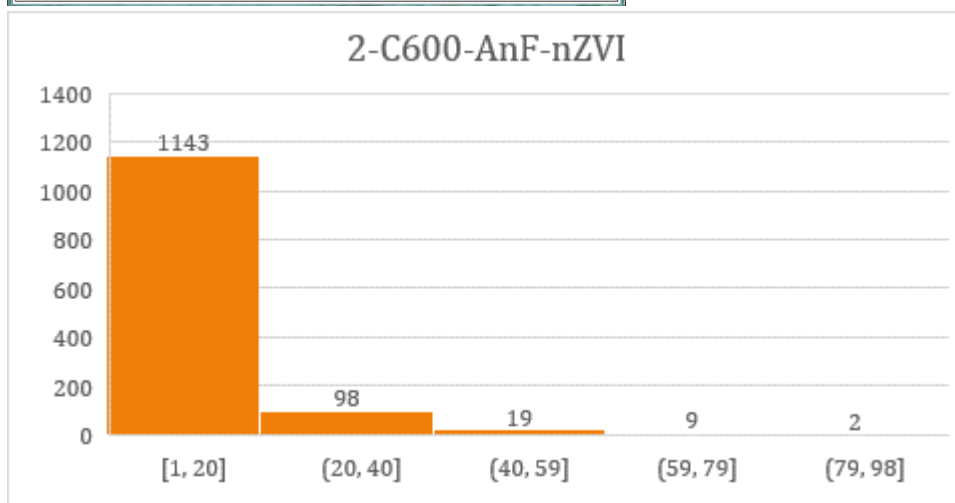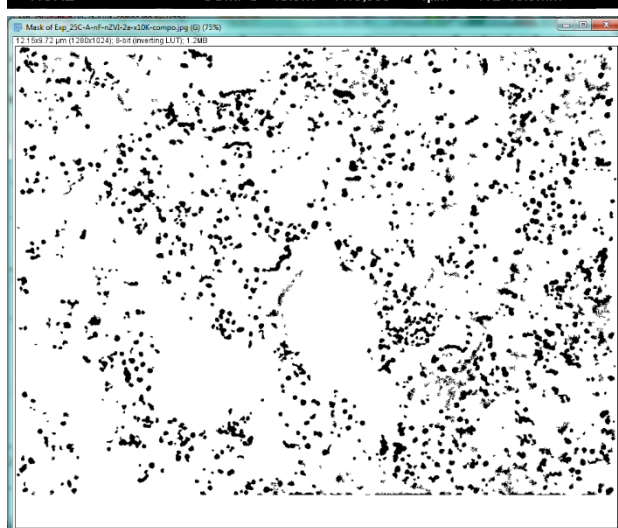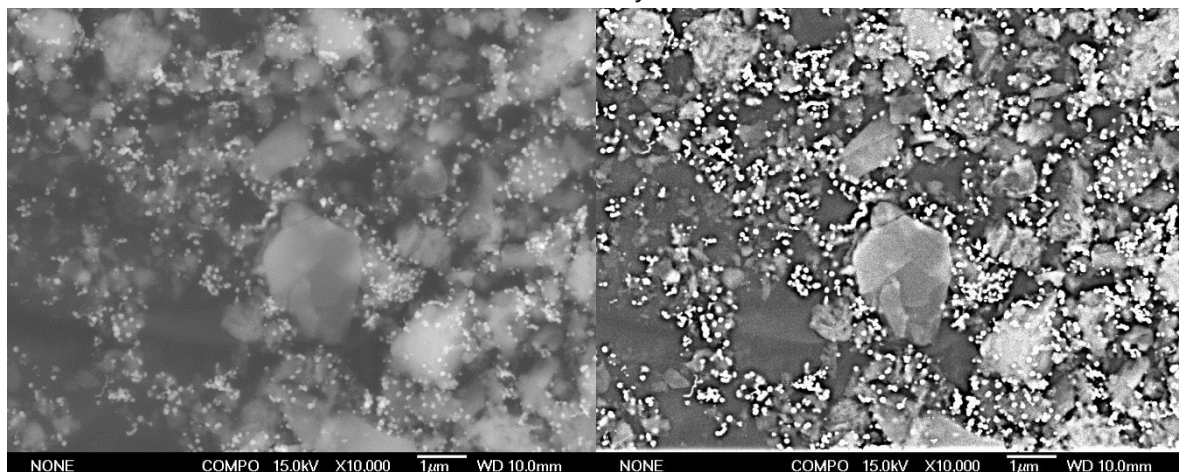
Mean = 8946 nm^2
SD= 10552 nm^2
% <2000 nm^2 : 90.0%

2-C600-AnF-nZVI 2   *A*=0.62   Entry 16
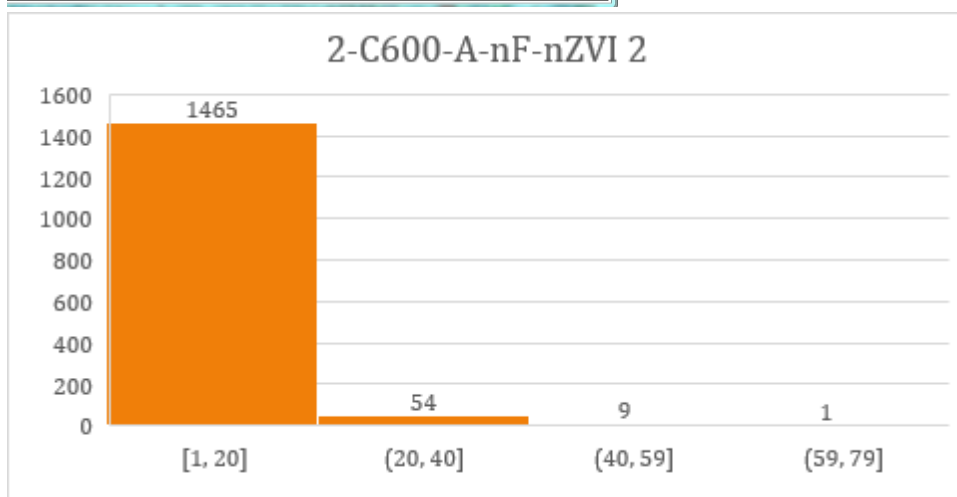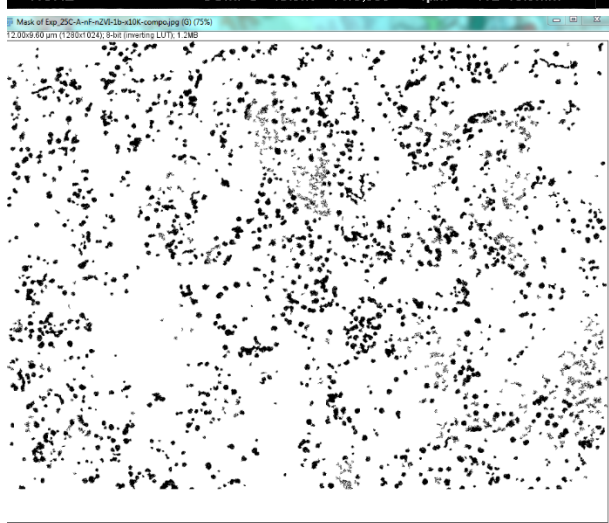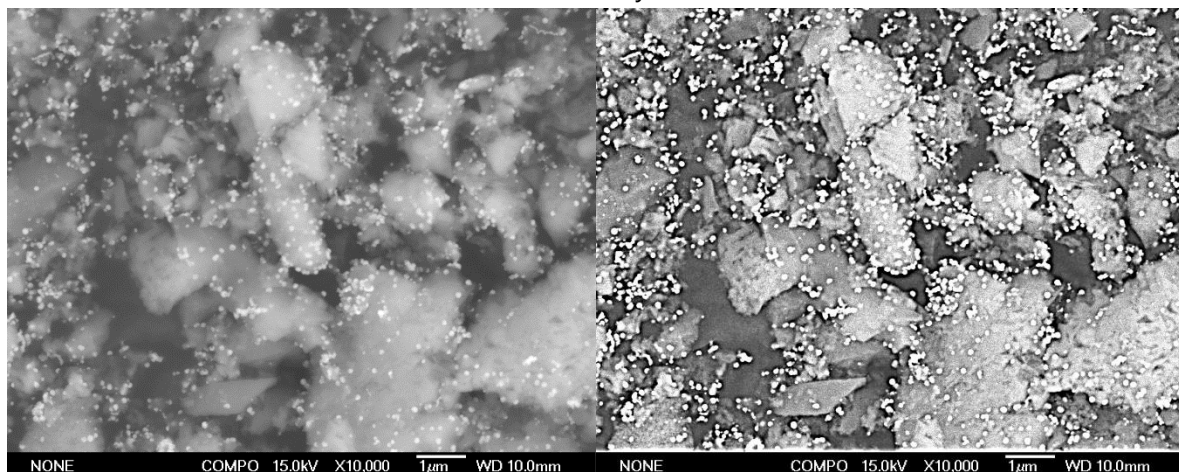
Mean = 6430 nm^2

SD= 6819 nm^2

% <2000 nm^2 : 95.8%

2-C600-nAF-nZVI   *A*=2.50   Entry 17
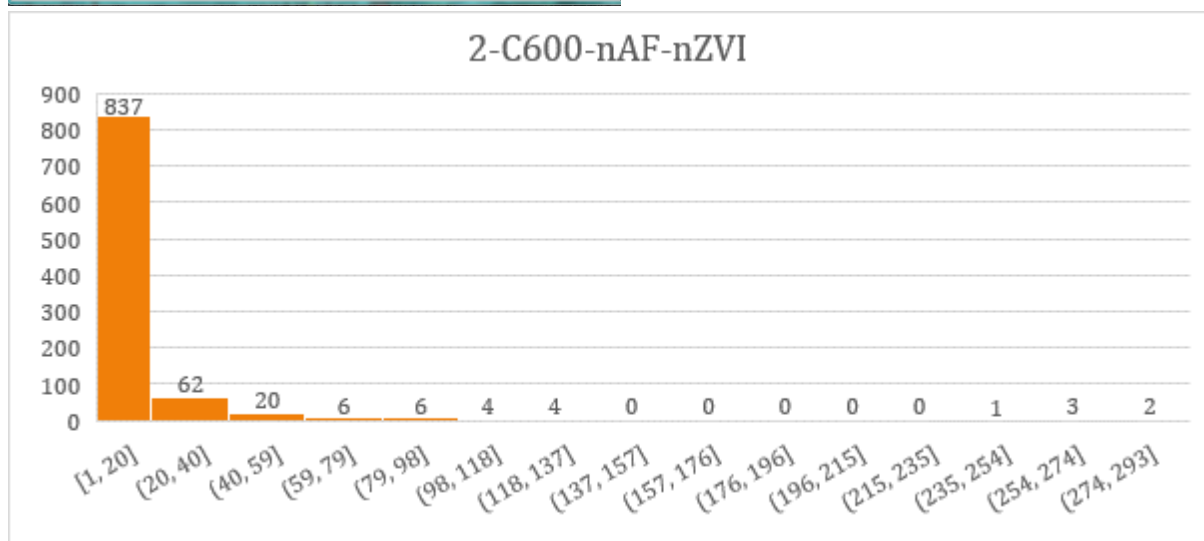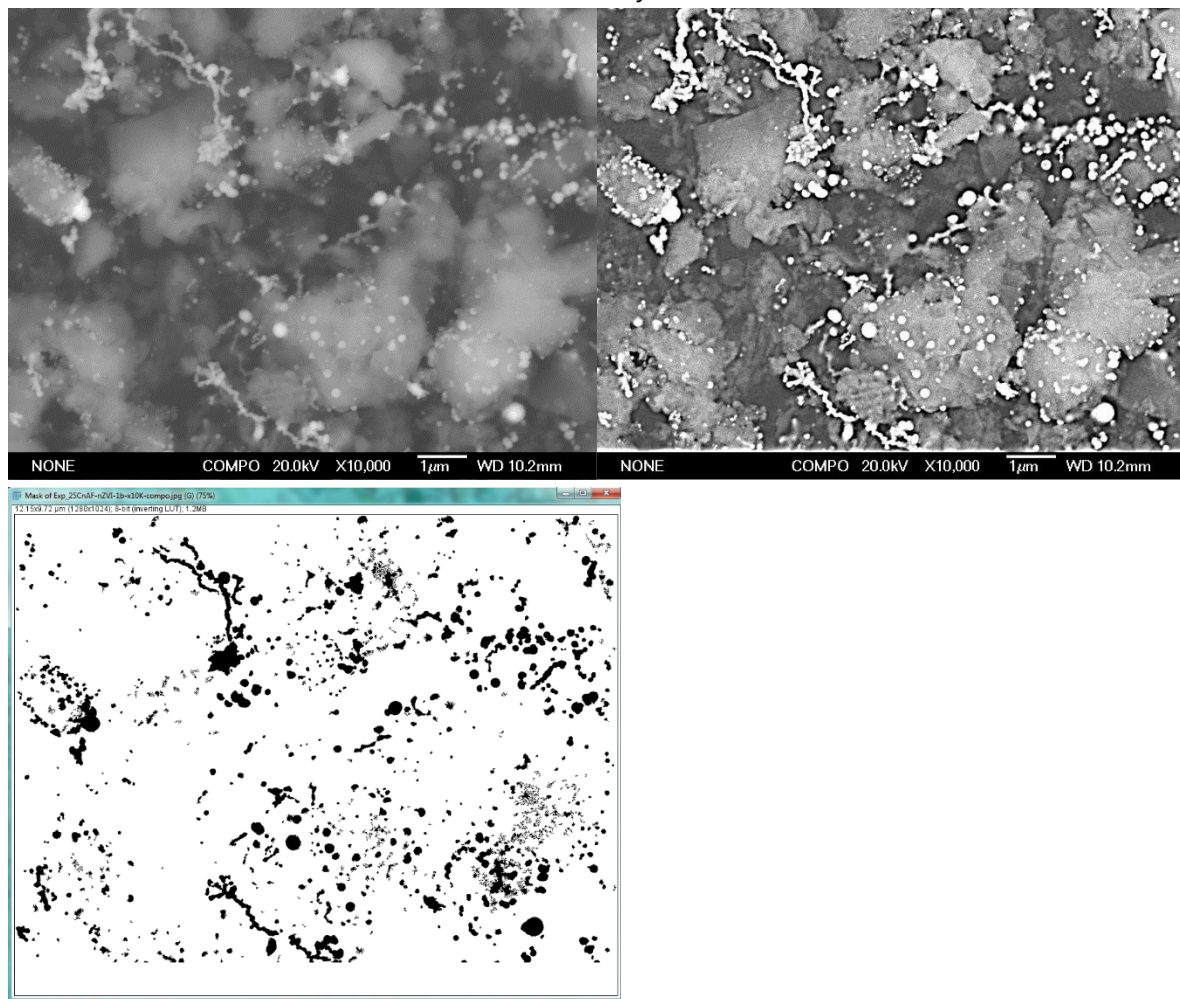
Mean = 10605 nm^2

SD= 25819 nm^2

% <2000 nm^2 : 88.6%

201

2-C600-nAF-nZVI 2   *A*= 0.55   Entry 18

Mean = 5650 μm^2
SD= 5633 μm^2
% <2000 nm^2 : 98.6%

2-C600-nAnF-nZVI 1   *A*=0.83   Entry 19

2-C600-nAnF-nZVI

Mean = 7215 nm^2
SD= 8976 nm^2
% <2000 nm^2 : 94.8 %

2-C600-nAnF-nZVI 2   *A*=3.39   Entry 20
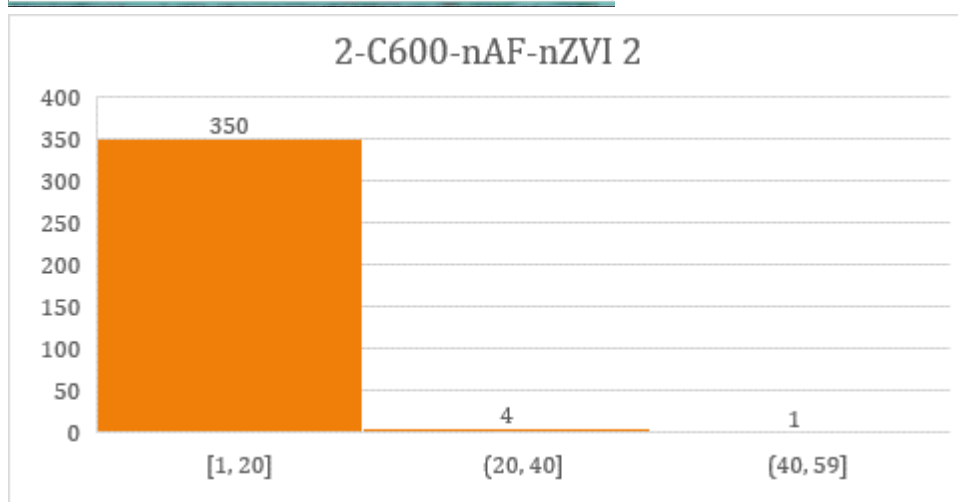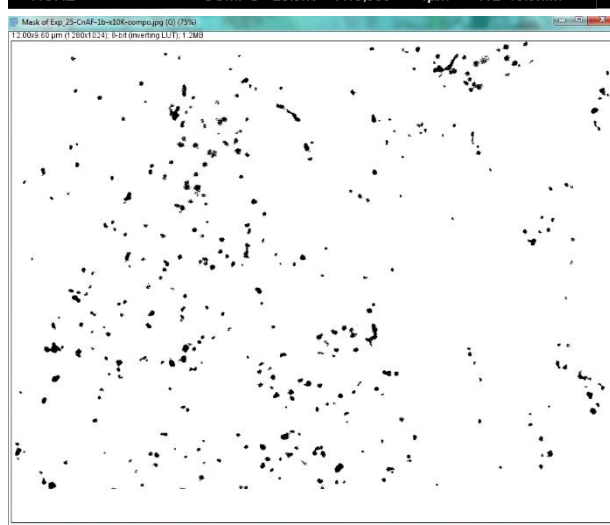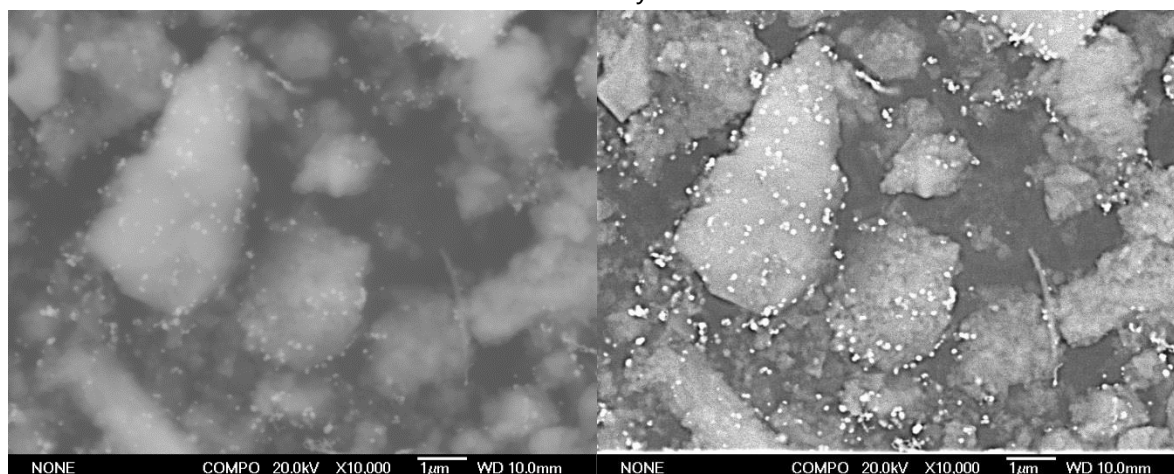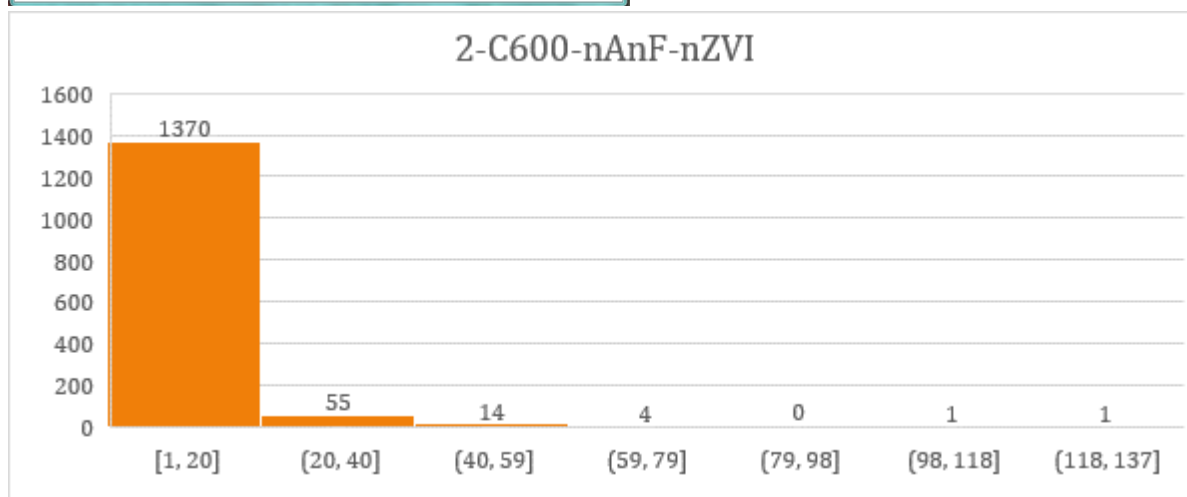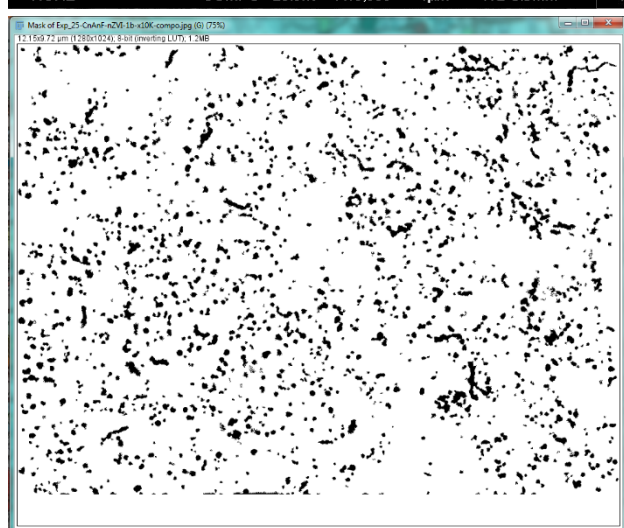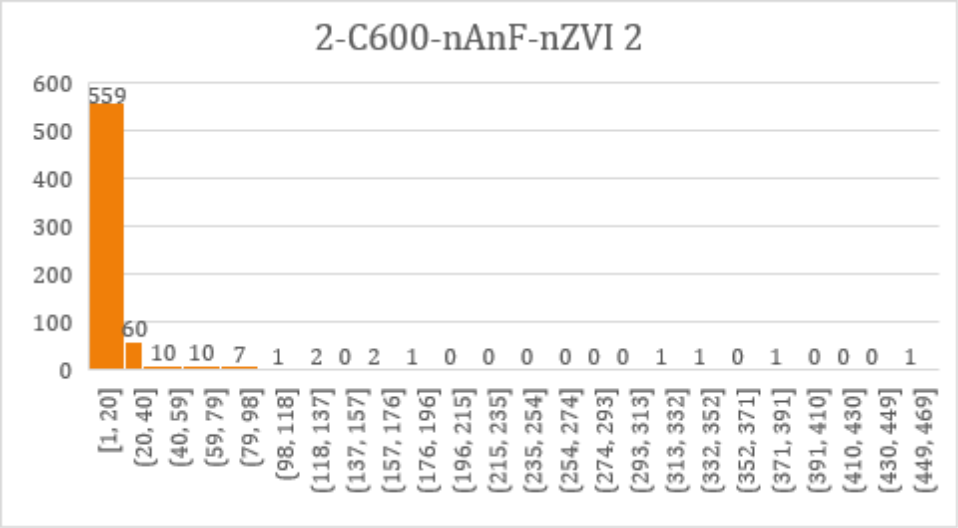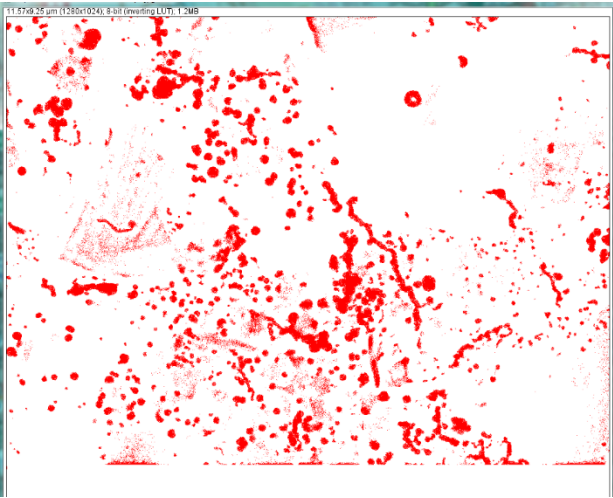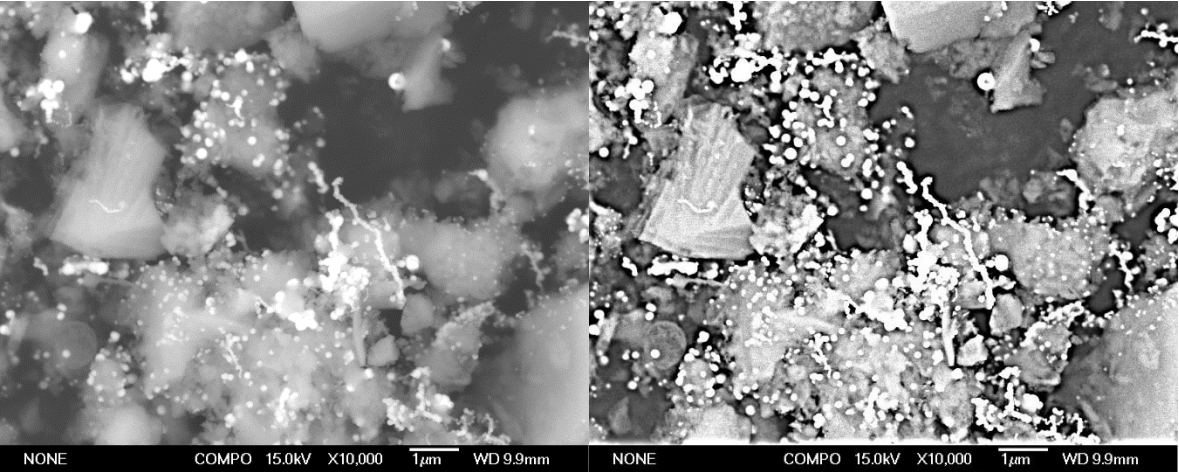
Mean = 13620 nm^2
SD= 34855 nm^2
% <2000 nm^2 : 85.2%

2-uC-AF-nZVI 1   *A*=0.92   Entry 21
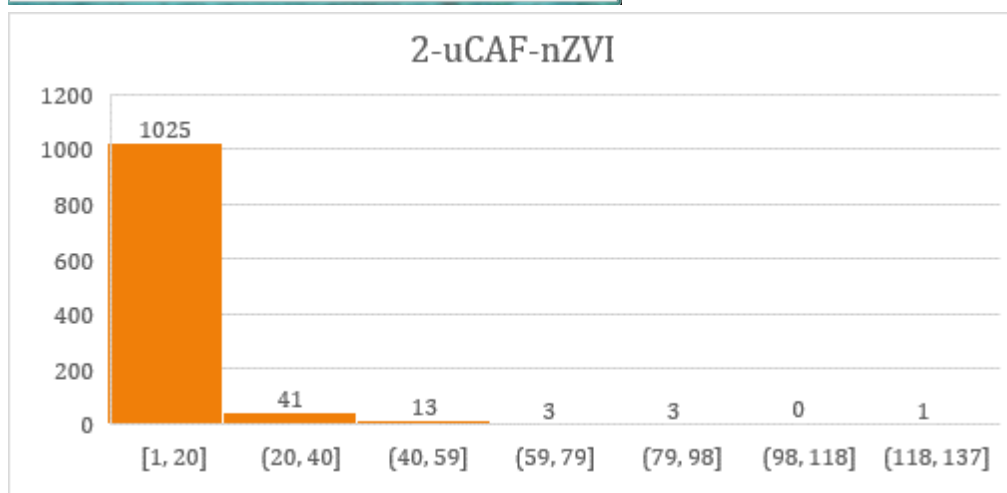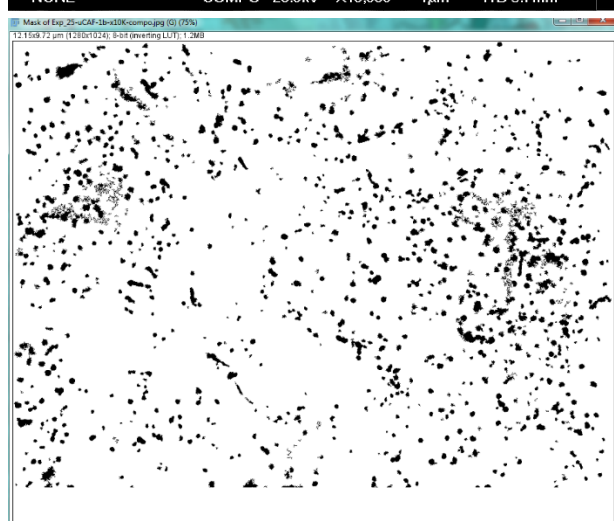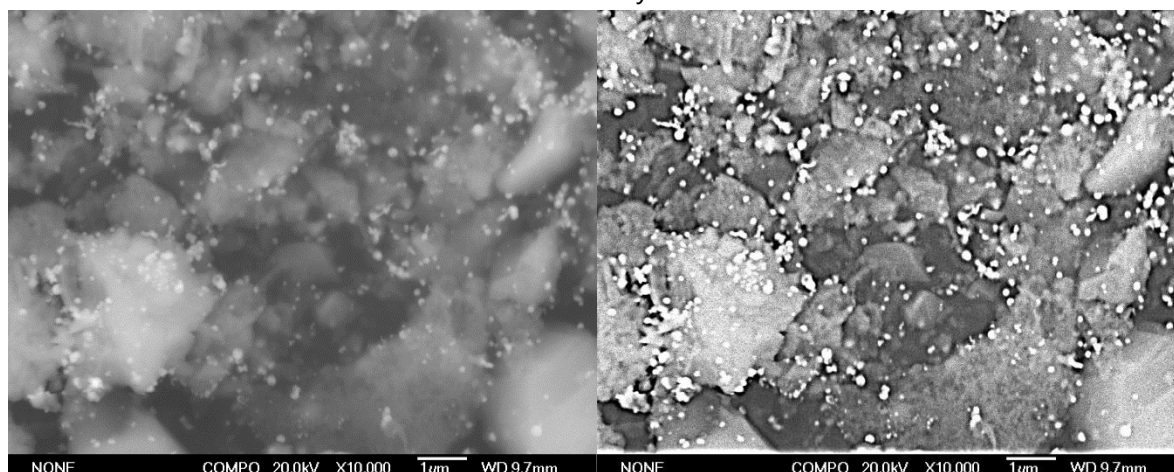
2-uCAF-nZVI

Mean = 7500 nm^2

SD= 9803 nm^2

% <2000 nm^2 : 94.4%

205

2-uC-AF-nZVI 2   *A*=0.60   Entry 22
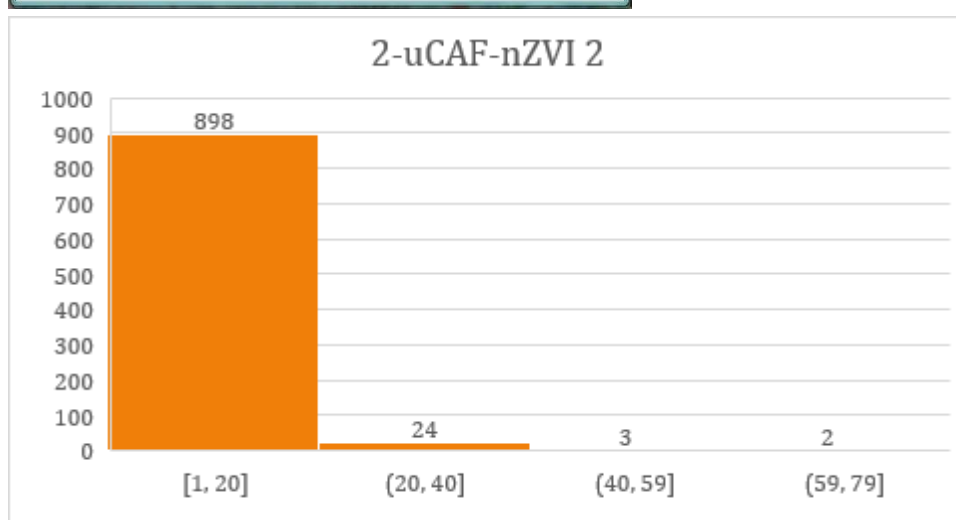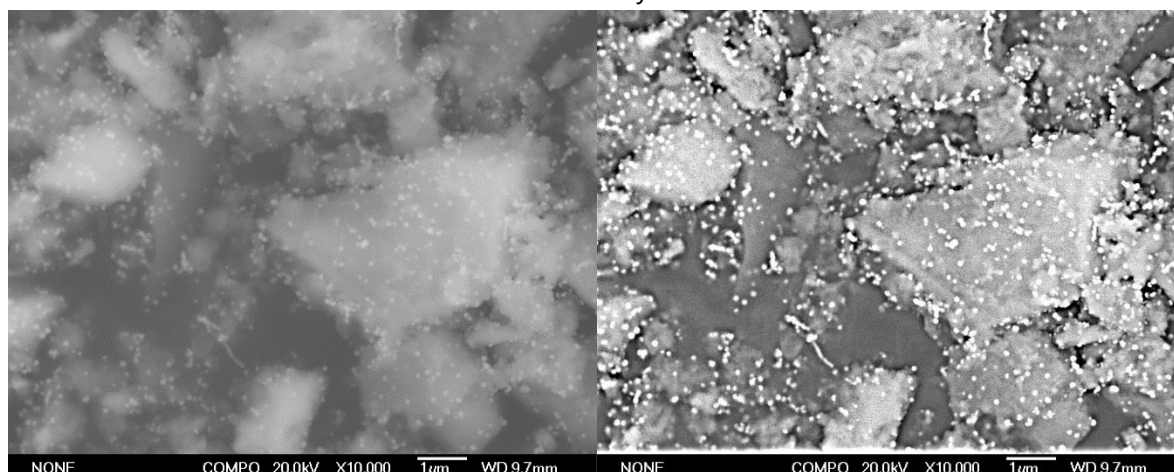
Mean = 6325 nm^2

SD= 6447 nm^2

% <2000 nm^2 : 96.9%

206

2-uC-AnF-nZVI   *A*=1.31   Entry 23
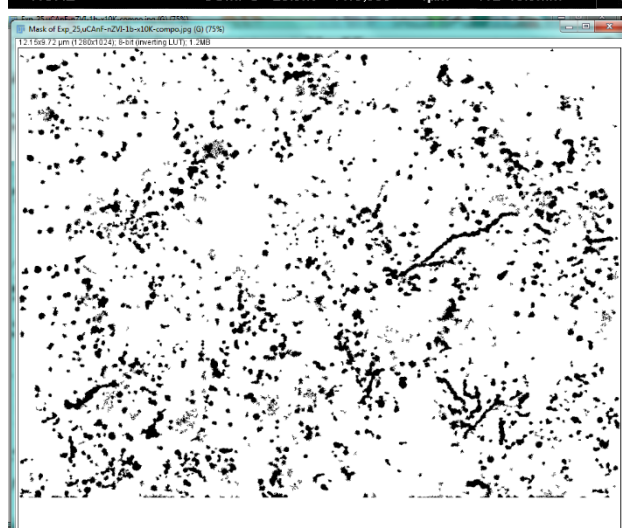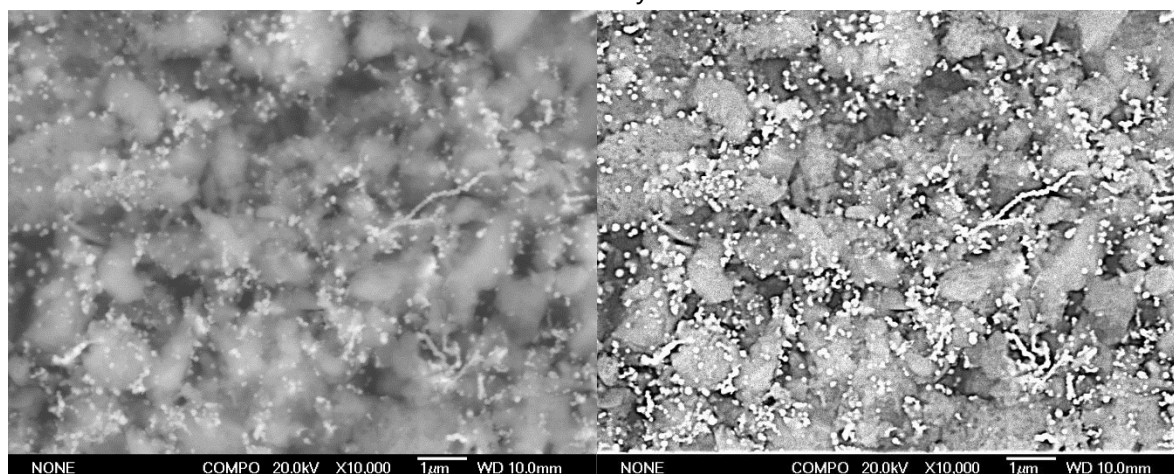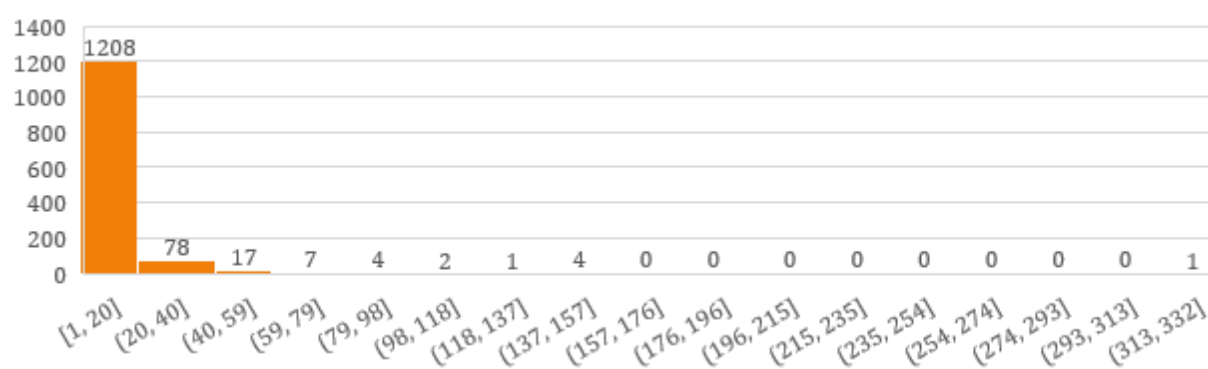
	With outlier	**Without outlier (322)**
Mean (nm^2)	8951	8714
SD (nm^2)	16305	13850
% of particles under 2000 nm^2	91.4	91.4

2-uC-nAF-nZVI 1   *A*=0.73   Entry 24
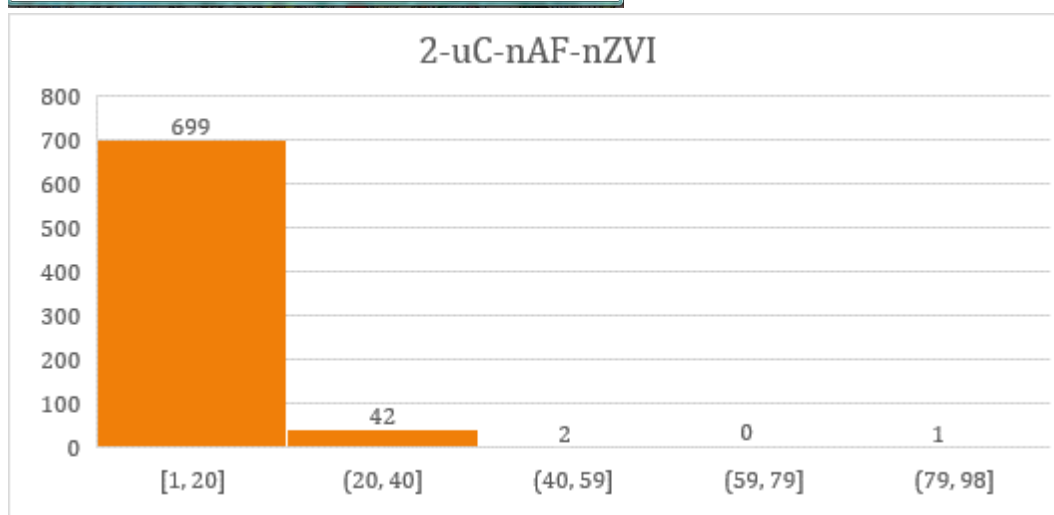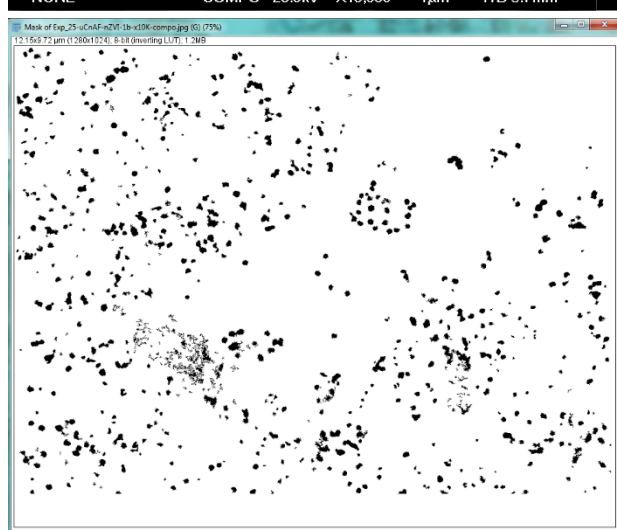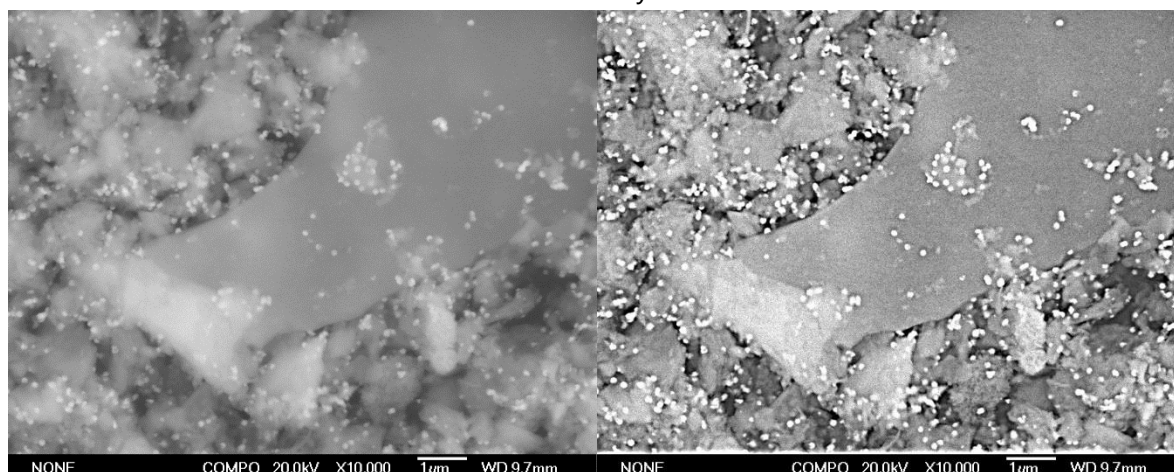
2-uC-nAF-nZVI

Mean = 7250 nm^2

SD= 7646 nm^2

% <2000 nm^2 : 94.0%

2-uC-nAF-nZVI 2   *A*=0.76   Entry 25
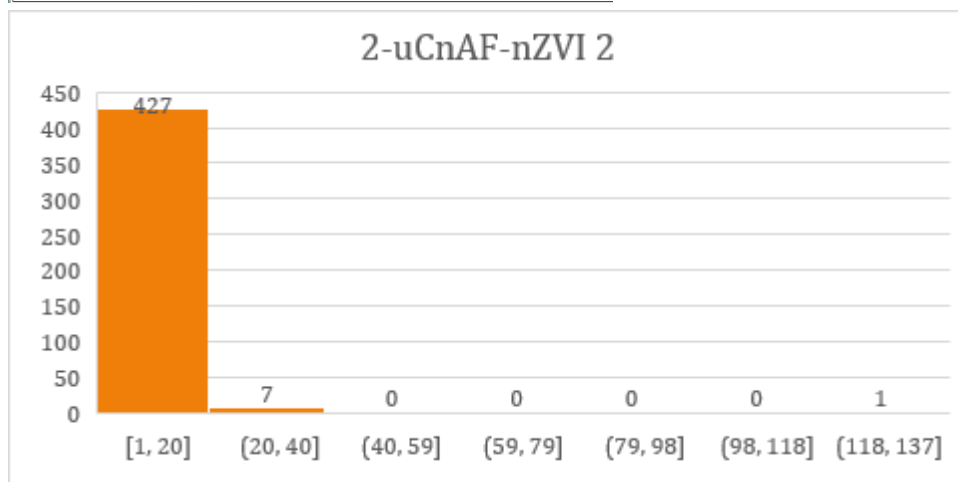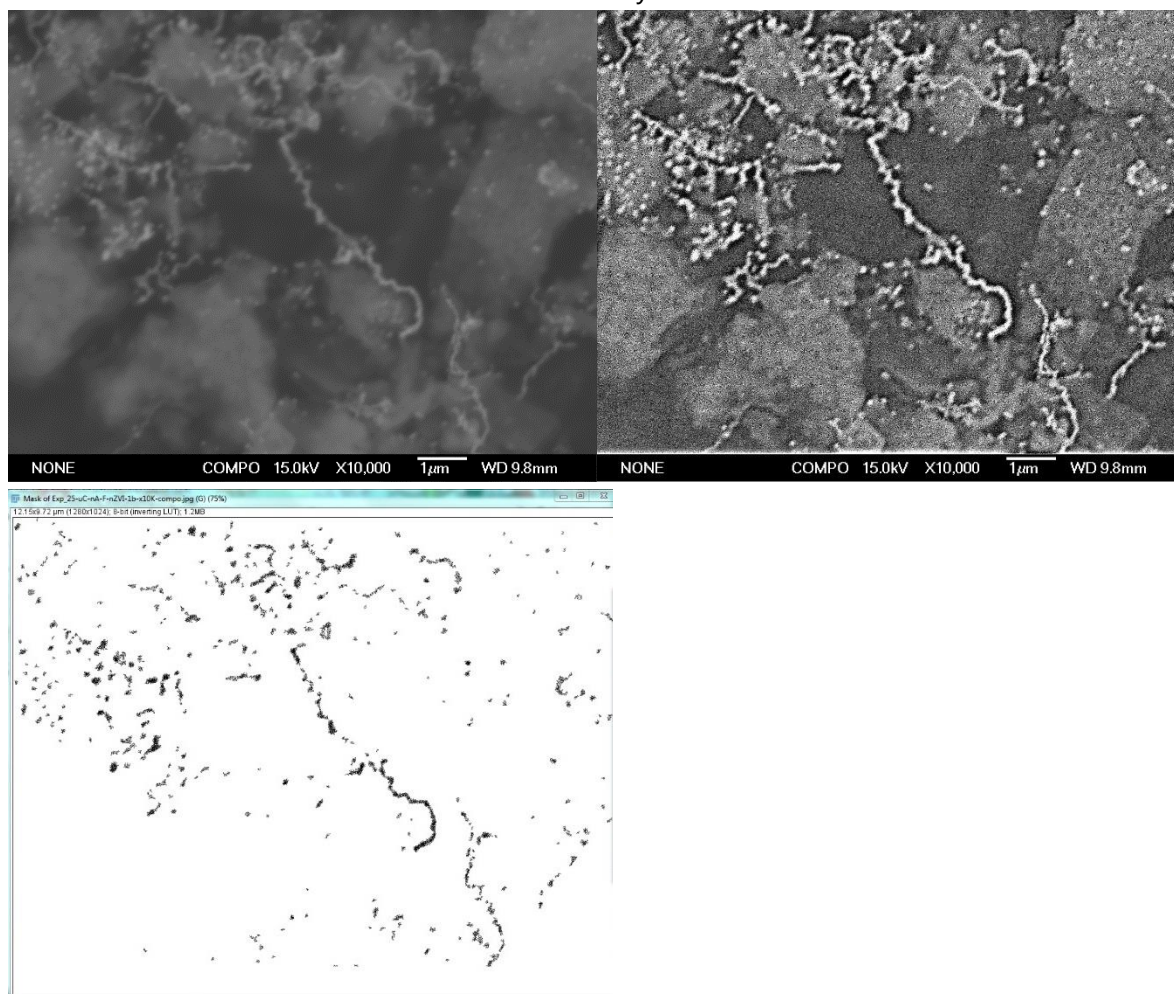
Mean = 4704 nm^2

SD= 7869 nm^2

% <2000 nm^2 : 98.2%

209

2-uC-nAF-nZVI 3   *A*= 0.54   Entry 26
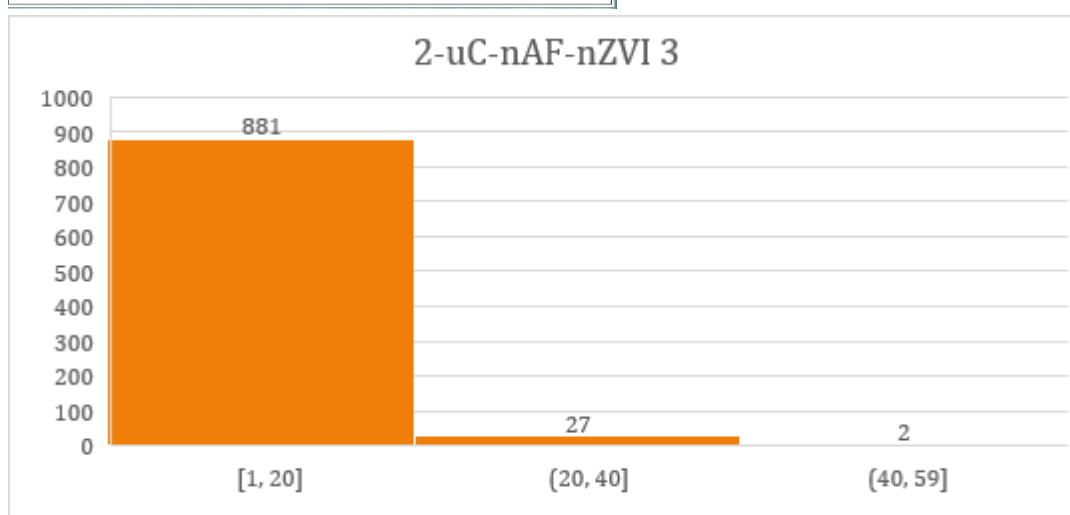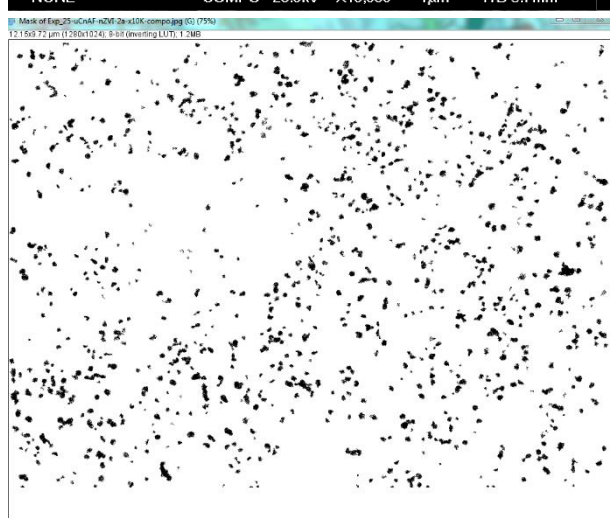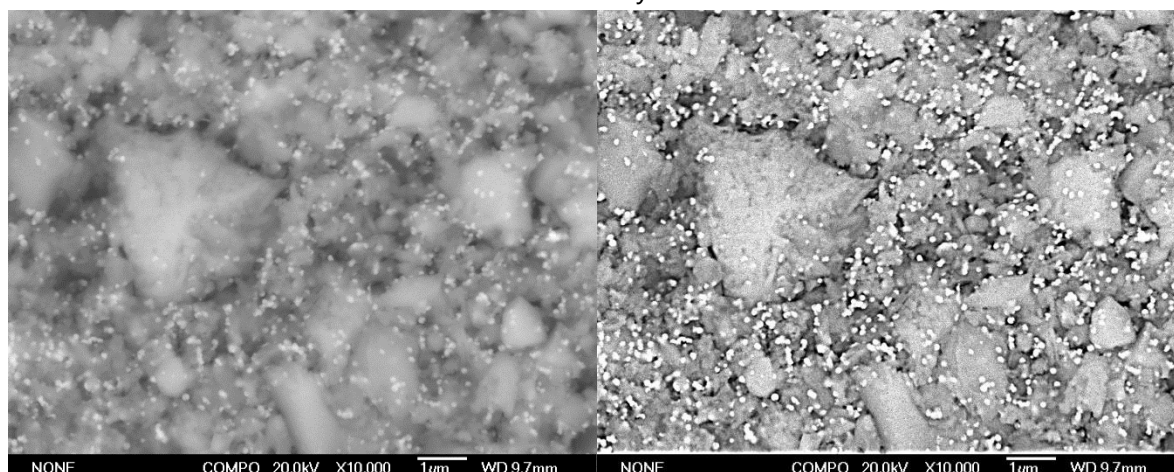
Mean = 6481 nm^2
SD= 5793 nm^2
% <2000 nm^2 : 96.8%

2-uC-nAnF-nZVI   *A*=1.18   Entry 27
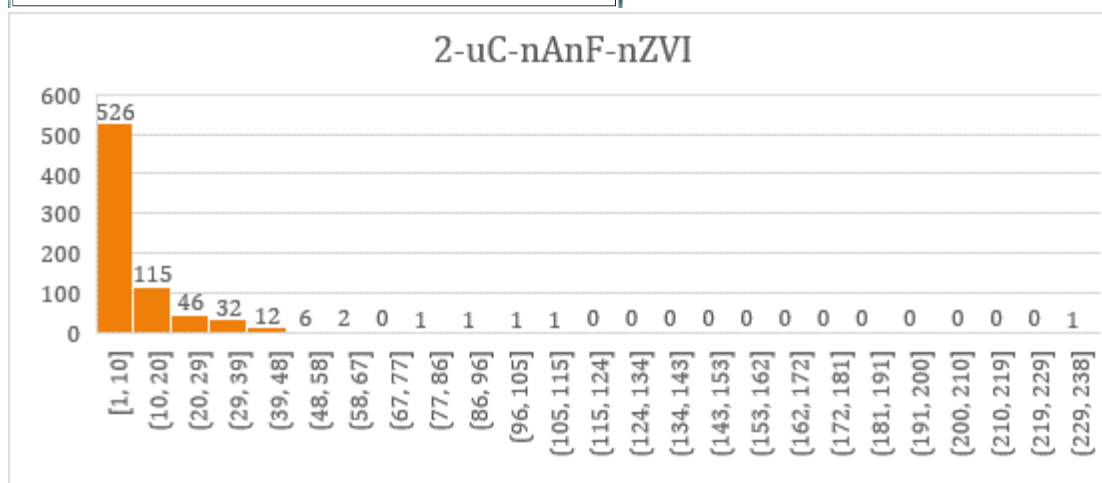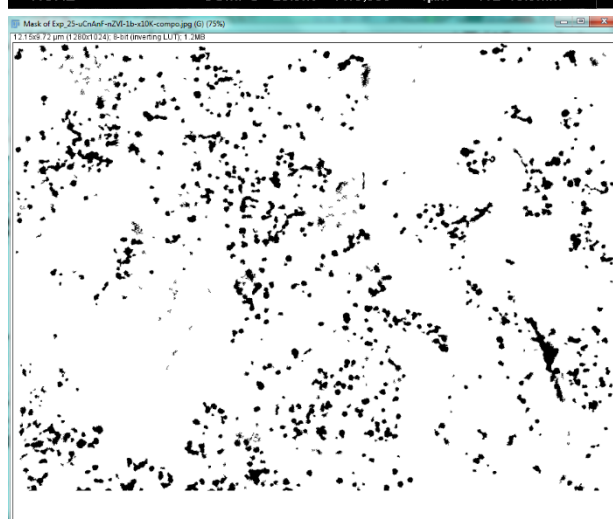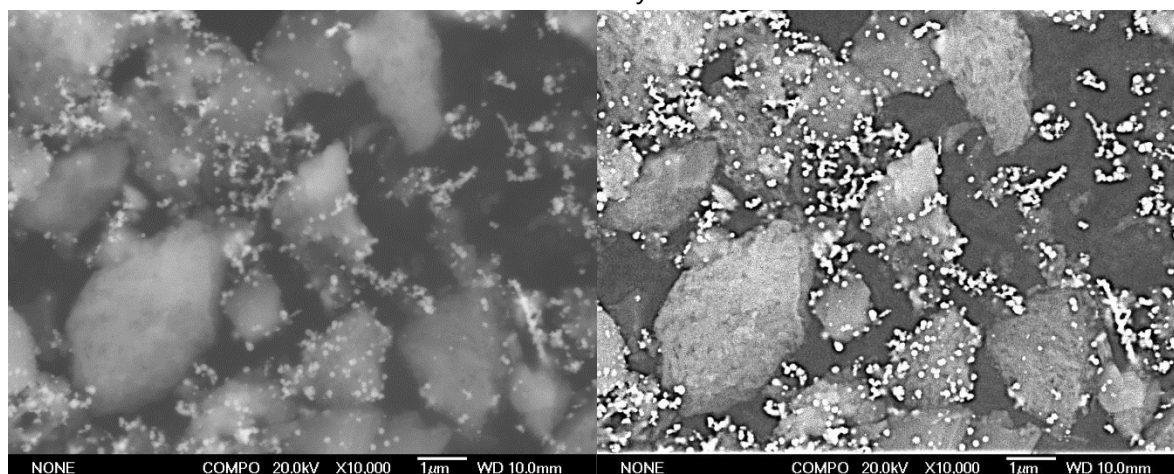
	With outlier	Without outlier (230)
Mean (nm^2)	10385	10090
SD (nm^2)	14653	12248
% of particles under 2000 nm^2	70.7	70.7

5-C600-AF-nZVI 1   *A*=0.52   Entry 28
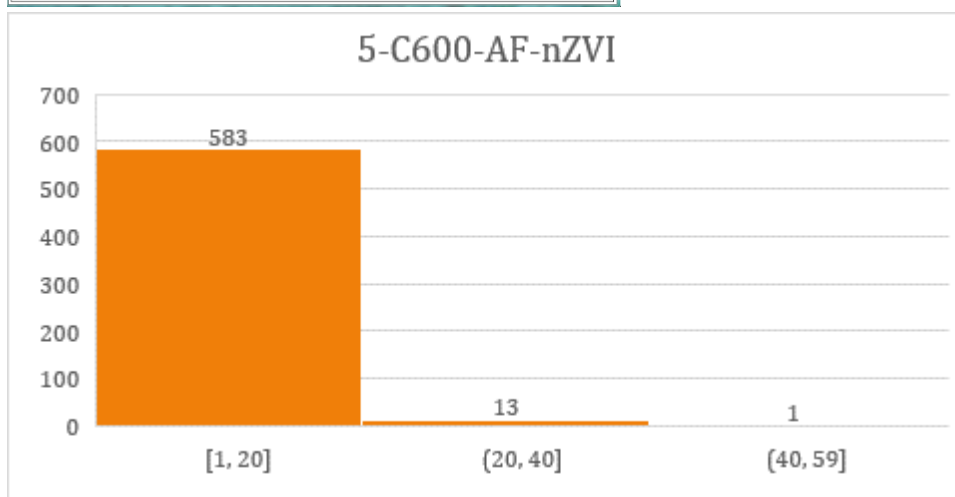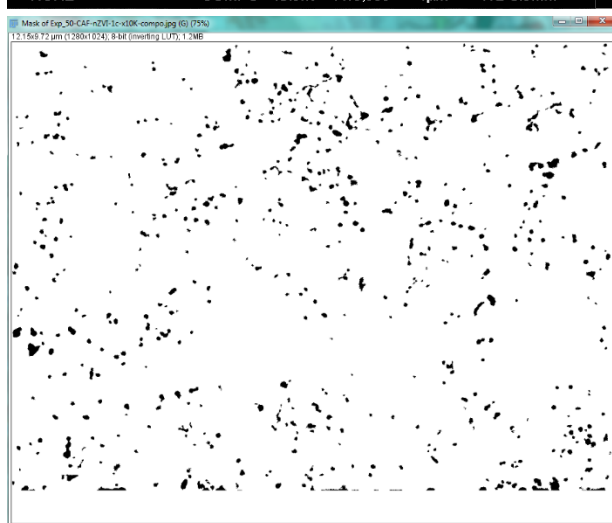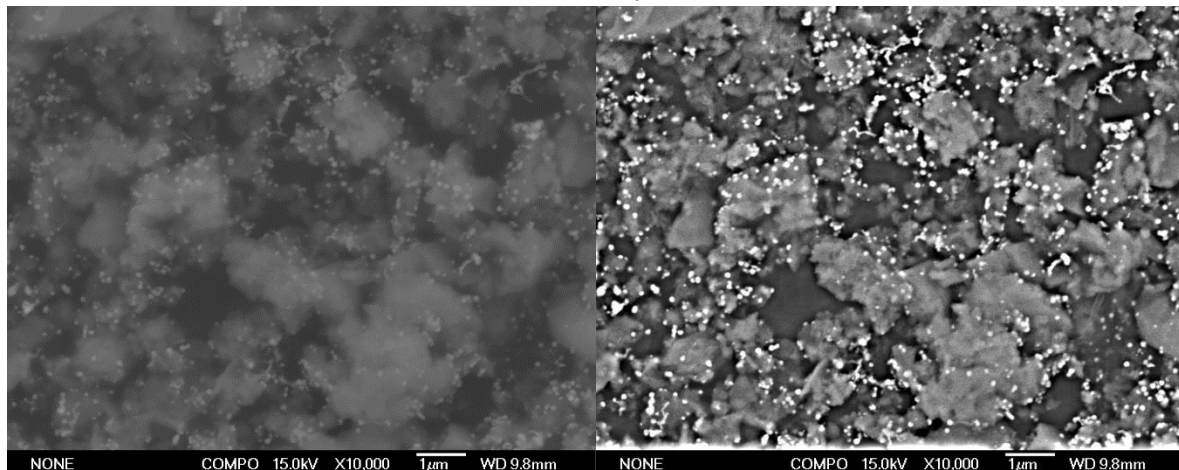
Mean = 5630 nm^2
SD= 5457nm^2
% <2000 nm^2 : 97.7%

5-C600-AF-nZVI 2   *A*=1.37   Entry 29
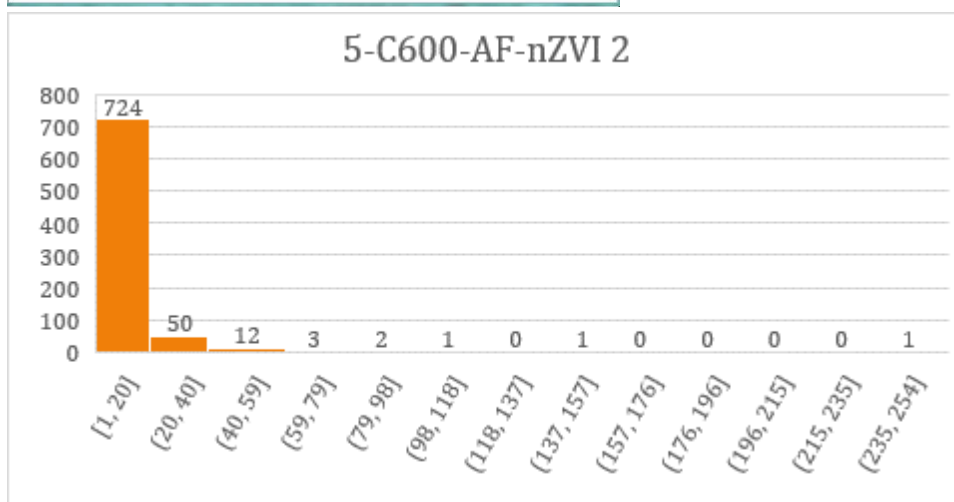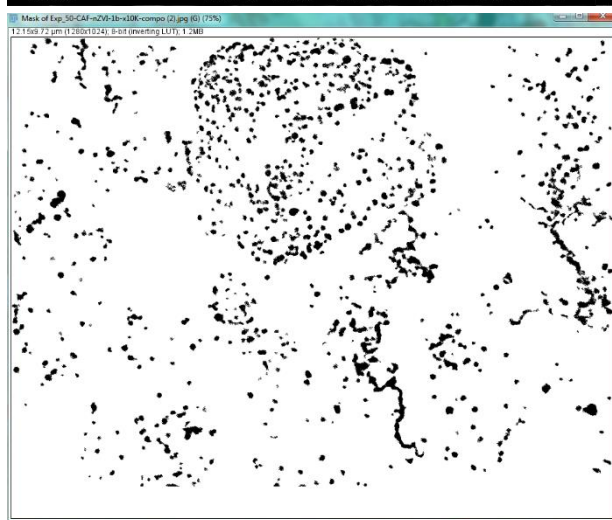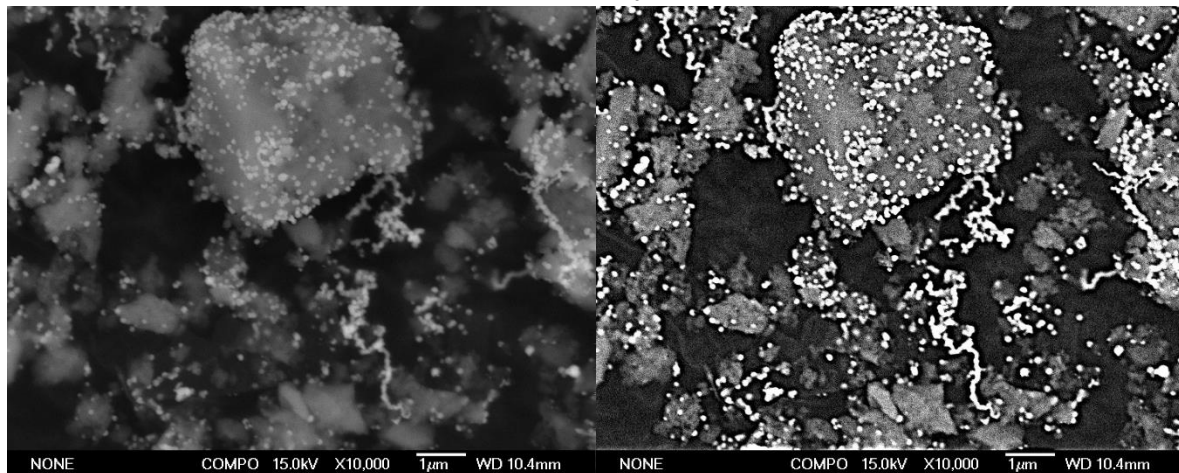
5-C600-AF-nZVI 2

Mean = 9434 nm^2
SD= 14196 nm^2
% <2000 nm^2 : 91.2%

213

5-C600-AF-nZVI 3   *d*=2.40   Entry 30
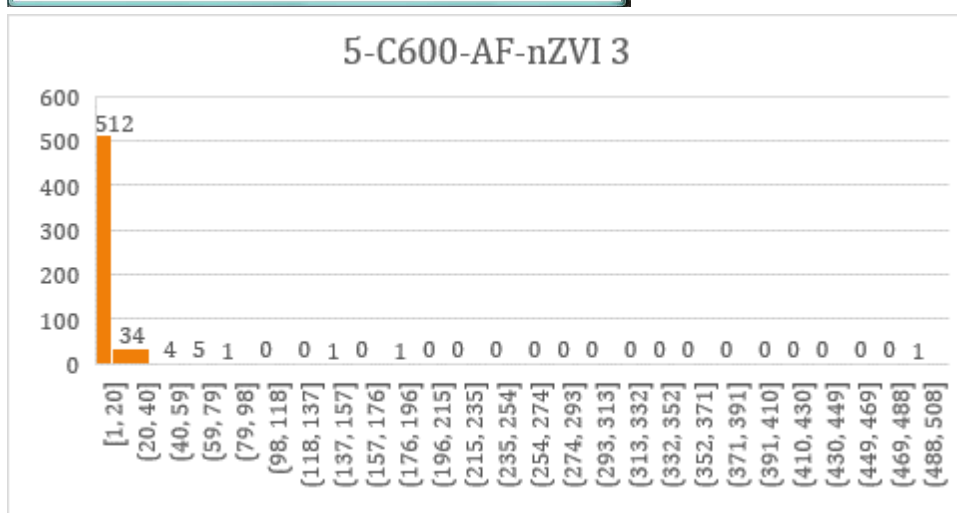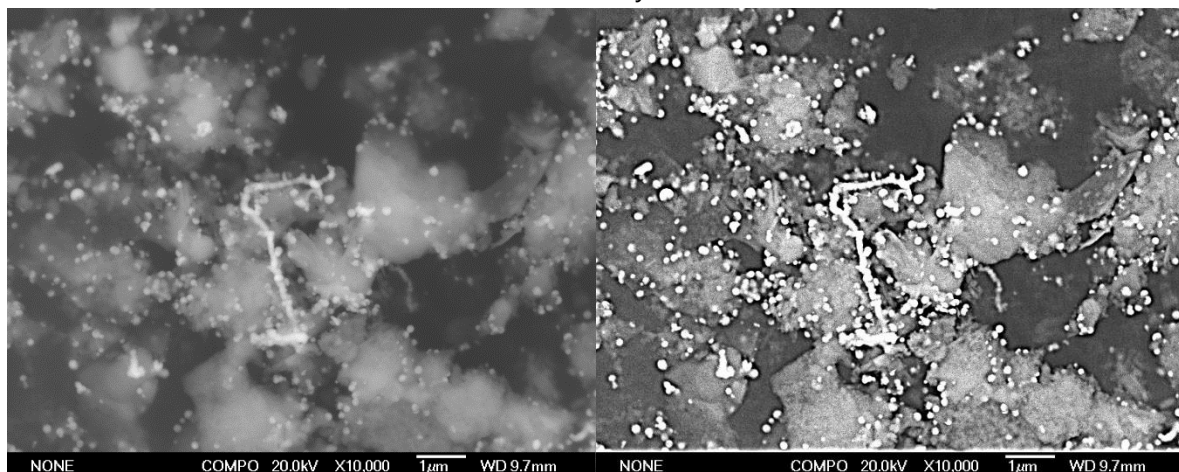
Mean = 10551 nm^2

SD= 24693 nm^2

% < 2000 nm^2 : 91.6%

214

5-C600-AF-nZVI-4   *A*=0.71   Entry 31

5-C600-AF-nZVI-4

	[1, 20]	(20, 40]	(40, 59]	(59, 79]	(79, 98]	(98, 118]
	569	17	2	0	0	1
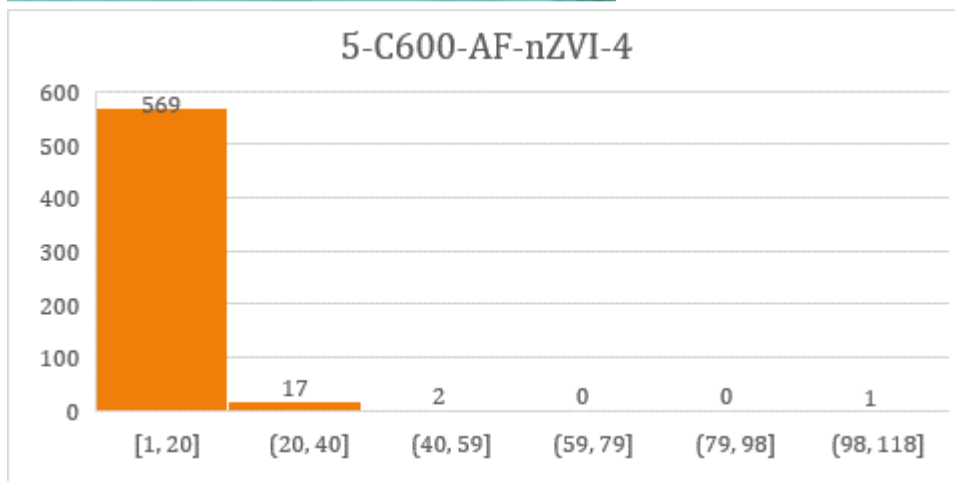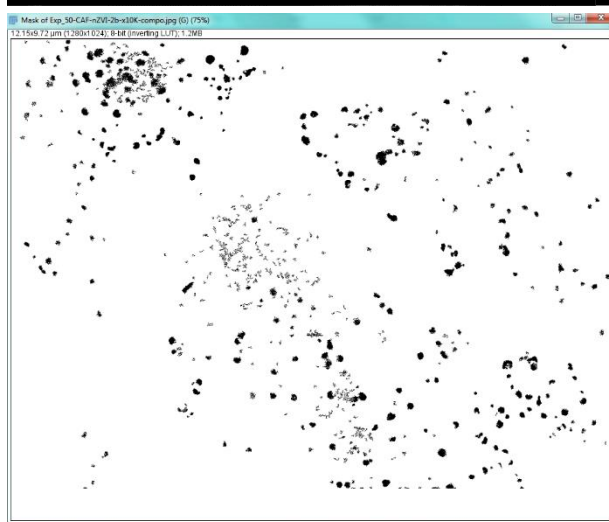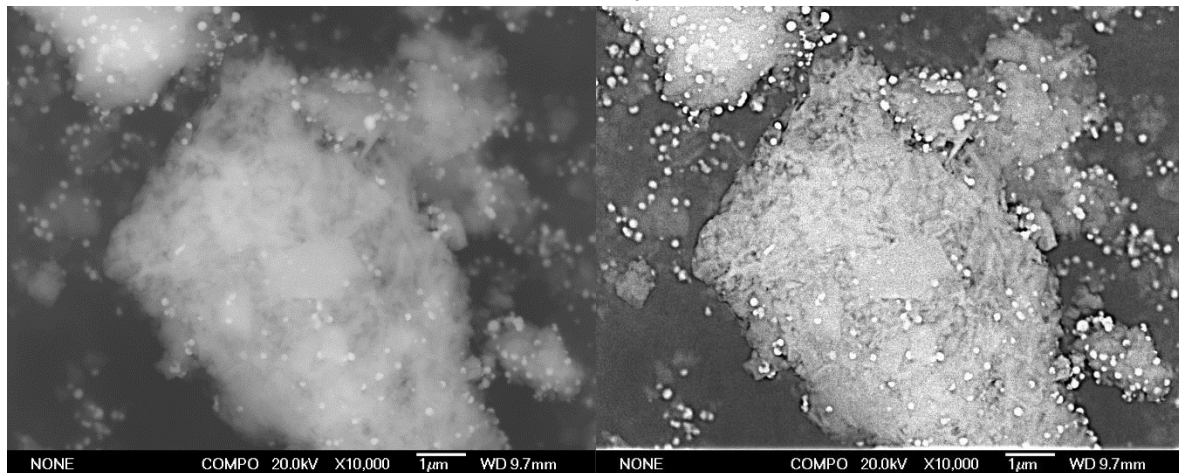
Mean = 5262 nm^2

SD= 7458 nm^2

% < 2000 nm^2 : 96.6%

5-C600-AnF-nZVI   *A*=0.84   Entry 32

5-C600-AnF-nZVI

	[1, 20]	[20, 40]	[40, 59]	[59, 79]	[79, 98]	[98, 118]	[118, 137]
Count	1284	36	12	4	0	1	2
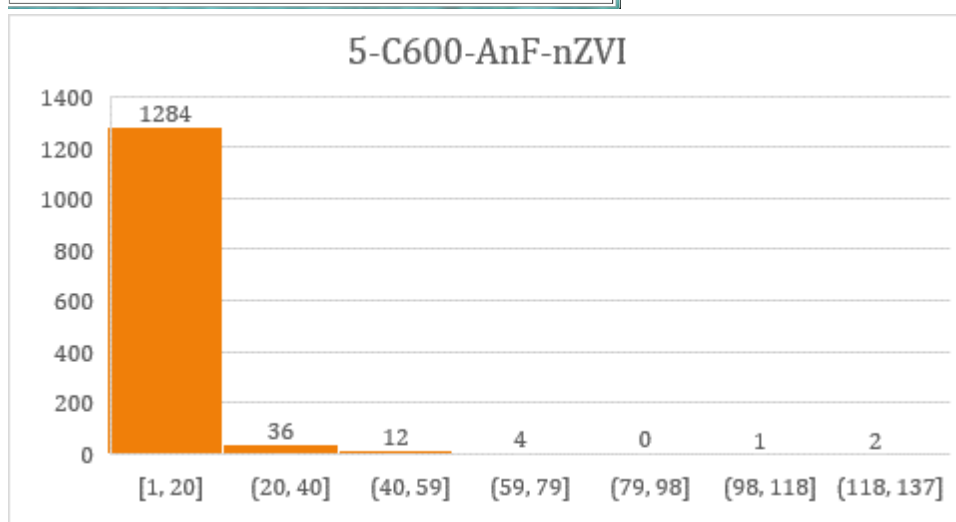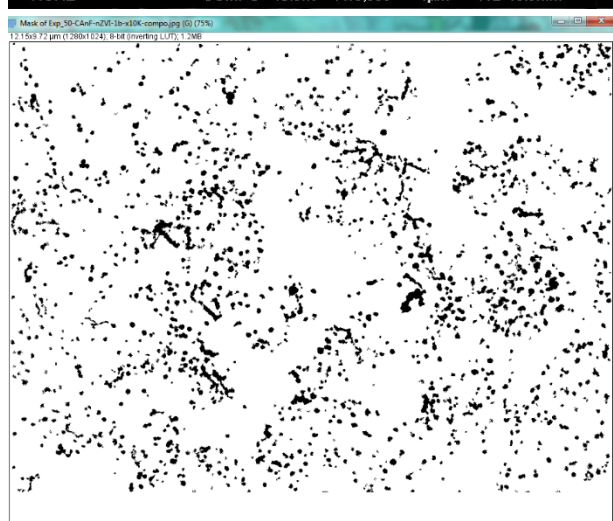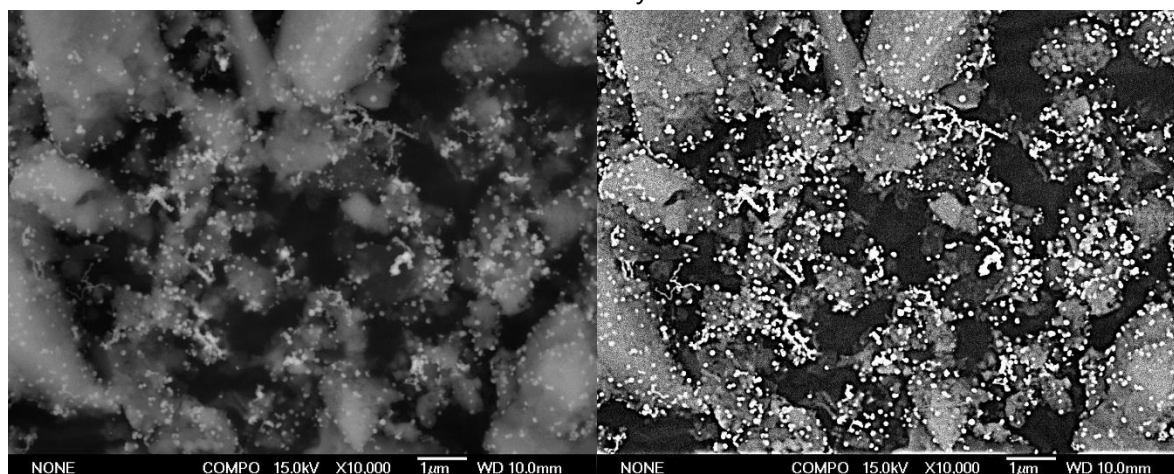
Mean = 6798 nm^2
SD= 9088 nm^2
% <2000 nm^2 : 95.9%

5-C600-AnF-nZVI 2   *A*=1.11   Entry 33
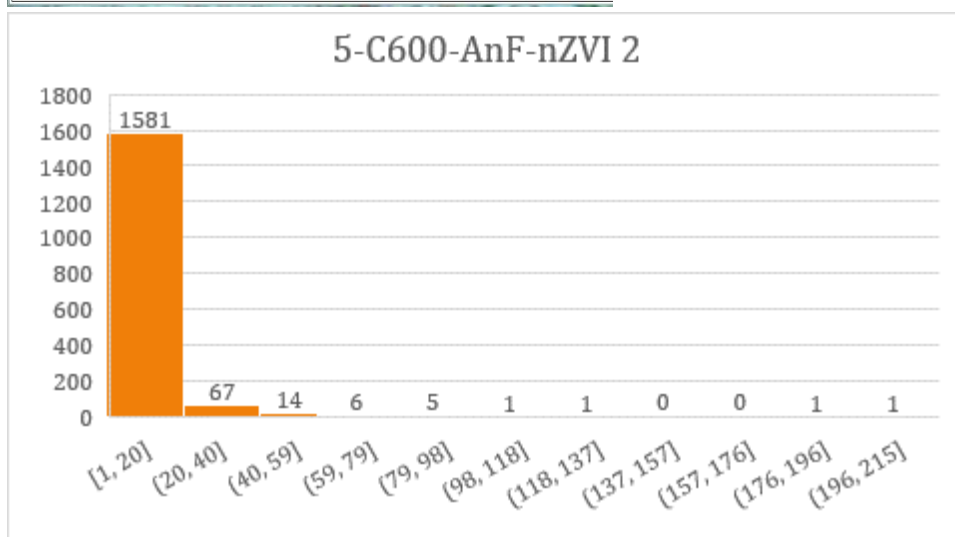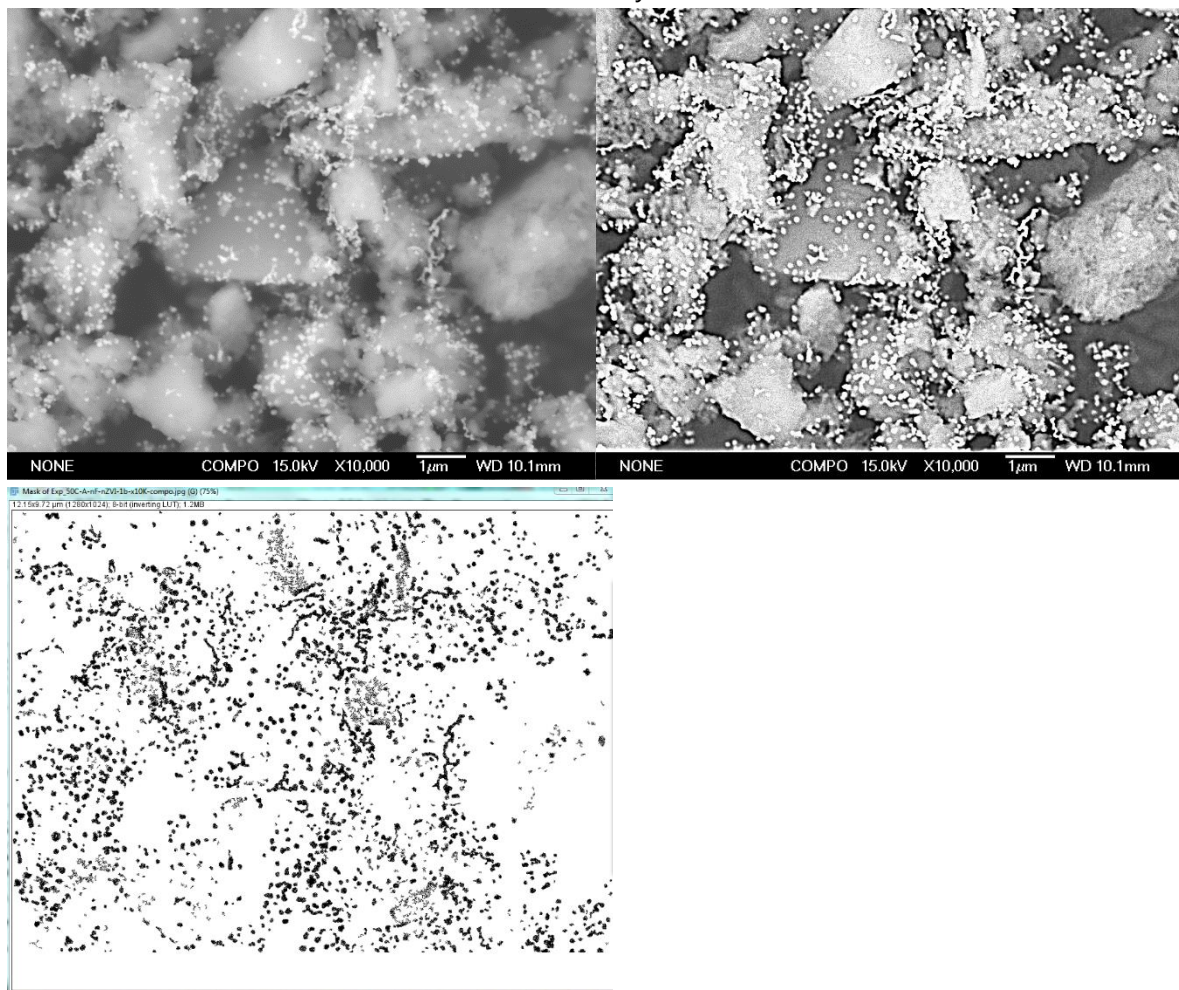
Mean = 7145 nm^2
SD= 11911 nm^2
% < 2000 nm^2 : 94.3%

5-C600-AnF-nZVI 3   *A*=1.24   Entry 34
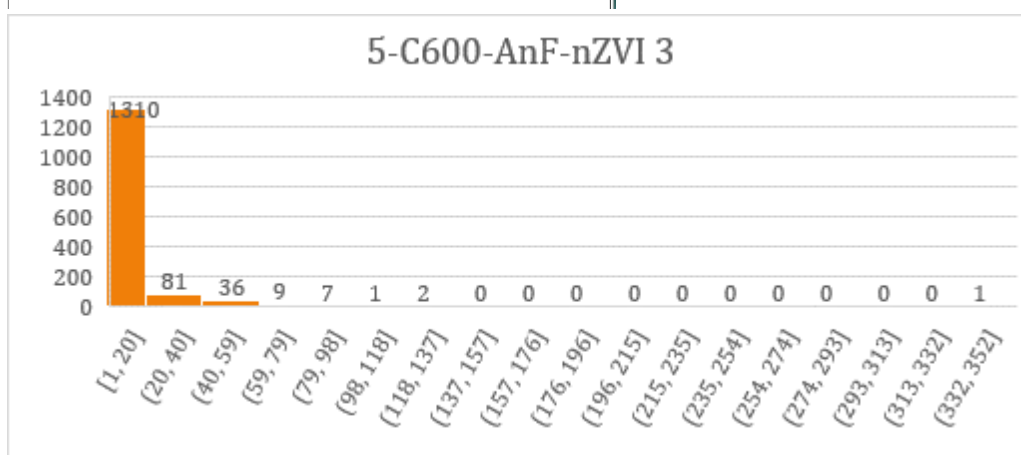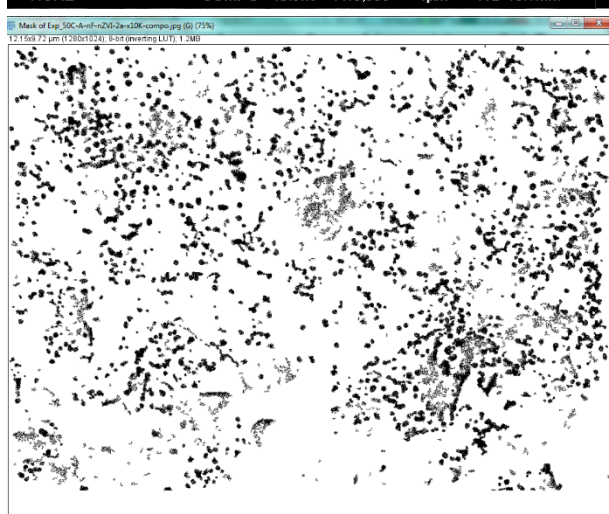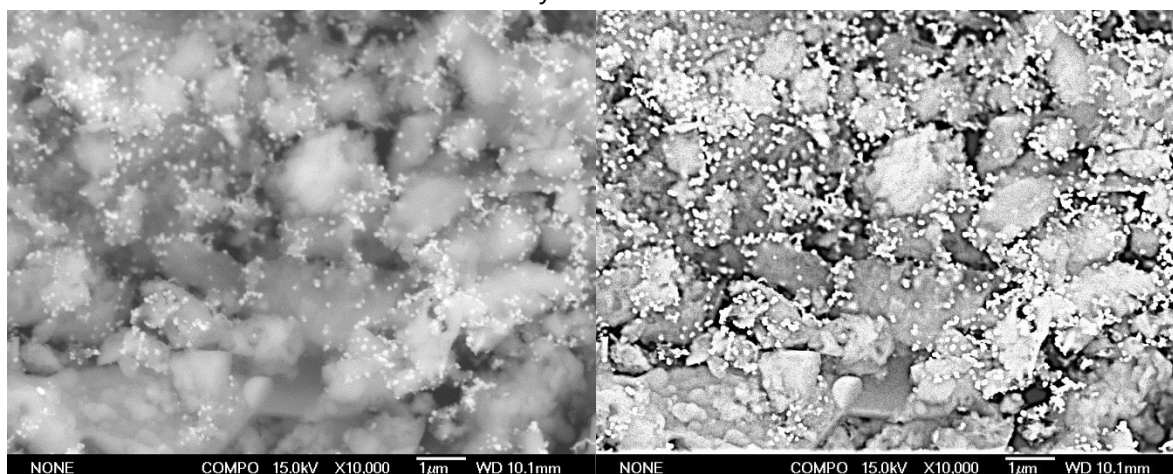
	With outlier	Without outlier (338)
Mean (nm^2)	9272	9044
SD (nm^2)	15721	13135
% of particles under 2000 nm^2	90.5	90.5

5-C600-nAF-nZVI 1   *A*=0.85   Entry 35
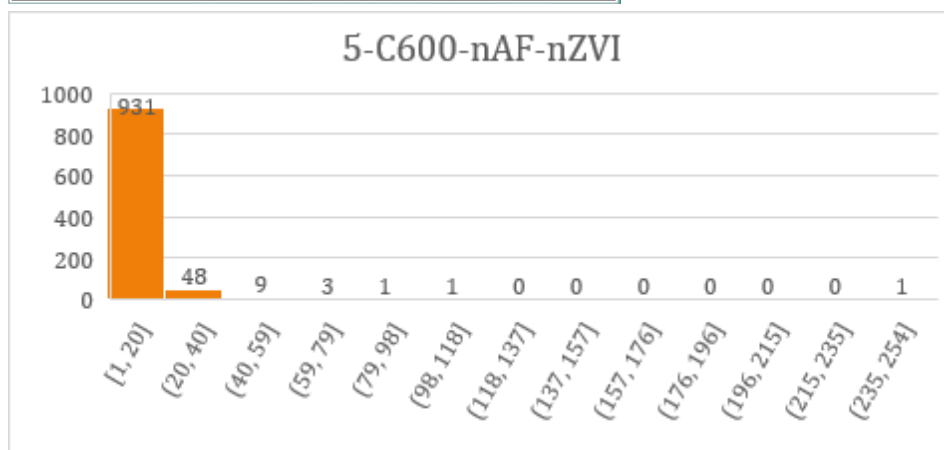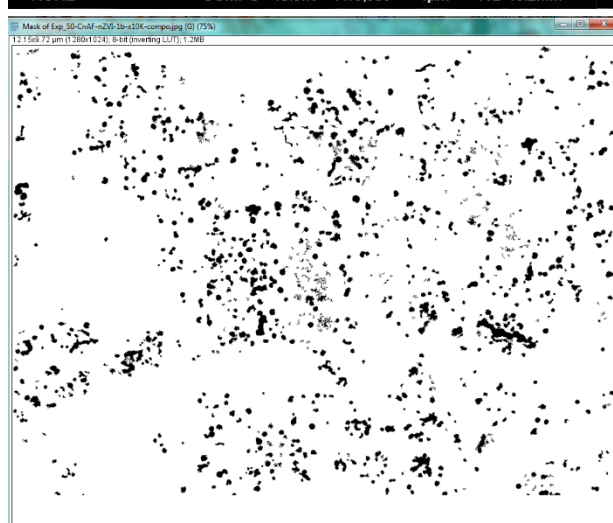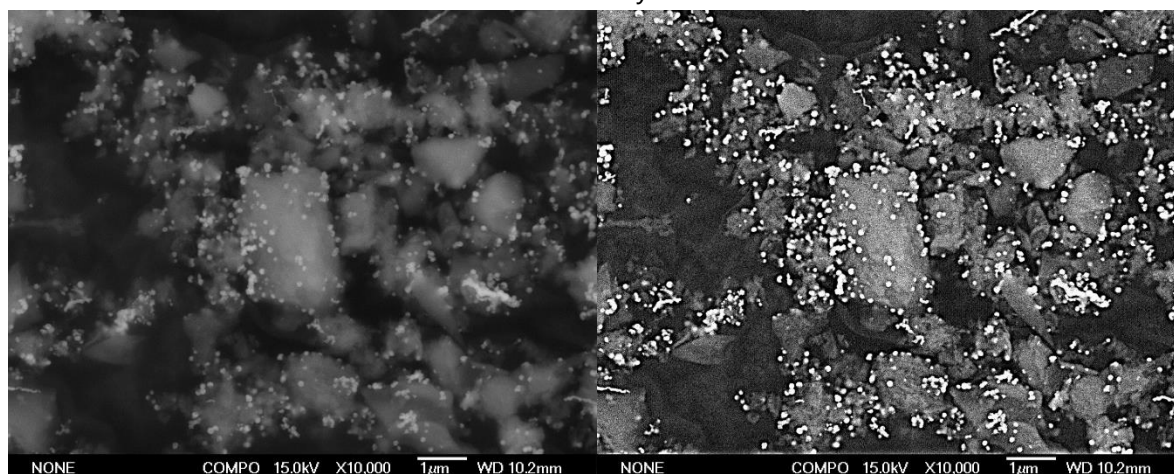
	With outlier	Without outlier (237)
Mean (nm^2)	7294	7063
SD (nm^2)	11593	9019
% of particles under 2000 nm^2	93.7	93.7

5-C600-nAF-nZVI 2 *A*=0.54   Entry 36
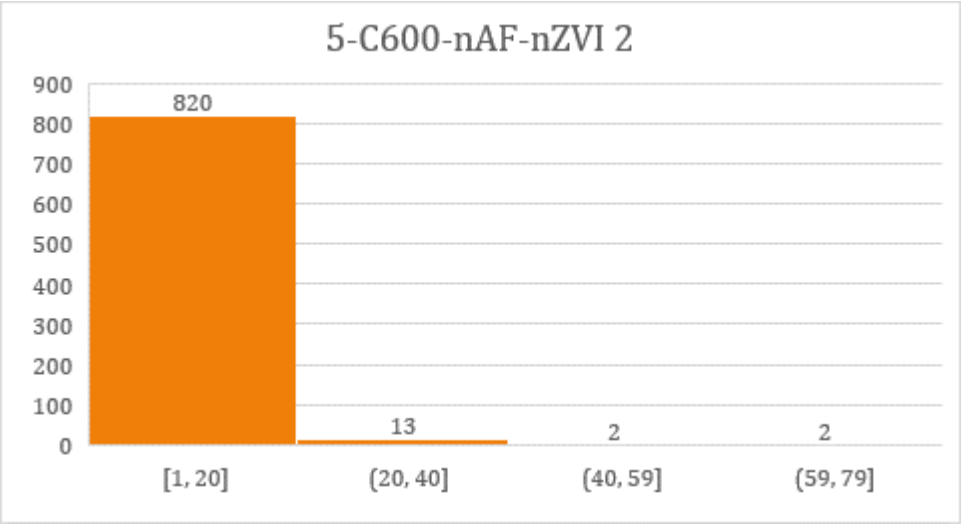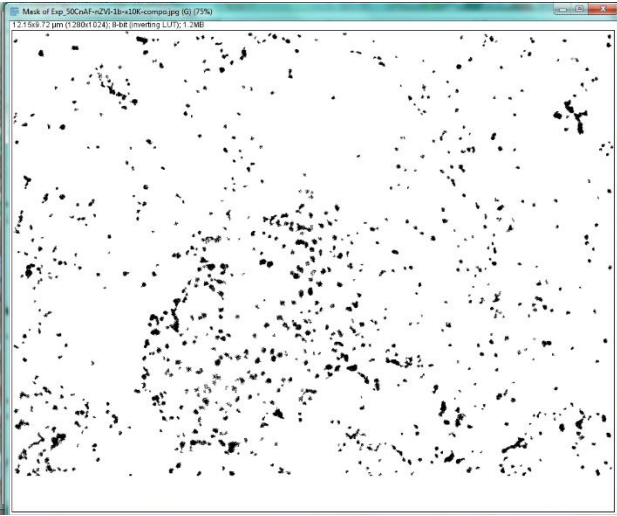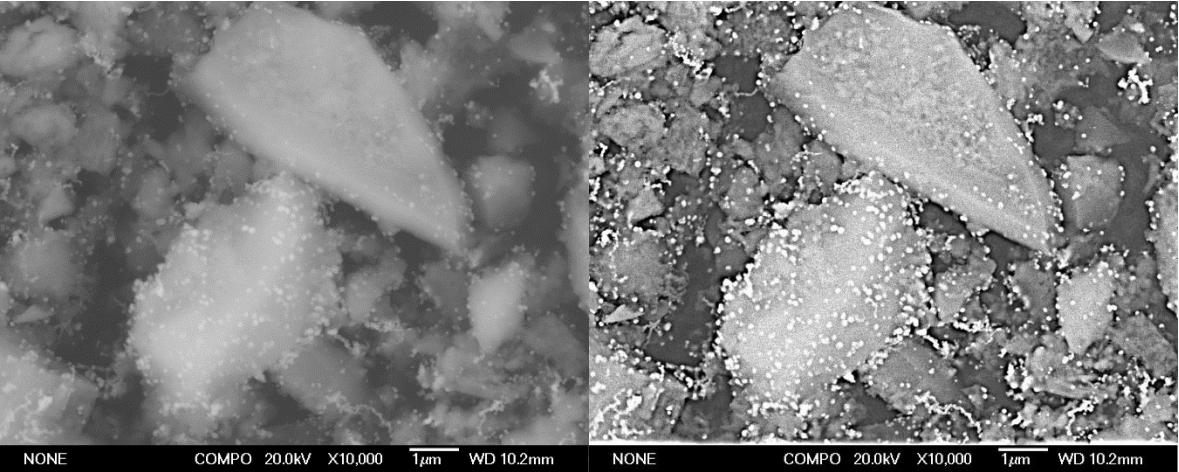
Mean = 4842 nm^2
SD= 5779 nm^2
% < 2000 nm^2 : 98.0%

5-C600-nAF-nZVI 3   *A*= 0.63   Entry 37
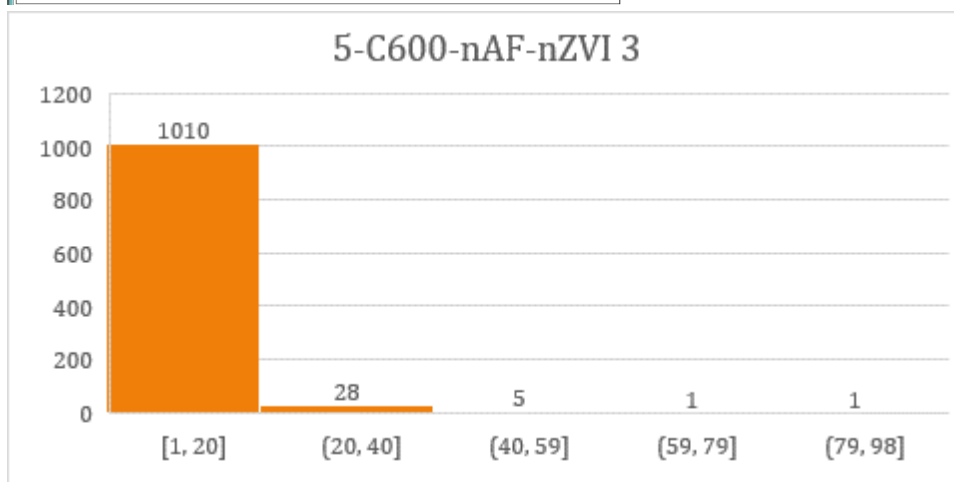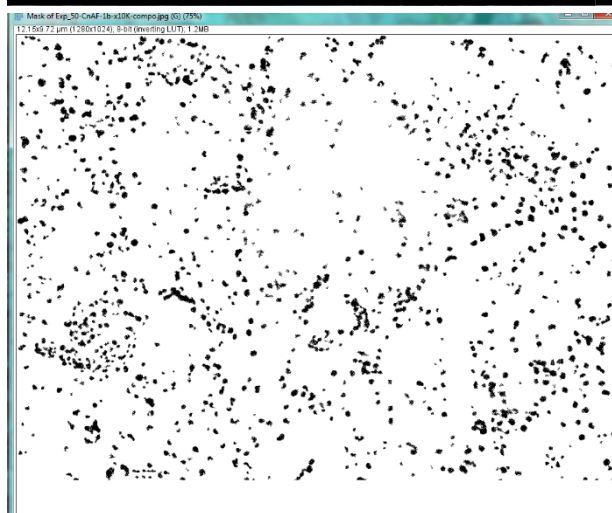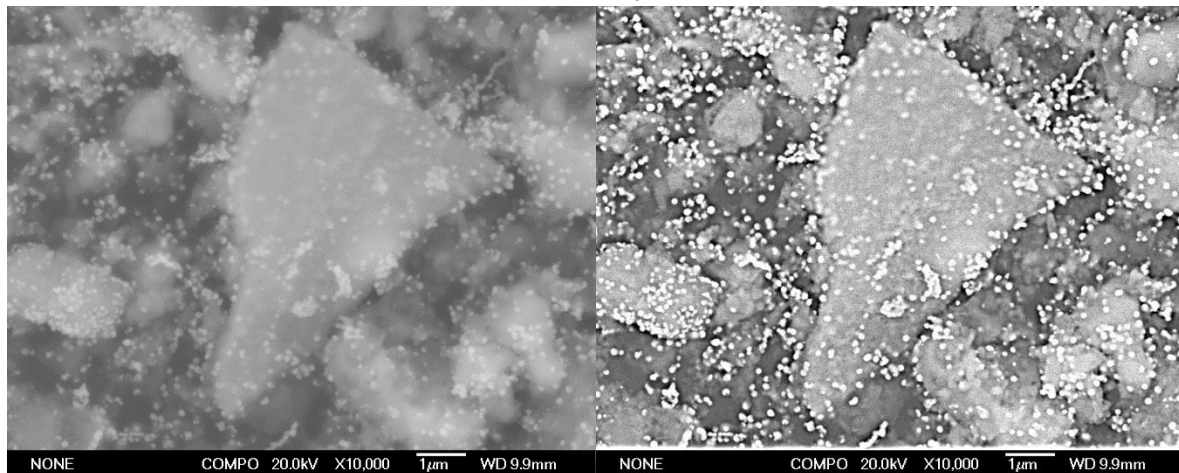
Mean = 6871 nm^2
SD= 6783nm^2
% <2000 nm^2 : 96.7%

221

5-C600-nAF-nZVI 4   *A*=0.68   Entry 38
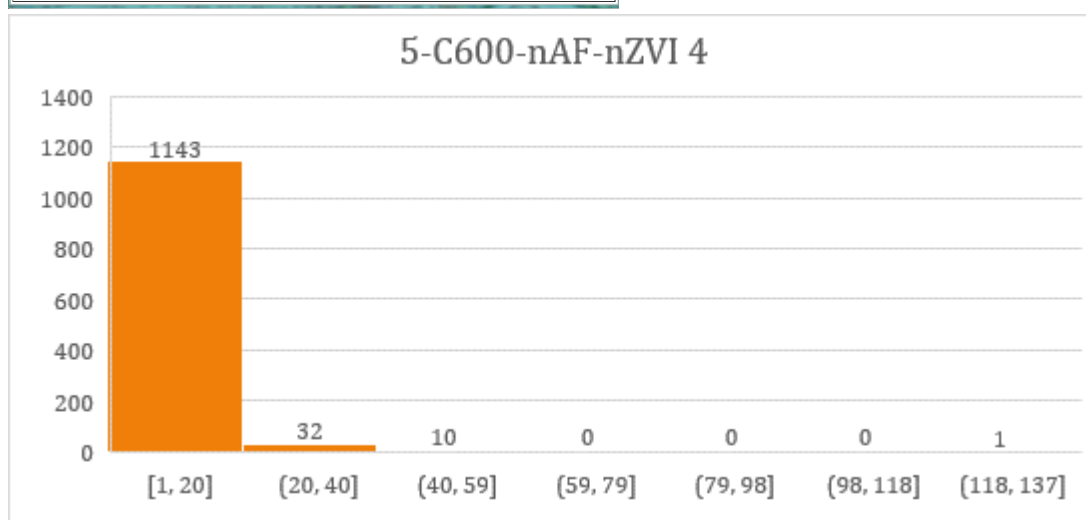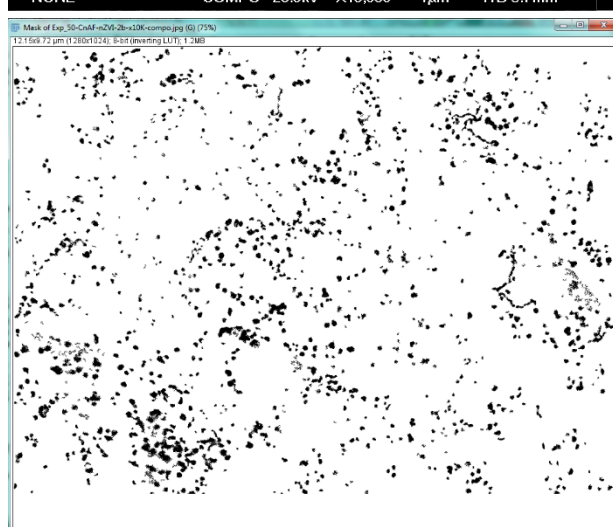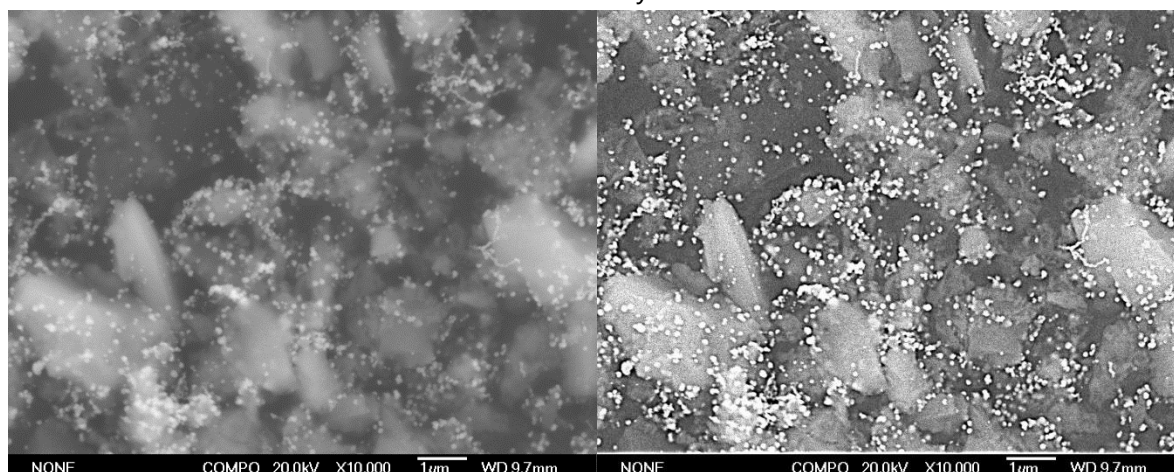
Mean = 5851 nm^2
SD= 7305 nm^2
% < 2000 nm^2 : 96.4%

5-C600-nAnF-nZVI   *A*=0.82   Entry 39
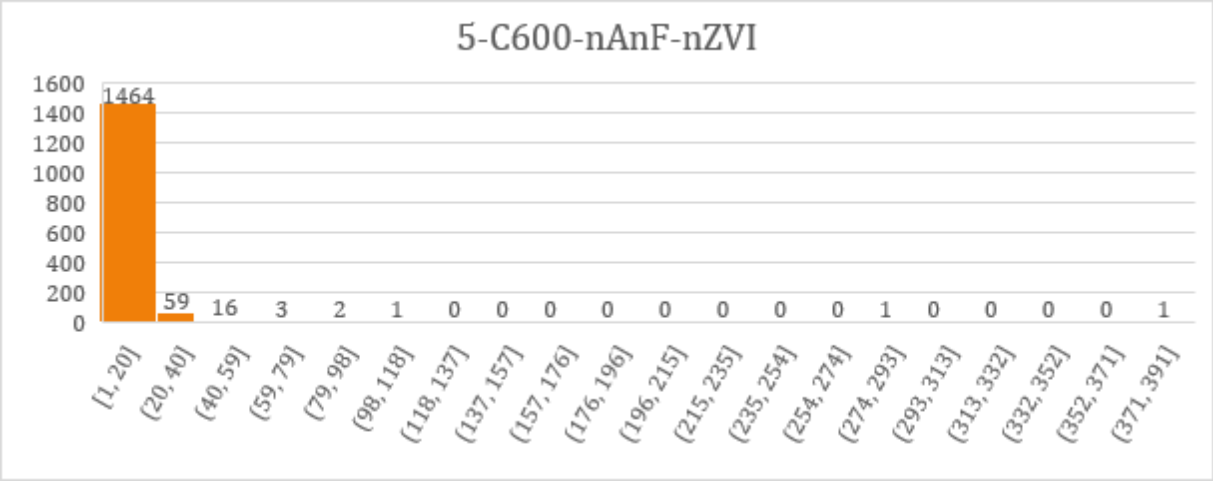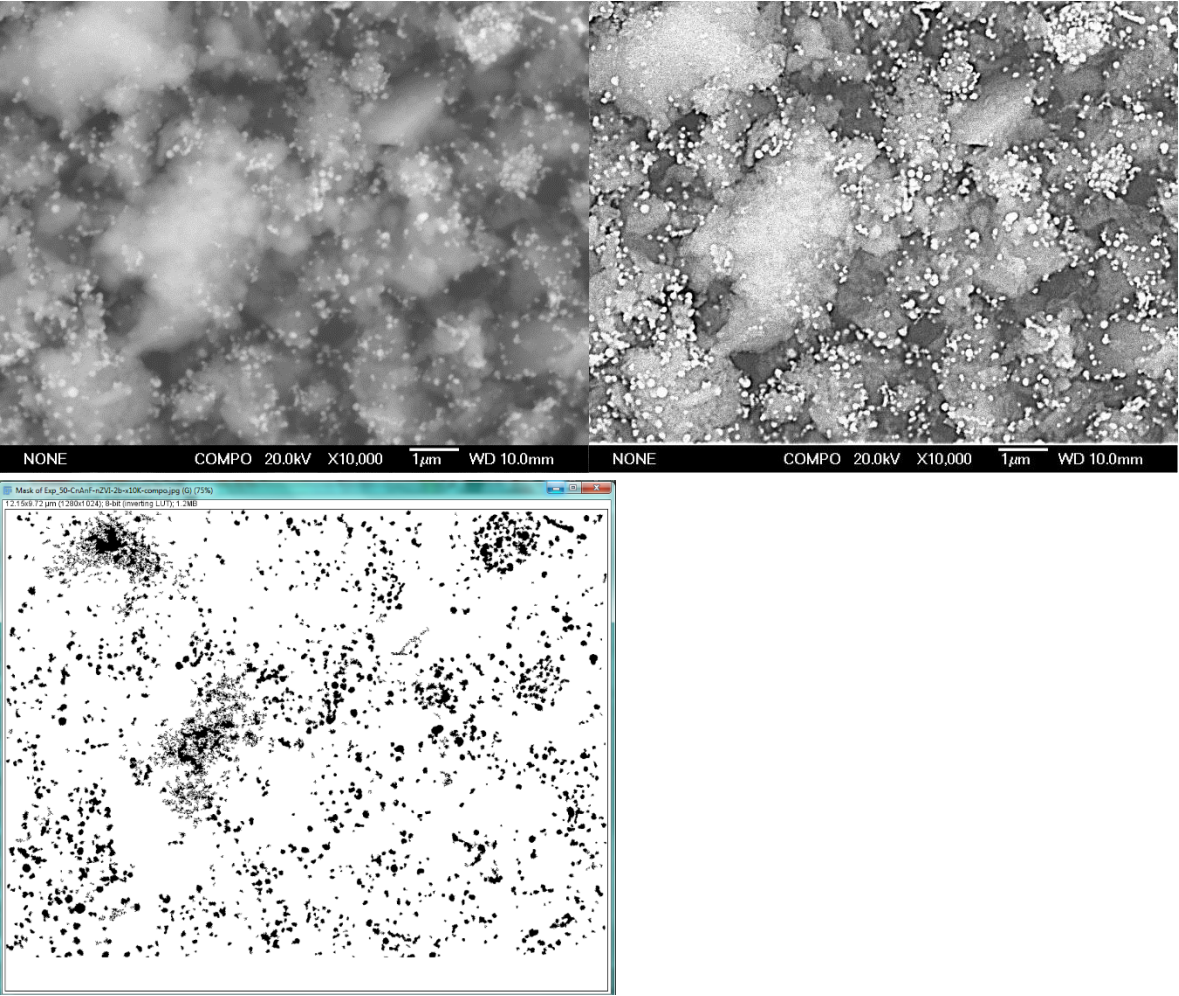
	With outlier	Without outlier (389)
Mean (nm²)	6986	6554
SD (nm²)	15035	8895
% of particles under 2000 nm²	94.6	94.6

223

5-C600-nAnF-nZVI 2   *A*=0.28   Entry 40
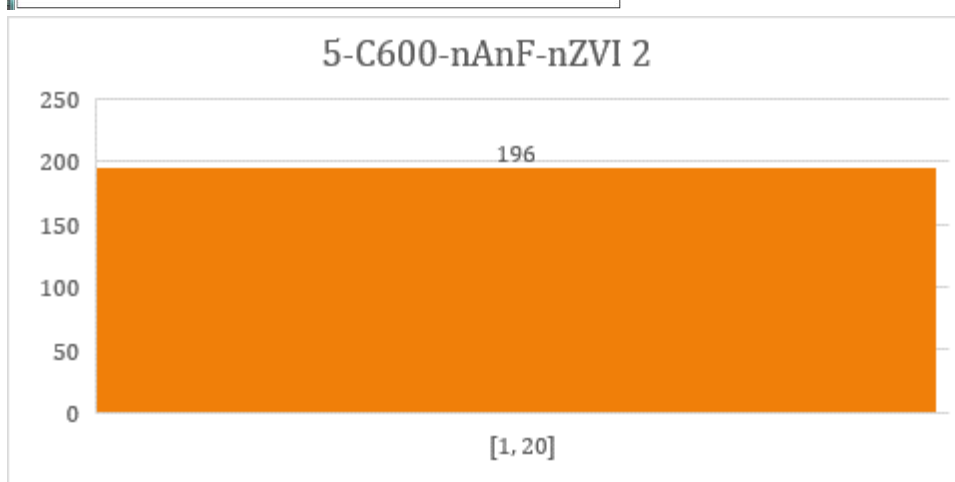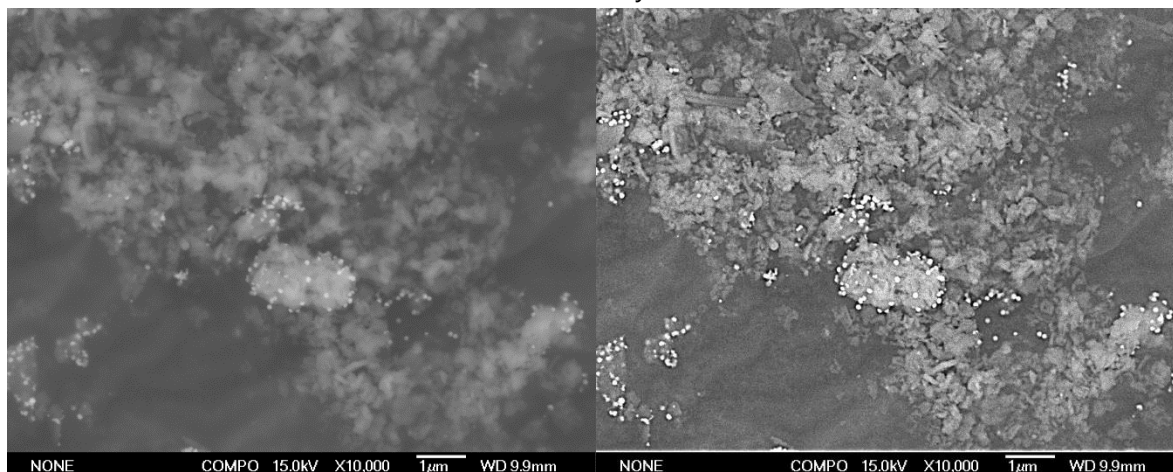
Mean = 4049 nm^2

SD= 2890 nm^2

% < 2000 nm^2 : 100%

5-uC-AF-nZVI   *A*=2.69   Entry 41
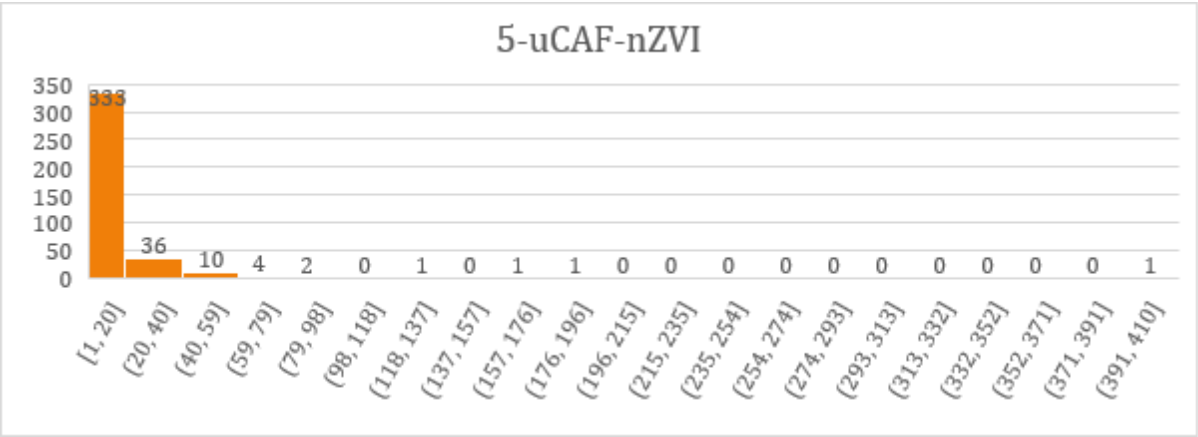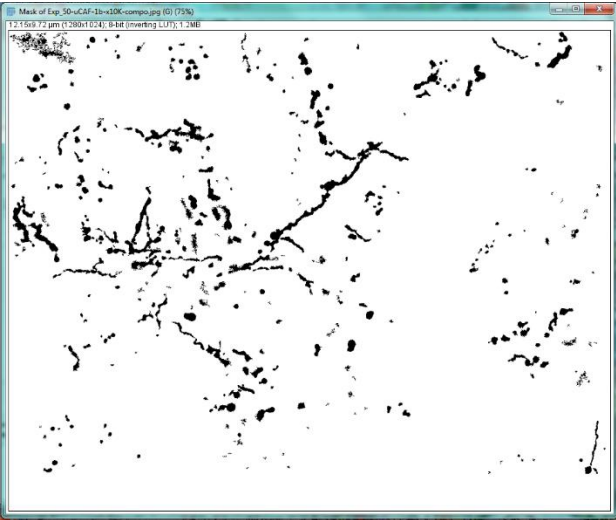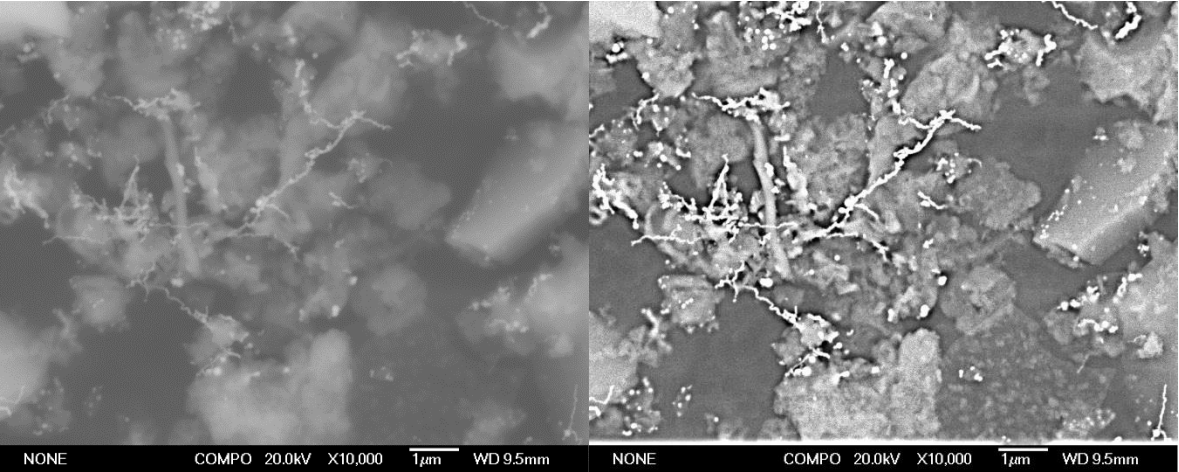
	With outlier	**Without outlier (404)**
Mean (nm^2)	11819	10808
SD (nm^2)	27594	19131
% of particles under 2000 nm^2	85.6	85.6

5-uC-AnF-nZVI   *A*=2.06   Entry 42
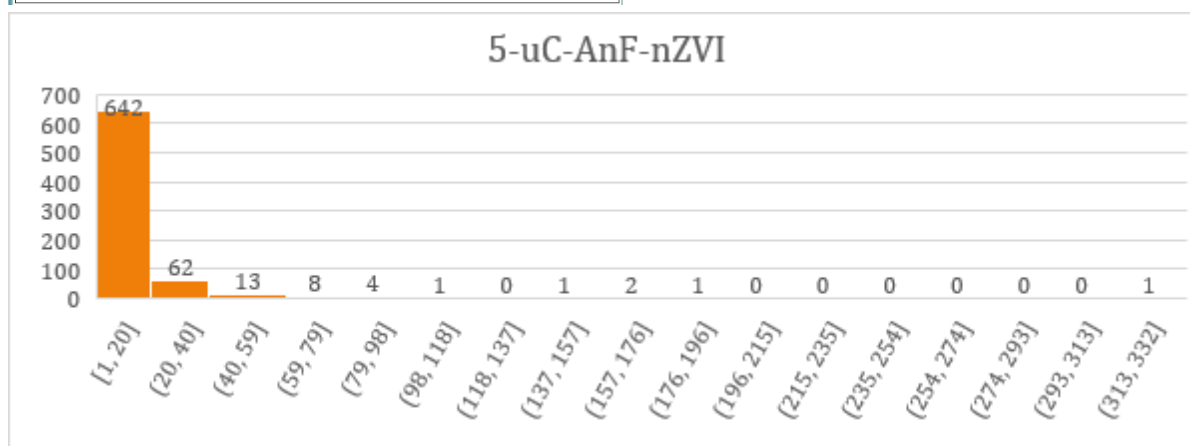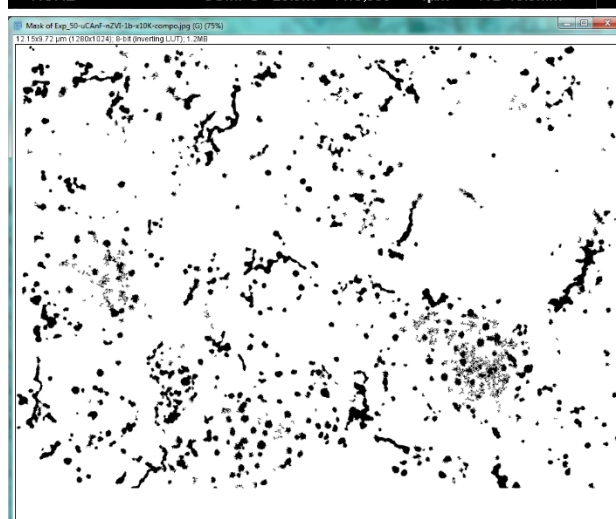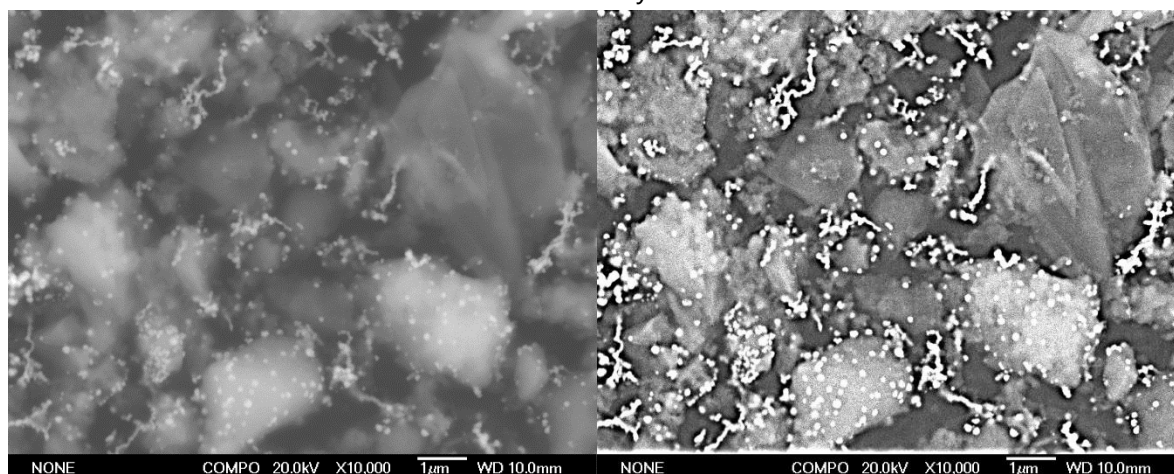
	With outlier	Without outlier (324)
Mean (nm^2)	11563	11138
SD (nm^2)	21316	17940
% of particles under 2000 nm^2	87.3	87.3

5-uC-nAF-nZVI   *A*=1.15   Entry 43
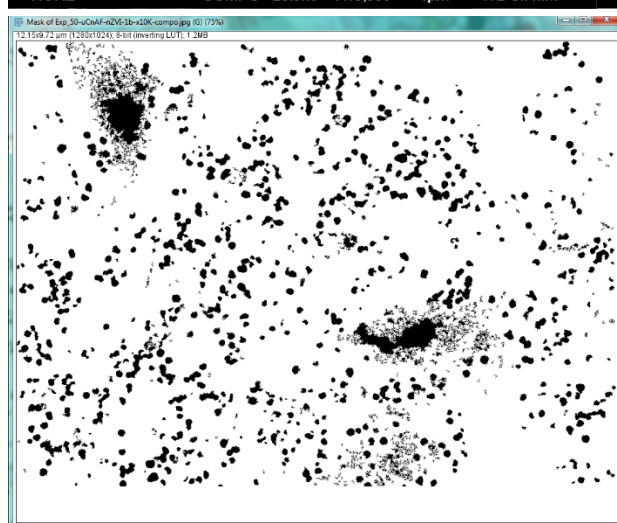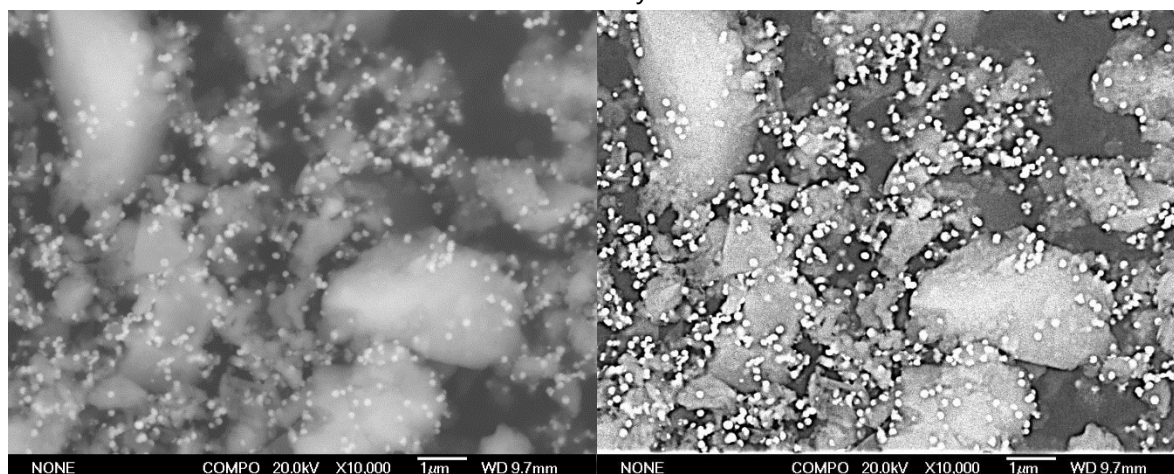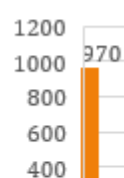
	With outlier	Without outlier (843 & 718)
Mean (nm^2)	11085	9688
SD (nm^2)	35047	12085
% of particles under 2000 nm^2	87.9	87.9

5-uC-nAnF-nZVI   *A*=0.88   Entry 44

Mean = 7042 nm^2

SD= 9369 nm^2
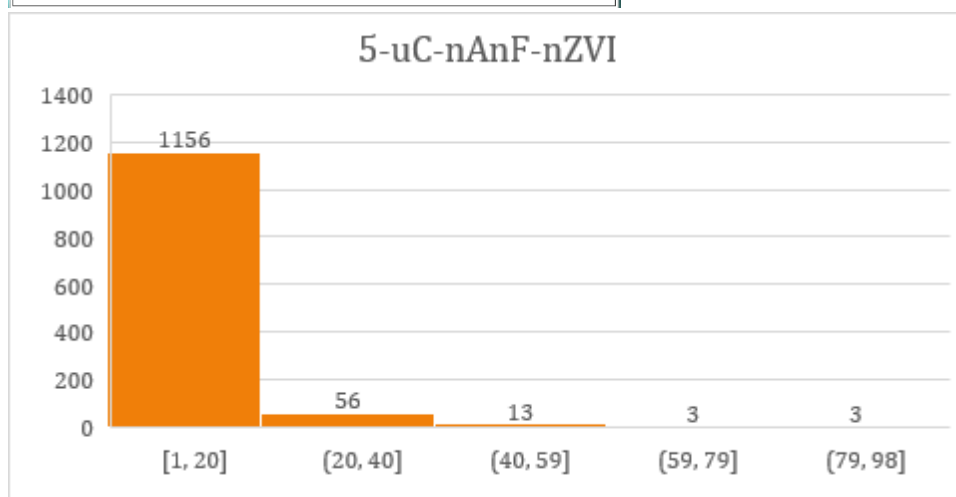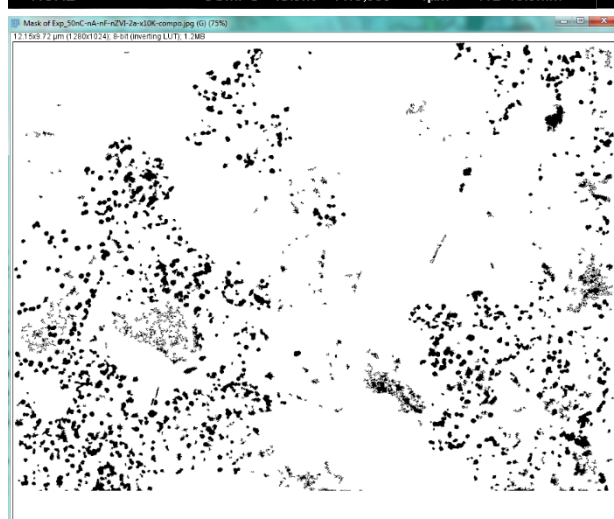
% <2000 nm^2 : 93.9%

C400-5-AF-nZVI   *A*=2.02   Entry 45
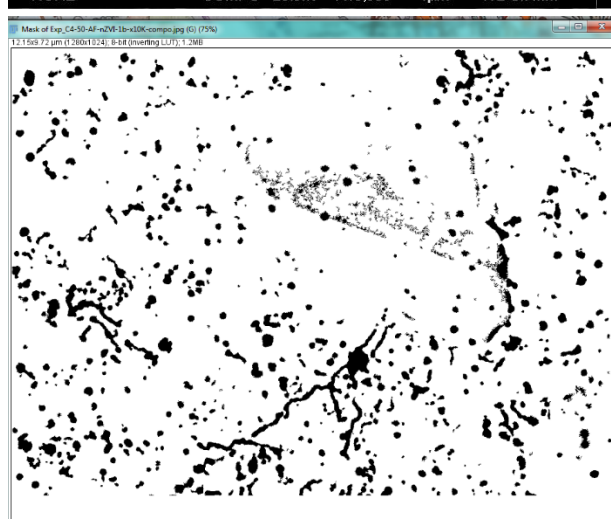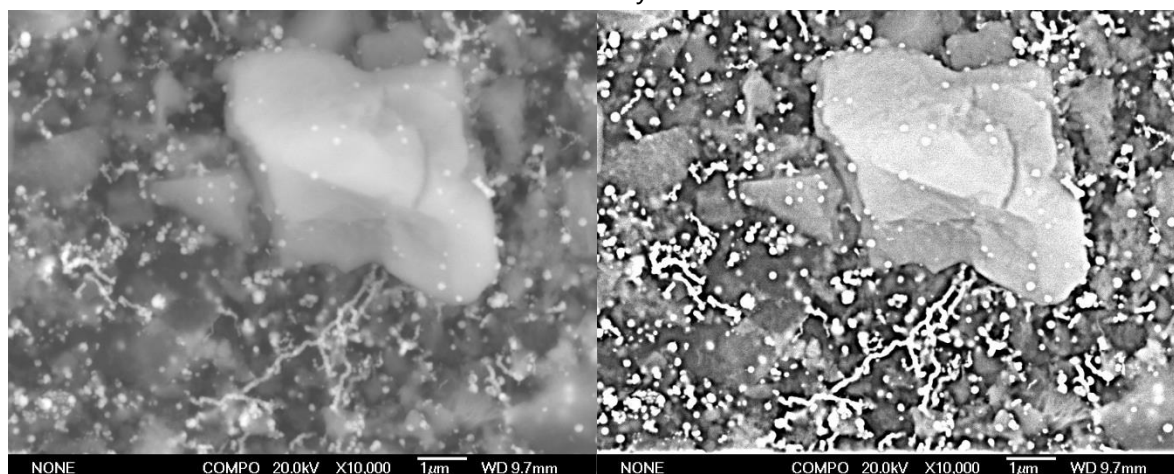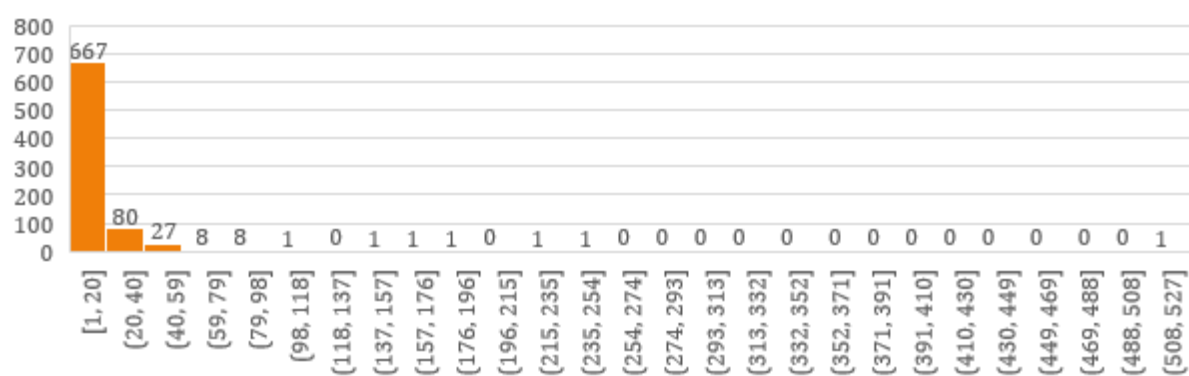
	With outlier	Without outlier (521)
Mean (nm^2)	13101	12463
SD (nm^2)	27598	20935
% of particles under 2000 nm^2	83.7	83.7

C400-5-nAF-nZVI   *A*=2.11   Entry 46
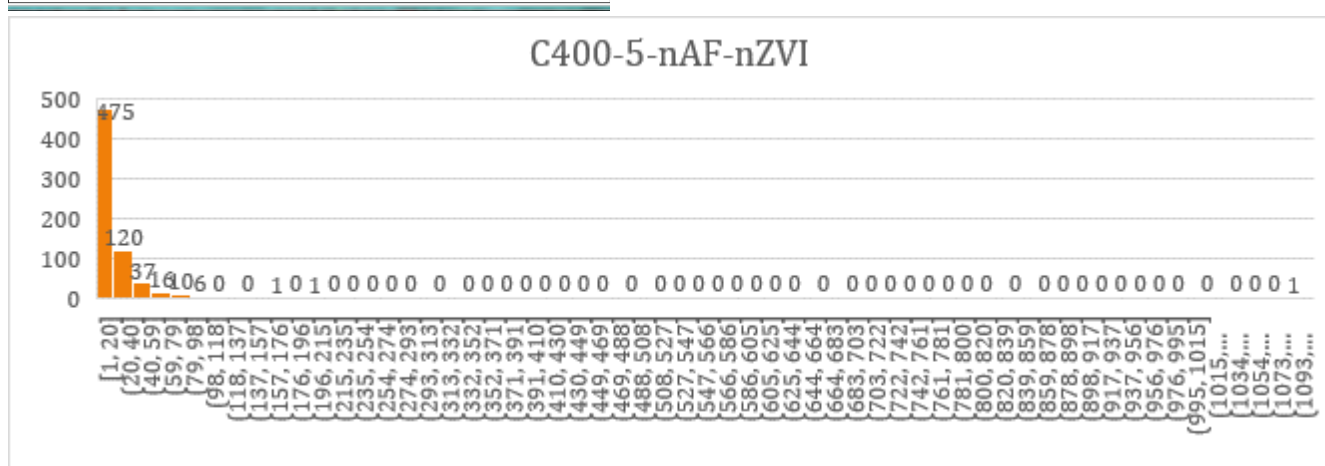
	With outlier	Without outlier (521)
Mean (nm^2)	18952	17336
SD (nm^2)	47043	2180
% of particles under 2000 nm^2	71.2	71.2

C400-5-nAnF-nZVI   *A*=2.10   Entry 47
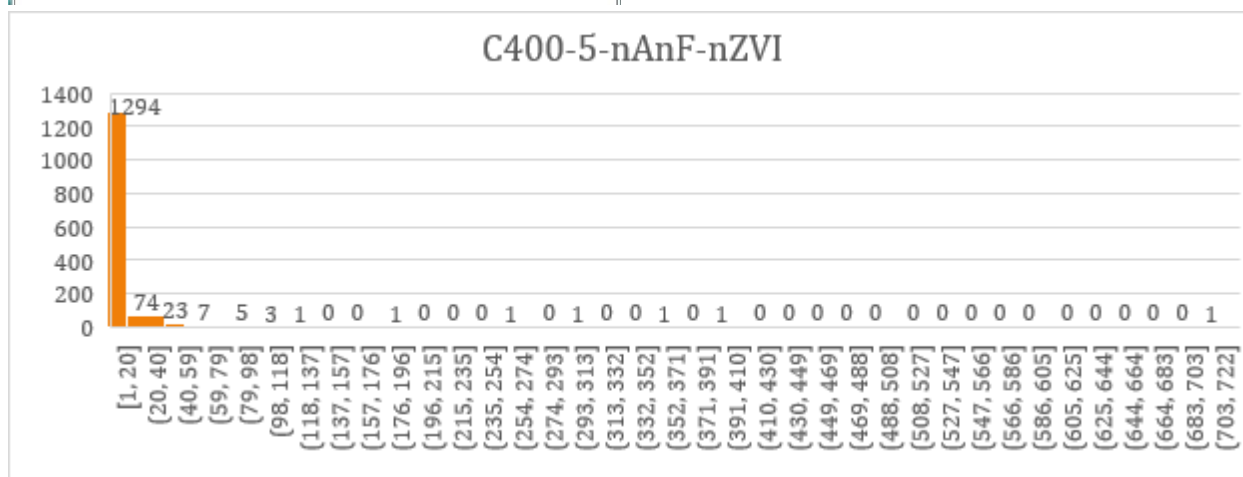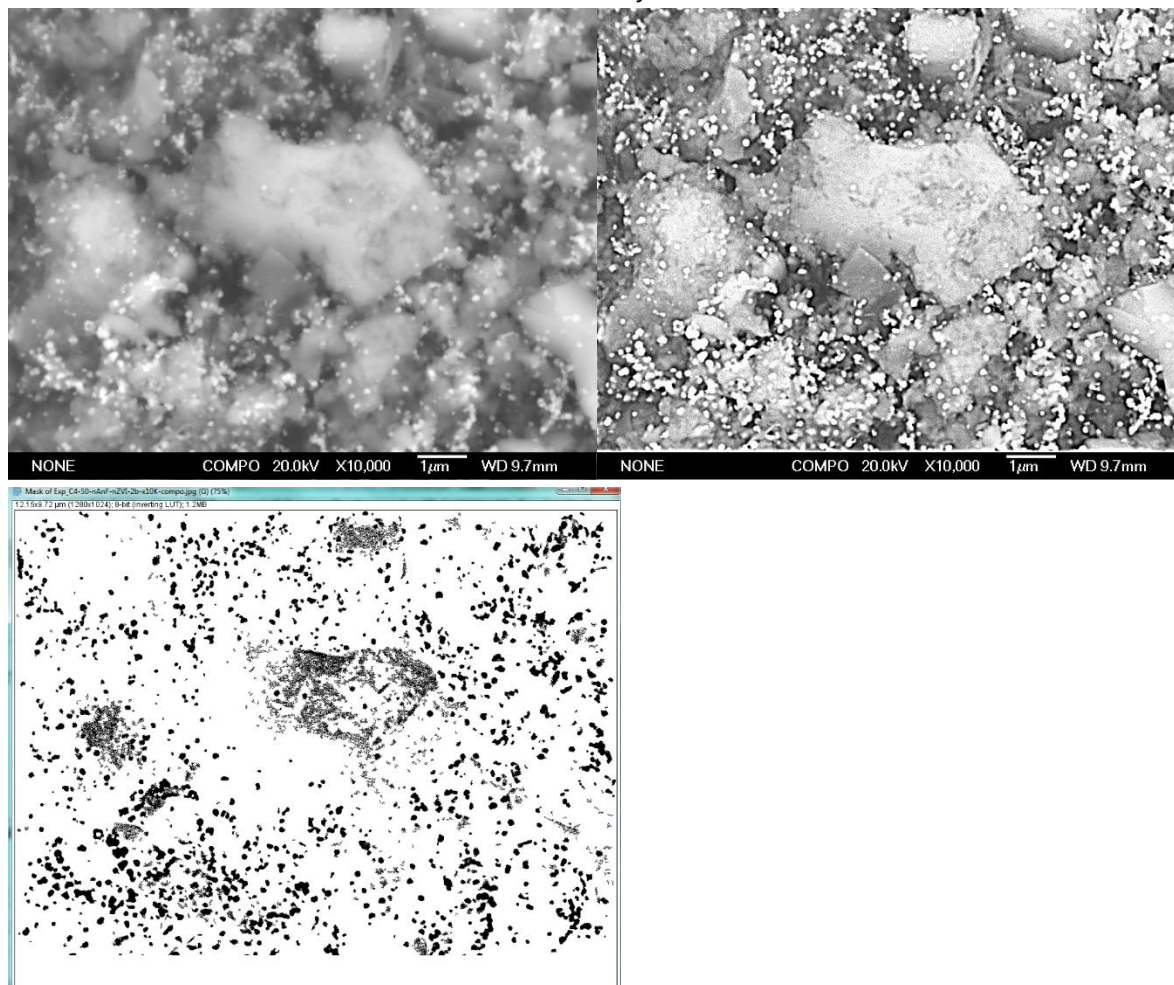
	With outlier	Without outlier (713)
Mean (nm^2)	9867	9369
SD (nm^2)	28843	21957
% of particles under 2000 nm^2	91.6	91.6

C400-AF-nZVI *d*=2.08   Entry 48
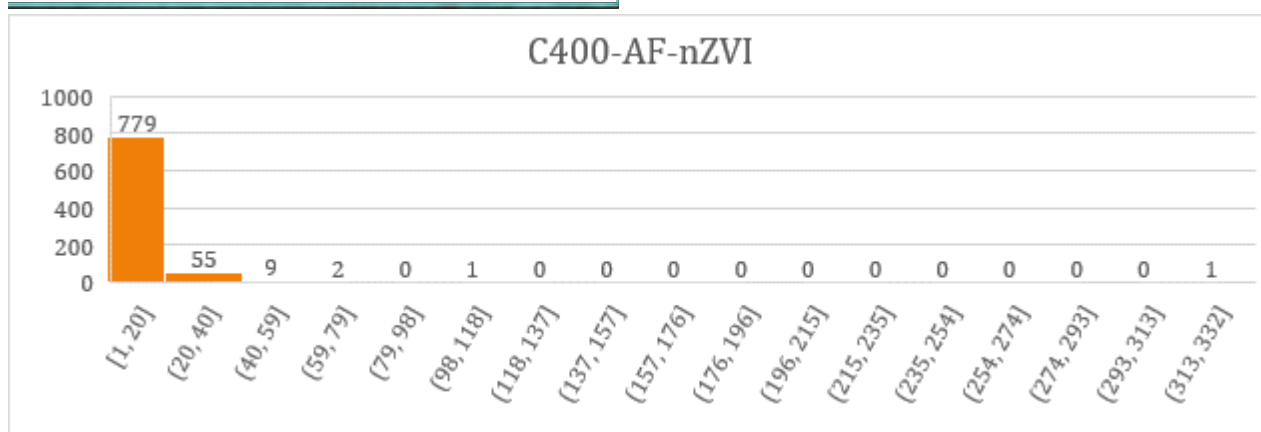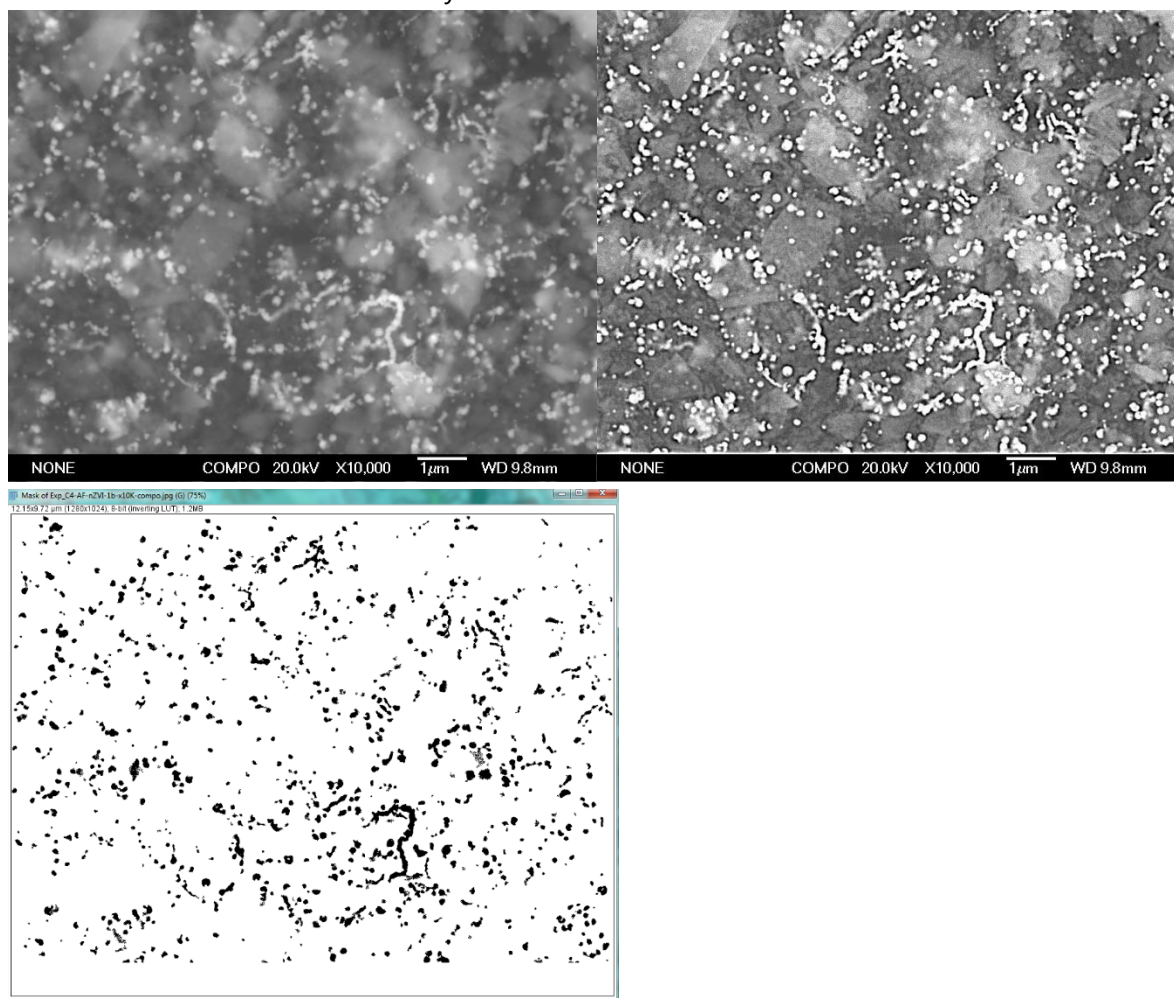
	With outlier	Without outlier (713)
Mean (nm^2)	8811	8432
SD (nm^2)	14249	9011
% of particles under 2000 nm^2	92.0	92.0

C400-AnF-nZVI   *A*=2.43   Entry 49
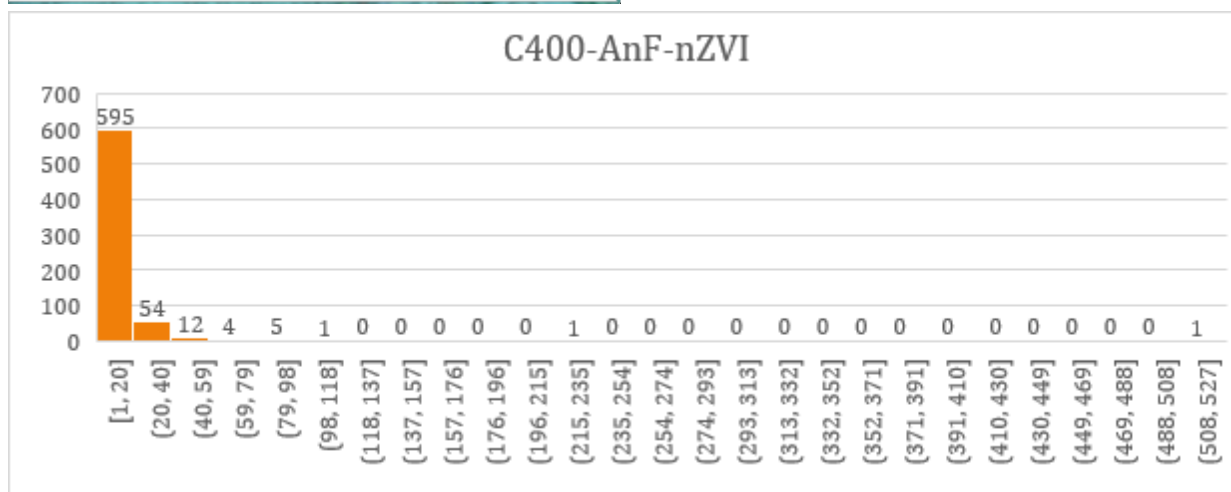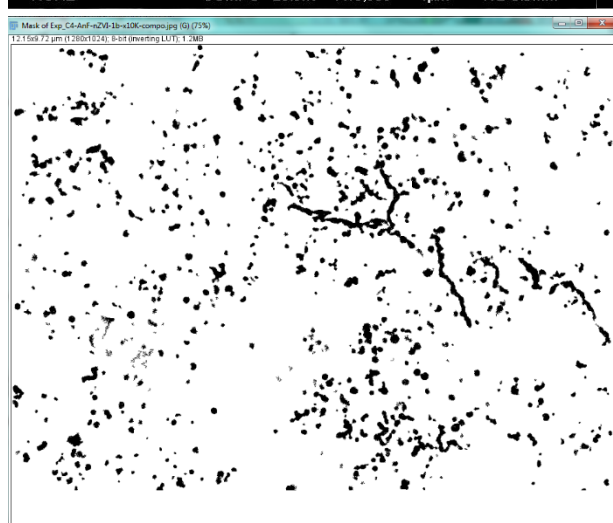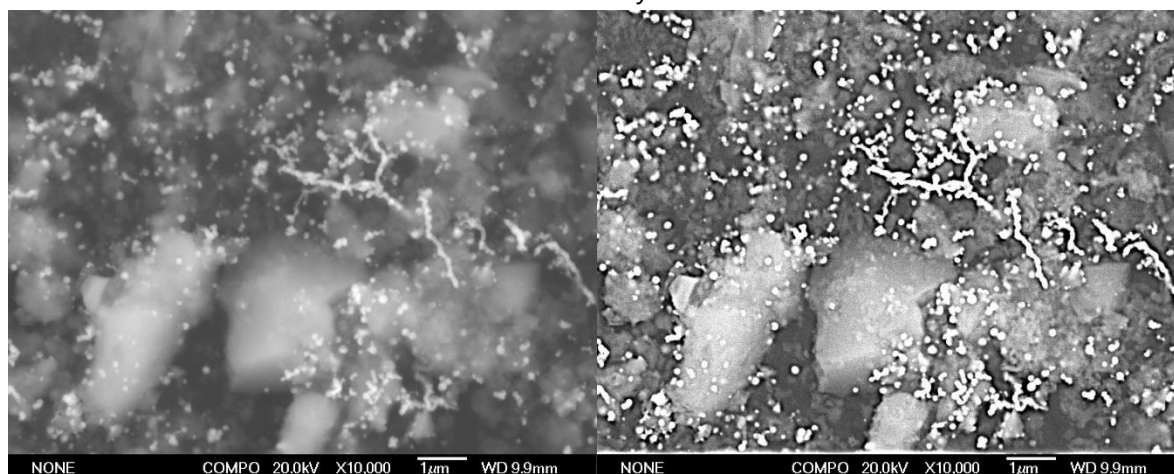
	With outlier	Without outlier (525)
Mean (nm^2)	11511	10747
SD (nm^2)	25005	15272
% of particles under 2000 nm^2	88.4	88.4

233

C400-nAF-nZVI   *A*=1.78   Entry 50
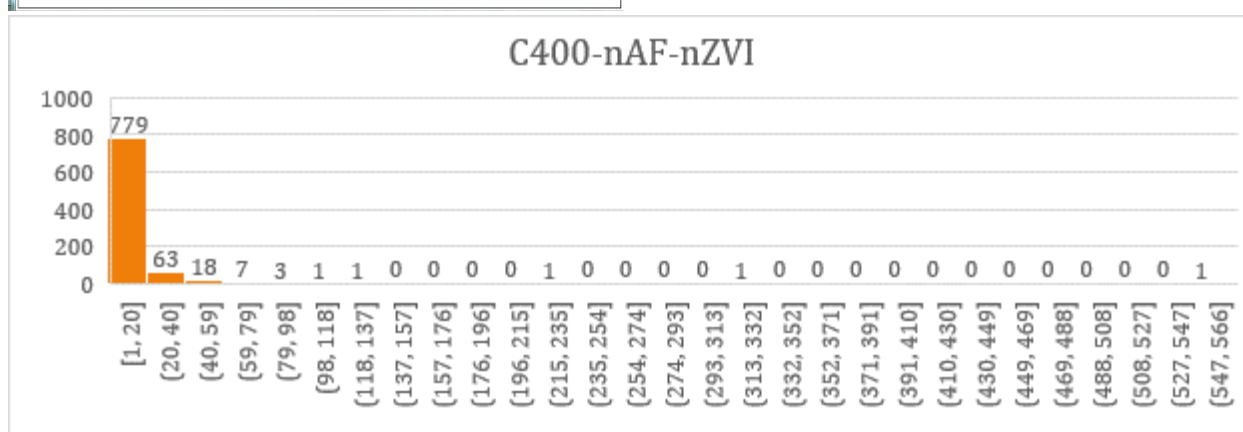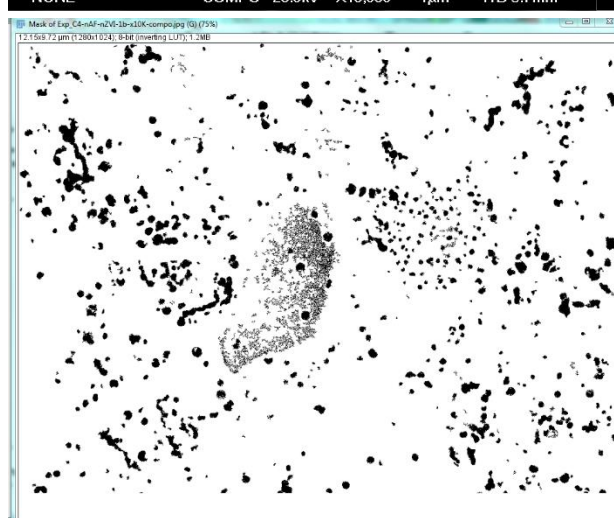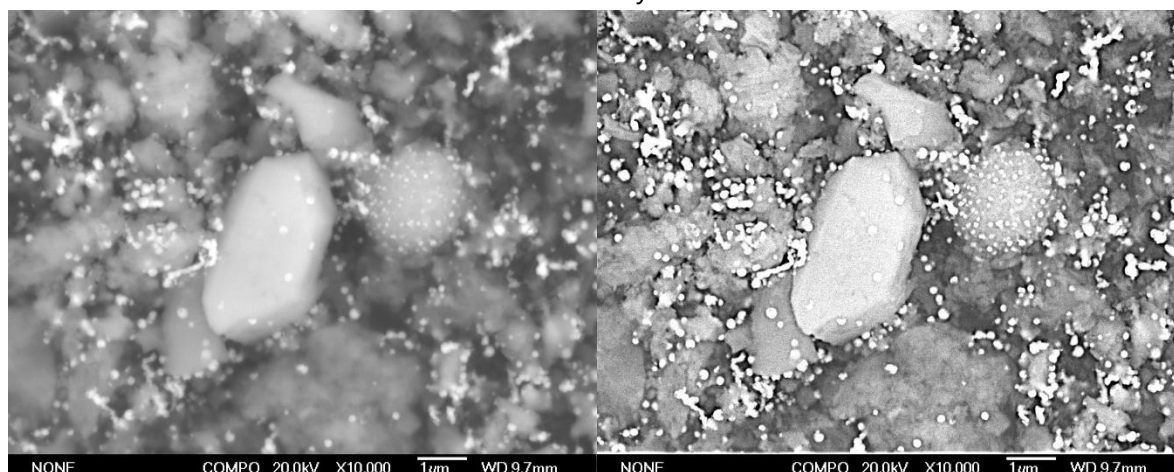
	With outlier	Without outlier (525)
Mean (nm^2)	9941	9316
SD (nm^2)	26117	18475
% of particles under 2000 nm^2	89.0	89.0

234

C400-nAnF-nZVI   *A*=0.65   Entry 51
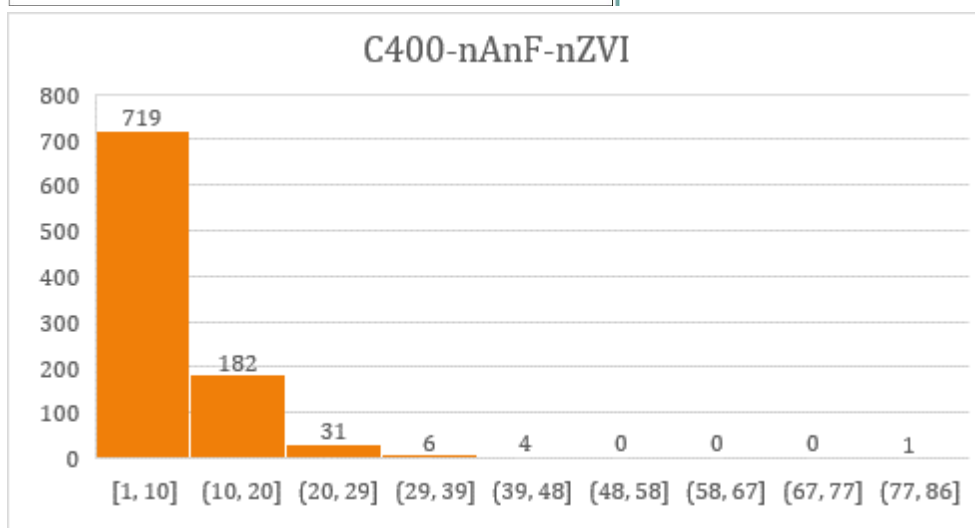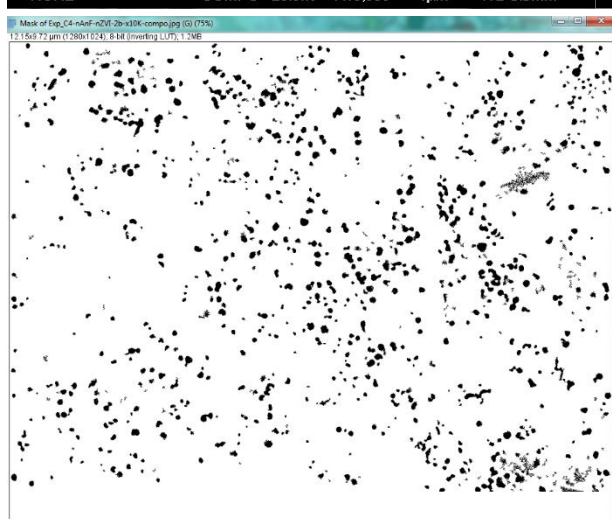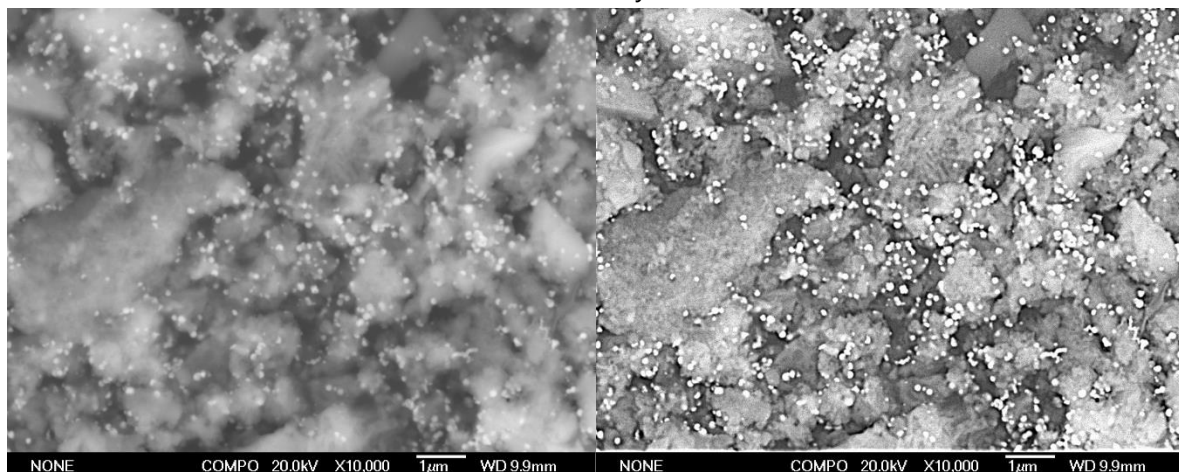
Mean = 7190 nm^2

SD= 6930 nm^2

% <2000 nm^2 : 96.3%

235

C600-5-AF-Nzvi 1   *A*=2.49   Entry 52
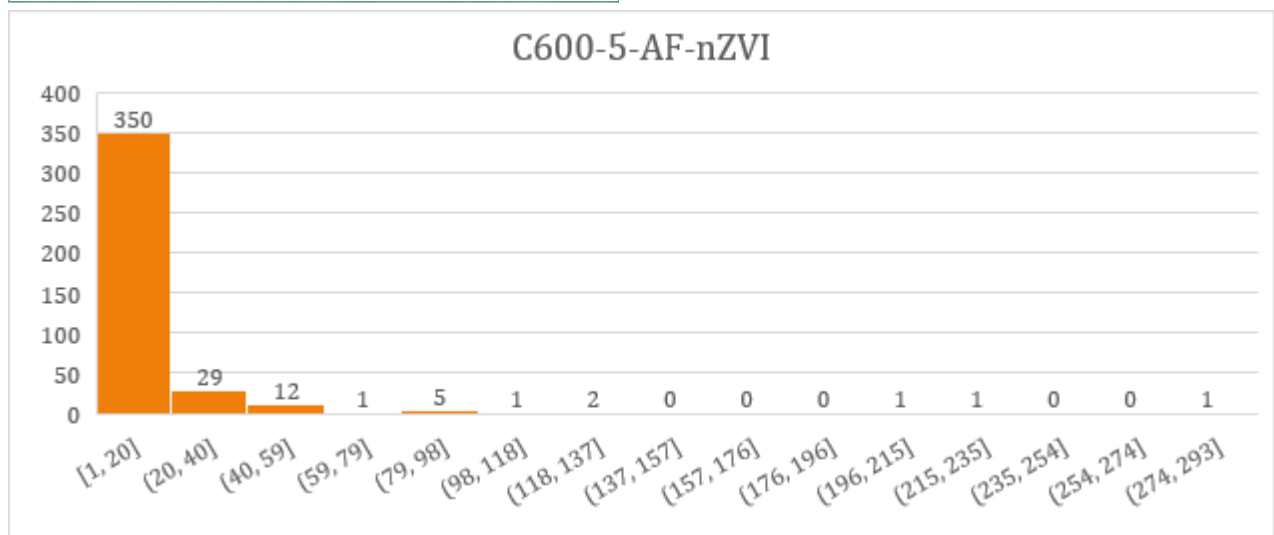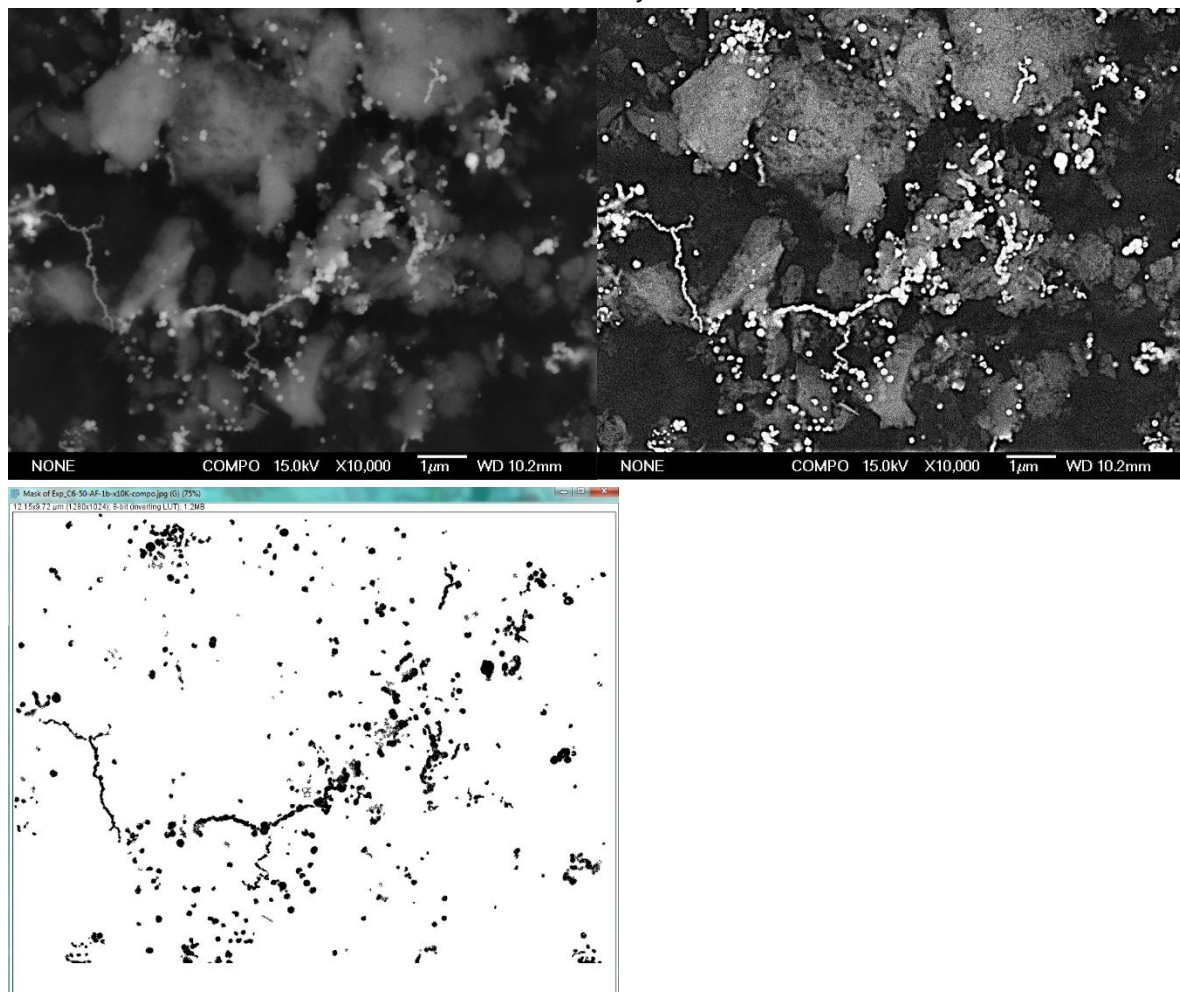
Mean = 12843 nm^2

SD= 25492 nm^2

% <2000 nm^2 : 86.8%

C600-5-AF-nZVI 2   *A*=1.17   Entry 53
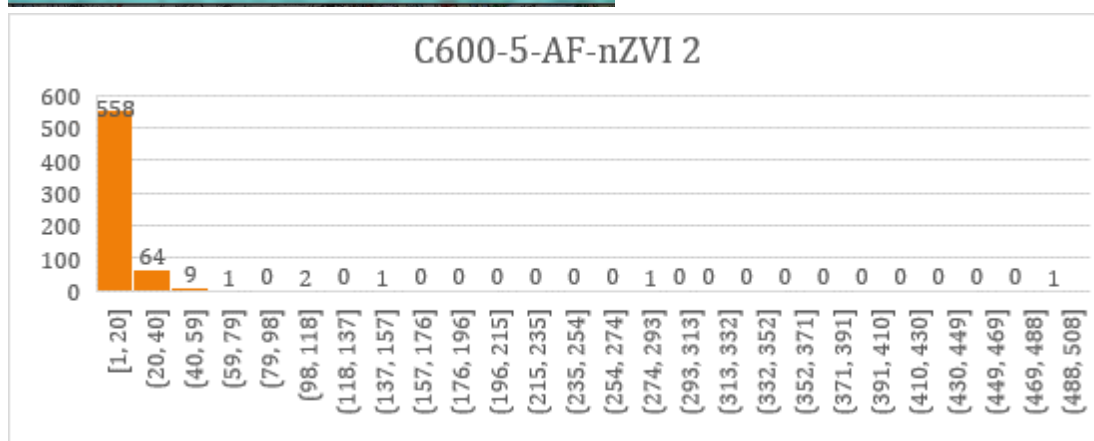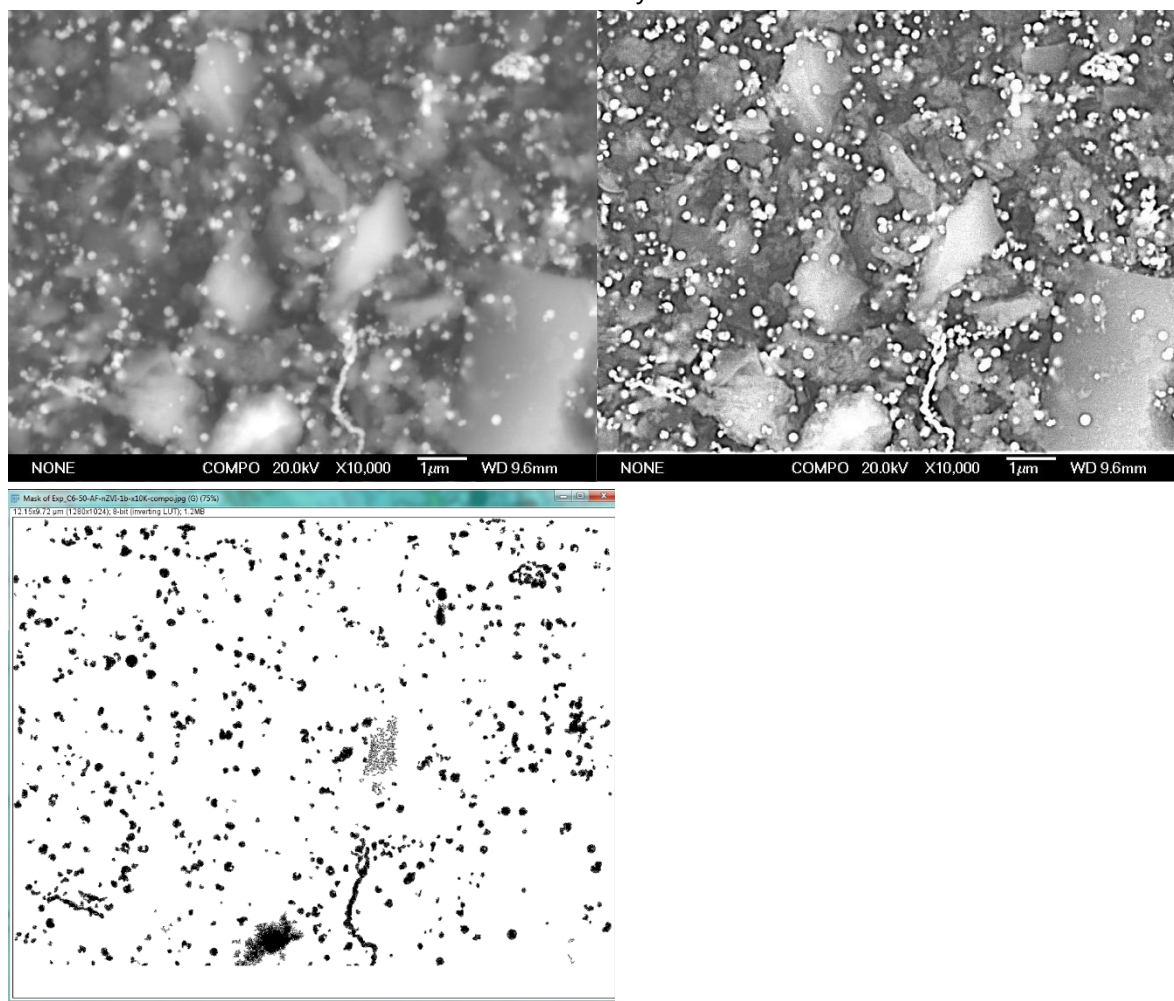
	With outlier	Without outlier (277&500)
Mean (nm^2)	11507	10320
SD (nm^2)	25174	12146
% of particles under 2000 nm^2	87.6	87.6

C600-5-AnF-nZVI   *A*=1.54   Entry 54
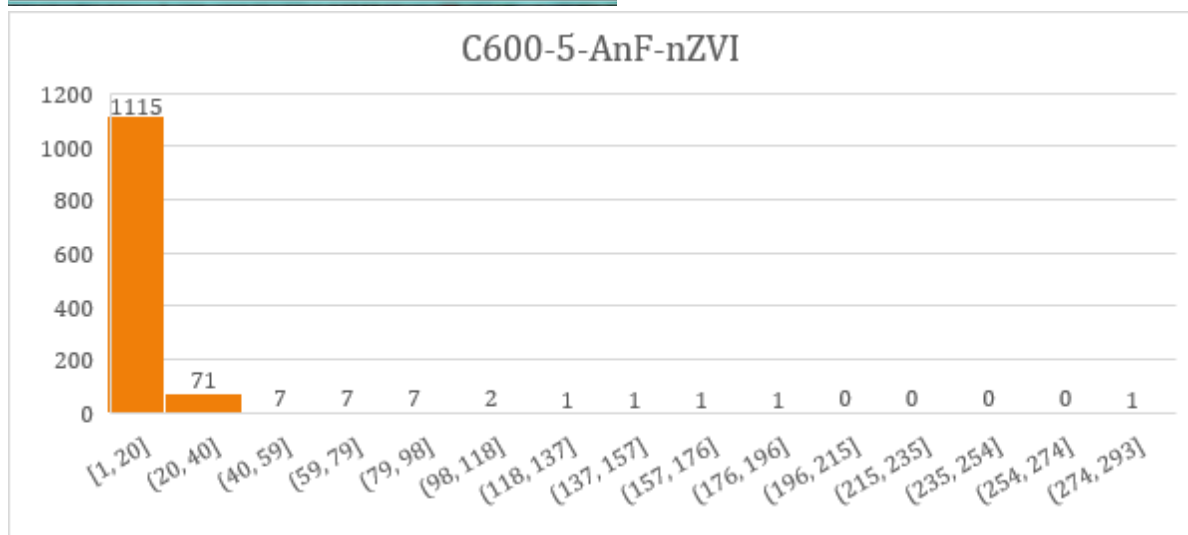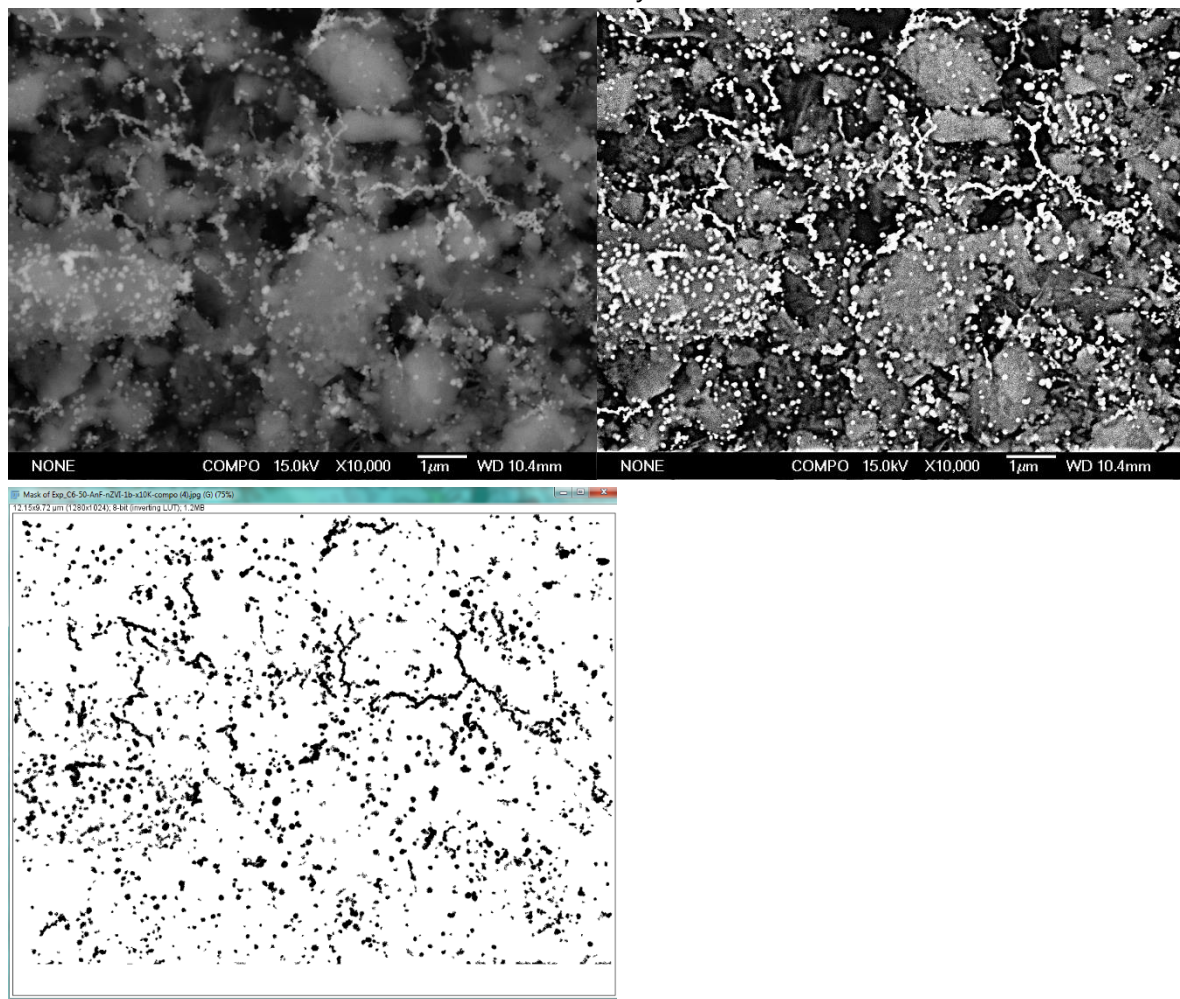
Mean = 8645 nm^2
SD= 16163 nm^2
% <2000 nm^2: 91.8%

C600-5-nAF-nZVI 1   *A*=1.21   Entry 55
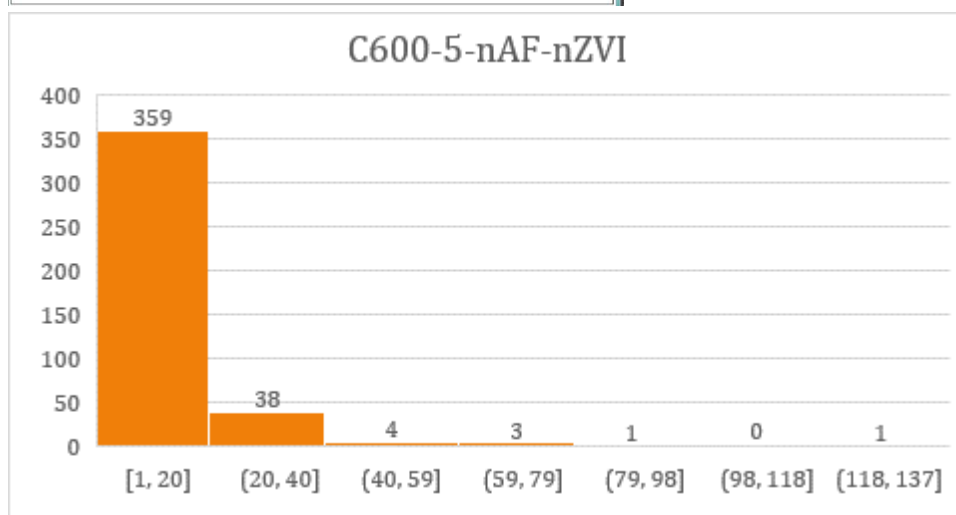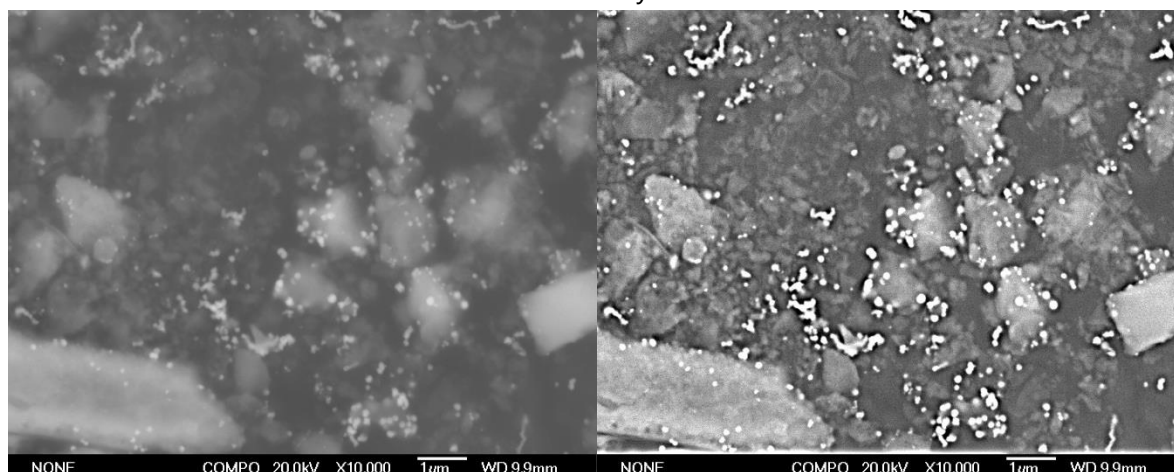
Mean = 9786 nm^2
SD= 12476 nm^2
% < 2000 nm^2: 88.4%

C600-5-nAF-nZVI 2   *A*=1.04   Entry 56
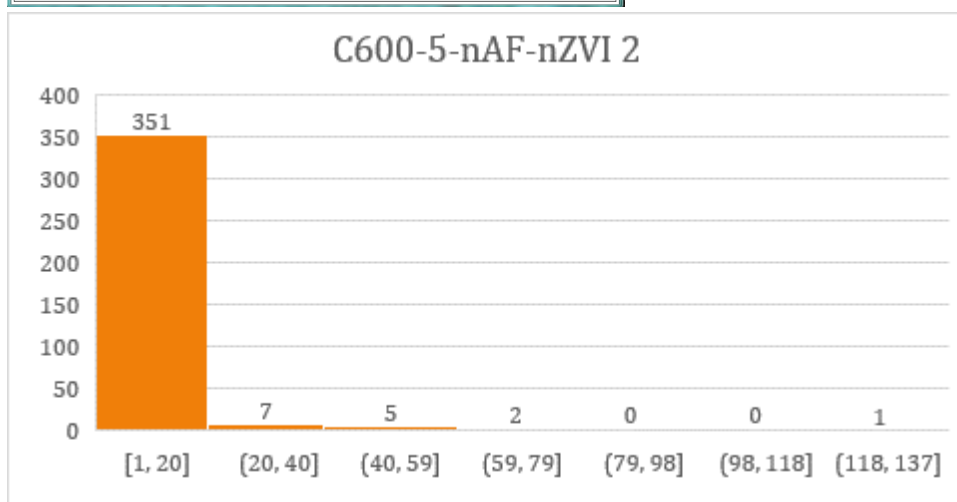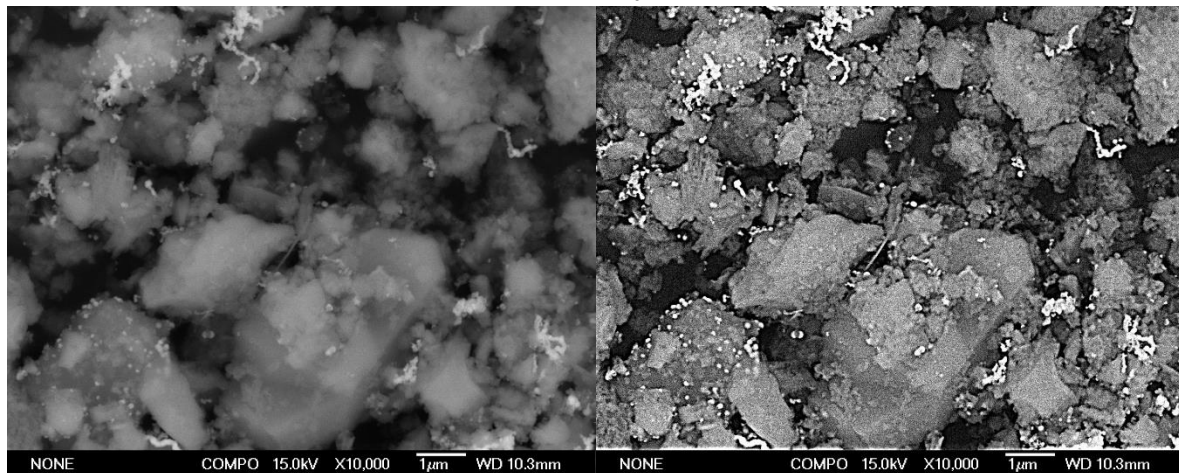
Mean = 5604 nm^2
SD= 10679 nm^2
% <2000 nm^2: 95.9%

C600-5-nAnF-nZVI   *A*=1.05   Entry 57
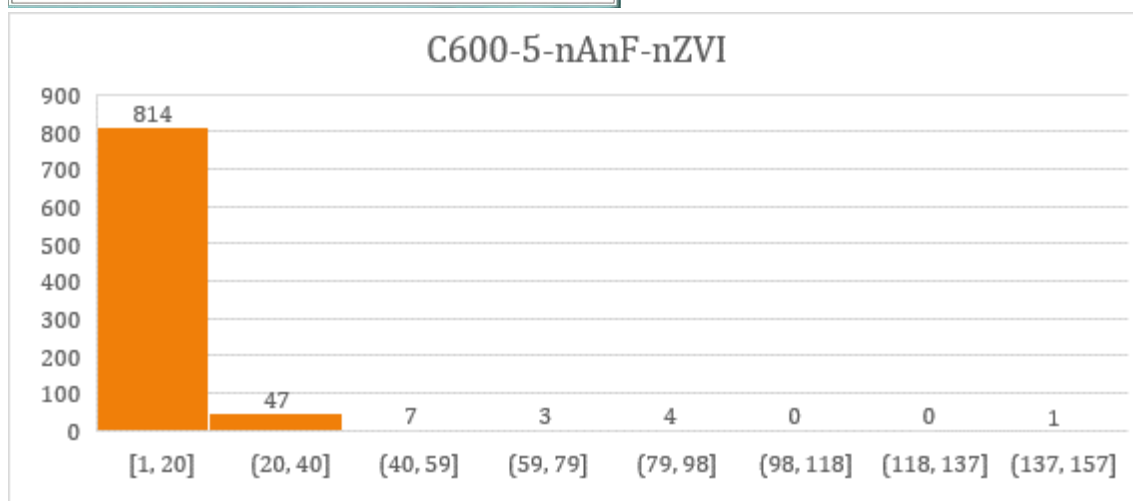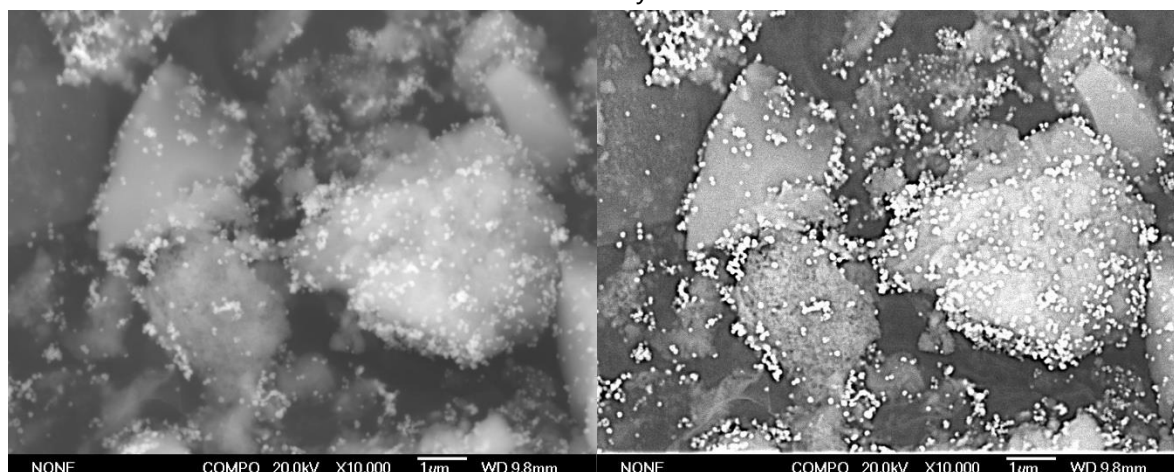
Mean = 7906 nm^2
SD= 10975 nm^2
% <2000 nm^2: 92.9%

C600-5-nAnF-nZVI 2   *A*=1.02   Entry 58
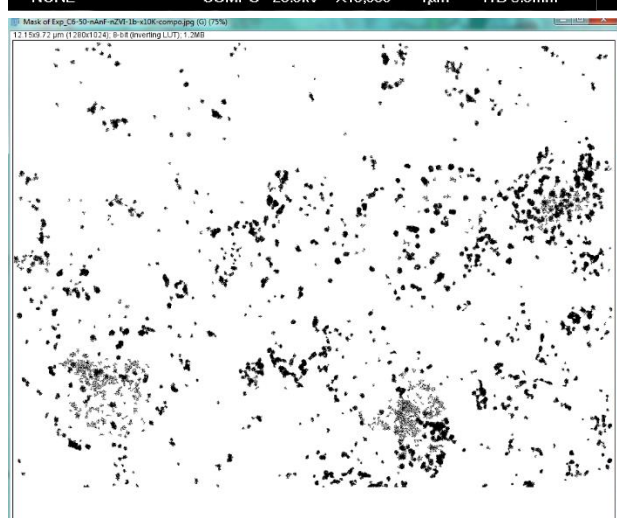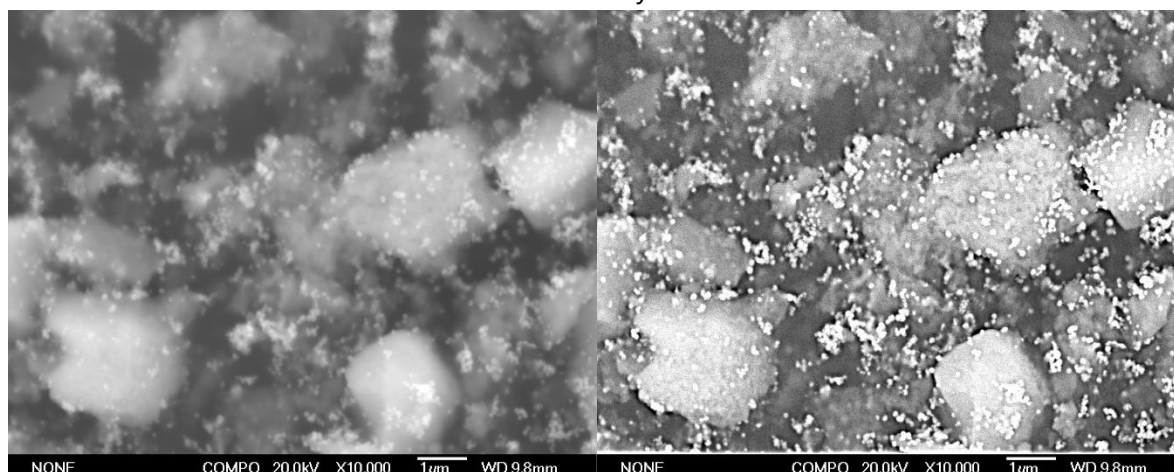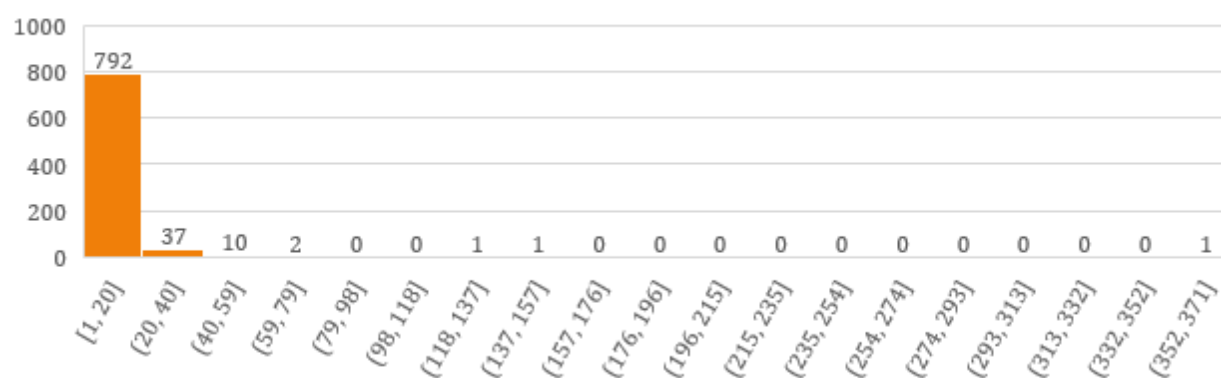
	With outlier	**Without outlier (362)**
Mean (nm^2)	7408	6987
SD (nm^2)	16192	10638
% of particles under 2000 nm^2	93.8	93.8

C600-5-nAnF-nZVI 3   *A*=0.64   Entry 59
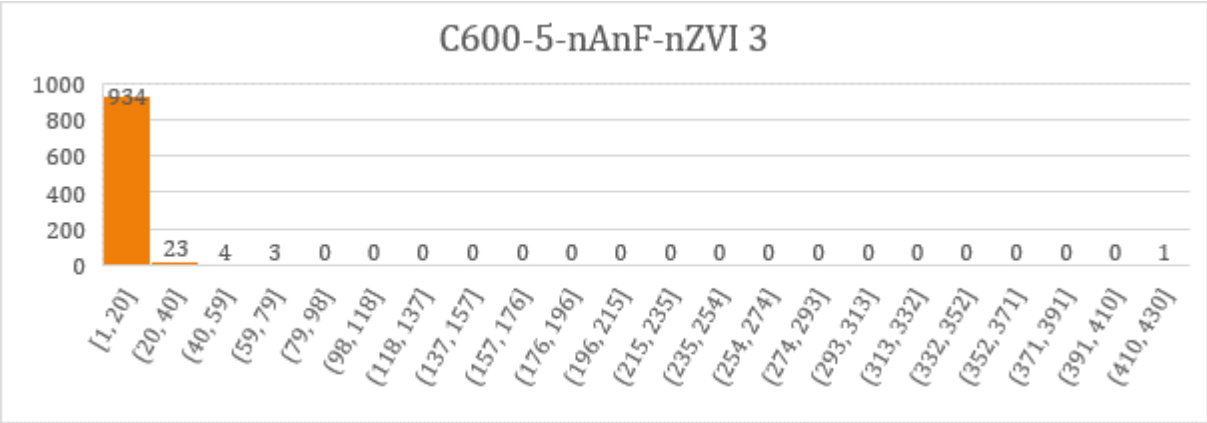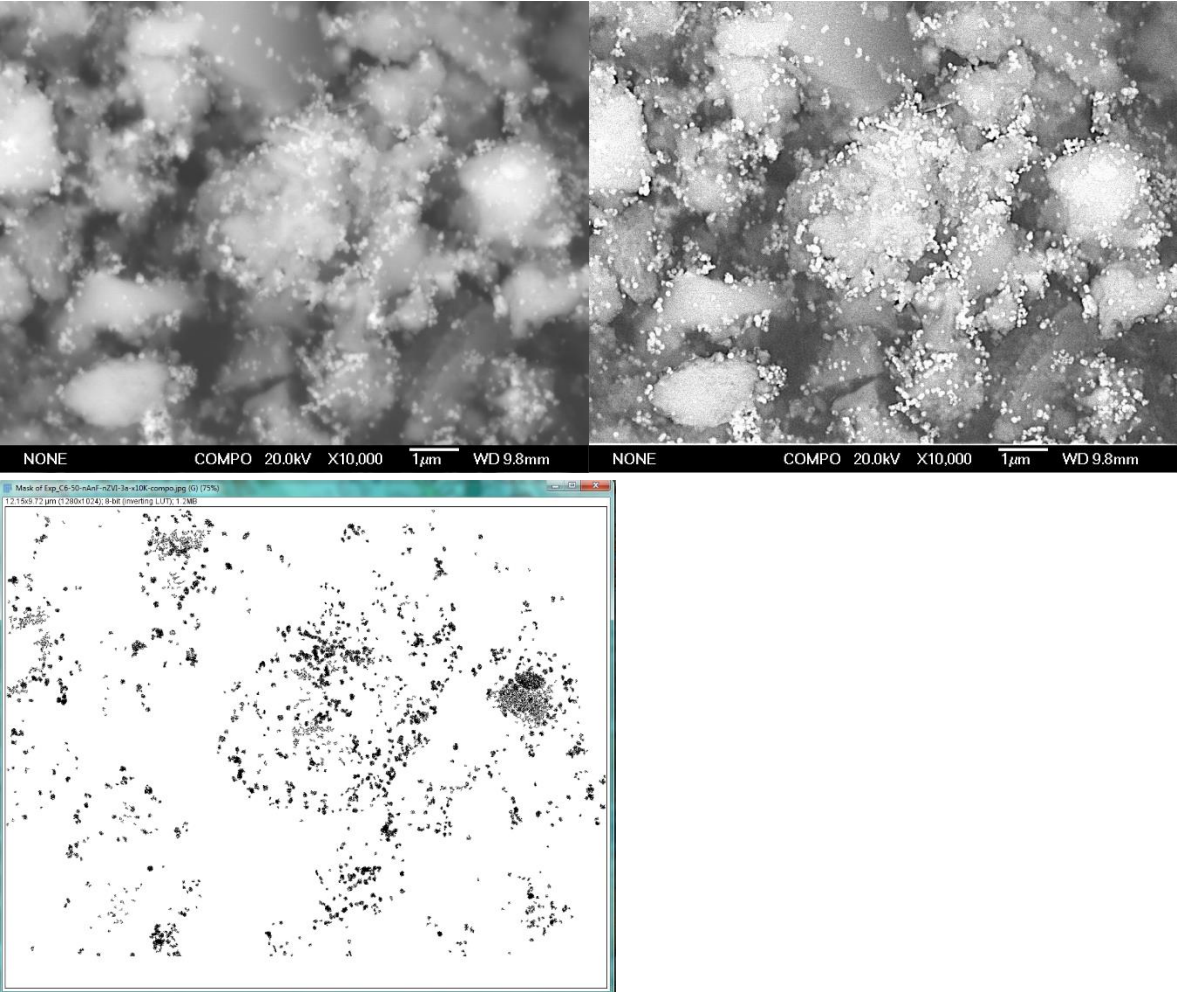
	With outlier	Without outlier (427)
Mean (nm^2)	4993	4555
SD (nm^2)	15213	6836
% of particles under 2000 nm^2	96.8	96.8

243

C600-AF-nZVI 1   *A*=2.00   Entry 60
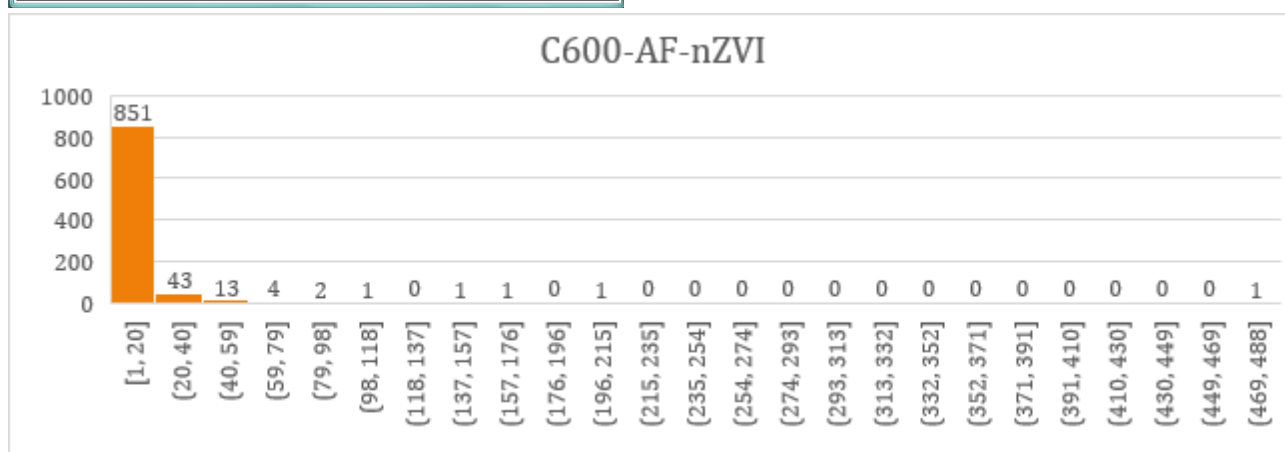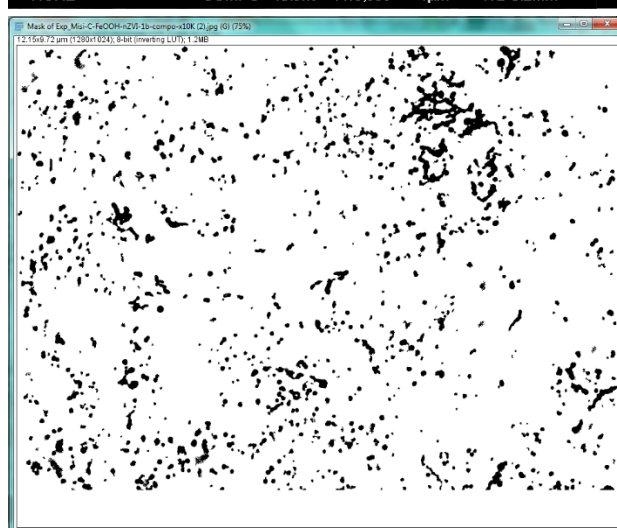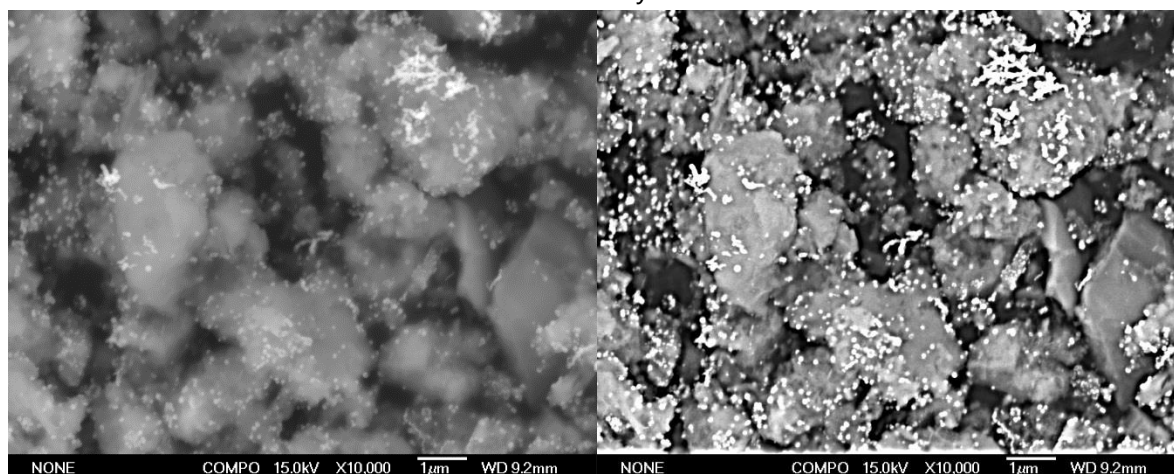
	With outlier	Without outlier (471)
Mean (nm^2)	9165	8661
SD (nm^2)	20776	14117
% of particles under 2000 nm^2	92.7	92.7

C600-AF-nZVI 2   *A*=2.04   Entry 61
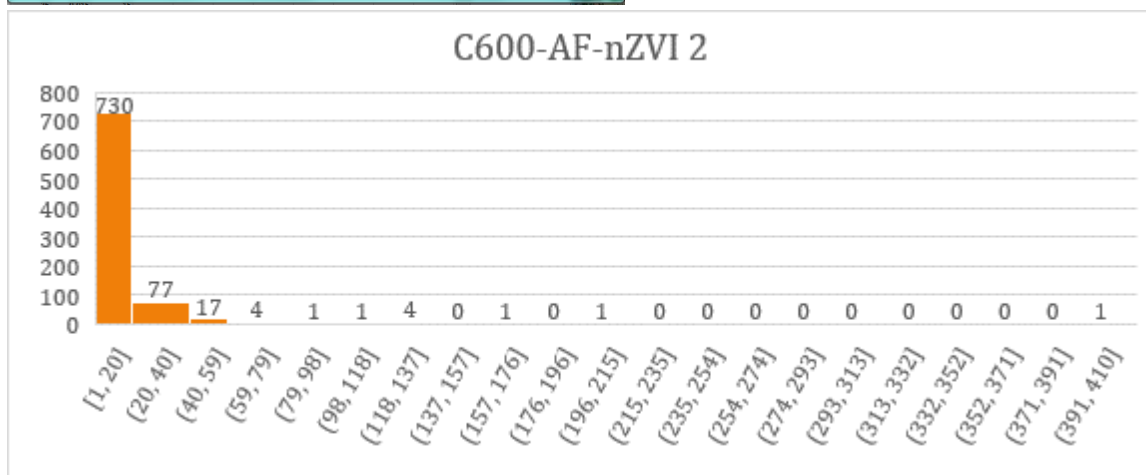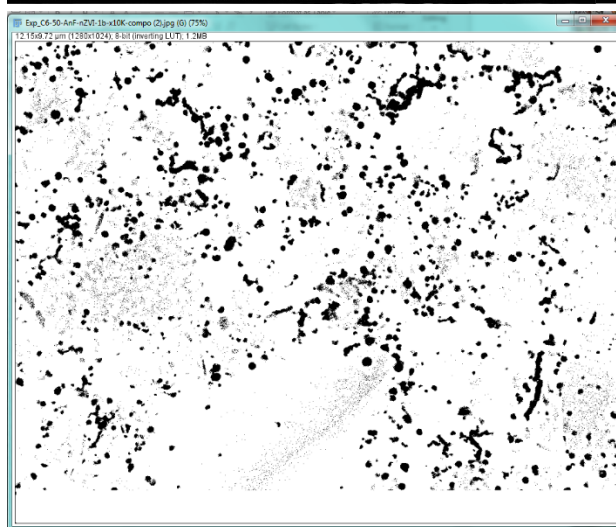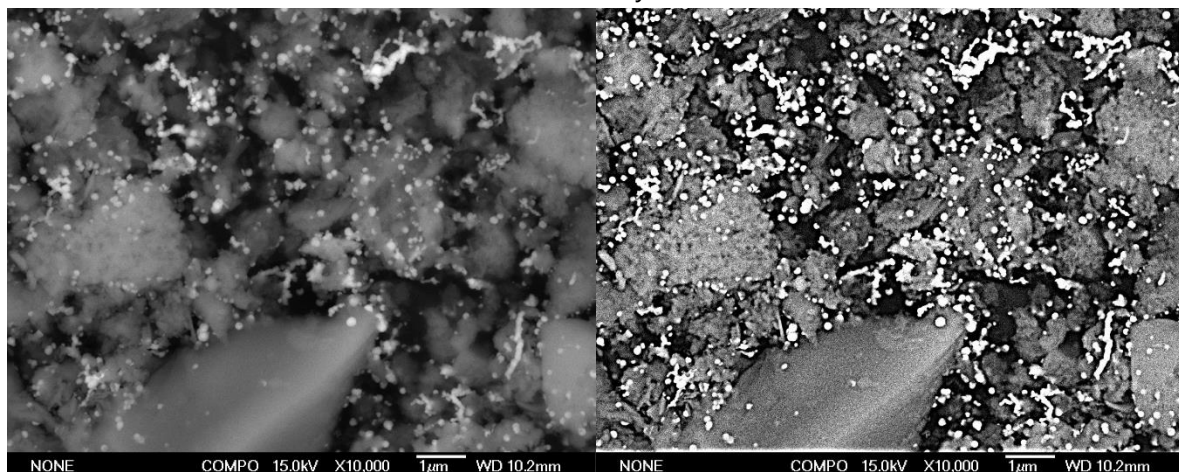
Mean = 11421 nm^2
SD= 21142 nm^2
% <2000 nm^2: 87.2%

C600-AnF-nZVI $\qquad$ A=1.76 $\qquad$ Entry 62
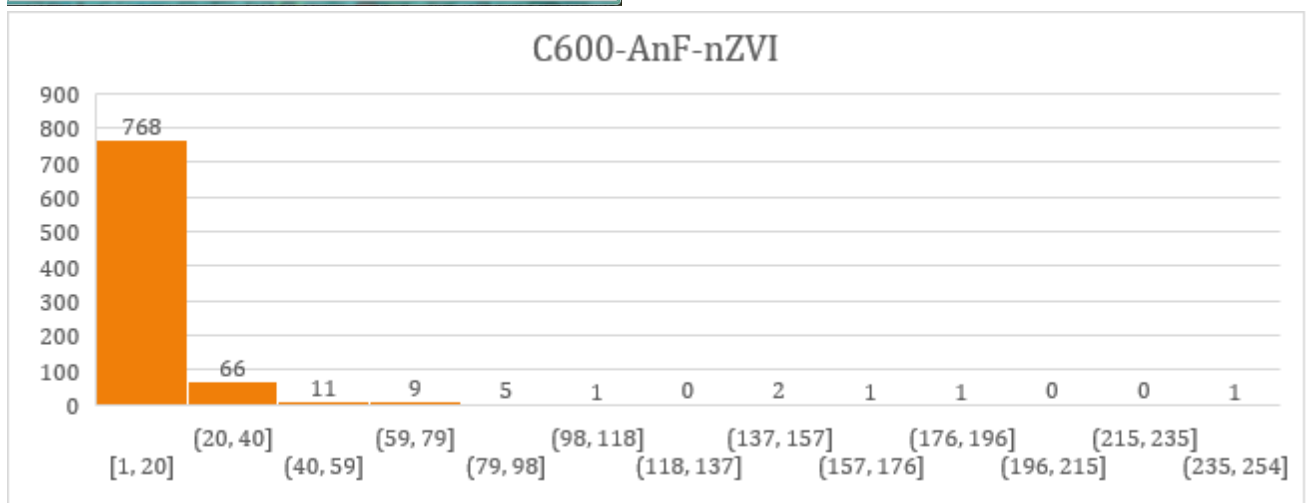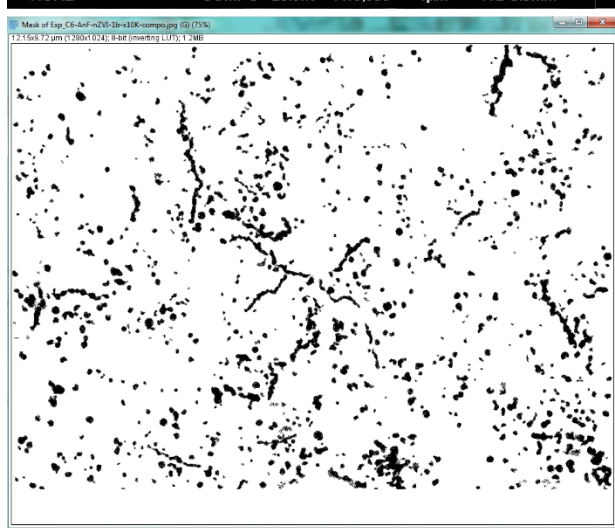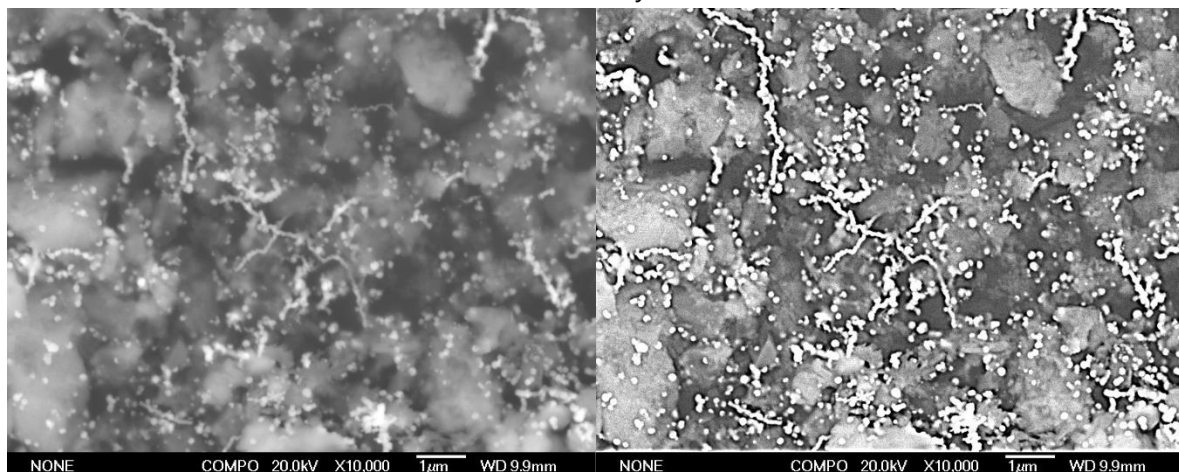
Mean = 10623 nm^2

SD= 18235 nm^2

% <2000 nm^2: 88.8%
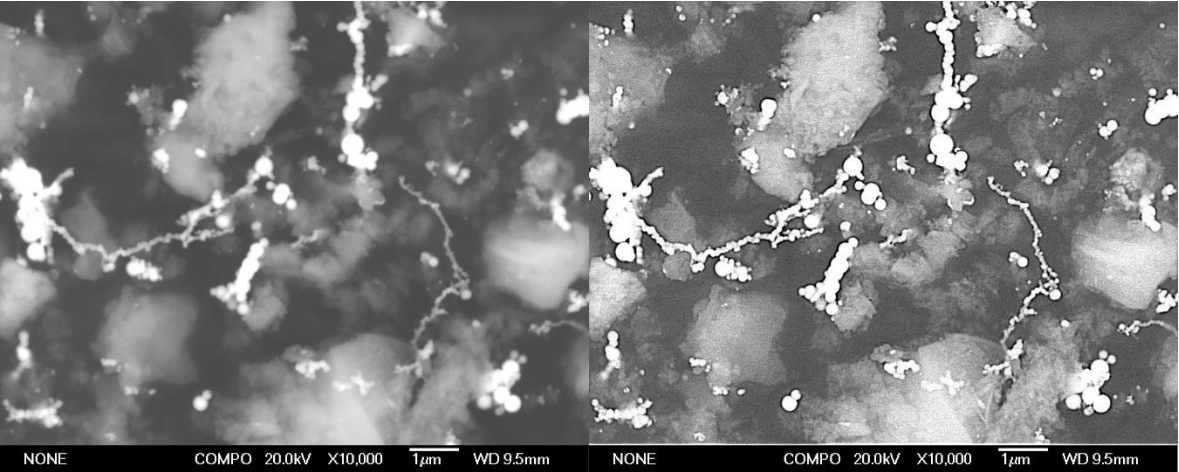
C600-nAF-nZVI 1   *d*=0.75   Entry 63
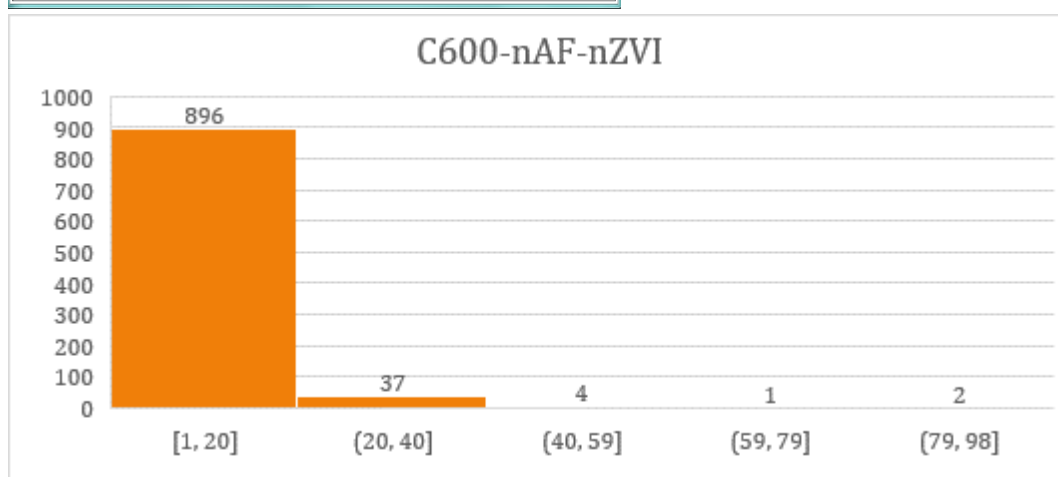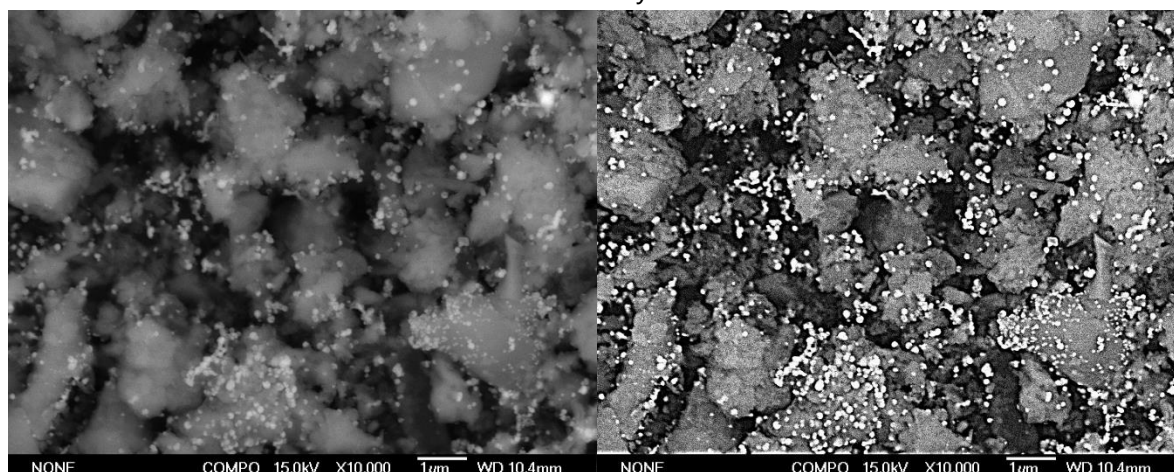
Mean = 6445 nm^2

SD= 7926 nm^2

% <2000 nm^2: 95.3%

247

C600-nAF-nZVI 2   *A*=5.07   Entry 64
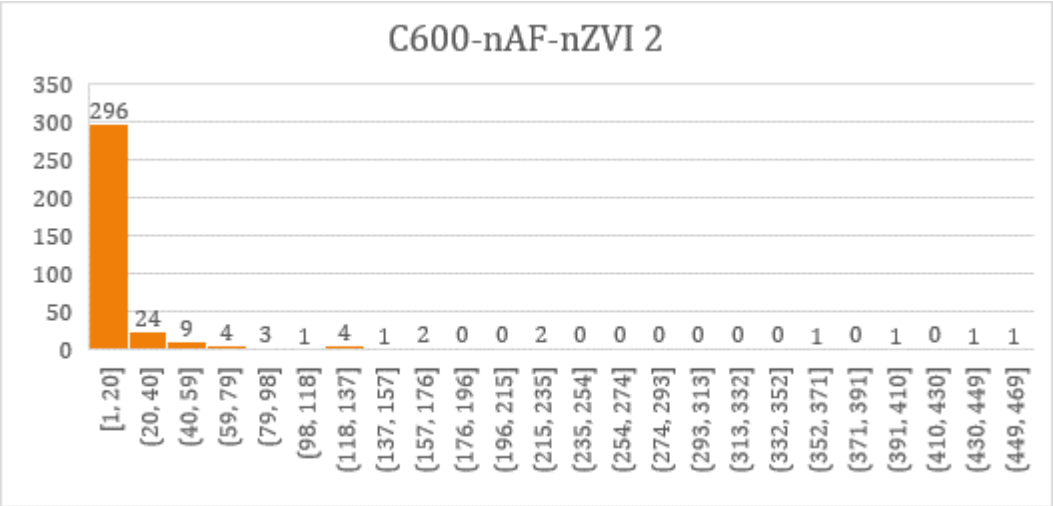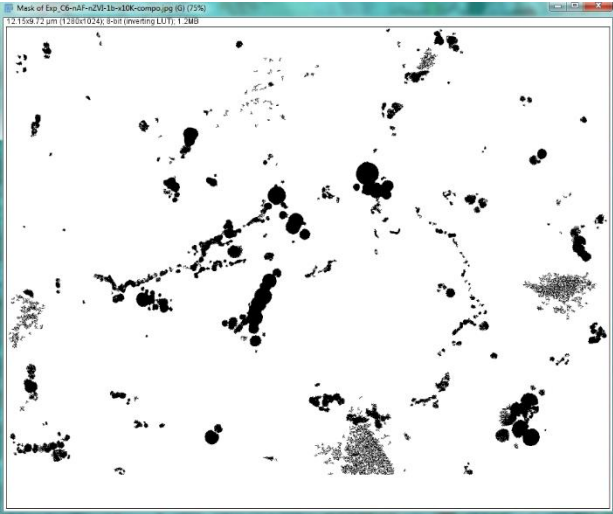
Mean = 16797 nm^2
SD= 51859 nm^2
% <2000 nm^2: 84.6%

C600-nAnF-nZVI   *A*=0.67   Entry 65
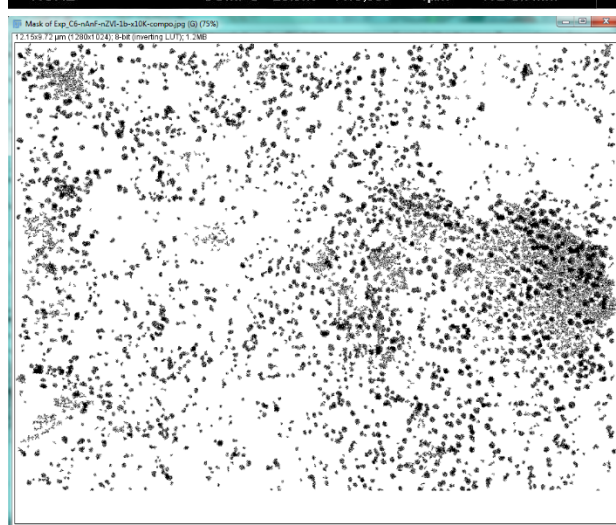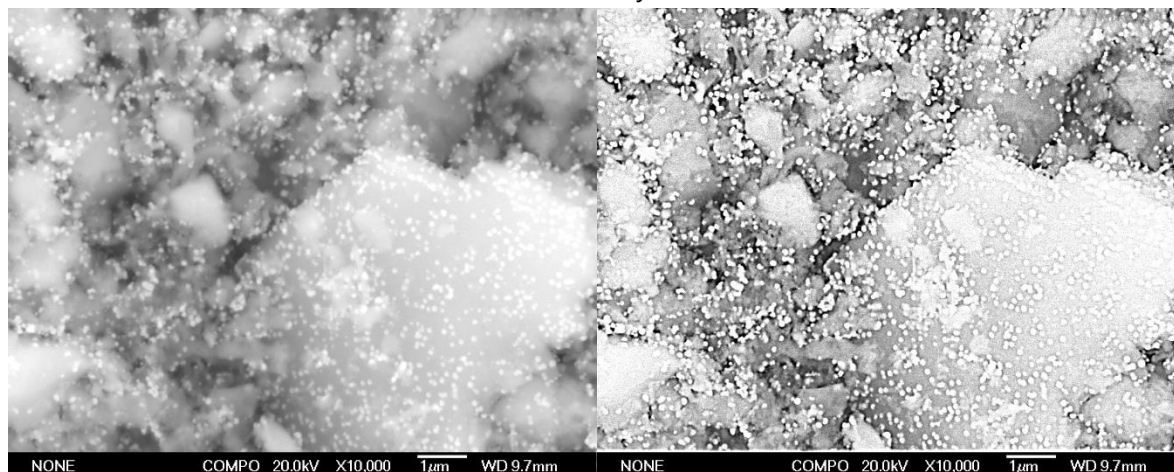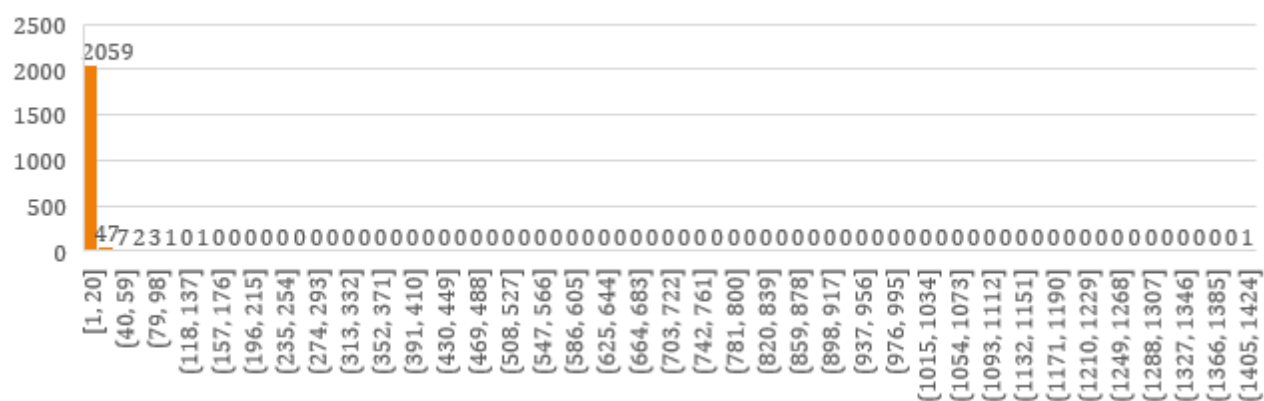
	With outlier	Without outlier (243)
Mean (nm^2)	6139	5478
SD (nm^2)	31394	7655
% of particles under 2000 nm^2	97.1	97.1